# Formation of polymer lipid nanodiscs for membrane protein studies

Tognoloni, Cecilia

*Award date:*
2017

*Awarding institution:*
University of Bath

# Formation of polymer-lipid nanodiscs for membrane protein studies

Cecilia Tognoloni

A thesis submitted for the degree of Doctor of Philosophy

University of Bath
Department of Chemistry

September 2017

*To my family and friends*
*and*
*To myself*

# Acknowledgements

These acknowledgements have not been read by anyone, so: sorry for any English/grammar/horrible mistake you will encounter. But after these 4 years people got to know me for this as well. So here we are. First of all I would like to thank my supervisor, Prof. Karen Edler. Thanks to have taught me so much, for never giving up on me and for being always so supportive. I would like to thank my second supervisor Prof. Gareth Price for letting me use his laboratory and for sharing his knowledge with me. I would like to thank all the beamline scientists I had the honour to meet over the "just few" experiments I carried out during my PhD. You are the brightest people I have ever met. I am not going to name you one by one, I would forget someone.

An exception must be made for my co-supervisor Dr. Ann Terry. Ann, if you will ever read this acknowledgements, I really want to thank you for everything. You made possible the unimaginable. You made SANS and SAXS (I will never forget the experiment on I22) enjoyable. Thank you for sharing your knowledges and your passion for science with me.

I am grateful to Dr. Stephen Roser, who helped me to fit reflectivity data and for sharing with me his knowledge. I wish I had asked more questions during these 3 years.

Thanks to all the collaborators in Birmingham. Prof. Tim Dafforn, Dr Sarah Lee and of course, thanks to Steve. I always had a good laugh when I carried out experiments with you.

A deep felt "thank you!" goes to the guys that have shared with me this adventure (T.V.O.S.): sorry guys to have written your name down in the page (the only one you are going to read of the whole thesis, probably). But, here you are. Thanks to Ilaria for being so supportive even from Lund. Duygu, you were

here nonetheless you are living in the US, thanks for our chat at 3 a.m. in the morning. Amani, I am still waiting for our trip to France, we will make it! Adri, well. The whole page would not be enough. You have always been supportive and constructive with your discussion on my data. You and Rosa were always there, telling me I could make it, it seems I did (you have probably done it because you wanted to eat my lasagna, but that is another story). Vincenzo, I am sorry that I met you just on the third year of my PhD. You have been a great colleague and an invaluable friend. Emily, thanks for your patience in the first couple of years, when you were doing monologues because I could barely speak. If I know few words and I got to the end of this adventure, I owe that to you. All the people in the group where fundamental to get at the end of this path, so many of you: Gavin, Sarah, Nomi, Oli, Drew, Yun, Andi, Marcelo, Julien, Antony, Yun-Chu. I forgot someone for sure. It has been an honour to meet you all. I hope our paths will cross again in the future.

I would like to thank Barbara and Tolga, and of course Pietro. Baba, je l'ho fatta! We have started our studies together. For better or worse, this adventure came to an end. I am deeply grateful to Andrea, Francesco, Enrico, Michela and Susanna. I don't know what I would have done without you. Micky Mouse, here and now I promise that I will become more tidy. I hope I did not drive you too crazy. You are the friend everyone should have whilst writing a PhD thesis. And of course, thanks to those guys from Italy that were always, always, always there, nonetheless the distance: Ombra, Vitty, Sara, amica Betty. Simply: thanks for being who you are.

And then, I really need to make this acknowledgements in italian...Un profondo e sentito grazie va alla mia famiglia: Aly, sempre breve e conciso, con quel "Anche se va male, lunedí cominci a lavorare!" mi hai dato tutto quello di cui avevo bisogno. Non in un milione di anni avrei mai pensato che avremmo avuto questo rapporto. Grazie per avermi sempre sostenuto. Gresta, Mauretto. Grazie per aver sopportato i miei sbalzi di umore e per aver sempre pensato che l'avrei potuta fare. Questa tesi é per voi. Spero di non deludervi.

# Abstract

Despite the crucial role that membrane proteins have in the biological field, the study of their structure is still a challenge for the scientific community. An obstacle is the dependency of their functional structure on the surrounding conditions. In the last decade a new platform involving poly(styrene-co-maleic acid) (SMA) copolymers has been developed for the extraction of membrane proteins without using any detergent into discoidal structures, referred to as nanodiscs. Nevertheless, even though progress has been achieved using this method, limitations of this system are the insolubility of the polymer at pH lower than 8 and the complexation of the acid groups in the presence of divalent cations. The polymer is also produced via an uncontrolled free-radical polymerisation route which means it has a polydisperse and random structure, making it difficult to correlate properties of the polymer with the structures of the nanodiscs.

In this project new styrene maleimide copolymers, soluble at pH lower than SMA, were investigated for their potential in forming stable lipid structures. Characterisation of their architectures was carried out using mainly scattering techniques. The stability of these structures were studied in the presence of divalent cations such as $CaCl_2$ and at low pH.

Moreover, SMA copolymers were synthesised with a narrow distribution of molecular weights and well defined architecture using a controlled radical polymerisation method. This demonstrated that the size and stability of the nanodiscs could be tuned directly via control of polymer structure. To achieve supramolecular assembly at a wider pH range, zwitterionic copolymers were also synthesised and their structures characterised.

The mechanism and kinetics of the polymer insertion into the lipid monolayer and the polymer self-assembly around the lipid tails as nanodiscs formed were

investigated using several techniques such as fluorescence, small angle neutron scattering and neutron and X-Ray reflectivity. The mechanism of disc formation is complex and appears to depend on the properties of both the polymer and the lipids.

# Contents

# List of Figures

# List of Tables

# Chapter 1

# Introduction

## 1.1 Soft matter and nano structure

The prefix "nano" comes from Greek "$\nu\alpha\nu\nu\omega\sigma$" which means "dwarf"; in the international metric system, nanometre (nm) corresponds to $10^{-9}$ m. The term and concept of nanostructure comes from Richard P. Feynman, an American Physicist, who, in his Nobel prize speech 1959, introduced people to the idea that in the future it would be possible to compress machine engineering into smaller and smaller scales yet with higher and higher performance [9]. With the term nanotechnology we mean the techniques and the methods that allow us to handle matter on atomic and molecular scales, and is applied from hard condensed matter through to soft matter to define structures and devices on the nanometre length scale. Pierre-Gilles de Gennes, who won the Nobel Prize in 1991, is the "father" and the inventor of the term *soft matter*. Before this scientists used to refer to this kind of material as a "complex form of matter" and prior to this was used "complex fluid". He introduced this new term for two reasons: firstly, not of all the systems studied are liquid and, secondly, so that students would not be scared by the word *complex*. He highlighted the two major features of soft matter: the *complexity* and *flexibility* [10]. When we talk about soft matter we include a wide range of materials, which includes liquid, colloids, polymers, foams, gels, granular materials and biological systems. All of

these systems have the characteristic that they can be easily deformed by thermal stresses or fluctuations. This is due to the energy that the system is bonded with, which is comparable to $k_B$T, where $k_B$ is the Boltman's constant and T is the temperature. In fact the kind of interactions involved are electrostatic, Van der Waals, hydrophobic and hydrophilic interactions. The advantage of soft matter, such as a polymer, is that a small change in the chemical conditions can cause a very large change in the mechanical properties [11]. It is the templating or creation of a nanostructure through modification and interactions of polymers and phospholipid aggregates which form the basis of the work in this thesis and will be further discussed in section 1.2.

## 1.2 Phospholipid aggregates and protein characterisation

Phospholipids are amphipathic molecules which have a hydrophobic or non-polar region and a hydrophilic or polar region (figure 1.1).

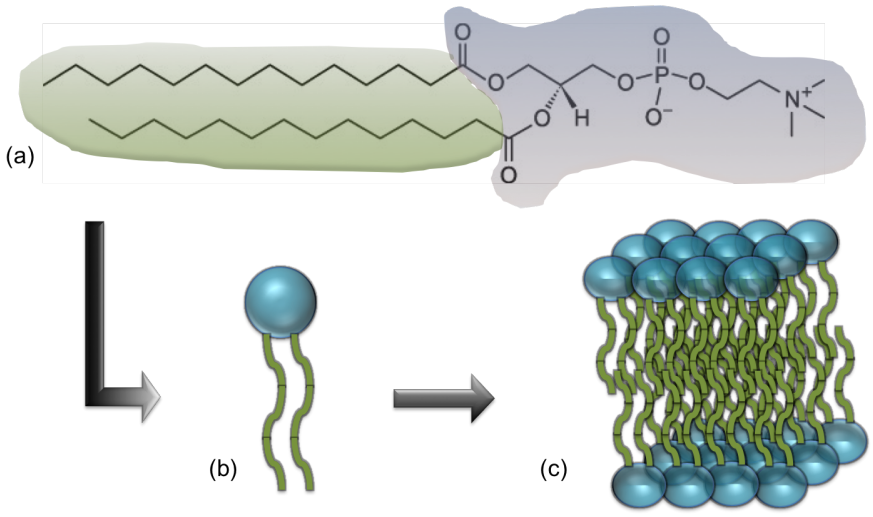


**Figure 1.1** (a) Chemical and (b) simplified representation of a structure of a phospholipid and (c) their assembly in a bilayer. Green regions correspond to the hydrophobic lipid tails and blue regions are the hydrophilic headgroups

When phospholipids are dispersed in water, or in any polar environment, they

arrange in a way that minimises the tail-water interaction. The contributions from both entropy and energy interactions play a key role in this self-assembly process. Entropy will drive the system to a random distribution of molecules, whereas the energetic interactions among neighboring molecules will bring them closer together, which can result in a phase separation or in multi-phase systems. The structures formed can be defined as a "phase" since they have uniform physical properties such as density and chain order parameters. The nature of the structures formed and their phase behaviour is complex, depending on the interactions mentioned above and as shown in figure 1.2 how changing the tail length, the head size and the water to oil composition of the solvent promote different phases.

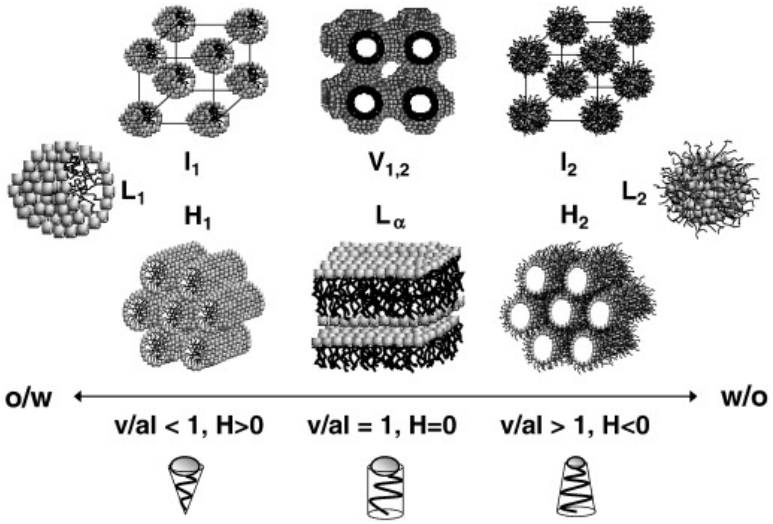


**Figure 1.2** Schematic of lipid phases upon changing the head and tail composition and lipid volume fraction in water-oil. Image reprinted with permission from [1]

### 1.2.1 Phospholipids and cellular membranes

The most common naturally occurrring aggregates of phospholipids occur in cell membranes (figure 1.3). The framework of the cell membrane is a phospholipid bilayer in which several other components can move relative each other in a fluid-mosaic model [12]. The hydrophobic tails of the lipids form the core of

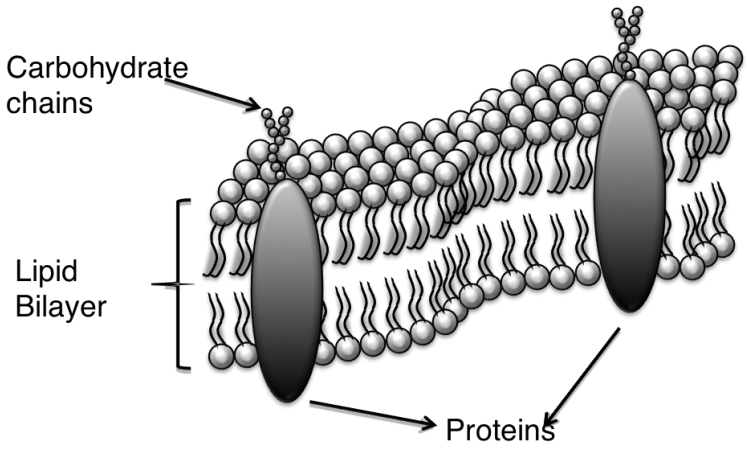


**Figure 1.3** Biochemical organization of cellular membranes

the membrane, whereas the hydrophilic heads are exposed to the external water environment. The proteins in the membrane exhibit a semi-fluidic behaviour as the protein can move but only laterally. [13].

Membrane proteins have a key role in every day life. In the cell membrane, membrane proteins are involved in the regulation of the cell and determine its functions. The activity of each cell is based on the different amounts and types of membrane proteins present in the cell membrane. [14] Until the beginning of 2000, the structure of membrane proteins was simplified and their orientation along the cell membrane was assumed to be perpendicular to the double phospholipid layer, thus making transmembrane helices [15]. However, in the last few years, more studies have been carried out on the relationship between the structure of the protein and its functions. It has been proved that the unfolding process of proteins causes diseases [16], for example, many degenerative conditions are caused by denaturation of proteins that aggregate into amyloid fibrils and plaques which cause syndromes such as Alzheimer's [17] and Parkinson's [18]. It is now well established that the functionality of the proteins is strictly correlated to their spatial arrangement, which is more complicated than a simple transverse channel across the membrane. Proteins can associate with the cell membranes in different ways as depicted in figure 1.4.

One of the most common types of proteins are channel proteins (figure 1.4a-b-c)

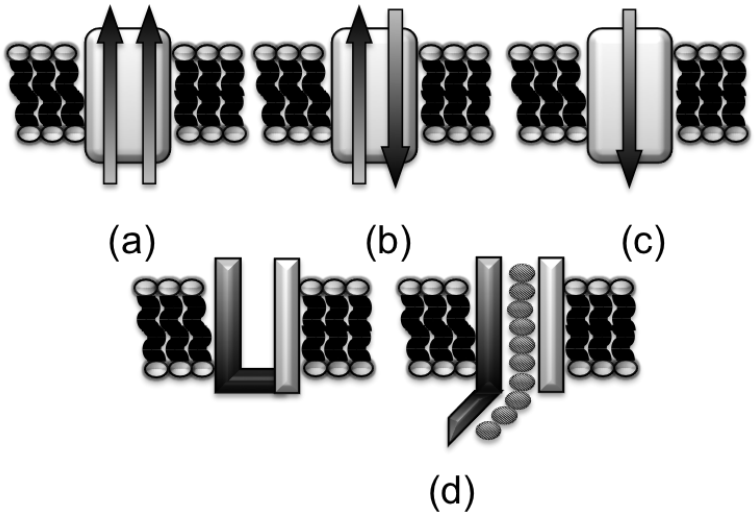


**Figure 1.4** Schematic diagram of a few possible arrangements of membrane proteins in a cell membrane

that control the flux of ions inside and outside the membrane. Membrane proteins are also correlated to the enzymatic activity of the cell. The enzymatic function of proteins is often used as a target for therapeutic applications and diagnosis [19].

Membrane proteins can be divided into two elementary regions: one hydrophilic and one hydrophobic. The first region will be intercalated and stabilized into the cell membrane in the lipidic head layer or the surrounding water. The hydrophobic core of the phospholipid bilayer instead will interact and anchor the hydrophobic region of the membrane protein. The way the phospholipids interact with membrane protein is based on the composition of the membrane. Five points must be kept in mind:

1. A protein can not move without regard to the surrounding lipids: lipids surrounding the membrane protein have to arrange hydrocarbon tails in a way that no void space is present (figure 1.5). Moreover, the stretching of the hydrocarbon tails must not be greater than the critical length.

2. Lipid configuration around the protein is different: Due to point 1, lipids surrounding the membrane protein must have different mobility in order to pack their tails into the membrane. The discrepancy between the mobility

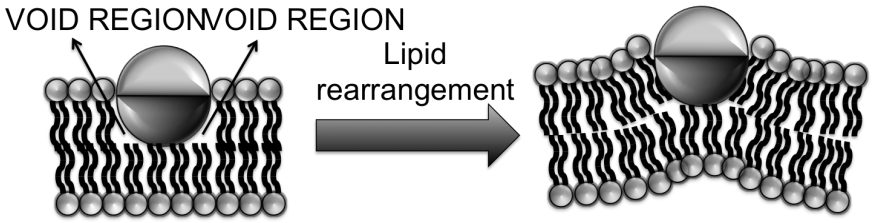


**Figure 1.5** Pictorial representation of (left) a membrane protein with a hydrophilic (grey) and a hydrophobic (black) region. and (right) the rearrangement of lipids in a membrane to avoid empty space

of the tails around the protein and those far away from the protein was detected using ESR (Electron Spin Resonance) and NMR [20, 21].

3. The way the lipids are packed will be different in the top and bottom leaflet due to changes in the curvature and the membrane function on both sides of the bilayer.

4. The mobility of the protein along the cell membrane will change in the presence of coupled regions.

5. Phase separation can occur around a protein: due to the concavity/convexity that the cell membrane has around a protein, there is a selectivity of lipids that can thermodynamically surround a protein. Since just a few lipids can, most of the time, match the properties so far explained, it is not uncommon to find phase separation of lipids around a membrane protein.

Due to the complexity of the interaction between membrane proteins and lipids, the conformation of one changes with the respect to the other, which leads to different configurations and, as a consequence, to different functionalities of the proteins in different lipidic environments [22]. The conformation of the latter is affected by changes in pH and salt conditions and thus tight control over these solution parameters is crucial to maintain the functionality of a protein. Figure 1.6 shows how two different cells can differ from each other with respect to lipid content.

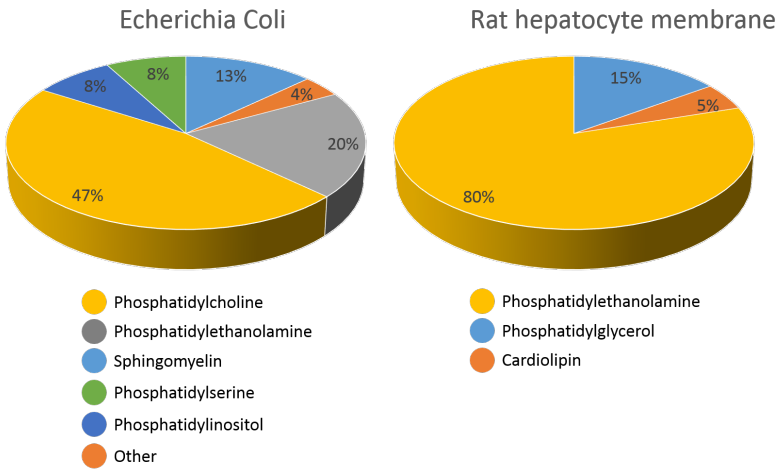


**Figure 1.6** Lipid composition for two different cell membrane: (left) *Escherichia Coli* and (right) Rat Hepatocyte Membrane.

Different phospholipid heads will affect the charge on the membrane surface whereas different tails will change the pressure that the protein experiences. All these parameters will affect the quaternary structure of a protein. In general the physiological environment controls the protein function, which can change from organism to organism, with age and disease [23].

A critical point for the scientific community is to then find the stability conditions for which the conformation of the membrane protein is preserved out of the native environment in order to study the role of the membrane in, for example, degenerative diseases. In fact, unlike soluble enzymes, membrane proteins aggregate into insoluble structures if removed from the native environment [24]. Therefore, to carry out a biological characterisation of a membrane protein, three parameters have to be satisfied:

- control of lipid environment
- control and definition of protein oligomeric state
- topology of the insertion

In order to satisfy the parameters specified above, membrane protein characteri-

sation has typically been carried out either using micellar or liposome phases as supports. In the first case, detergent is used to solubilise the protein in a micellar structure. The detergent can lead to an inactive or denatured structure, as well as interferring with the probing technique used for the characterization [24]. Moreover, the small particle size of micellar structures leads the system to have dynamic fluctuations [25], which are different to fluctuations in the native layer. For a long time liposomes have also been used to characterise membrane proteins [26–28] due to the similarity of the structure to that of a cell membrane. This system is still used to study channel proteins where the discrimination between the inside and the outside of the membrane is fundamental to the functionality of the protein [29]. The main disadvantages of this system, though, arise from the impossibility to have a tight control over the phospholipid composition, which, as discussed above, has a huge effect on the structure of the membrane.

## 1.3 Nanodiscs: a literature review

The direct self-assembly of simple molecular components into a complex structure is still a controversial field which has fascinated the science community for the last few decades [30–32]. Examples of self-assembly emerge from several subjects, for example, in the chemistry of polymers arising from a mixture of monomers [33]. In biology the three dimensional structure of proteins is also driven by the "monomers"; in this case, the amino acid sequence. The supramolecular order seems to be the main driving force for phase separation and symmetry breaking in the formation of anisotropy at the mesoscopic level.[34] With the goal to study membrane proteins, in order to avoid the limitations described above with using liposomes and micelles as model systems, the scientific community recently came up with another self-assembled system: the *nanodisc*.

The nanodisc is a non-covalent self-assembled system made from a bilayer of phospholipid wrapped by either a Membrane Scaffold Protein (MSP) [35] or a polymer in a belt-like configuration [36].

The advantages of the nanodisc structure is that the oligomeric state of the target membrane protein is controlled and the protein is solubilised at the single molecule level. This allows structural and functional studies of the protein by techniques that before were confined only to soluble proteins [37, 38].

### 1.3.1 MSP stabilised nanodiscs

MSP is a synthetic protein based on the apolipoprotein A-1 sequence, which consists of a chain of 200 amino acids which construct an amphipathic alpha helix. The globular N-terminal domain present in the native protein is substituted by a histidine tag and Factor X cleavage[35]. The MSP encircles the phospholipid bilayer, stabilising the structure in a disc-like configuration. Two or more chains of MSP are involved in this process [39, 40]. A so-called MSP2 was engineered in such a way as to fuse two chains of MSP; this allowed the self-assembly process to proceed using only one chain [35]. The procedure for the self-assembly process from a cell membrane to a protein embedded in its lipids' native environment has been exhaustively reported in the literature [23, 24, 34, 35]. The process is summarised in figure 1.7 and described below.

Initially, the lipid to MSP concentration must be determined. This is usually done by titration of MSP against several lipid concentrations. As Sligar *et al.* [35] has already shown, monodisperse nanodiscs are generated when lipids is added to MSP in correct proportions. If the concentration of lipids is too high, large aggregates in solution are formed. Conversely, for a too low concentration of lipids, the MSP will still interact with the lipid tails, but the resulting structure will be deformed and most likely will not have a nanodisc shape. In general, when the lipid to polymer ratio is not optimal, then polydisperse structures are made [24].

Once the ideal ratio is established, the engineered MSP protein is solubilised in a detergent and mixed with the lipids. The self assembly process begins when the MSP and lipids are dialysed against water where the surfactant diffuses into

the water and the protein therefore starts to interact with lipid tails. The system finds its minimal energy configuration with the MSP surrounding the lipid tails on the perimeter of the disc shielding them from the solvent [35].
The optimal disc radius arises from the length of the MSP[34]; engineered MSP were generated with several lengths and show that upon increasing the length of the MSP, larger discs are created [34].
However, even though control of the size nanodisc is possible using this method, a surfactant must be initially used for the protein extraction. Moreover, in order to extract the membrane protein from the cell membrane several steps must be undertaken and in fact the MSP cannot be used directly to extract the membrane protein from the cell membrane.

In the last decade, however, a new method using a block copolymer of styrene and maleic acid has been developed to extract membrane protein from the cell membrane in one step, without requiring the use of detergent.

## 1.4 Polymer stabilised nanodiscs

IPolymer stabilised nanodiscs use polystyrene-co-(maleic acid) (SMA) to extract membrane proteins out of the cell membrane. When SMA is added to either artificial or natural membranes, the polymer disrupts the membrane and stabilises, in similar structures to MSP, the lipid tails on the perimeter of the discs. The structures made are called SMALP (**SMA L**ipid **P**articles). The great advantage of this method is that it is detergent free and the protein is preserved in its native environment. SMALP (SMA Lipid Particles) nanodiscs made with this polymer have a size range between 10 and 25nm [41, 42]. In the last decade many membrane proteins have been extracted using this polymer. The characteristics and features of this polymer are extensively explained in section 1.5.1
The self-assembly process that leads to either MSP or polymer stabilised nanodiscs is reported in figure 1.7

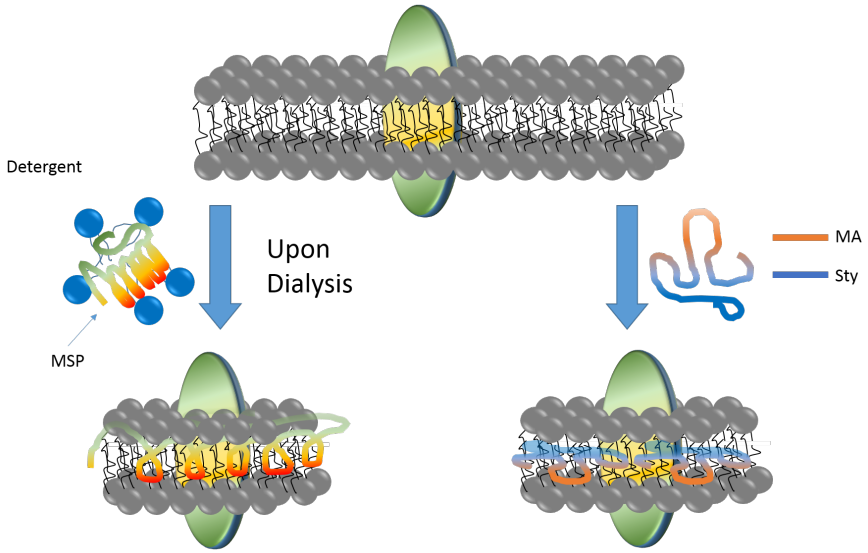


**Figure 1.7** Schematic of the self-assembly process that leads to the assembly of (left) MSP or (right) SMA in stabilised nanodiscs.

### 1.4.1 Latest developments using SMALP

The development of SMALP for the three-dimensional study of membrane proteins has increased the number of membrane protein extracted in their lipid native environment from simple cells like as *Escherichia Coli* [43]. Membrane proteins like AcrB [44], ABC transporter PgP [45], the potassium channel KcsA [46] and more, have been extracted and a library of membrane protein structures in their native lipid environments has been formed. In addition to their use as a platform for membrane protein reconstruction, SMA stabilised discs have been used also as a pseudo stationary phase in electrokinetic chromatography (EKC), instead of membrane stabilised nanodiscs. A good performance of SMALP was observed in terms of mobility and migration range thanks to the maleic acid charged group. [47].

Recently, nanodiscs have proven successful in the detection of phosphorylation using NMR [48]. The SMALP platform has allowed the characterisation of $\alpha$-synuclein ($\alpha$-syn), a membrane protein responsible for neurodegenerative diseases such as Parkinson's disease. The aggregation of this protein has been observed in neurons, however, there is evidence that in its functional form, this protein

has a high alpha helices content and can make a tetramer, the functionality of which remains unclear. Using SMALP as a platform for $\alpha$-syn showed their ferrireductase activity in its functional form in the tetrameric state [49].

## 1.5 Polyelectrolyte block copolymers

Poly(styrene-co-maleic acid) is just one of a wide range of polymers called polyelectrolytes. In this specific case, SMA, as well as being a polyelectrolyte, is also a block copolymer species. Polyelectrolyte block copolymers are widely used in disciplines such as biology, physics and chemistry. In general a polyelectrolyte is a polymer whose monomers contain an electrostatic charge, which can be either positive or negative [50]. Due to the charge on the molecule, polyelectrolytes are soluble in water environments, which make them suitable for green and sustainable chemistry, biological and medical application [1].

### 1.5.1 Poly(styrene-co-maleic acid) (SMA)

Poly(styrene-co-maleic acid) is the product of the hydrolysis of a widely available commercial copolymer: poly(styrene-co-maleic anhydride) (figure 1.8).
Poly(styrene-co-maleic anhydride) (SMAh) is produced on a large scale by many companies such as Polyscope, Sartomer, Cray Valley and Syngenta. Due to its thermoplastic and chemical-resistance properties, it has been used in the past for the production of objects such as plastic trays and automobile parts.
The anhydride form is still interesting as a polymer with a wide range of applications such as ink, coatings and leather tanning agent due its hydrophobicity and polarised beat from styrene and maleic anhydride respectively. But, due to the insolubility of this polymer in aqueous solution, it is not attractive for the biology community.
On the other hand, poly(styrene-co-maleic acid) (SMA) has been widely used by the scientific community for many purposes: to make photoactive polymer micelles [51], to control the growth of crystal nanoparticles [52] etc. SMA has

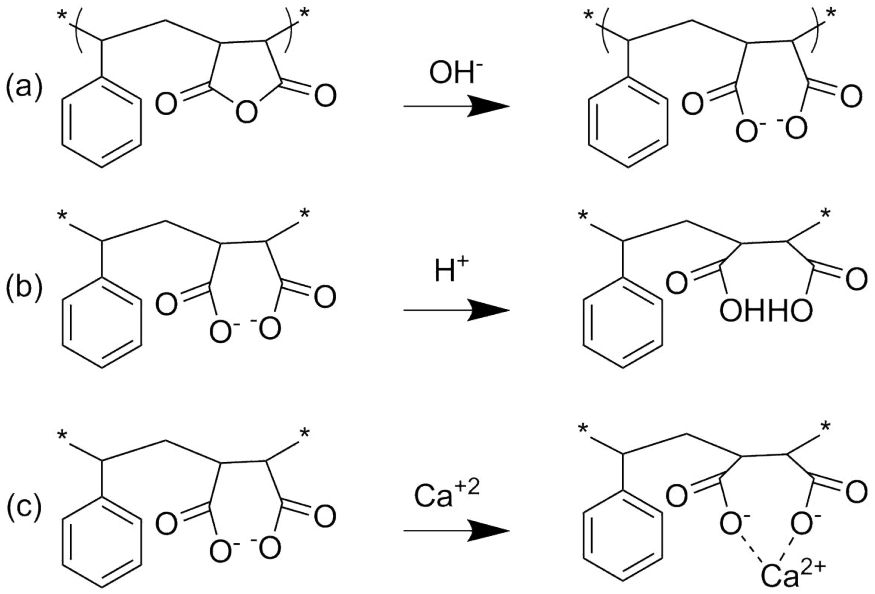


**Figure 1.8** Schematic of (a) the hydrolysis of maleic anhydride to maleic acid in an alkaline environment, (b) the protonation of maleic acid in an acidic environment and (c) the chelation of maleic acid with divalent cations.

also been used in medicine and biochemistry in conjugation with cancer-therapy drugs [53].

One of the most recent applications of SMA is to make SMALP, as described in section 1.4. From the structural point of view, SMA is a polyelectrolyte copolymer made of styrene and maleic acid. The double acid group present in the latter monomer makes the polymer soluble in aqueous solution. Maleic anhydride undergoes a ring-opening reaction in presence of a base as shown in figure 1.8a. There are limitations to the use of this polymers which mainly arise due to the chelating properties of maleic acid. In fact when a divalent cation is added into solution, maleic acid makes a complex which neutralises the polymer charge on the surface (figure 1.8c); this leads to a precipitation of the polymers. Moreover SMA copolymer is not stable in acidic solutions due to the protonation of the carboxylic group (figure 1.8b).

### 1.5.2 Poly(styrene-co-maleimide)

Positively charged polyelectrolytes have been widely investigated due to their ability to disrupt the cell membrane. This property gives rise to antimicrobial applications[54], and is also used in gene delivery[55]. Polystyrene maleimide is a resin which changes its physical properties depending on the percentage and the type of maleimide [56]. Styrene maleimide co-polymers have been developed due to their interesting thermal properties. The thermal resistance of this polymer is increased compared to styrene - maleic anhydride co-polymers [57, 58].

Direct copolymerisation of styrene and maleimide can be carried out using Atom Transfer Radical Polymerization (ATRP), but this method is not the most commonly used because maleimide, unlike maleic anhydride, can homopolymerise, so must be handled with care prior the polymerisation [58]. For this reason, large scale production of SMI has been achieved by conversion of the SMA copolymer. The main advantage to use the SMA copolymer as a starting material arises from its large availability, and moreover SMA copolymers are well characterised for MW, PDI and styrene to maleic anhydride ratio. The modification occurs either in the liquid or in the gas phase. The conversion of the maleic anhydride depends on the concentration of the amine used, which can be ammonia [58, 59] or a R–$NH_2$ reagent. This copolymer, other than being used as a resin for photolithography and photoengraving applications [60] has already been used in biology to make giant hybrid macromolecules [61].

As for SMA, SMI can become a polyelectrolyte upon the protonation of the imine group, as reported in figure 1.9.

Polycationic species are interesting and have been widely studied for their ability as a antimicrobial agent. In fact it has been shown that polycationic species can disrupt the cell membrane [54].

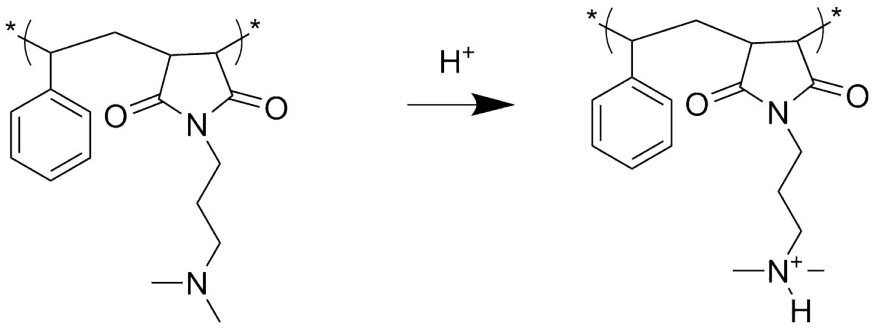


**Figure 1.9** Schematic of the protonation of SMI used during the project.

## 1.6 Aim and objectives

To determine whether commercial SMI can be used to make stable aggregates with DMPC or not, an in-depth study of the polymer alone, and then in the presence of lipids it is discussed in chapter 3.

However, the commercial SMA did not show a clear correlation between the molecular weight of the polymer and the diameter of the discs. That is why a controlled polymerisation of this copolymer has been made. In order to correlate the features of the polymer with the nanodiscs properties, the structure of the polymer has been slightly modified as shown in chapter 4.

The controlled synthesis of the copolymer led to the possibility to deuterate part of the structure and to follow the early stages of the penetration of the polymer into a lipid monolayer. This will be discussed in chapter 5.

# Chapter 2

# Material and Methods

This chapter introduces the theory of the characterisation techniques. A brief introduction of the scattering theory will be discussed first.

## 2.1 Wave-matter duality and scattering theory

The first debates about wave-particle duality date back to the XVI century. Two divergent opinions were held by Isaac Newton and Huygens, respectively, about the nature of light. Newton published his treatise "*Opticks*"[62], in 1704, where light was described as a particle, whereas Huygens in 1690 described in his *"Trait de la Lumiere"* (treatise on light) the first mathematical description of light as a wave. In the 20th century, Einstein advanced the hypothesis of a wave-matter duality. He wrote: *"It seems as though we must use sometimes the one theory and sometimes the other, while at times we may use either. We are faced with a new kind of difficulty. We have two contradictory pictures of reality; separately neither of them fully explains the phenomena of light, but together they do".*
Given then the dual wave-matter nature of radiation when this hits a particle, whether this is light, X-rays or neutrons when it hits a particle the scattering event can be described using classic mechanics due to its particulate nature. When a scattering event occurs, two pathways are available: the incident beam hits the particle and transfers part of its energy to the sample (inelastic scattering) or energy is conserved (elastic scattering) [63]. Scattering experiments can be per-

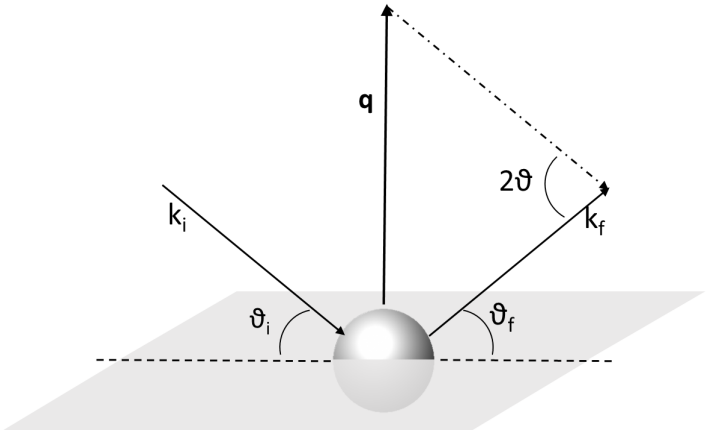


**Figure 2.1** Representation of a scattering event.

formed in order to elucidate the structure or dynamics of the system under study. In the case of neutrons and X-rays, only structural experiments using elastic scattering were performed in this work: these are discussed in sections 2.2.1 and 2.2.2. Depending on the nature of the source of radiation (neutron, X-ray, light etc), different information can be extracted. In fact, the interaction of each radiation with the same sample is different: neutrons will be scattered from nuclei, X-Rays will be scattered from the electronic cloud and light will be scattered by a dipole-dipole interaction[64]. Even though different information will arise from any of those scattering events, these techniques return complementary information and can be described with the same basic equations and laws[65]. The general event of scattering can be summarized as in figure 2.1

The incoming radiation has an initial vector, magnitude and direction when it hits the scattering particle and leaves from it in a different direction with either an equal or different final vector magnitude. In the first case the event is called elastic scattering and no energy exchange happens, whereas the second case is called inelastic scattering where the incident particle does not preserve its kinetic energy. Since only elastic scattering was used to investigate the systems, in this thesis, only this type of phenomenon will be described in-depth.

## 2.2 Small angle scattering (SAS)

Small Angle Scattering (SAS) is an elastic scattering technique, typically used to study the size, shape and orientation of particles in solution. The incoming radiation used to probe the sample in SAS can be light, neutrons or X-rays [64]. In general, in an elastic collision, the total energy (E) is preserved, in other words, the kinetic energy is not converted to other forms and we can express it as reported in equation 2.1

$$E = \hbar\omega_i - \hbar\omega_f \tag{2.1}$$

where $\hbar$ is the Planck constant 6.626069x10$^{-34}$Js, $\omega_i$ and $\omega_f$ are the frequency of the radiation before and after the collision with the scattering object. As both the total energy and the momentum are preserved in elastic scattering, we can then express this as equation 2.2.

$$P = \hbar(k_i - k_f) \tag{2.2}$$

where $k_i$ and $k_f$ are the wave vectors before and after the radiation hits the object. As depicted in figure 2.1, the scattering vector $q$ is quantified as the difference of the final and initial wave vector $(k_f - k_i)$. The magnitude of the scattering vector can be quantified considering that $\mid k \mid = \frac{2\pi}{\lambda}$, where $\lambda$ is the wavelength of the incident light. From the geometry described in 2.1 and from the magnitude of the wave vectors, it is possible to rewrite (2.3) to express $q$ as a function of $\lambda$ and the incident angle of the radiation and where $\theta$ is half of the scattering angle.

$$q = \frac{4\pi \sin\theta}{\lambda} \tag{2.3}$$

If we consider a system of isotropic centrosymmetric particles 1 (our analyte) surrounded by particles 2 (the solvent), the intensity of the scattered radiation arising from this sample is proportional to equation 2.4

$$I = N_P \cdot \Delta\rho^2 \cdot V_P^2 \cdot P(q) \cdot S(q) + B \tag{2.4}$$

where $N_P$ is the number of particles, $V_P$ is the volume of the particle $I_0$ is the intensity, $P(q)$ and $S(q)$ are the form and structure factor respectively, $\Delta\rho$ is the difference in the scattering length densities between the particles and the matrix around this and $B$ is the background contribution. The scattering length density (SLD) is defined in equation 2.5

$$\rho = \frac{\sum_{i=1}^{N} b_i}{V_m} \tag{2.5}$$

where $b_i$ is the scattering length and accounts for the contribution of each i-atom to the scattering and $V_m$ is the molar volume of the molecule. For a general scattering experiment, the scattered intensity is measured at different q values, either by varying the angle $\theta$ or the wavelength $\lambda$

The scattering length, in terms of the physical interaction, describes how strongly the incoming radiation interacts with matter. Due to the different nature of the interactions of neutrons and X-rays with matter, as described in section 2.1, the scattering length is also different for the two cases. In the case of neutrons $b_i$ is randomly distributed along the periodic table. In the case of X-rays, since the interaction arises from the electronic cloud, it increases with increasing atomic number of the atoms involved in the event and is defined as equation 2.6:

$$b_{X-Ray} = Z r_e \tag{2.6}$$

where $Z$ is the atomic number and $r_e$ is the scattering cross section for an electron which is defined as in equation 2.7

$$r_e = \frac{e^2}{4\pi\epsilon_0 m c^2} = 2.8x10^{-5}\mathring{A} \tag{2.7}$$

where $\epsilon_0$ is the vacuum permittivity, $m$ is the mass of an electron and $c$ is the speed of light.

For a typical biological sample, the most common atoms involved in the structure are C, H, O, N, P. Neutron and X-Ray scattering lengths for these atoms are reported in table 2.1.

**Table 2.1** Values of $b_i$ for common elements in biology

| | Scattering Length | |
|---|---|---|
| | Neutrons ($10^{-6}$Å) | X-Rays ($10^{-6}$Å) |
| H | -0.37 | 0.28 |
| D | 6.67 | 0.28 |
| C | 6.65 | 1.69 |
| O | 4.23 | 2.25 |
| N | 9.36 | 1.97 |
| P | 5.13 | 4.23 |

### 2.2.1 Neutron scattering

Neutrons interact and can be scattered by matter in a different way to other scattering events, such as light or X-ray scattering. When an incoming beam hits the sample, neutrons will interact with the nuclei rather than the electronic cloud. Advantages of this technique are:

- Wavelength

  Neutrons are between 0.6 and 20nm in wavelength. This is much smaller than the wavelength of visible light (400-700 nm). The shorter wavelength leads the neutrons to achieve an atomistic resolution, compared to light scattering. [63].

- Low Energy

  An electromagnetic radiation has an energy given by $E = \lambda\nu$ where $\nu$ is expressed as $c/\lambda$. Due to the mass of the electron ($m = 1.674\text{x}10^{-27}$Kg), the kinetic energy can be calculated (equation 2.8).

$$E = \frac{h^2}{2m\lambda^2} = \frac{mv^2}{2} \tag{2.8}$$

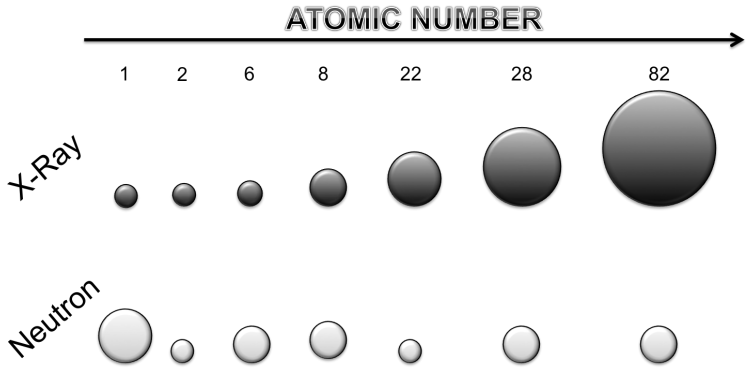


**Figure 2.2** Schematic of scattering lengths for some elements.

Considering $\lambda = 1.8$ nm for a neutron or 0.1 nm for an X-Ray, we can calculate $E$ which is 25 meV or 8.2 keV for neutrons or X-Rays respectively[64]. The great advantage of neutrons, then, is the low energy level of the incoming beam, which does not damage organic and biological samples. In the last few years many research fields and companies have used neutrons to investigate X-ray radiation sensitive samples, such as in food science research [66].

- Labeling

  Isotopic labelling is widely used in several techniques. The signal arising from a sample when compared with the surrounding media is key for any measurement such as NMR or spectroscopy techniques. For a scattering experiment, as shown in equation 2.4, the intensity of the signal is proportional to the square of the difference in SLD between the solvent and the sample. For neutrons the cross section of atoms is isotope-dependent, unlike for X-rays where it is proportional to the atomic number. A schematic representation of this phenomenon is reported in figure 2.2.

  Due to the large difference in the scattering length of hydrogen and deuterium, the contrast variation in neutron scattering experiments is usually done by exchanging the hydrogen with deuterium; this hydrogen can be either in the solvent or within components in the sample. Variation of the contrast allows the highlighting of specific parts of a molecule and to

hide others without modifying the chemical behaviour of the sample, e.g. without having to leave out any of the components or add other labels like fluorescence markers. This is crucial in biology, since it is possible to hide or highlight part of macromolecules just by exchanging hydrogen with deuterium in water, which is omni-present in biological samples and thus is relatively cheap. It is usually assumed assumed that this does not change the properties of the studied sample, e.g. the hydrogen bonding network.

### 2.2.2 X-Ray scattering

X-rays are electro-magnetic waves with a wavelength range between 0.01 and 10 nm [67]. This wave is the result of an electric and magnetic field that propagate perpendicularly to each other. Due to the X-ray-matter interaction, the strength of the interaction of the beam with the sample is congruent with the electron density of the sample, as shown in figure 2.2 There are many advantages to using X-ray techniques such as:

- **Fast** Due to the high flux and energy of the beam, it is possible to acquire a large amount of data in a short time
- **Resolution** Short wavelengths from X-rays have been often used in the last century to investigate the crystal structures of proteins with subatomic resolution.

## 2.3 Small angle neutron scattering (SANS) instruments

In this project SANS data was acquired in central facilities in Grenoble, France (ILL) and Didcot, UK (ISIS). Two SANS instruments were used at each facility, LOQ and SANS2d at ISIS and D11 and D33 at the ILL. The two facilities produce neutrons in different ways, ISIS by spallation arising when a proton beam collides

with a heavy metal target and ILL utilizing a research nuclear reactor. This means that the SANS instruments at both facilities are subtly different, ISIS using polychromatic beams to increase the useful neutron flux and time of flight methods, ILL using (approximately) monochromatic beams. A representation of a monochromatic beam small angle scattering technique is reported in figure 2.3.

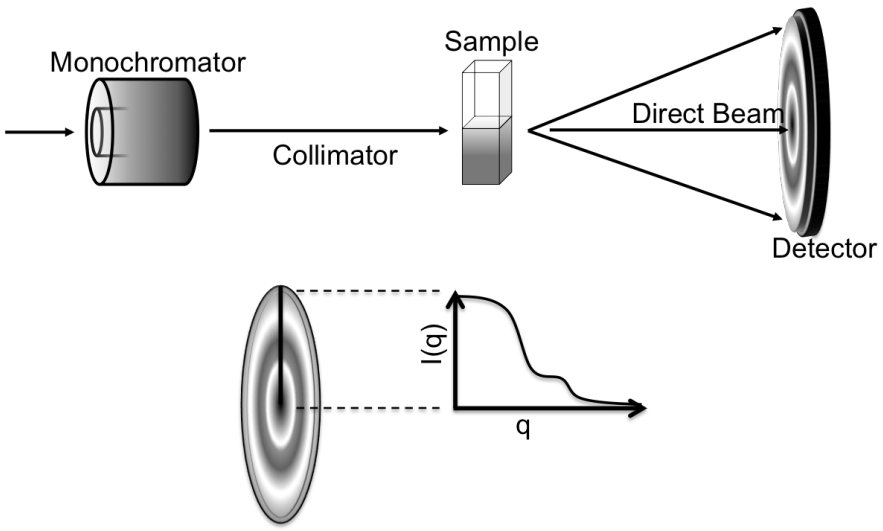


**Figure 2.3** Generic representation of a SAS beamline

LOQ [68] is a time of flight SANS instrument at ISIS. The instrument has a chopper that allows the selection of wavelengths from 2 to 12 Å. At about 11 m from the first chopper is the sample environment thermostatically controlled using a water bath. The sample changer used for experiments has 20 positions available. The sample changer used for the experiments has 20 positions available. Samples are loaded into quartz Hellma cells 1 mm thick and 1cm wide. At a distance of 4m from the sample position is a 64 cm x 64 cm $^3$He-$CF_4$ filled ORDELA detector with a resolution of 5 mm. Calibration of the instrument is performed using a copolymer of 50% perdeuterated/protonated polystyrene, called TK49. In all measurements, the instrumental background and solvent contribution are also collected, as is the incident wavelength spectrum of neutrons incident on the sample and the intensity of the transmitted beam with wavelength. All of the above are used to reduce the data to absolute intensities with respect to scattering

angle, using Mantid [69], an open source software.

D11 [70] is a SANS instrument based in Grenoble at the Institute Laue Langevin (France). The instrument is placed about 100 m from the nuclear reactor. Neutrons are beforehand moderated and the energy is selected by a monochromator (ASTRIUM). Neutrons are selected through a velocity selector that consists in a helical path, allowing the forward transmission of neutrons with a distribution of 9% around the mean wavelength. The wavelength for the experiments carried out on D11 was set at 6 Å. Neutrons arising from the monochromator are collimated using movable mirrors. The sample zone is equipped with a thermostated sample rack that can hold 20 samples. The detector is situated in a vacuum vessel after the sample environment and can move to any sample-detector distance between 1.2 and 39 meters. For our purposes, three sample-detector distances are necessary to cover the entire q-range used for our data interpretation: 1.204 m, 6.994 m and 13.495 m. As for LOQ, samples are loaded into quartz Hellma cells 1 mm thick and 1cm wide. To calibrate the instrument to an absolute intensity, water is run as a standard. Medium and high angle scattering patterns are collected for every sample. The low angle is collected only for those samples that appear aggregated (cloudy via visual inspection) or which contained large structures from preliminary analysis of the scattering patterns. Scattering patterns from different detectors are merged before being analysed. To subtract the background properly, every buffer is run for each angle and merged. Data are reduced using the software LAMP [71].

SANS2d [72] is a time of flight SANS instrument based at Target Station 2 (TS2) in ISIS. SANS2d has two movable detectors. The sample environment is placed at 17 m from the chopper. Two different types of experiment are performed. The sample area is equipped with a rack that can accommodate up to 40 samples in 1mm thick quartz Hellma cells for the experiments using a sample changer. The environment is kept at constant temperature using a water bath. A Bio-Logic SFM-400 stopped flow equipment, (which is further explained in section 2.6.3 below)is also used to follow the kinetic processes of the polymer interacting

with lipid vesicles. Two 0.96 m square $^3$He multiwire proportional counters (Ordela21000N) are placed after the sample area and can be moved from 3.5 to 12.5 m from the sample. The higher angle detector of the two can be moved 1.3 m sideways and rotated to be perpendicular to the scattered beam from the sample. Both detectors are displaced 0.15 m vertically relating to the transmitted (direct or unscattered) beam.

D33 [73] is a small angle neutron scattering instrument at ILL that can work either in TOF or monochromatic mode. For our purposes, only the monochromatic mode has been used. The wavelength of the neutrons (6Å) is selected by a velocity selector, as for D11. The detector, a $^3$He multi detector, is placed in a 20 m evacuated tube. It can move along the tube to modulate the Q-range. For our experiments the detector is moved to positions of 1.2 m and 12 m from the sample. Two sample environments are used on D33: a stopped flow device (Bio-Logic SFM-400) and a sample changer. Background is subtracted and the data are reduced using LAMP [71].

## 2.4 Small angle X-Ray scattering (SAXS) instrument

SAXS data were collected in Diamond, RAL, Didcot, the instruments used being B21 and I22. A schematic representation of I22 is reported in figure 2.4

I22 is a SAXS instrument built at the Diamond Light Source. The sample area is adaptable to allow a wide range of experimental set ups. For experimental data shown in chapter 3 and 4 from I22, 1.5 mm wide quartz capillaries are used. During the experiment the temperature is not controlled within the sample changer but the room is thermostatically controlled at 22°C. The incoming beam has a wavelength of 1 Å. The beam pipe and the wedge shaped nosecone can be moved in order to minimise the pathlength of the X-ray beam through air. The sample-detector distance used was 4.7m. Data reduction is carried out using DAWN [74].

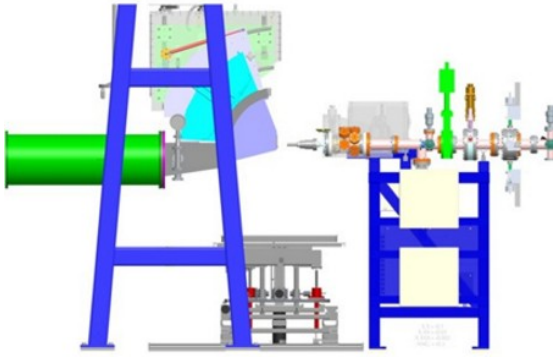

**Figure 2.4** Schematic of I22 beamline in Diamond. Picture reprinted with permission from [2]

B21 is a SAXS instrument specifically built at Diamond Light Source for BioSAXS (biological SAXS). The scattering vector, $q$, is varied between 0.015 and 0.3 Å$^{-}$1. TThe wavelength of the incoming beam is fixed at 1 Å. A Pilatus 2M detector at 4.15 m from the sample area is also used in a fixed position. The X-ray scattering experiment is performed using robotic sample handing equipment. A 96 well plate is loaded with samples and placed in the hutch. A sample handing robot loads the sample into a 1 mm quartz capillary. Before each sample is loaded, the capillary is washed with buffer, ethanol, buffer and then filled with the sample. The exposure time is 1 min collected in 1 s frames to check for beam damage. All data are acquired at 25 °C. Data is reduced to I(q) vs q using the DAWN [74] software package . Silver behenate and collagen are used to calibrate both of the SAXS instruments.

## 2.5 X-Ray and neutron reflectivity

Reflectivity is widely used in industry and academia to study the surface and interface properties of thin layers. In this project liquid-air interface reflectivity was used to probe the penetration of the polymer into a lipid monoalyer. These experiments are described in chapter 5.

The way the incoming radiaiton interacts with matter is the same as has been discussed for SAXS and SANS in section 2.1. In neutron and X-ray reflectivity

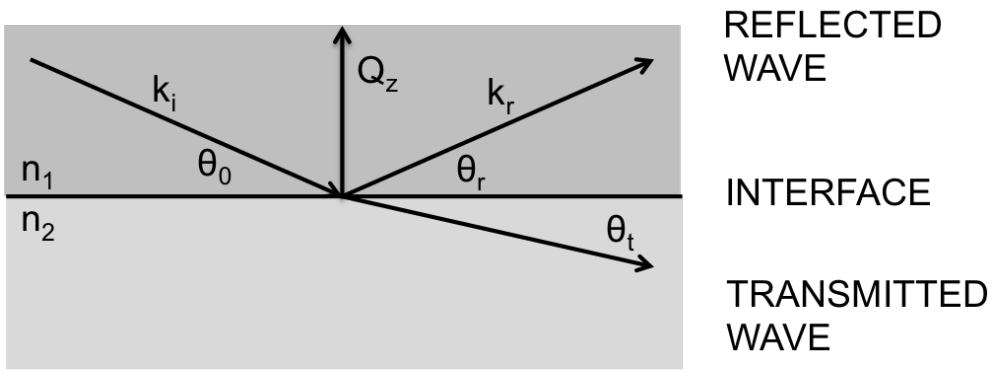


**Figure 2.5** Schematic of a reflectivity event

(NR and XRR, respectively) the probing beam is almost parallel to the surface. A schematic of a reflectivity event is represented in figure 2.5.
In terms of geometry, the momentum transfer for this event is the same calculated for a scattering event in equation 2.3:

$$Q = \frac{4\pi \sin \Theta}{\lambda}$$

Similar to SAS, the principle laws for the technique apply no matter what kind of radiation is used to probe the sample. In general the refractive index of a material has a real and a complex part (equation 2.9)

$$n = 1 - \delta + i\beta \tag{2.9}$$

where $\delta$ is the real part of the refractive index and is defined as:

$$\delta = \frac{\lambda^2}{2\pi}\rho \tag{2.10}$$

where $\lambda$ is the wavelength of the incoming wave and $\rho$ is the scattering length density for either X-rays or neutrons. $\beta$ is the absorption coefficient and is usually neglected because it is significantly smaller than $\delta$, of the order of $10^{-5}$-$10^{-6}$. The incident and reflected beams are named $k_i$ and $k_r$ respectively. Snell's law (equation 2.11) states that when an incoming wave hits a surface the radiation can undergo either transmission or reflection. The angle at which transmission occurs

depends on the refractive index of the two materials where the wave propagates:

$$n = \frac{n_1 \Theta_0}{n_2 \Theta_t} = \frac{n_1 \cos k_i}{n_2 \cos k_r} \tag{2.11}$$

where $\Theta_0$ is the incident angle and $\Theta_t$ is the transmitted angle formed by the neutron or X-ray beam to the surface normal and $n_1$ and $n_2$ the respective refractive indices for the subphase and the sample.
Below a certain angle the so-called critical edge ($\Theta_c$), the incoming beam is totally reflected. Equation 2.11 can be rearranged considering the $\Theta_0 = \Theta_c$ and $\Theta_t = 0.0$. Combining equation 2.9 and 2.11 we can define the critical edge as:

$$\Theta_c = \lambda \sqrt{\frac{\Delta\rho}{\pi}} \tag{2.12}$$

Therefore,the position of the critical angle provides information regarding the composition of the subphase. Changing the angle of the incident beam then allows the study of the surface in terms of its scattering length density as a function of the distance from the interface. When neutrons or X-rays hit the surface at an angle above the critical edge, the reflectivity is given by Fresnel's equation (2.13)

$$R_{Fresnel}(Q) = \left| \frac{Q_0 - Q_1}{Q_0 + Q_1} \right|^2 \tag{2.13}$$

where $Q$ is defined in equation 2.3 and $Q_1 = \sqrt{Q^2 - Q_c^2}$. This equation is derived as shown in references [75, 76] and does not account for imperfections within the surface, e.g. the roughness of the surface results in a decreased specular reflection due to diffuse scattering events rather than reflection. The nature of the surface is taken into account by adding an exponential decay to the Fresnel equation (equation 2.14):

$$R = \frac{Q_0 - Q_1}{Q_0 + Q_1} e^{-Q_0 Q_1 \sigma^2} \tag{2.14}$$

A schematic of a neutron reflectometer is shown in figure 2.6

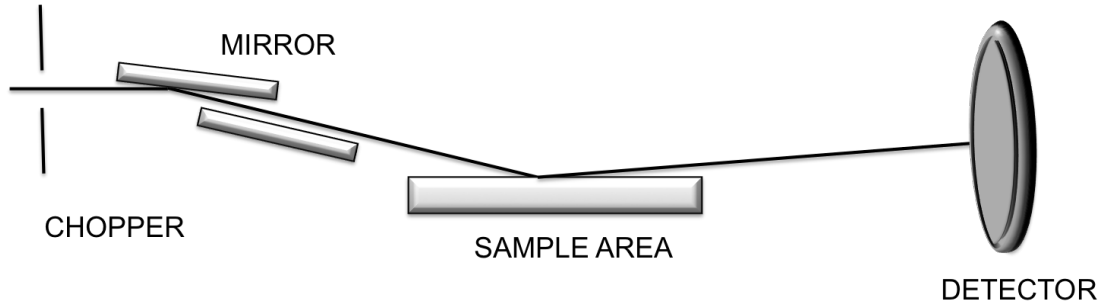


**Figure 2.6** Schematic of a reflectometer.

FIGARO (ILL) was used to carry out the NR liquid-air reflectivity experiment, whereas X-ray reflectrometry was performed on I07 (Diamond Light Source) . A brief description of these two instruments is given below.

- **Figaro** [77] is a neutron reflectometer at the ILL. The wavelengths of neutrons are selected using a chopper and can change between 2 and 30 Å. Neutrons are then collimated and conducted to the sample changer. In our case a 40 mL Langmuir trough is used. This is situated on a anti-vibration table to avoid any interference during the experiment. A laser is used to align the trough and to check the volume of the liquid in the trough as described in section 2.10. Data is background subtracted and reduced to reflectivity against Q, using Cosmos.

- **I07** [78] is an X-Ray reflectometer at Diamond Light Source. The energy of the incoming beam is 12.5 keV. Multiple aligned teflon adsorption troughs are used for the experiment. Similar to Figaro, troughs are placed on an anti-vibration table at ambient temperature (22°C). Data are collected with a Q-range from to 0.09 to 0.6 $Å^{-1}$.

## 2.6 SAS and reflectivity data analysis

As discussed in section 2.2, contrast variation has a key role in neutron techniques [79]. In order to fit scattering and reflectivity patterns, the scattering length densities of the used materials were either calculated or taken from the literature.

### 2.6.1 Polymer solution scattering analysis

The SLDs (equation 2.5) for the polymers used were calculated using the NIST online calculator apart from SLDs for and , which were calculated by running a solvent contrast variation experiment to determine the match point. In order to do that, a 1.5% wt polymer solution was made up in different contrasts: 100% mol $D_2O$, 75% mol $D_2O$, 50% mol $D_2O$ and 35% mol $D_2O$. The intensity was extrapolated to Q=0 and was plotted against percentage of $D_2O$ (figure 2.7). A linear fit to the data was done and the SLD for the two polymers were obtained where this line crossed $I_0$=0, which is called the match point. The match point indicate that both of the polymers have about same SLD within the error which is 1.96x$10^{-6}$ Å$^{-2}$.

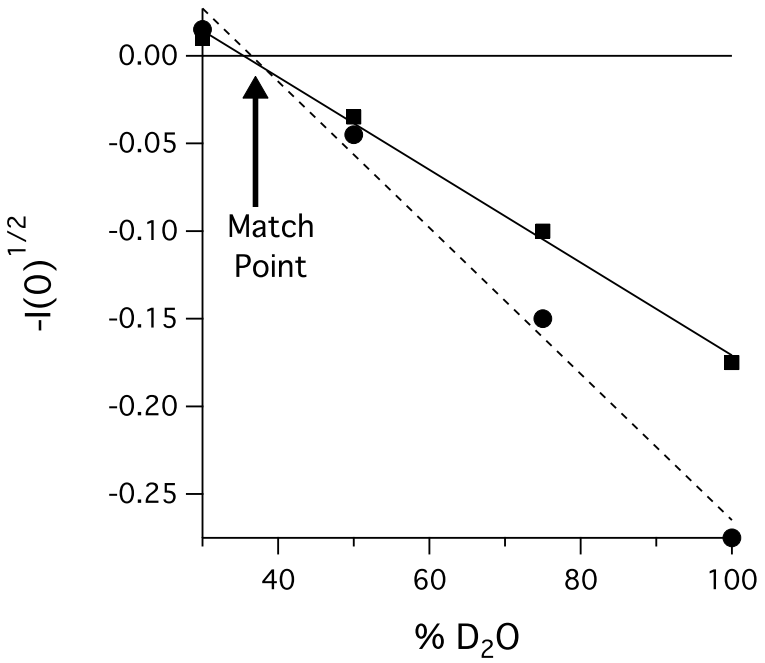


**Figure 2.7** Solvent match point data for $SMI_{1000}$ and $SMI_{2000}$.

Analysis of the SAXS patterns for the 1.5% solutions of the polymers alone revealed a sphere shape for the polymers at low salt concentrations, and could be fitted with a spherical form factor, whereas an elongated shape was found for higher salt concentration. The latter data were fitted with an ellipsoidal shape. The two models are described below:

- **Polydisperse sphere**

  The model, schematically represented in figure 2.8, calculates the form factor, P(q), for a spherical particle with uniform scattering length density. The form factor is normalized to the particle volume as shown in equation 2.15 described below. No structure factor is included in this model, as the data were collected within the dilute (non-interacting) regime. The model uses a Schultz distribution for the polydispersity of the radius.

$$P(q) = \frac{scale}{V}\left[\frac{3V(\Delta\rho) - qr\cos(qr)}{(qr)^2}\right]^2 + bkg \tag{2.15}$$

| Parameters | Values |
|---|---|
| Volume Fraction | 0.01 |
| Mean Radius (Å) | 60 |
| PDI (sig/ave) | 0.2 |
| SLD sphere ($Å^{-2}$) | $1.96x10^{-6}$ |
| SLD sphere ($Å^{-2}$) | $6.3x10^{-6}$ |
| Inch. Bkg | 0.01 |

**Table 2.2** Typical values for sphere model

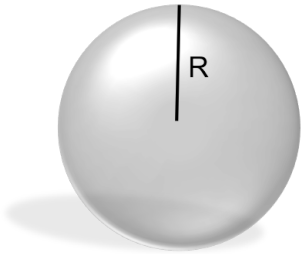


**Figure 2.8** Sphere model

- **Uniform Ellipsoid**

  The form factor for this model is calculated for a monodisperse ellipsoid with uniform SLD. This is normalised to the particle volume and integrated over all possible orientations of the particles as above. No structure factor is included in this model. The form factor is calculated as reported in equation 2.16

$$P(q) = \frac{Scale}{V_{ell}}(\Delta\rho)^2 \int_0^1 f^2[qr_b(1 + x^2(v^2 - 1))^{1/2}]dx + bkg \tag{2.16}$$

  where:

$$f(z) = 3V_{ell}\frac{(\sin z - z\cos z)}{z^3} \tag{2.17}$$

$$V_{ell} = \frac{4\pi}{3} r_a r_b^2 \tag{2.18}$$

$$v = \frac{r_a}{r_b} \tag{2.19}$$

A schematic representation of the model used is reported in figure 2.9

| Parameters | Values |
|---|---|
| Scale | 0.01 |
| $R_a$ (Å) | 60 |
| $R_b$ (Å) | 60 |
| SLD ellipsoid (Å$^{-2}$) | 1.96x10$^{-6}$ |
| SLD solvent (Å$^{-2}$) | 6.3x10$^{-6}$ |
| Inch. Bkg | 0.01 |

**Table 2.3** Ellipsoid model parameters

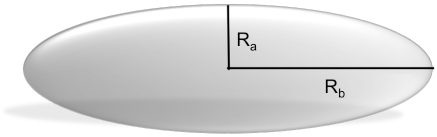


**Figure 2.9** Graphic of ellipsoid model

- **Polymer micelle**

  This model calculates a form factor for a micelle with a spherical core and a Gaussian coil representing the polymer chains on the surface of the micelle. It is usually applied for describing the micelles formed by block copolymers. This model calculates the form factor for an inner sphere of radius $r$ which makes the core and for Gaussian coil chains around of this sphere of additional radius $R_g$. A schematic of the model is reported in figure 2.10. It is assumed that the chains forming the corona do not penetrate into the core.

- **Fuzzy sphere**

  This model was used to fit zwitterionic copolymers in solution. It calculates the form factor for a sphere and convolutes this function with a Gaussian gradual drop-off in the scattering intensity at the edge of the sphere, i.e. a fuzzy layer.

$$P(q) = \frac{3[\sin(qR) - qR\cos(qr)]}{qR^3} e^{\frac{-\sigma_{surf} q^2}{2}} \tag{2.20}$$

| Parameters | Values |
|---|---|
| Scale | 0.01 |
| Radius $r$ (Å) | 40 |
| $R_g$ (Å) | 20 |
| SLD core (Å$^{-2}$) | 1.4x10$^{-6}$ |
| SLD corona (Å$^{-2}$) | 2x10$^{-6}$ |
| Inch. Bkg | 0.01 |

**Table 2.4** Polymer micelle parameters

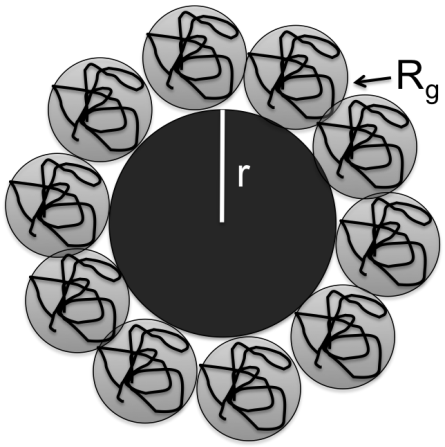


**Figure 2.10** Graphic of polymer micelle

### 2.6.2 Nanodiscs analysis

The scientific community, after several models were initially proposed [39, 80–83] for protein stabilised phospholipid nanodiscs, adopted a commonly accepted theory of a discoidal structure of the nanodiscs. Therefore here we have used the same model for polymer stabilised nanodiscs based on their apparently similar shape from previous TEM and SANS studies [84]. Data from small angle scattering experiments were fitted using a concentric cylinder model which is graphically shown in figure 2.11. This model is made of an inner cylinder divided into 3 parts:

- Top and Bottom: those parts represent the head of the phospholipid
- Central: This part represents phospholipid tails in the bilayer disc

The external hollow cylinder models the polymer belt that surrounds the lipid tails (external dark grey cylinder in figure 2.11). In order to account for polydispersity in the model, the radius of the inner cylinder is convoluted with a Schultz distribution. This model has 15 parameters reported in table 2.5. The mean radius represents the radius of the inner cylinder which corresponds to the phospholipid bilayer. This is represented in figure 2.11 as A. The core length is represented in figure 2.11 as C and is the length of the phospholipid tails. The rim thickness is the thickness of the polymer surrounding the phospholipid tails and is represented as B. The SLD of the core represents the scattering length density

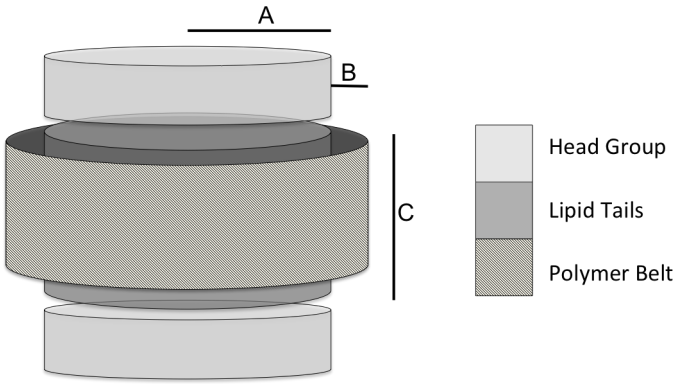


**Figure 2.11** Schematic representaion of the polydisperse bicelle model used to fit SAS data [3]

of the tails (showed in figure 2.11with the inner dark grey cylinder). Due to the large number of parameters, the SLD of the polymer, the lipid heads and lipid tails, dielectric constant [85], temperature, monovalent salt concentration, and the thickness of the lipid heads and tails were calculated or found from literature and usually fixed during fitting. Exceptions are noted in the description of the model in the following chapters. The salt concentration was set to the concentration of the buffer (50 mM) plus that of the added NaCl in each case. As an example, in a 50 mM NaCl buffer solution, the salt strength is considered to be 0.1M. The water content in the rim and in the lipid head regions was used for fitting purposes rather than the SLD. Thus for the polymer rim and lipid heads this value had to conform to the scattering from several contrasts rather than being evaluated separately for each contrast. The structure factor was calculated using a Hayter-Penfold charged sphere approximation [86]. Using this routine, the software calculates the structure factor for charged particles in a dielectric medium by assuming the discs are tumbling in solution so that a spherical approximation can be used.

**Table 2.5** Parameters and typical values used to fit the model reported in figure 2.11

| Parameters | Values |
|---|---|
| Volume Fraction | 0.01 |
| Mean Radius (Å) | 60 |
| PDI (sig/ave) | 0.2 |
| Core Length (Å) | 28 |
| Rim Thickness (Å) | 10 |
| Head Thickness (Å) | 8 |
| SLD core ($Å^{-2}$) | $7.2x10^{-6}$ |
| mol frac $_{H_2O}$ in face | 0.57 |
| mol frac $_{H_2O}$ in belt | 0.5 |
| SLD solvent ($Å^{-2}$) | $9.46x10^{-6}$ |
| Charge | 39 |
| Conc. Monovalent Salt (mol/L) | 0.25 |
| Dielectric constant | 78 |
| Temperatuere (K) | 298 |
| Background ($cm^{-}1$) | 0.01 |

### 2.6.3 Stopped flow analysis

Stopped flow experiments were performed on D33 and SANS2d. A general experimental set up is showed in figure 2.12. The stopped flow apparatus was a commercially produced unit made by BIO-LOGIC, model SFM-400, modified to hold a quartz cuvette for SANS measurements.

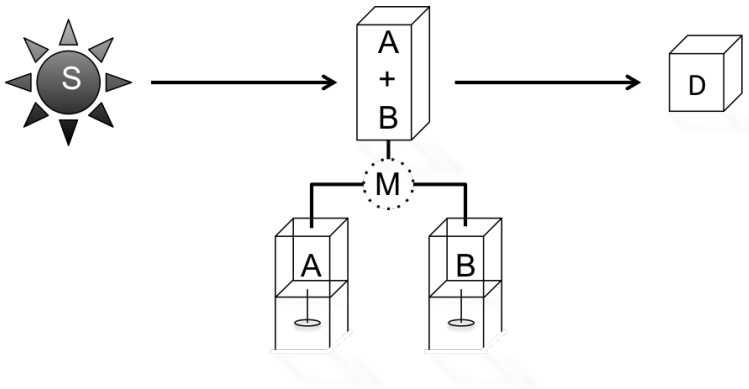


**Figure 2.12** Schematic of a stopped flow set up

Stopped flow was also used for experiments following changes in the fluorescence of tagged lipid vesicles interacting with the polymer.

In figure 2.12 ia schematic of the stopped flow setup used for both fluorescence and neutron experiments is shown. A and B are the cuvettes where the sample solutions are loaded. The desired solutions are pushed from the reservoirs, respectively, into the mixer chamber M where they are mixed before passing into the measurement cuvette. The incoming radiation source from (S) hits the mixed sample in the cuvette (A+B) and goes to the detector (D). In order to fit the scattering patterns of the DMPC vesicles formed in the stopped flow experiment, the data were fitted using a 3 shell polydisperse hollow sphere model. A schematic of the model and the fitting parameters are reported in figure 2.13 and table 2.6 respectively. The vesicle model was summed with a disc model and most of the parameters were held constant. The ratio of the two models were analysed to determine how the concentration of both species changed with time.

| Parameters | Values |
|---|---|
| Scale | 0.01 |
| Core Radius(Å) | 60 |
| Core PDI (sig/ave) | 0.3 |
| Core SLD ($Å^{-2}$) | $6.3x10^{-6}$ |
| Head Thick(Å) | 10 |
| Head SLD ($Å^{-2}$) | $-4x10^{-7}$ |
| Tail Thick(Å) | 28 |
| Tail SLD ($Å^{-2}$) | $7.2x10^{-6}$ |
| Solv. SLD ($Å^{-2}$) | $6.3x10^{-6}$ |
| Bckg ($cm^{-1}$) | 0.001 |

**Table 2.6** Pathree shell model parameters

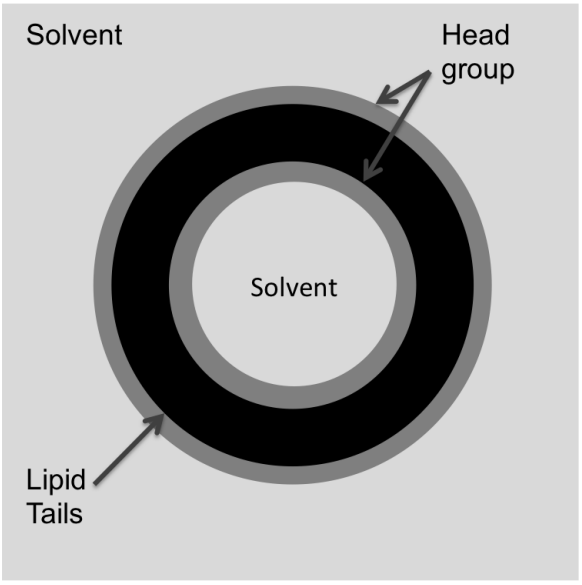


**Figure 2.13** Three shell modell scheme

### 2.6.4 Reflectivity analysis

Reflectivity data were analysed using either MOTOFIT [87] by the candidate or RasCAL [88] with the assistance of Dr Stephen Roser as will be explained in the next paragraphs.

#### MOTOFIT

The Motofit software is developed by Dr Andrew Nelson and implemented in IGOR Pro. In order to fit reflectivity data this software uses the Abeles matrix method which calculates the reflection of a source from a multilayer surface. Each layer is approximated to be smooth and with a characteristic SLD. The mathematical development of this method is given in references [75, 87, 89].
With this method implemented into Igor Pro it is possible to model the system by subdividing it into several layers, each of which has an associated surface roughness, SLD, thickness and a hydration percentage. The hydration percentage is implemented into the model and calculated as reported in equation 2.21 For our purpose the lipid monolayer has been divided in two layers: one models the head groups, whereas the other models the tails. This is a good approximation due to the pronounced difference in the SLDs for the head and tails (1.6x$10^{-5}$ Å$^{-2}$ and 8 x$10^{-5}$ Å$^{-2}$ respectively). The SLD of the layer is calculated as a linear combination of the SLD of the species itself and the SLD of the solvent used that penetrates into the layer:

$$\rho_{layer} = \rho_{dry} x_{dry} + \rho_{solv} x_{solv} \tag{2.21}$$

where $\rho_{layer}$ is the effective SLD of the layer, $\rho_{dry}$ is the SLD of the "dry" layer and $\rho_{solv}$ is the SLD of the solvent used. x is the mole fraction for each component.

#### RasCAL

RasCAL is a software developed for the fitting of reflectivity data from either X-ray and neutrons. It is implemented in Matlab and fits reflectivity patterns using

a SLD distribution defined by a sum of Gaussians. The model implemented to fit the data used the scattering length and the molecular volume for each component of the layer. Similar to MOTOFIT, the hydration of the layer was included in the model along with the tilt of the lipid tails in the monolayer.

## 2.7 Dynamic light scattering (DLS)

Dynamic Light Scattering (DLS) is commonly used to detect the particle size of sub-micron particles in a solution [90]. Due to its non-invasive nature, this technique is often used to analyse biological samples and inorganic nanoparticles [91–93]. In addition, the absolute scattered intensity (averaged over time or frequency) provides information about the mass or molecular weight of the scattering objects [94].

When the radiation hits the sample it is scattered from the particles in the solution and goes to the detector. Fluctuations in the scattered light signal are due to the movements of particles in the medium [95] . In order to analyse the data, it is assumed that the particles follow a Brownian motion movement [96], also called a Random walk . The second assumption for the data analysis is that the particles in solution behave like hard spheres. A typical set up for a DLS experiment is reported in figure 2.14. A laser produces the incoming light that hits the sample. The light is scattered and is collected at 173° by a photon counting device. The detector sends the signal to a correlator device which returns a correlation function by which decay is related to particle size; the smaller the size of the particles, the higher the decay rate (figure 2.14-b).

In general an autocorrelation function is defined as the correlation of a signal with itself, in other words it is the similarity between 2 functions delayed in time with each other. For a short time, it is assumed the function is highly correlated, but it will not be correlated for long range of time. The correlation function [97] (equation 2.22) is described with an exponential decay for monodispersed particles is undergoing Brownian motion, which depends on the diffusion coefficient as

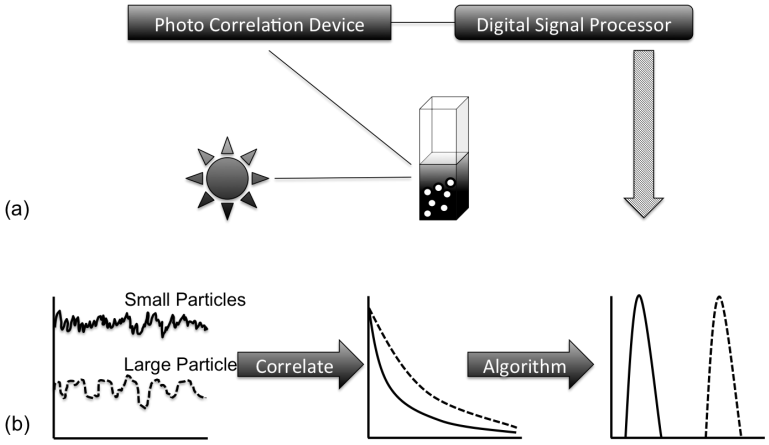


**Figure 2.14** Schematic of DLS setup

shown in equation 2.23

$$G_2(\tau) = \int I(t)I(t+\tau) \tag{2.22}$$

where

$$\tau^* = \frac{1}{2dq^2} \tag{2.23}$$

When a DLS measurement is performed it measures the translational coefficient diffusion cofficient of the particles. This, using the Stokes - Einstein equation, is related to the particle diameter as shown in equation 2.24 [98]:

$$D_0 = \frac{kt}{3\pi\eta d} \tag{2.24}$$

where $D_0$ is the diffusion coefficient, $T$ is the temperature, $\eta$ is the viscosity of the solution and $d$ is the particle hydrodynamic diameter. This is bigger than the actual diameter of the particle due to the hydration shell around the particle (figure 2.15).

The hydration shell is influenced by factors such as the ionic strength of the solvent or the chemistry of the polymer on the surface of the particle. Figure 2.15 shows how the hydrodynamic size of the particle changes with ionic strength and with different surface environment. Measurements were undertaken on a

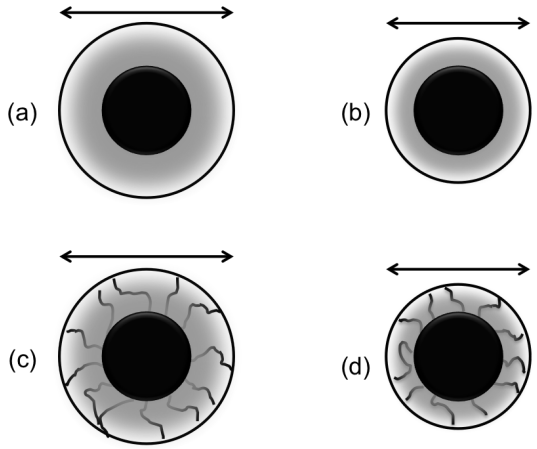


**Figure 2.15** Schematic of hydrodynamic diameter changing with electronic double layer (a) and (b) and with the nature of the surface (b) and (c)

Malvern Zetasizer Nano ZS. The incoming radiation from a He-Ne laser has a wavelength of 633 nm and a detector that operates at an angle of 173° . The software used to collect and analyse the data was the Zetasaizer Software version 7.11 from Malvern. 50 $\mu$L of each sample was measured in disposable polystyrene cuvettes with a pathlength of 10 mm.

## 2.8 Nuclear magnetic resonance (NMR)

This technique uses the electromagnetic radiation absorbed or emitted from the system under investigation when this is placed in an external magnetic field. Since the intensity (I) of the radiation absorbed depends on the spin quantum number ($I$) of the atom present (equation 2.25), a prerequisite to be able to study a sample using NMR is that it must have a nuclear spin, this means that the nuclei studied have either odd numbers of protons or odd numbers of neutrons.

$$I = \frac{h}{2\pi}\sqrt{I(I+1)} \tag{2.25}$$

Since nuclei possess electric charge as well, they also produce a magnetic moment vector $\mu$ (equation 2.26)

$$\mu = g_N \beta_N I \tag{2.26}$$

where $g_N$ is a dimensionless constant and $\beta_N$ is the so-called nuclear magneton which is a constant equal to 5.051x10$^{-27}$J/T. When there is no magnetic field applied, the nuclear spins are randomly distributed in space and possess the same energy. When a magnetic field is applied, this condition is lost and an energy splitting in the levels occurs as shown in figure 2.16.

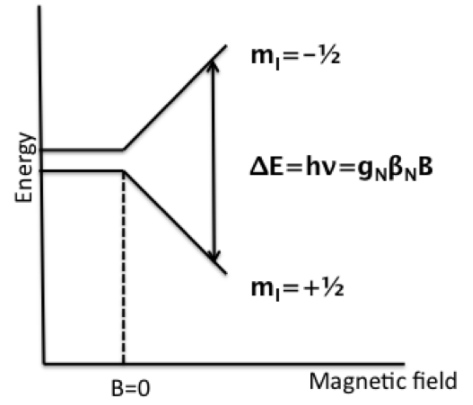


**Figure 2.16** Splitting of the energy levels of the nuclei when they are exposed to a magnetic field

In a molecule nuclei are shielded by the electrons orbiting around them. The

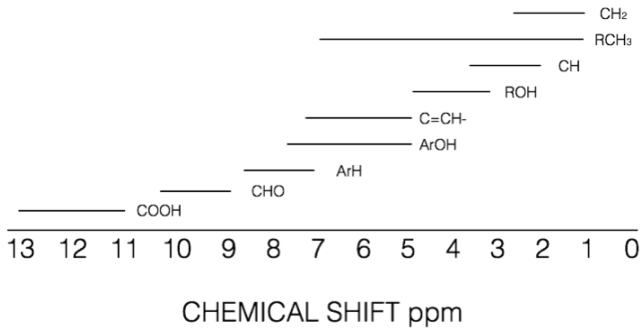


**Figure 2.17** Common shifts for protons in $^1$H NMR

moving electric charge of the electrons produces a magnetic field opposed to the magnetic field applied. Then the effective magnetic field $B_{eff}$ is:(equation 2.27)

$$B_{eff} = B_0(1 - \sigma) \tag{2.27}$$

where $\sigma$ is the chemical shift. The energy gap due to the energy spitting $\Delta E$ will depend on $B_{eff}$ (equation 2.28)

$$\Delta E = g_N \beta_N B_0(1 - \sigma) \tag{2.28}$$

In order to make the measurement independent from the magnetic field used, a standard is used to calibrate the instrument. For $^1H$ NMR tetramethylsilane (TMS) is typically used. The value arising from comparison of the unknown species investigated to the signal from TMS leads to a dimensionless value, the so-called chemical shift $\delta$ (equation 2.29)

$$\delta = (\delta_{TMS} - \sigma) \cdot 10^{-6} \tag{2.29}$$

The most common chemical shifts relative to TMS for protons in organic functional groups are reported in figure 2.17.

In this work $^1$H NMR was used to characterize the monomer conversion and the ratio of styrene to maleic anhydride in polymers synthesised in the project. Samples were made up by dissolving the polymer powders in d-acetone with a concentration of 15mg/mL. Samples were run on a Bruker 300 MHz Avance NMR

spectrometer.

## 2.9 Size exclusion chromatography

Size exclusion chromatography, as the name suggests, separates the components of a mixture by their size [99]. The experiment can be summarized by 3 components:

- Mobile phase
- Stationary phase
- Sample

Depending on the mobile phase chosen for the experiment, the technique changes name: gel permeation chromatography (GPC) for organic solvent or gel filtration chromatography (GFC) for aqueous solutions. GPC is more often used to study polymeric molecular weight distributions, while GFC is used more for the separation of structures soluble in aqueous solutions, such as membrane proteins or biological systems. The first eluted particles are the biggest and these are followed by the smaller. This because the bigger particles cannot get into the pores in the stationary phase, in contrast the smaller particles spend more time in the pores with the result that they have an increased elution time. A schematic representation of this technique is reported in figure 2.18

In GPC or GFC experiments, the stationary phase is equilibrated with the mobile phase, which fills the pores in the column. The sample is then injected into the column and, from a previous calibration, from the elution time, the molecular weight of the polymer can be calculated. Unless the unknown polymer is the same as the polymer used for the calibration, the GPC analysis of molecular weight is a relative measurement. Correct choice of the solvent is crucial to achieve a meaningful result. In general, the solvent should not itself interact with the column, should be able to dissolve the sample and should not lead to an interaction between the sample and the column. If the sample is not soluble in a solvent, it is possible to increase the temperature to help it dissolve. During

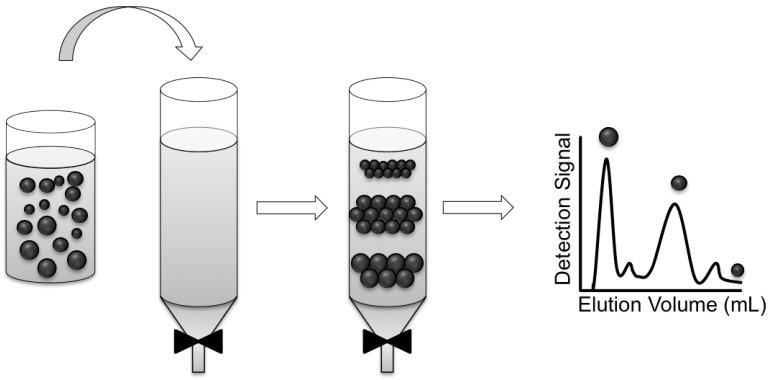


**Figure 2.18** Schematic of size exclusion chomatography apparatus

the measurement many factors can influence the analysis: the temperature, pH, particle size, particle size distribution, flow rate and viscosity either of the sample or the buffer. When the sample is eluted, an instrument to follow the elution of the sample is needed.

In this work, SMA was synthesized and characterised by GPC. The instrument used was a 1260 GPC/SEC MDS from Agilent. The separation was done using two columns PL HFIPgel 300x7.5 mm with a guard column PL HFIPgel 50x7.5 mm. The mobile phase is GPC-grade THF flowing at 1 mL/min. The detection was done using a differential refractive index detector. The columns and the detectors are maintained at 35°C. The column calibration is done using a set of polystyrene samples of known molecular weight. Even though the standard is not the same as the polymer analysed, polystyrene standards are often reported in literature for the analysis of the molecular weight of poly(styrene-co-maleic anhydride) co-polymers [100, 101]. Most of the time the detection instrument associated with the GPC instrument is a spectrophotometer.

Gel Filtration Chromatography was also used to purify nanodiscs from the excess of polymer. The instrument used was a GE health care AKTAprime plus, the column used was a Superdex 10/300. The instrument is equipped with an automated fraction collector. The sample was injected using a 5mL loop. UV-Vis detection at 254 nm allowed the identification of aggregates containing styrene. To ensure the fractions contained similar sized aggregates, fractions were col-

lected and analysed with DLS prior being mixed together and concentrated. The final concentration of the sample was detected with UV-vis. Due to the low concentration of the solution after purification through the column, the sample was centrifuged using a spin concentrator (MW cut off 10KDa). When used for SANS experiments, the sample was dialysed against the desired buffer. The concentration of the polymer was estimated afterwards by UV-Vis. An UV-spectrum is acquired before the gel filtration process. After gel filtration values for absorbance were considered acceptable if they had a value within 1/3 of the initial value.

## 2.10 Surface tension and Langmuir trough

Surface tension is the phenomenon that arises due to cohesive forces among molecules in a solution. Molecules at the interface will bind more strongly with each other due to the lack of molecules surrounding them. This stronger interaction creates at the interface a sort of film, the strength of which is measured in mN/m [102]. When a species is at the interface the cohesion between interfacial molecules changes. In this project, surface tension measurements were undertaken to study the hydrophobicity of the copolymer in solution using the Du Noüy method [103, 104] or a Wilhelmy plate [105]. In this experimental set up a ring is immersed in the solution. The force measured is the force that the apparatus needs to lift the immersed ring through the surface. Equation 2.30 shows how this force is related to the surface tension.

$$\gamma = \frac{F}{2\pi(r_i + r_a)} \tag{2.30}$$

where $F$ is the force in mN, $r_i$ and $r_a$ are the inner and outer radius of the ring and $\gamma$ is the surface tension in mN/m. A schematic representation of the apparatus is reported in figure 2.19.

For the measurement, a 40 mL vessel was used. Since the measurement is sensitive to any impurity, both the vessel and the ring were washed with water and ethanol and then flamed to remove any organic impurity. This procedure was

done twice. The surface tension of water was then run as a standard. In the case of disagreement between the values obtained and literature the cleaning procedure was repeated.

Surface tension is related to surface pressure as described in equation 2.31

$$\Pi = \gamma_0 - \gamma \tag{2.31}$$

where $\gamma_0$ is the surface tension of the pure subphase and $\gamma$ is the surface tension of the interface when the analyte is spread at or has diffused to the interface. This is usually done using the Wilhelmy plate [105]. In this project a Langmuir trough and Wilhelmy plate were used to study the diffusion of the polymer to the interface under a lipid monolayer. The insoluble lipid monolayer was spread on the surface of the trough from a 0.5 mg/mL solution in chloroform and the polymer solution injected underneath. (See chapter 5 section 5.3 for details).

In this project, surface tension measurements with use of a Du Nouy Ring were undertaken on on an Attension Force Tensiometer Sigma 700/701. The Langmuir trough used was a NIMA technology trough type 611.

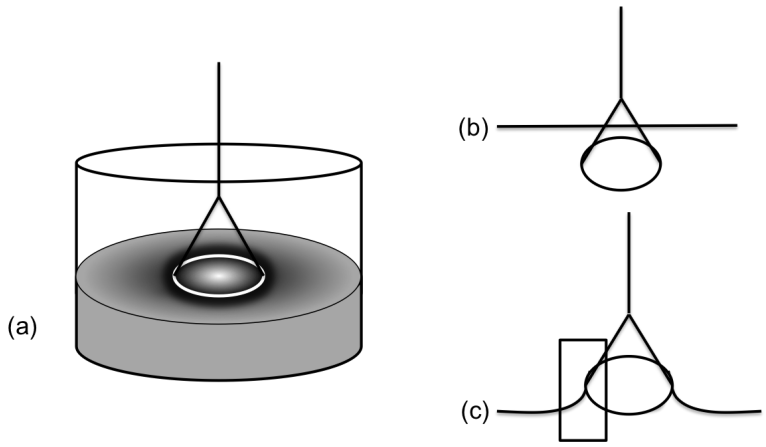


**Figure 2.19** Schematic of a surface tension apparatus

## 2.11 Fourier transform infrared spectroscopy

Fourier Transform Infrared Spectroscopy (FTIR) is a spectroscopic technique that uses light that has wavenumbers with an energy between 4000 and 400 $cm^{-1}$. The incoming radiation is absorbed by the particles and promotes transitions in the vibrational energetic level [106]. The wavenumber is related to the wavelength of the radiation as shown in equation 2.32.

$$\tilde{\nu} = \frac{1}{\lambda} \tag{2.32}$$

The incoming radiation interacts with the dipole moment of the molecule which is connected to the moieties in the organic molecules and does not change, apart from a slight shift occurring due to the chemical environment that can increase or decrease the energy gap between the vibrational modes. So FTIR is used to characterize the organic molecules and their functional groups. In a molecule, each atom can move independently from each other in a three-way oscillation. A pictorial representation of the vibrational mode of a triatomic molecule is represented in figure 2.20

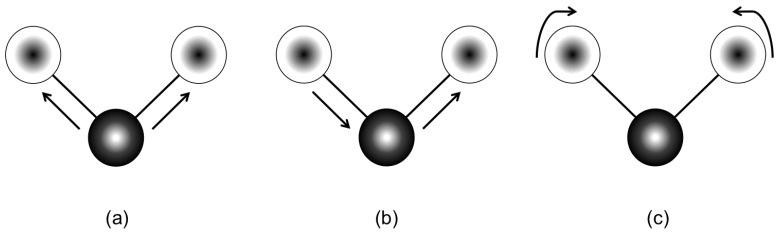


**Figure 2.20** Pictorial representation of vibrational modes of a molecule

In this work, FTIR was used to check the successful hydrolysis of the polymer and to check the conversion of the anhydride group to imide when SMA was converted to SMI. The sample was measured by placing the polymer powder on the glass sensor. The spectrometer used was a Perkin Elmer Spectrum 100 Series FT-IR spectrometer at the University of Bath. A pictorial representation of the instrument is reported in figure 2.21.

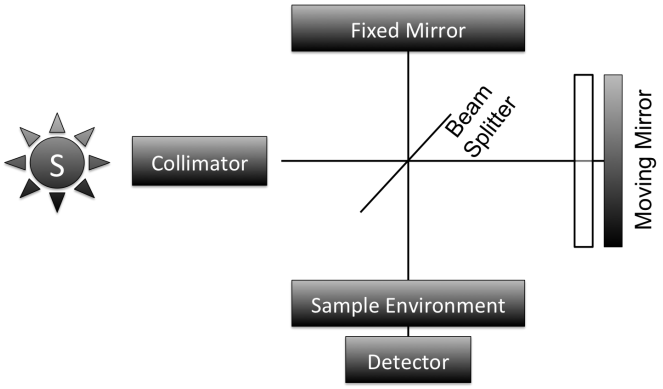


**Figure 2.21** Schematic of FTIR instrument

## 2.12 Fluorescence

Fluorescence is a reversible process that involves three stages where radiation is first absorbed and then emitted from a sample. The phenomenon is governed by three laws:

- Kashas's rule [107]: The fluorescence emission occurs from the lowest excited state
- Stokes' shift [108]: The emitted light has less energy than the excitation.
- Mirror Image Rule [108]: This law is related to the Frank-Condom principle and states that the emission spectra give information on the energy level of the ground state.

The incoming light is adsorbed from the sample only if the incoming photon energy is equal to the energy gap between the ground state and the excited state. When the system achieves the excited state, at the vibrational level $v^* = n$, it will relax through non-radiative processes to $v^* = 0$. At the lowest energy level of the excited state the system will release the absorbed energy. This emission process is called fluorescence [108]. The process is represented in figure 2.22
To perform the fluorescence measurements a Horiba FluoroMax 4 spectrometer was used. A schematic of the instrument is reported in figure 2.23. The excitation light is emitted by a neon lamp. The light produced goes through a monochromator and hits the sample. The intensity and the monochromaticity of the radiation

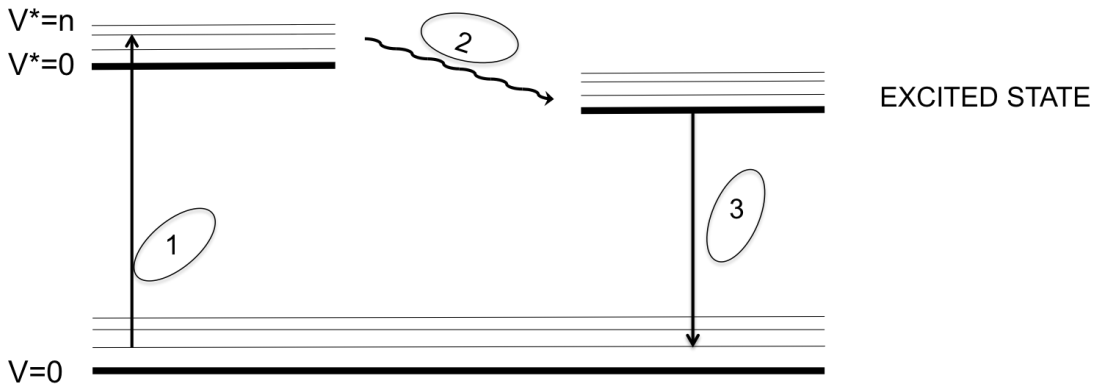


**Figure 2.22** Schematic of the absorption and emission of a photon for a fluorescence process

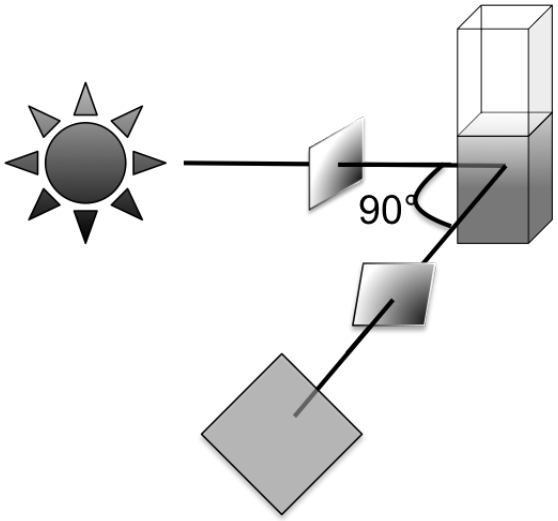


**Figure 2.23** Schematic of fluorimeter

is regulated through slits with variable aperture. Once the sample is hit by the radiation, it emittes radiation isotropically, i.e. in all directions equally. Even though a few fluorphores have a quantum yield close to unity, fluorescence is not usually an intense emission. For this reason the radiation is collected at 90°, so that the excitation light does not influence the measurement and the fluorescence can be detected.

For the measurements in chapter 5, 0.4 mL of solution containing vesicles containing fluorescently labelled lipids were injected and mixed with 0.4 mL of polymer to give a final concentration of 1.5 wt.% polymer and 0.5 %wt of lipid. The ex-

periment was followed between 0 and 0.2 seconds (1000 points) and between 0.2 and 20 sec (1000 points). 8 repeats for each experiment were run and averaged. A quartz cuvette of 1 cm path length was used. The experiment was carried out at 25°C. The schematic of the experimental set up is similar to that described in 2.6.3.

## 2.13 Experimental procedures

In this section the general sample preparation and solutions used in chapters 3, 4 and 5 will be discussed.

### 2.13.1 Buffer preparation

Buffer solutions are often used in chemical and biological environments to maintain a constant pH even during the addition of acids or bases to the solution. Depending on the polymer used (SMA or SMI), two different buffers were used to ensure the polymer was ionized and thus soluble. Buffers were made at different pH and at several salt concentrations.
Salts added to the buffers in this project, their supplier and purity of the chemicals are listed below:

- Sodium chloride (NaCl, BioXtra, $\geq$ 99.5%, Sigma Aldrich)
- Calcium chloride ($CaCl_2$, BioXtra, $\geq$ 99.5%, Sigma Aldrich)
- Magnesium chloride ($MgCl_2$, BioXtra, $\geq$ 99.5%, Sigma Aldrich)
- Magnesium sulfate ($MgSO_4$, BioXtra, $\geq$ 99.5%, Sigma Aldrich)
- Sodium bromide (NaBr, BioXtra, $\geq$ 99.5%, Sigma Aldrich)

The table 2.7 reports the pH and concentration of the salt used.
The following procedures were used to make acetate buffer (ABS) and phosphate buffer solutions (PBS):

**Table 2.7** Summary of the pH and salt concentration used.

| Kind of Buffer | pH | Strength (mol/L) | Salt Concentration (mol/L) |
|---|---|---|---|
| Acetate | 4 & 5 | 0.05 | 0, 0.05, 0.1, 0.2, 0.5, 1, 2 |
| Phosphate | 8 | 0.05 | 0, 0.05, 0.1, 0.2, 0.5 |

- Acetate Buffer: To make an Acetate Buffer Solution (ABS) at pH=5, at strength of 50 mM two solutions of glacial acetic acid (AcOH, Aldrich, ≥99%) and sodium hydroxide (NaOH,BioUltra, ≥ 98.0% ) with a concentration of 50 mM were made. Sodium hydroxide reacts with the acetic acid in a ratio 1:1 forming the sodium salt of acetic acid. To make 2L of acetate buffer at pH=3.5, 1.894 mL of 50 mM acetic acid was mixed with 106 mL of 50 mM sodium hydroxide. The buffer pH was adjusted with a pH-meter, METTLER TOLEDO. To make ABS at pH=5, 1.280 L of acetic acid was mixed with 0.720 L of sodium hydroxide with both at a concentration of 50 mM. Once a large amount of buffer was made, the solution was portioned in several aliquots and sodium chloride was added to make different concentrations of the salt at the same buffer strength.

- Phosphate Buffer Solution (PBS): To make PBS, two solutions of 0.2M of sodium phosphate monobasic ($NaH_2PO_4$, ≥99.0%, Sigma-Aldrich) and sodium phosphate dibasic ($Na_2HPO_4$, BioXtra, ≥99.0%) were made. 5.3 mL of 0.2M $NaH_2PO_4$ solution was mixed with 94.7 mL of 0.2 M $Na_2HPO_4$ solution and diluted to 400 mL to obtain a strength of 50 mM. The solution was portioned into several aliquots and salt was added to make different concentrations of the salt at the same buffer strength.

### 2.13.2 Making nanodiscs

A standard preparation to make nanodiscs was made as follows:
5mg of DMPC purchased from Sigma-Aldrich (99% pure) were suspended in 0.77 mL of buffer (prepared as described above). The choice of the buffer depends on the characteristics and the solubility of the polymer that was used. The solution

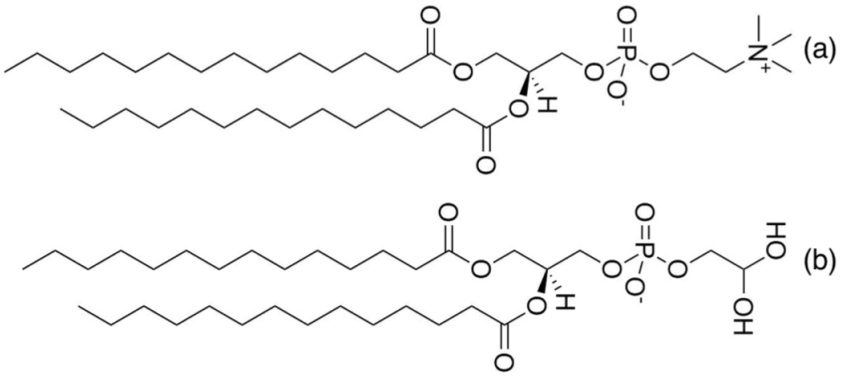


**Figure 2.24** Chemical structure of (a) DMPC and (b) DMPG

was sonicated in a water bath (Fisherbrand FB 11020) for about 20 minutes until a cloudy homogeneous solution was obtained. A 0.23 mL of a 6.5% wt solution of a polymer in the same buffer was added to this solution. The solution instantly turns clear, suggesting that the phospholipids in solution are incorporated into nanometer size structures which no longer scatter light. The final concentration of the solution was 1.5% wt of polymer and 0.5% wt of lipids. The nanodisc solutions were usually prepared at least 12 hours before use.

In order to mimic the complexity of the cell membrane, DMCP and DMPG mixture were used in some experiments. In order to make those samples, two separate solutions of different lipids were made, and the lipid suspensions were mixed in the ratio desired, such that the final concentration of the lipids remained 0.5%wt. Structures of the lipids used are reported in figure 2.24.

### Gel filtration

Gel filtration was used to purify nanodisc samples and remove the free polymer from the solution. Nanodiscs were made following the procedure in section 2.13.2 and left equilibrating overnight. While nanodiscs are equilibrated, buffer is run through the column for 1.5 time the volume of the column. The sample is then manually injected and run through the column. An autosampler made of 100 tubes collected the sample each 5 mL of eluted volume.

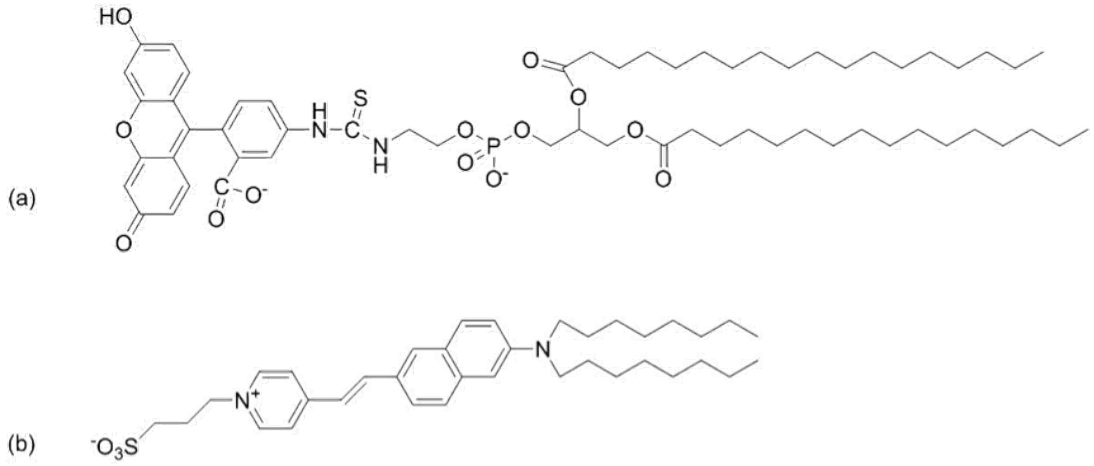


**Figure 2.25** structural formula of (a) FPE and (b) di-8-ANEPPS

### 2.13.3 Making FPE/Di-8 Anepps vesicles

Studies of the interaction of phospholipids with polymers using fluorescence was carried out for different lipid compositions in the vesicles and different polymers. The styrene-maleic acid copolymers used were either the commercial SMA2000P (6.4 KDa 2:1 ratio styrene:maleic acid) or a $SMA_{RAFT}$ copolymer synthesised at the University of Bath (6KDa, 2:1 ratio of styrene:maleic acid). For the following experiment lipid liposomes composed of either 100% of DMPC or 80%DMPC-20%DMPG ($DMPC_{80}DMPG_{20}$) were used. Phospholipids were purchased from Sigma ($\geq$99 % purity) and used as received.

Liposomes were made at a stock concentration of 13 mM and further diluted and used for experiments at a concentration of 400 $\mu$M. The first step was make a solution of phospholipid in chloroform and let this dry until a thin film is made. This was rehydrated with buffer in order to get a solution of vesicles with a concentration of 13 mM. Four freeze-thaw cycles were then done in order to get a monolamellar vesicle sample which was then extruded using a 100 $\mu$m membrane to obtain a monodisperse sample. Liposomes were tagged with either FPE or Di8 (figure 5.2) and incubated at 25°Cfor 24 hours before being used. The size of the vesicles were checked using DLS and they did not change over time until 30 days.

# Chapter 3

# SMI stabilised nanodiscs

In this chapter the stability of poly(styrene-co-maleimide) copolymers and their ability to form nanodiscs at acidic pHs will be discussed. The chapter is divided into two parts. In the first part the stability of the polymer in solution alone is considered. In the second part of this chapter the lipid-polymer aggregates are discussed. The morphological analysis of both the polymer and the lipid aggregates has been carried out using small angle scattering techniques.

## 3.1 Introduction

In the last few years, much effort has been invested in the use of poly(styrene-co-maleic acid) (SMA) by the biology community to immobilise membrane proteins. [44, 109, 110]. However poly(styrene-co-maleimide) (SMI) is also a potentially interesting copolymer for the formation of nanodiscs since it carries a positive charge rather than the negative charge of SMA. The physical properties of SMI also lead the polymer to be suitable for biological applications. One such example includes the increased solubility of SMI at lower pH compared to SMA, which is not soluble at pH lower than 8. A polymer that is soluble at lower pH would allow the extraction of proteins that have an isoelectric point in the pH range between 4 and 6. [111, 112]. Moreover, poly(tertiary) amines have been widely investigated from the structural point of view since they can undergo a completely reversible conformation change given the protonation state of the tertiary amine

group. The protonation process is reported in figure 1.9. Indeed, despite the overall positive charge on SMI it does not precipitate following the addition of a divalent cation to the system. This gives an advantage for SMI over SMA since SMI is not influenced by the presence of $CaCl_2$ which is commonly found in biological solutions. The molecular structure for poly(styrene-co-maleimide) is reported in figure 3.1. Commercial names for this polymers are SMA1000I, SMA2000I and SMA3000I where the molar ratio of styrene to maleimide is equal to one, two or three, respectively. To avoid confusion with the name of the others copolymers made of styrene and maleic anhydride, in this thesis this copolymer will be named $SMI_{1000}$, $SMI_{2000}$and $SMI_{3000}$, respectively. Values for molecular weight ($M_w$), molecular number ($M_n$) and polydispersity index (PDI) are reported in table 3.1

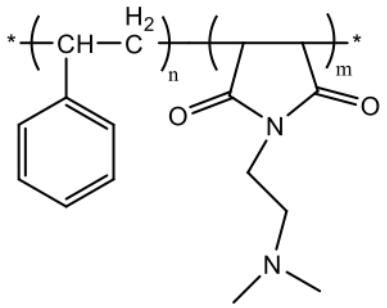


**Figure 3.1** SMI molecular structure

**Table 3.1** Values for the polymer used in this project obtained from [7]

| Ratio Sty:MI | Commercial name | Name in this project | $M_n$ (g/mol) | $M_w$ (g/mol) | PDI ($M_w/M_n$) |
|---|---|---|---|---|---|
| 1:1 | SMA2000I | $SMI_{1000}$ | 2000 | 5500 | 2.75 |
| 2:1 | SMA2000I | $SMI_{2000}$ | 3000 | 7500 | 2.5 |
| 3:1 | SMA2000I | $SMI_{3000}$ | 3800 | 9500 | 2.5 |

## 3.2 SMI characterisation

The commercial SMI copolymers used in this work were kindly supplied by Cray Valley. Only one batch of each copolymer was used for the entirety of this thesis. In order to use the SMI copolymer, the ternary amine needs to be protonated as reported in figure1.9 to be water soluble. To achieve a final concentration of 13%wt of polymer in solution the following formula 3.1 was used to calculate the amount of acid that had to be used to solubilise the resin.

$$mL_{acid} = \frac{(SMI_{wt})(SMI_{index})(ACID_{MW})(ExcessFactor)}{1000(Acid_{conc})} \tag{3.1}$$

**Table 3.2** Polymer index and amount of polymer and acid used for the solubilisation of the resin

| Polymer | Index | $H_2O$ (mL) | AcOH (mL) |
|---|---|---|---|
| $SMI_{1000}$ | 3.15 | 6.746 | 0.902 |
| $SMI_{2000}$ | 2.50 | 6.942 | 0.712 |
| $SMI_{3000}$ | 2.05 | 7.077 | 0.587 |

where $mL_{acid}$ is the volume of acid used (mL), $SMI_{wt}$ is the weight percentage of the polymer in solution (g/mL), $Acid_{MW}$ is the molecular weight (MW) of acid used and $Acid_{conc}$ is the concentration of the bulk acid solution used to dissolve the resin. $SMI_{index}$ (meq/g) is a parameter specified by the company and depends on the resin dissolved. These values were obtained from the supplier and are reported in table 3.2. The standard procedure for solubilisation and a list reagents used is reported next.

For a typical solubilisation of the polymer, the as-supplied polymer resin was initially ground in a pestle until a fine powder was obtained. 6.75 mL of MilliQ water (18.2 M) from ELGA PURELAB ultra was stirred before adding 1 g of resin. The solution was continuously stirred for 15 minutes after which 0.9 mL of glacial acetic (Aldrich, $\geq$99%) was added. The temperature was then raised to 60°C and left under reflux for 4 hours to fully protonate the polymer. The solution was cooled in a water bath. The pH of the final solution was 5 as tested

using pH paper. The stock solution (13% wt) was then diluted and used without further purification. The same procedure was also followed to solubilise $SMI_{2000}$ and $SMI_{3000}$. Different amounts of H2O and AcOH were used to dissolve these polymers when compared to $SMI_{1000}$as reported in table 3.2. Once the polymer was dissolved, the solution was stored in the fridge at 4°C. Before starting the characterisation of the phospholipid structures, an analysis on the polymer alone was carried out.

### 3.2.1 pH working range

All the polymers ($SMI_{1000}$, $SMI_{2000}$ and $SMI_{3000}$) were titrated in order to find the variation in the polymer solubility. Two different methods were used: manual titration and an automated titration using DLS. For the latter method a 0.5% wt polymer solution in water initially at pH=4 was titrated with 0.1M NaOH solution. The $pK_a$ was determined from the graph (figure 3.2a). The values obtained for the different polymers are slightly different: 6.8, 6.4 and 6,1 for $SMI_{1000}$, $SMI_{2000}$ and $SMI_{3000}$ respectively. In fact, depending on the hypercoiled structure of the polymer in solution, the amine group will be more or less exposed to the protons. This results in a change in the $pK_a$ [113]. This is in agreement with the fact that $SMI_{2000}$ and $SMI_{3000}$ have a higher hydrophobic to hydrophilic ratio compared to $SMI_{1000}$. As shown in table 3.1, the ratio of styrene to maleimide is of 1:1, 2:1 and 3:1 for $SMI_{1000}$, $SMI_{2000}$ and $SMI_{3000}$, respectivelly; the higher percentage of styrene results in those polymers being more hydrophobic. The polymer reorganises its structure in an aqueous solution in order to minimize the contact of the hydrophobic parts with water so that fewer acid groups will be available for protonation [113]. The hydrophobic part will reorganise in order to minimise the contact with water. Adding NaOH to the solution causes the positive charge of the polymer to be neutralised. Microdomains of positively charged amines will form in order to have as many positively charged groups on the structure surface as possible. This reorganisation of charges leads the polymer to be soluble below the $pK_a$ as shown by the transition point in figures 3.2b. The

titration curves are reported in figure 3.2a. Automated titration of the polymer was followed using a Malvern Nano ZS instrument and is depicted in figure 3.2b. Here the size of the polymer in solution is followed with changing pH. As the charge on the polymer is decreased the polymer becomes less soluble, and thus form larger aggregates.

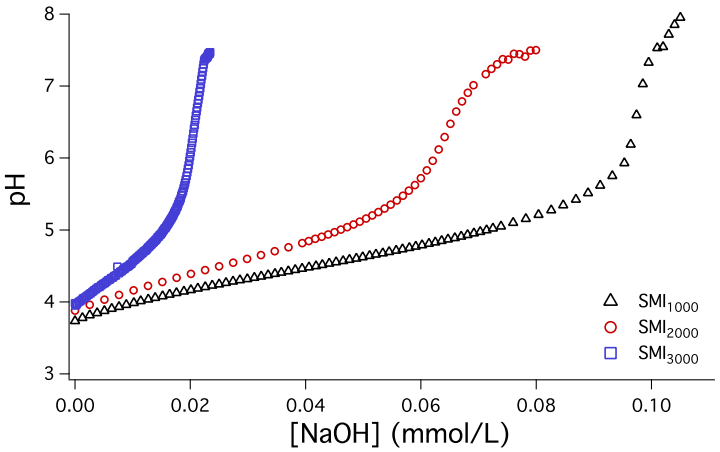


**(a)** pH meter titration

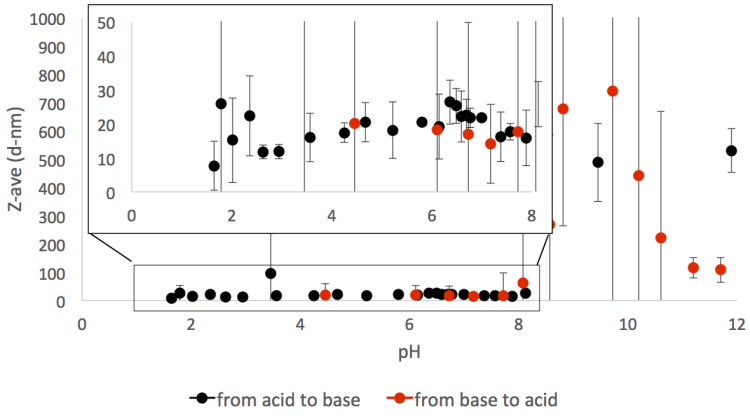


**(b)** DLS titration

**Figure 3.2** Titration of $SMI_{1000}$ and $SMI_{2000}$ using (a) pH-meter and (b) ZS nanosizer autotitrator

From figures 3.2a and 3.2b it is possible to note increasing Z-average and intensity values for pH $>$ 7.5, which indicates an aggregation of the polymer into a larger macromolecular structure. Upon increasing pH, the amine group is deprotonated and the resulting polymer becomes insoluble. This visibly manifests in a change to a cloudy consistency of the solution. This process is reversible as shown in

figure 3.2b. The blue data points show the titration of the same polymer solution from alkaline pH to acidic pH. The structure returns to the original size for pH lower than the $pK_a$. A different transition point is revealed by the two different methods. Even though the polymer is above its $pK_a$ at values of pH $> 6.5$ the solubility of the polymer up to pH $= 7.5$ allows for experiments to be carried out at pH up to 7. When the titration with acid is done using the DLS instrument, the transition point occurs at higher pH. This is explained by the presence of microdomains where the protonated uncharged moieties make the core of the coil and the still available protonated amine makes the polymer soluble in solution. The transition point found with DLS matches the plateau of the titration carried out with the pH meter, which indicates a fully unprotonated polymer [113]. A similar behaviour has been reported in the literature for diethylaminoethyl methacrylate, a weak poly base which is protonated at pH over 7.1. For more alkaline pH this polymer arrange in a micellar structure made of chains collapsed together [114].

### 3.2.2 pH and salt effects on SMI in solution

SMI copolymers were analysed under different pH conditions whilst keeping the buffer concentration constant at 50mM. The pH range was varied between 3.5 and 7.

#### DLS analysis

The solution properties of the polymer were analysed at different salt concentrations using either SAXS (B21 beamline at Diamond, RAL), SANS (SANS2D at ISIS) or DLS. The procedure for preparing the buffer and salts used is reported in section 2.13.1. The co- and counterions were changed in order to evaluate the stability of the system under different salt conditions. This parameter is fundamental when studying biological systems. Several kinds of salts are present in the bloodstream as well as and in the inside and outside of the cell membrane. Their different concentrations inside and outside the membrane is responsible for the

electrostatic membrane potential [115]. It is important to study the independent system, in our case the polymer itself, and its range of stability before applying it to a more complicated structure. Indeed, the requirment for the stability of the system studied varies as a function of the final application. In the case of drug delivery systems it is important to have structures that can be disrupted in order to realese the drug. pH responsive polymers are used for this purpose [116, 117]. In our case, since we want the polymer to encircle lipids and proteins to stabilise them, our purpose is to find the range of stability for which the polymer on its own does not precipitate out of the solution. Therefore an in depth analysis of the polymer in different conditions has been carried out in order to check the stability and the working range at which the polymer can be used without causing precipitation

In order to correlate the conformation changes of the polymer changes with the physico-chemical characteristics of the nanodiscs, the polymer was dissolved in solutions containing the same amounts of salt using the same buffer strength at the same pH (3.5 and 5) used to make nanodiscs. The graph reported in figure 3.3 shows DLS measurements for the SMI polymers dissolved at different salt concentrations at pH=5.

Looking at the intensity graphs, $SMI_{1000}$ presents polymer aggregates with a size around 400 nm. Even though the DLS measurements give the hydrodynamic radius, which consists of the particle and its solvation shell rather than the true radius of the dissolved samples, a trend is still visible where the smaller structures are getting bigger as the salt concentration is increased, whereas the structures around 400 nm are not changing in size but they do decrease in intensity. The change in size of aggregates containing charged species upon increasing salt concentration has been studied in the literature for a wide range of soft matter compounds, from surfactants [118–120] to polyelectrolytes [121, 122]. For the case of polyelectrolytes, the chain usually adopts a Gaussian coil conformation for ideal dilute solutions. Electrostatic charges on the corona repel each other causing a certain sized structure to be formed. When salt is added to those solutions, the

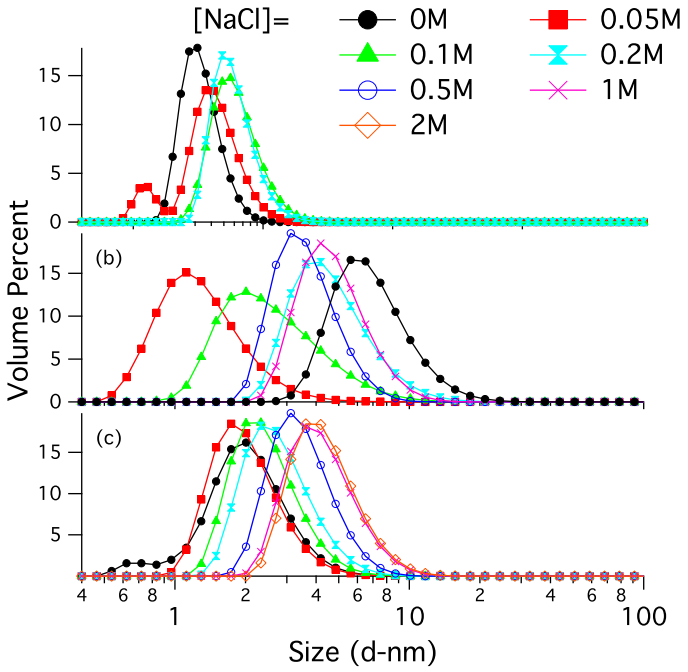


**(a)** DLS volume

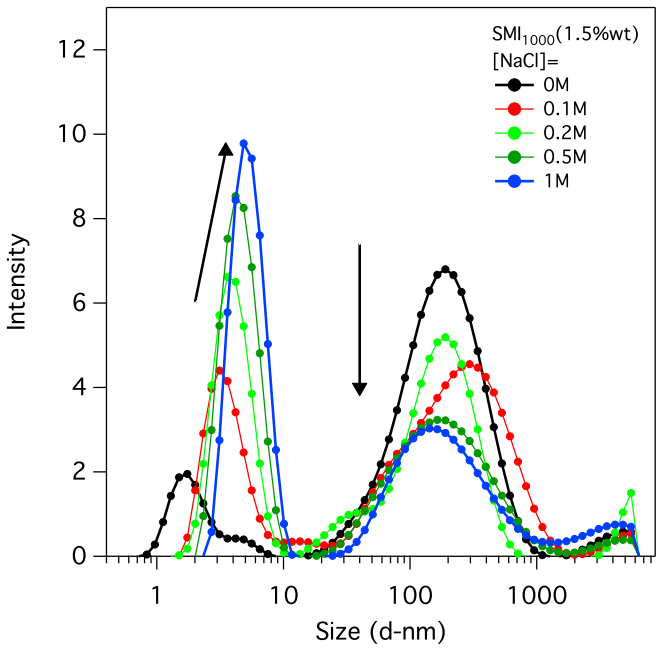


**(b)** DLS intensity

**Figure 3.3** DLS measurements plotted as intensity or volume percent vs hydrodynamic diameter carried out for a 1.5%wt solution of polymer using acetate buffer at pH=5, varying concentration of NaCl as reported in above for (a) $SMI_{1000}$, (b) $SMI_{2000}$ and (c) $SMI_{3000}$.

charges are screened and a shrinkage in the radius is detected because of the neutralization or reduction of the charge on the polymer moieties [123]. However, DLS measurements throughout this thesis were run at high concentration (1.5% wt). At these concentration polymers do not arrange in a Gaussian coil distribution. Due to the hydrophobicity of the polymer, at 1.5 % wt the polymer is likely to be arranged in a supramolecular structure rather than as a Gaussian coil. Studies of block copolymers have been carried out extensively, for example, by Borisov and his collaborators, as a function of salt concentration [124]. The commercial SMI studied here, however, has a more complicated structure than a block copolymer. SMI is commercially produced from the commercially available SMA. This leads the SMI to have the same random structure of the carbon backbone as for SMA. Further discussion on the moieties distribution along the SMA backbone is reported in chapter 4. The random distribution of hydrophobic and hydrophilic moieties along the polymer chain potentially leads this system to show a different behaviour. The hydrophobic part of the polymer will tend to minimise the contact with water making a structure similar to a micelle. The neutralisation of the charges induced by the salt, along with the hydrophobic effect of the polymer, is likely to cause aggregation of the polymer in solution, as observed experimentally by the precipitation of the $SMI_{3000}$ at a lower salt concentration when compared to $SMI_{1000}$ and $SMI_{2000}$. As discussed before, $SMI_{3000}$has a higher hydrophobicity and precipitated at a concentration of salt where the other two formed stable aggregates concentration of salt where the other two formed stable aggregates, e.g. $SMI_{3000}$ precipitated at 0.2 M NaCl concentration. For concentrations up to 2 M NaCl however, $SMI_{1000}$ is still soluble whereas $SMI_{2000}$also precipitated. For $SMI_{3000}$ precipitation occurs even at a NaCl of 0.2 M concentration. Moreover the solutions of $SMI_{3000}$were unstable over the period of one day. For this reason, no further characterisation for other salts has been carried out for $SMI_{3000}$. The experimental observation of $SMI_{1000}$ getting smaller with increasing salt concentration it is not completely clear. Firstly, the polymer concentration at which DLS measurements were run are not ideal. Moreover, the DLS results,

as presented in this thesis, were not analysed further than the automatically produced results from the Malvern Instrument software. The software assumes that the particle is spherical and calculates the hydrodynamic diameter accordingly. However, as previously discussed, the high concentration of the polymer leads the chains to aggregate not in a Gaussian coil and thus this assumption might be invalid. As a consequence, 400nm may not be the real size of particles in solution. However, for the purpose of this thesis, qualitative results show structures which reduce in radius upon the addition of salt.

$SMI_{1000}$ is the co-polymer that has the highest hydrophilic to hydrophobic ratio. Hydrophilic moieties (charged tertiary amines) allow a stretched conformation in water. Along with the hydrophilic effect, however, the polymer experiences the hydrophobic interaction of styrene moieties among polymer backbones. The ratio close to 1:1 of hydrophobic and hydrophilic moieties, along with the random distribution of styrene and maleimide moieties, causes an uncharacterised structure in solution. In the case of $SMI_{2000}$ and $SMI_{3000}$, the hydrophobic to hydrophilic ratio is higher. The higher hydrophobic effect leads the chain to have a collapsed structure even though charges on the surface are not shielded. When salt is added to these two copolymers, chains behave more like block copolymer with a micellar structure reported in literature.

As a concluding remark for the behaviour of $SMI_{1000}$, $SMI_{2000}$ and $SMI_{3000}$, it can be stated that further studies must be carried out in order to fully understand the aggregation of $SMI_{1000}$ at low concentration of salt. $SMI_{1000}$ and $SMI_{2000}$, however, have been further investigated in the presence of different anion/cation since they have shown a stable response over a wide range of pH and concentration of salt. On the other hand, $SMI_{3000}$ will not be discussed further in this thesis because it has shown poor stability at concentrations of salt higher than 0.2M inserted a new section to discuss NaBr and $CaCl_2$

### 3.2.3 Hofmeister serie: counter ion effect

DLS measurements were also carried out for $SMI_{1000}$ and $SMI_{2000}$ using $CaCl_2$ and NaBr (figure 3.4a and 3.4b).

Other than the concentration of salt itself, co- and counter ions play a key role in polymer self assembly. More than a century ago Hofmeister studied the influence of salts on the conformation of proteins [125]. Their conformation and size are affected by the kind of salt as well as its concentration. For proteins it was found that anions had a much stronger effect on solubility than cation. Hofmeister established a series of anions that that increased or decreased the solubility of proteins. In the scientific field, this phenomena is also known as a salting in or salting out effect, respectively. The Hofmeister series is reported below from the weakest to the strongest binding:

$$SO_4^{2^-} < OH^- < F^- < HCOO^- < CHCOO^- <$$

$$< Cl^- < Br^- < NO_3^- < I^- < SCN^- < ClO_4^-$$

Solubility effects described by this series are valid for many other fields in soft matter such as the aggregation point of polymers, the surface tension of electrolytic solutions or the mesoporous arrangement of silica templates [126, 127]. Even though, due to the complexity of systems such as polymer micelles or protein structures, it is not possible to write a general law that explains uniformly every system, the series is still legitimate to give a rough prediction of the behaviour of a system. The validity of this series is due to the general laws that control this phenomenon. For a long time, the different behaviour of supramolecular structures in the presence of different anions was explained via the different packing of molecules of water around the ion. In the biological field it is not uncommon to find names such as structure maker or breaker, or low/high density water to describe the interface with membranes and the effect of salts [128]. In the last decade, however, dispersion forces have been claimed to better explain the behaviour of structures in solution in the presence of ions. Independently

from the structure that is affected (micelle, vesicle, proteins), for the anion it is suggested that the higher the atomic number, the larger the polarisability of the electronic cloud. This leads the system to have a different interaction with the surrounding media through dispersion forces [127] which leads to a more effective binding of the anion on the surface of the structure.

The validity of the Hofmeister series has been validated for polymers studied in this project as well. Figure 3.4 shows the behaviour of $SMI_{1000}$ and $SMI_{2000}$ in the presence of different anions/cations at different salt concentrations. The summary graphs (figure 3.4a and 3.4b) show the values for the smaller structures detected in solution. Errors are calculated as a standard deviation from 3 different readings of the same sample. Values are reported in table 3.3

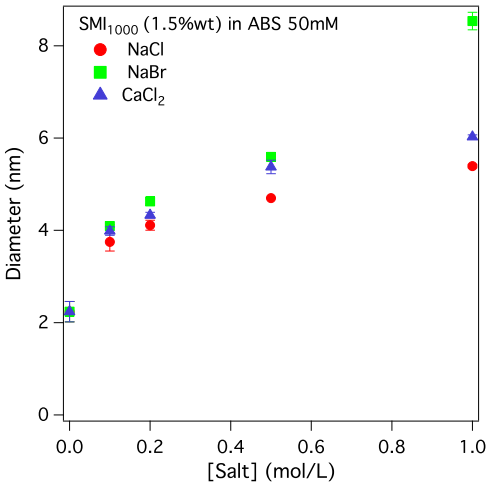


(a) $SMI_{1000}$

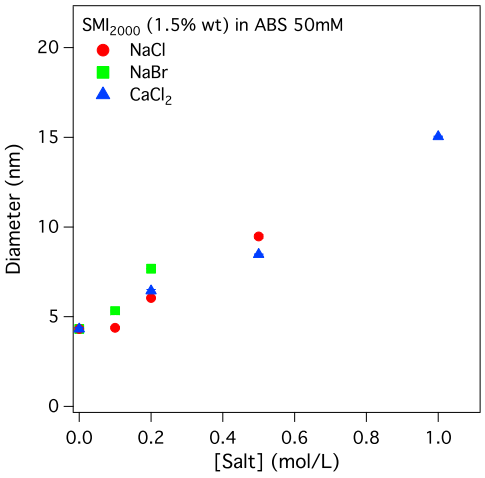


(b) $SMI_{2000}$

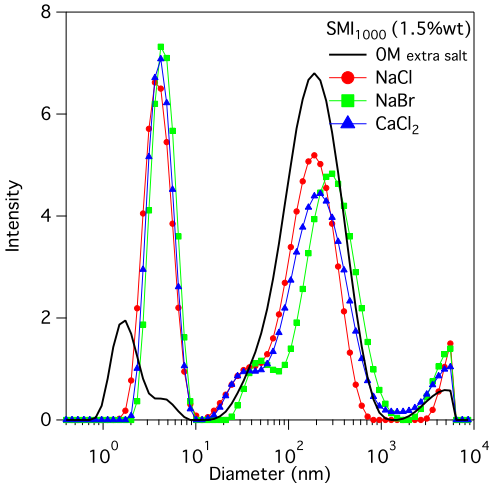


(c) $SMI_{1000}$, [salt]=0.2M

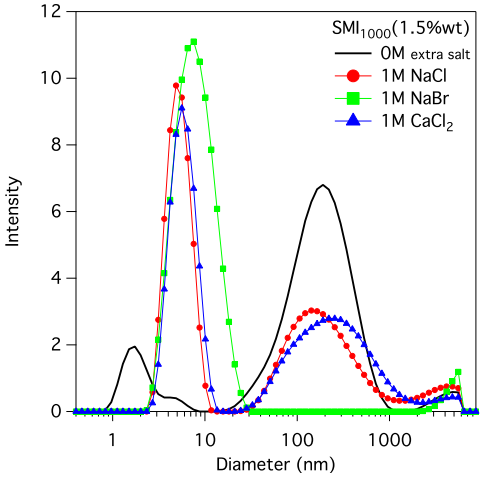


(d) $SMI_{1000}$, [salt]=1M

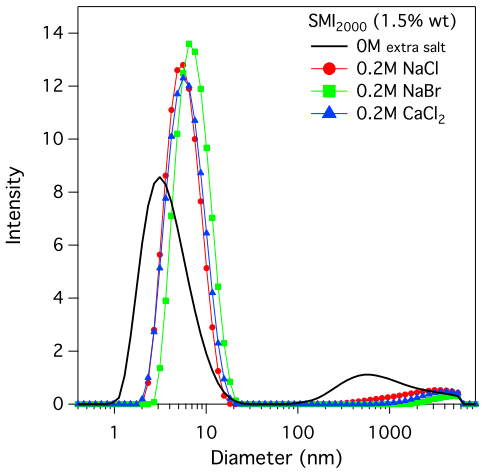


(e) $SMI_{2000}$, [salt]=0.2M

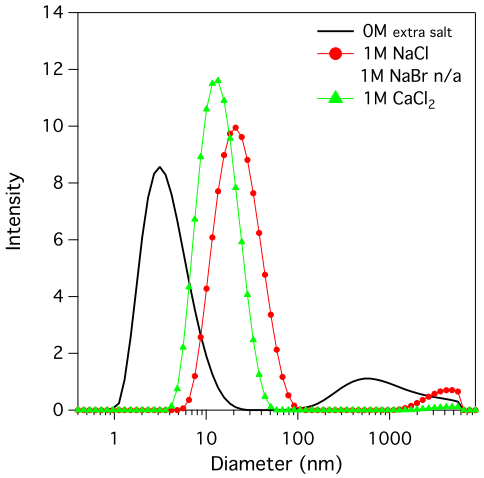


(f) $SMI_{2000}$, [salt]=1M

**Figure 3.4** Summary of DLS measurements carried out for (a)$SMI_{1000}$ and (b)$SMI_{2000}$at 1.5%wt in ABS (pH=5, 50mM) with different salt concentration. Several salts were used: NaCl (red dot), NaBr (green square) and $CaCl_2$ (blue triangle).

**Table 3.3** DLS values size for $SMI_{1000}$ and $SMI_{2000}$ at different salt concentrations for NaCl, NaBr and $CaCl_2$. Values reported refer to the smaller structures in figure 3.4. The low intensity is due to the presence of large aggregates which give a higher DLS signal.

| | | NaCl | | NaBr | | $CaCl_2$ | |
|---|---|---|---|---|---|---|---|
| | | Size (d-nm) | Int (%) | Size (d-nm) | Int (%) | Size (d-nm) | Int (%) |
| $SMI_{1000}$ | 0M | 2.2 ±0.2 | 12.4 | | | | |
| | 0.1M | 3.7±0.2 | 26.8 | 4.1±0.1 | 33.4 | 4.0±0.1 | 36.4 |
| | 0.2M | 4.1±0.1 | 38.9 | 4.6±0.1 | 37.9 | 4.3±0.1 | 37.2 |
| | 0.5M | 4.7±0.1 | 49.3 | 5.6±0.1 | 59.8 | 5.4±0.1 | 36.7 |
| | 1M | 5.4±0.5 | 52.5 | 8.5±0.2 | 96.7 | 6.0±0.1 | 51.3 |
| $SMI_{2000}$ | 0M | 4.3±0.1 | 82.3 | | | | |
| | 0.1M | 4.4±0.1 | 99.1 | 5.3±0.1 | 100 | 5.0±0.1 | 98.7 |
| | 0.2M | 6.0±0.2 | 93.5 | 7.7±0.1 | 98.4 | 6.4±0.1 | 96.4 |
| | 0.5M | 9.4±0.3 | 88 | n/a | - | 8.5±0.1 | 100 |
| | 1M | 25±0.6 | 95.4 | n/a | - | 15.0±0.5 | 99.3 |

Both chloride and bromide anions, as predicted from the Hofmeister series, have a stronger binding effect compared to the acetate. This was observed when a buffer made at 2M buffer strength did not precipitate any polymer. Without any further addition of salt to the solution, the structures for $SMI_{2000}$ are bigger compared to $SMI_{1000}$, yet both of the polymers have about the same molecular weight. The bigger size of $SMI_{2000}$ is likely to be due to the higher hydrophobic ratio compared to $SMI_{1000}$. Due to this higher hydrophobic contribution, the effect of added salt is more pronounced for $SMI_{2000}$. In the case of $SMI_{2000}$ no big structures were detected with DLS (figure 3.4d).The polymer, however precipitated for NaBr concentrations higher than 0.2M (figure 3.4f). This behaviour agrees with the Hofmeister series, which predicts that bromide ions bind more strongly to the surface. This leads to a pronounced change in conformation of the polymer structures in solution at lower concentrations of NaBr compared to those of NaCl. Even though the NaBr did not lead to a precipitation of $SMI_{1000}$, a remarkable increase in size is observed. The hypothesis made about big clusters being disrupted by the neutralisation of counterions, is reinforced from the behaviour that $SMI_{1000}$ has in the presence of NaBr. In fact no big structures are

detected in 1M NaBr solution for $SMI_{1000}$. The stronger binding effect of bromide predicted from the Hofmeister series may cause the stronger interaction of the anion with the polymer clusters, which are disrupted more easily by bromide than chloride. Moreover, the percentage in intensity of small structures in the presence of NaBr increases linearly with the salt concentration going from 33 to 97%. This hypothesis is validated by looking at the behaviour of the polymer in the presence of $CaCl_2$. The percentage intensity for $CaCl_2$ is comparable to the intensity observed for NaCl. This is due to the fact that SMI co-polymers are positively charged, so just a small effect on the aggregation point of the polymer is detected when $CaCl_2$ is used. This is important since it will enable SMI to be used to extract or support membrane proteins in systems where $CaCl_2$ is important for the protein function or stability, such as GCPR [129, 130].

### Small angle scattering analysis

Even though DLS analysis is fast and gives the hydrodynamic diameter of the particle, it does not return structural information on the shape of the polymer in solution. It has been shown in the literature that a structural transition from a sphere to an ellipsoidal shape occurs increasing the salt concentration. Small angle scattering data were therefore collected on solutions of $SMI_{1000}$ and $SMI_{2000}$ in the presence of different salts, to determine the detailed structures of these polymers in solution and the effect of electrolyte concentration. Data for $SMI_{1000}$ and $SMI_{2000}$ were acquired on B21 at Diamond. Scattering patterns feature present an increasing background signal due to the increasing concentration of salt present in solution. The background subtracted from the following data set was kept at a sodium chloride salt concentration of 0.2M, thus the background contribution from the increasing NaCl in solution is taken into account by using a flat background term in the models applied during fitting. The data were fitted using two different models: a sphere model with a Schultz polydispersity distribution for the radius and a uniform ellipsoid model, as described in 2.6.1. For the fitting the salt concentration was set to the concentration of the buffer (50 mM) plus that

of the added NaCl in each case. As an example, in a 50 mM NaCl solution, the salt strength is considered to be 0.1M. The large amounts of salt present in these systems means that the charge on the scattering object is largely screened so the fit was not sensitive to this parameter and it was fitted from data at 0M concentration of NaCl and was set to be 39. Data from $SMI_{2000}$ and $SMI_{3000}$ at the same concentration (1.5%wt) were also fitted. Parameters related to dielectric constant, temperature, salt concentration, incoherent background, SLD of the solvent and the polymer are reported in table 3.4 and fixed during subsequent fitting. Scattering data and fits to these models are shown in figure 3.5.

**Table 3.4** Summary of parameters used that were calculated and hold or fitted to fit polymer scattering data using two different models: a polydisperse sphere or an uniform ellipsoid. both with a Hayter-Penfold structure factor to account for interactions between charged objects in an electrolyte solution. (*)SLD calculated using the NIST software [8]. (**) SLD determined with solvent match point.

| Schultz Spheres | | Ellipsoid | |
|---|---|---|---|
| Volume Fraction | Fitted | Scale | Fitted |
| Mean radius (Å) | Fitted | Rotation axis (a) (Å) | Fitted |
| PDI | Fitted | Rotation axis (b) (Å) | Fitted |
| Common Parameters | | | |
| Dielectric Constant | | 78 | |
| Charge | | 39 | |
| Temperature (K) | | 298 | |
| SLDs ($Å^{-2}$) | | | |
| | | X-Ray | Neutron |
| Solvent | $D_2O$ | 9.46 x $10^{-6}$ | 6.3 x $10^{-6}$ (a) |
| | $H_2O$ | | -0.54 x $10^{-6}$ (b) |
| SLD polymer (sphere or ellipsoid) ($Å^{-2}$) | | | |
| $SMI_{1000}$ | | 1.19 x $10^{-5}$ * | 1.96 x $10^{-6}$ ** |
| $SMI_{2000}$ | | 1.09 x $10^{-5}$ * | 1.96 x $10^{-6}$ ** |
| $SMI_{3000}$ | | 1.04 x $10^{-5}$ * | |

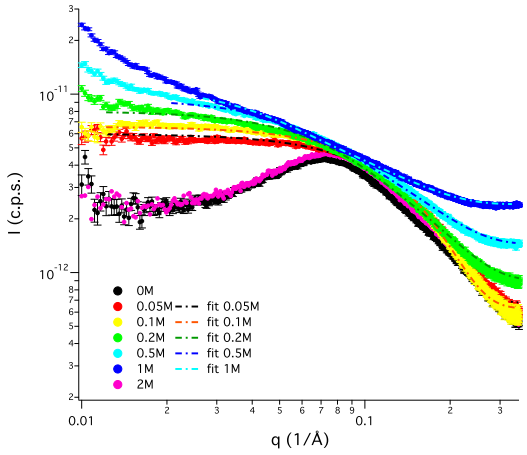


**(a)** $SMI_{1000}$

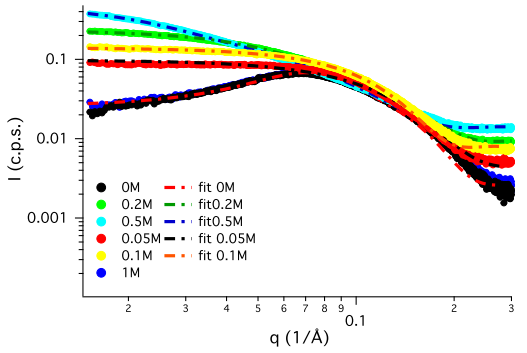


**(b)** $SMI_{2000}$

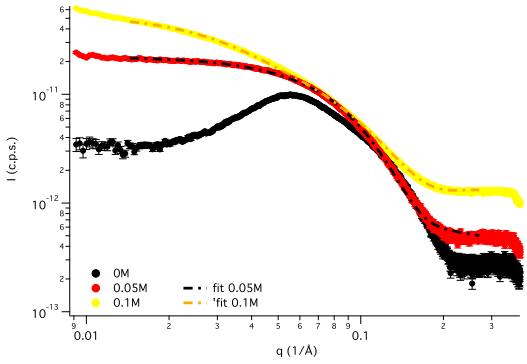


**(c)** $SMI_{3000}$

**Figure 3.5** SAXS patterns for (a) $SMI_{1000}$, (b) $SMI_{2000}$and (c) $SMI_{3000}$ solutions at 1.5% wt in ABS (ph=5, 50mM) with different NaCl concentrations. The dashed line is the best fit to this data using the models described in section 2.6.1

The results for the fitting reported in figure 3.5 are summarised in table 3.5. Errors were estimated from the changing values for parameters used for the fitting. The error was approximated to be a value that sensitively diverts the fitting curve from the experimental data.

**Table 3.5** Fitting parameters for a model of a polydisperse sphere fit to scattering data from a solution of $SMI_{1000}$, $SMI_{2000}$ at 1.5%wt run in ABS 50mM, pH=5 at several concentration of added NaCl

| | $SMI_{1000}$ | | |
|---|---|---|---|
| Salt concentration | 0M | 0.05M | 0.1M |
| Radius (Å) | 11.7 ±2 | 12.9±2 | 10.9±2 |
| PDI | 0.21 ±0.1 | 0.15±0.1 | 0.28±0.1 |
| | $SMI_{2000}$ | | |
| Radius (Å) | 16.7 ± 2 | 17.4 ± 2 | 15.6 ± 2 |
| PDI | 0.16 ± 0.1 | 0.14 ± 0.1 | 0.27 ± 0.1 |

Increasing the salt concentration leads to a change in the polymer shape, from a spherical to an ellipsoidal shape. Transitions in shape upon an incresaing salt concentration have been previously reported in the literature by Borisov *et al*[121]. For NaCl concentrations over 0.2M, for both $SMI_{1000}$ and $SMI_{2000}$, an ellipsoid model was used to fit the scattering data, the coefficients of which are reported in table 3.6

$SMI_{1000}$ and $SMI_{2000}$ structures in ABS solution were also analysed when mixed with NaBr and $CaCl_2$ using SAXS. The transition from a sphere to an ellipsoid was observed when the polymer was dissolved in the presence of NaBr and $CaCl_2$. In a similar manner to polymers dissolved in NaCl, a transition is present for increasing salt concentration. The values for fitting the SAXS data are reported in table 3.7 and SAXS patterns are reported in figure A.1 in section A.1. A transition from spherical micelle to elongated structures such as ellipsoids or rod-like shapes has been widely seen for many ionic surfactant solutions [120, 131–133]. The transition is ascribed to the screening effect that the salt has on the charged headgroups in the micelle corona. Electrostatic repulsion becomes lower and structures, in order to minimise their energy, fuse together. The effect of the co-

**Table 3.6** Ellipsoid model coefficients used to fit SAXS scattering from polymer solution of $SMI_{1000}$, $SMI_{2000}$ and $SMI_{3000}$ for structures in solution with a concentration of 1.5%wt and at several salt concentrations.

| | $SMI_{1000}$ | | |
|---|---|---|---|
| [NaCl] | 0.2M | 0.5M | 1M |
| R(a) rotation axis (Å) | 37.3 ± 2 | 42.8 ± 2 | 69.9 ± 1 |
| R(b) (Å) | 10.4 ±1 | 11.0 ± 1 | 12.1 ± 1 |
| | $SMI_{2000}$ | | |
| [NaCl] | 0.2M | 0.5M | 1M |
| R(a) rotation axis (Å) | 83.5 ± 4 | 169.0 ± 5 | |
| R(b) (Å) | 15.6 ± 1 | 18.7 ± 1 | |
| | $SMI_{3000}$ | | |
| [NaCl] | 0.1M | 0.5M | 1M |
| R(a) rotation axis (Å) | 83.5 ± 4 | | |
| R(b) (Å) | 15.6 ± 1 | | |

and counterion has a huge effect on the size and the transition from a micelle to a rod-like structure. Cetylpyridinium halide micelles were studied in the presence of both both NaCl and NaBr. In a similar manner to the experiments carried out in this work, the temperature and the concentration of the surfactant was held constant. SMI copolymers can be compared to small molecule surfactant since they also form micelle-like aggregates in solution. It was shown that NaBr increased the micellar size of cetylpyridinium halide micelles [119]. Studies reported in literature show that bromide is more effective to cause this transition, from a micelle to a globular structure [134, 135]. Bromide anions are less solvated and tend to have a stronger interaction with the surface of the micelle. The supramolecular structure changes more rapidly with increasing NaBr concentration than for NaCl [136]. Similar to the effect seen in literature, for both $SMI_{1000}$ and $SMI_{2000}$ bigger structures were detected with either DLS and SAXS when NaBr is used as a salt. In the same manner to the surfactants and polyelectrolyte solutions studied in by others, a transition from a sphere to an elongated structure occurs. For NaBr containing solutions of $SMI_{2000}$ the polymer precipitated for NaBr concentrations higher than 0.2M. The higher precipitation effect of the bromide anion was also reported in literature for trimethylammonium surfactants

[136]. When the polymer was dissolved in acetate buffer at the same pH no big change in size or shape was observed when $CaCl_2$ is used instead of NaCl. This is not surprising since the counterion is the chloride for both salts.

**Table 3.7** Fitting parameters for $SMI_{1000}$ and $SMI_{2000}$ fitted to a polydisperse sphere ($SMI_{1000}$ at [NaBr]=0.1 M) and to an uniform ellipsoid. $SMI_{1000}$ and $SMI_{2000}$ at 1.5% wt dissolved in acetate buffer, pH=5 for different salt concentrations of NaBr and $CaCl_2$. Graphs showing the fitted data are reported in section A.1 (figure A.1)

| | | $SMI_{1000}$ | | |
|---|---|---|---|---|
| | | 0.2M | | 0.5M |
| | Radius (Å) | 14.9 | | 14.5 |
| | PDI | 0.19 | | 0.26 |
| | | $SMI_{2000}$ | | |
| **NaBr** | | 0.2M | | 0.5M |
| | Radius (Å) | 18.5 | | |
| | PDI | 0.21 | | |
| | Rot Axes A | | | 61.7 |
| | Rot Axes B | | | 19.3 |
| | | $SMI_{1000}$ | | |
| | | 0.2M | 0.5M | 1M |
| | Rot Axes A | 47.0 | 85.0 | 147.5 |
| | Rot Axes B | 9.3 | 9.7 | 14.7 |
| **CaCl2** | | $SMI_{2000}$ | | |
| | | 0.2M | 0.5M | 1M |
| | Rot Axes A | 47.8 | 93.5 | |
| | Rot Axes B | 14.2 | 13.7 | |

The stability of SMI polymers in the presence of $CaCl_2$ is a great advantage for the membrane protein community. As discussed in chapter 1, one disadvantage of using SMA is the precipitation caused by divalent cations due to the complexation of the acid group (figure 1.8). As shown in figure 3.4, instead, adding $CaCl_2$ up to 1 M does not precipitate SMI copolymers, so they can potentially be used for membrane protein support when $CaCl_2$ is required.

## 3.3 Remarks on the properties of SMI copolymer properties

DLS measurements show that the counterion changes the properties of the dissolved polymer. Smaller aggregates detected in DLS matched the sizes of structures detected in small angle scattering measurements made on beam lines I22 and B21. Fitting of the SAXS patterns does not show big structures, but highlights only the small structures since structures shown in DLS bigger than 300 nm size are out of the detection range.

Comparing the SAXS results with the DLS measurements, the DLS returns larger sizes for the polymer. This is in agreement with the fact that DLS measures the hydrodynamic radius of the particle in solution, whereas SAXS measures the unsolvated size of the particle. In the case of the ellipsoidal structures, though, DLS has a smaller size. This is again due to the way the instruments works: DLS analyses data on the assumption that the sample is made of spherical particles. The sizes are averaged over all the possible orientations. The rotational axis, for example, for $SMI_{1000}$ at 1 M $CaCl_2$ has a radius of 147 Å, so the overall size of this particle should be 147x2=294 Å= 29 nm. The smaller rotational axis though, is 14.7 Å. Due to the averaging over all the possible orientations, the size found with the DLS of 6 nm is not unrealistic. The same considerations hold for the $SMI_{2000}$ structures.

SAXS played a key role to resolve the structural change in the polymer conformation in solution. Similar to micelles and polyelectrolyte micelles reported in literature, a transition from a micelle/spherical structure to an elongated structure was observed. The neutralisation of the charge of the polymer was observed causing an increased hydrophobicity of the polymer. Precipitation of the polymers occurred at lower concentration of the salt for polymers with an increased hydrophobic to hydrophilic ratio, and for NaBr compared to NaCl due to the stronger binding of the bromide anion to the polymer.

## 3.4 SMI stabilised phospholipid nanodiscs

After the polymer behaviour was measured, nanodiscs made with $SMI_{1000}$, $SMI_{2000}$ and $SMI_{3000}$ were analysed, without any further purification, using DLS, SAXS and SANS. The procedure to make nanodiscs is reported in section 2.13.2.DLS was used as a preliminary characterisation to check the size of structures in solution, even though no structural analysis could be carried out. In order to compare results to previous works, the polymer to lipids composition has been kept the same throughout the thesis, unless stated otherwise at 1.5% wt of polymer and 0.5% wt of lipids. These concentrations were stated to be the optimal conditions to form nanodiscs in the literature [84][137].

### 3.4.1 DLS analysis

Similar to the characterisation carried out for polymer on its own, the electrostatic stabilisation of SMI-DMPC aggregates was investigated by changing the concentration of salt in the buffer solutions. DLS measurements for $SMI_{1000}$, $SMI_{2000}$ and $SMI_{3000}$ with DMPC lipids are reported in figure 3.6.

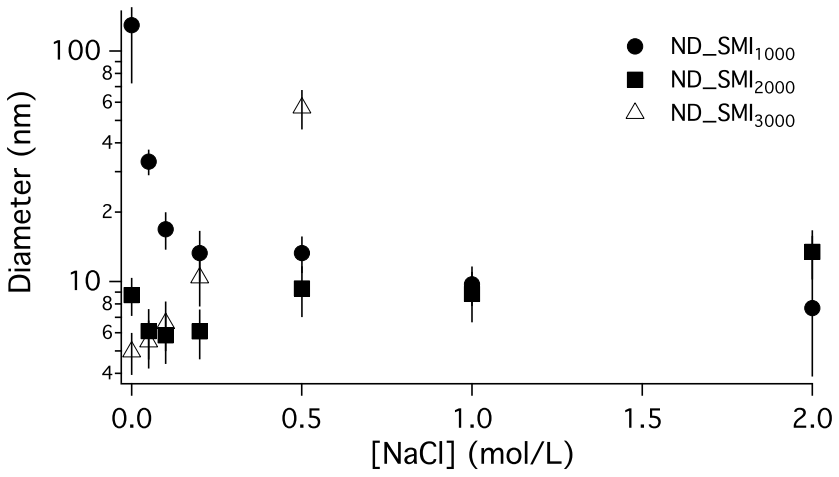


**Figure 3.6** Behaviour of SMI-lipids aggregates at different salt concentrations made with different polymers: $SMI_{1000}$ (dot), $SMI_{2000}$ (square) and $SMI_{3000}$ (triangle). The DMPC concentration was 0.5% wt and the solutions were prepared in 50 mM ABS at pH 5

DLS measurements show that the behaviour of lipid aggregates made with $SMI_{1000}$ and $SMI_{2000}$ differ from those made with $SMI_{3000}$. As figure 3.6 shows, increasing the salt concentration for aggregates made using $SMI_{1000}$ and $SMI_{2000}$ causes the sizes of the structures in solution to become smaller, up to a salt concentration of 0.2 for $SMI_{1000}$ and 0.1 M for $SMI_{2000}$. This is probably due to the screening effect of salt on the polymer, which gets to a saturation point where the aggregate size becomes constant. Looking at the aggregates made with $SMI_{3000}$ we have a different effect: this polymer shows increasing aggregate size with increasing salt concentration. The set of data reported for $SMI_{3000}$ goes up to a salt concentration of 0.2M NaCl because for higher concentration of the salt the solution became too viscous and was not suitable for DLS measurements. High viscosity, however, suggests that these solutions contined elongated or gel-like structures and not nanodiscs. Furthermore, aggregates made using $SMI_{3000}$ with DMPC were not stable in the fridge since the solution became a gel. This behaviour is probably due to the higher hydrophobicity of the polymer given the higher percentage of styrene present along the backbone, which leads the polymer to have a tendency to aggregate in aqueous solutions and to precipitate when salt is added (see section 3.2.2). For aggregates made using $SMI_{2000}$, however, the structures are stable for a salt concentration higher than 0.1M

The electrostatic contribution for nanodiscs stabilisation was checked by varying the salt concentration, using the same concentration of polymer as used for DLS measurements in section 3.2.2 and phospholipids. Co- and counter ions were changed as well along with the concentration of salt (figure 3.7).

The values of the diameter of the structures found with DLS are reported in table 3.8 along with the intensity percentage of the scattered light.

Unlike for polymer alone in solution, which showed an increasing size along with the salt concentration for the small structures, aggregates with DMPC decreased in size when $SMI_{1000}$ is used. Theoretical studies from Borisov *et al.* [124] showed a decreased size for the corona of micelles made of amphiphilic block co-polymers. As discussed for the polymer alone, this behaviour has been shown for micelles

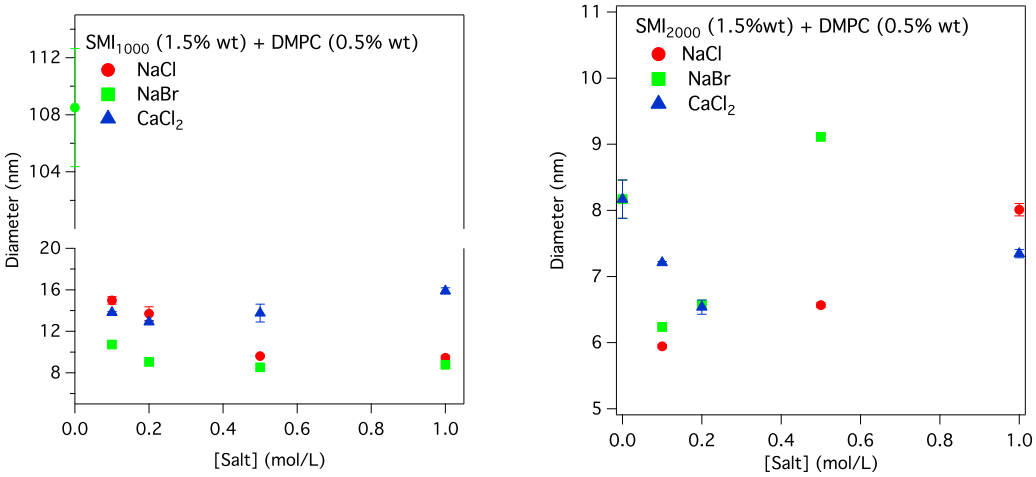


**(a)** $SMI_{1000}$ **(b)** $SMI_{2000}$

**Figure 3.7** Summary of DLS measurements carried out for (a) $SMI_{1000}$ and (b) $SMI_{2000}$ at 1.5%wt in ABS (pH=5, 50mM) with different salt concentration. Several salts were used: NaCl (red dot), NaBr (green square) and $CaCl_2$ (blue triangle). Error bars are calculated as standard deviation among three measurements

**Table 3.8** Summary of values found from DLS measuraments (figure 3.7)for structures made with $SMI_{1000}$ and $SMI_{2000}$ (ABS pH=5, 50mM, 0.5% wt) and different concentration of NaCl, NaBr, $CaCl_2$. (*) sample was not suitable for the analysis and was not measured

| | | NaCl | | NaBr | | $CaCl_2$ | |
|---|---|---|---|---|---|---|---|
| | | Diam. (nm) | Int (%) | Diam. (nm) | Int (%) | Diam. (nm) | Int. (%) |
| $SMI_{1000}$ | 0M | 158 ±12 | 98.1 | | | | |
| | 0.1M | 15.0±0.1 | 85.6 | 10.7±0.2 | 84.4 | 13.8±0.1 | 93.0 |
| | 0.2M | 13.7±1 | 68.7 | 9.1±0.2 | 85.7 | 12.9±0.1 | 91.7 |
| | 0.5M | 9.6±0.2 | 83.0 | 8.5±0.2 | 84.3 | 13.8±1 | 78.7 |
| | 1M | 9.4±0.1 | 88.7 | 8.8±0.3 | 98.1 | 15.9±0.2 | 95.1 |
| $SMI_{2000}$ | 0M | 7.9±0.3 | 79.4 | | | | |
| | 0.1M | 6.1±0.1 | 90.9 | 6.2±0.1 | 89.6 | 6.9±0.1 | 84.8 |
| | 0.2M | ±0.1 | 93.5 | 7.2±0.1 | 98 | 6.7±0.1 | 91.7 |
| | 0.5M | 7.2±0.1 | 97.3 | 10.6±0.1 | 99.6 | 11.1±0.3 | 92.4 |
| | 1M | 9.0±0.1 | 99.1 | gel | * | 8.0±0.5 | 96.9 |

made of small amphiphilic molecules and is claimed to be due to the neutralisation of charges among charged moieties. For the polymer stabilized DMPC aggregates, the hydrophobic effect among polymer chains is less effective due to

the stabilization of styrene moieties with the hydrophobic tails of the lipids. It is well established that the supramolecular aggregation of soft matter is a delicate balance of many effects. When the $SMI_{1000}$ is stabilised with DMPC, the reduced hydrophobic effect among styrene with the polymer chains allow the amine to behave more like a micelle and to decrease in size when salt is added. Similar to what is observed for the polymer, NaBr has the greatest effect on the structure. The structures made with $SMI_{2000}$ show a different behaviour compared to $SMI_{1000}$. This polymer behave more like the polymer alone. As will be shown in section 3.4.2, this is likely to be due to the fact that the polymer makes a thicker belt around the core of the lipids. The thicker belt suggests that the polymer interacts less effectively with the lipid tails, and a similar behaviour for the polymer alone in solution is detected. However, it is interesting to note the trend of $SMI_{2000}$ in the presence of $CaCl_2$. The decreasing size could be due the fact that the actual concentrations of counter ions are double with respect to that of NaCl. The increased hydrophobicity of the polymer due to the neutralisation of charges can lead the polymer to interact more strongly with the DMPC tails and the remaining hydrophilic portion of polymer that does not interact with the tails behaves like $SMI_{1000}$. Even though speculations can be made, more in-depth studies must be carried out in order to understand the properties of this system in terms of the special arrangement of polymer and DMPC lipid.

### 3.4.2 Small angle scattering analysis

Even though DLS is useful to analyse rapidly the size of structures in solution, it does not allow a structural analysis to demonstrate that the structures formed are discs. For this purpose Small Angle Scattering (SAS) experiments were carried out. As discussed in section 2.13.2, nanodiscs were run without any further purification, or after gel filtration to remove free polymer from the solution. Gel filtration patterns for nanodiscs made with either $SMI_{1000}$ and $SMI_{2000}$ are reported in figure 3.8

For the gel filtered sample, a polydisperse bicelle model (see section 2.6.2) was

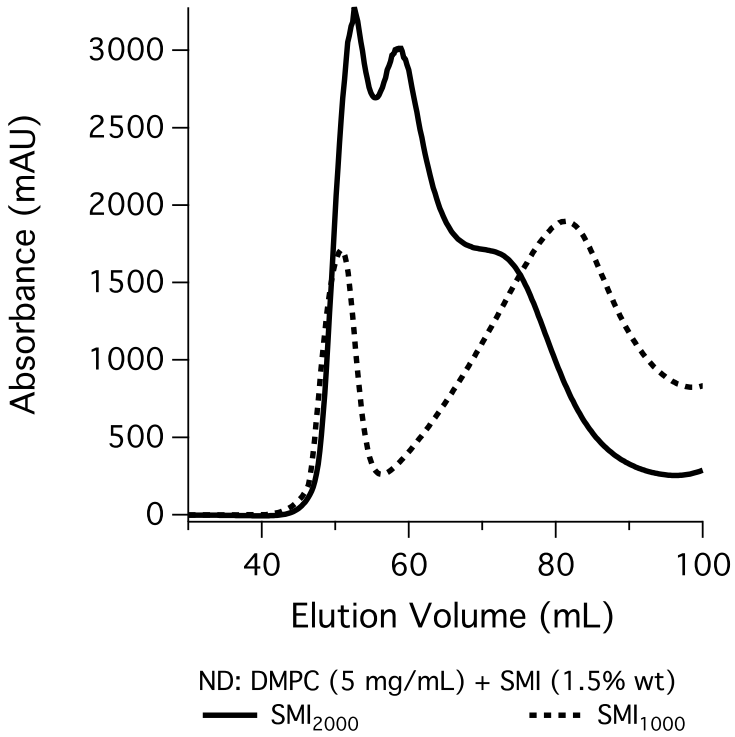


**Figure 3.8** Gel Filtartion for $SMI_{1000}$ (dotted line) and $SMI_{2000}$ (solid line).

used to fit the data, whereas for samples which had not been purified to remove the free polymer, two models were summed together to fit this scattering data. This is because in subsequent gel filtration measurements, free polymer was detected in solution. Therefore one model is used to represent the nanodisc, using the polydisperse bicelle model, whereas, either an ellipsoid or a sphere is used to model the free polymer remaining in solution. For a discussion on the mathematical models used please see sections 2.6.1 and 2.6.2. By plotting the two different models separately and summing the result, it is possible to observe that the polymer pattern (sphere or ellipsoid) forms the background of the scattering pattern (dashed line). The dotted line, instead, represents the polydisperse bicelle, which models the nanodiscs in solution. This pattern presents a fringe around $0.1\text{Å}^{-1}$. This fringe arises from the contrast of the phospholipid heads with the surrounding solvent. Figure 3.9 shows that the position of the fringe

is not altered by the polymer model which acts as a background, increasing the signal at low Q. 3.9

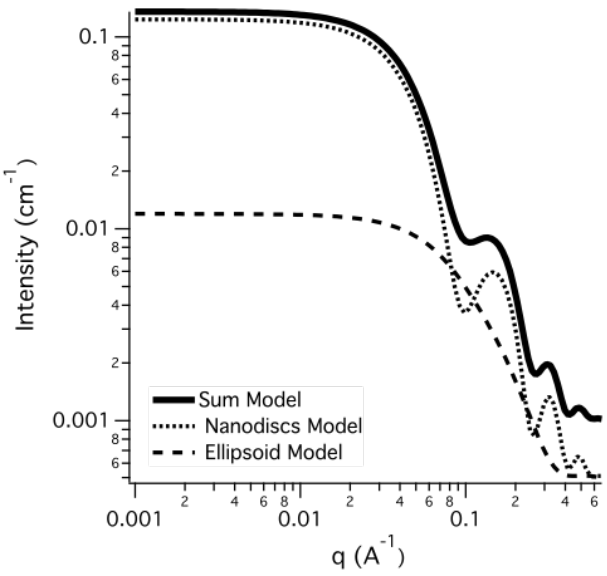


**Figure 3.9** Separated pattern of an ellipsoid (dashed line), a nanodisc (dotted line) and Sum model (black line)

From figure 3.9 it is clear that the fringe from the scattering pattern is due to the polydisperse bicelle model, whereas the polymer scattering acts as a background. Due to the large number of parameters, the polymer data were not fitted, but were fixed to correspond to that of the polymer-only scattering data obtained during the same experiment at the same salt and polymer concentration (1.5% wt of polymer at different salt concentration) as reported above. The SLDs of the polymers are reported in table 3.4 and were held during the fitting. The salt concentration was held fixed during the fitting and was calculated as mentioned in section 3.2.3, as a sum of all the salt in solution. The thickness of the DMPC bilayer and lipid heads were fixed at 28 and 8 Å respectively (values from [138]). The incoherent background was obtained from the high Q data where the intensity had plateaued.

From the gel filtration patterns in figure 3.8 it can be deduced that the nanodiscs made with $SMI_{2000}$ are smaller than the nanodiscs made with $SMI_{1000}$ . In fact the first peak, which is the one collected and analysed in SAXS and SANS, for $SMI_{1000}$

has a shorter retention time, which is associated with bigger structures. DLS results for $SMI_{1000}$ and $SMI_{2000}$ showed similar behaviour, with bigger structures formed when $SMI_{1000}$ is used to make nanodiscs (figure 3.6). Comparing values of structures made with $SMI_{1000}$ with the one reported in literature for nanodiscs made using the SMA commercial copolymer SMA 2000P, the $SMI_{1000}$-DMPC structures are slightly bigger in size. The diameter for nanodiscs made from $SMI_{1000}$ is 12.5nm whereas for SMA2000P it was found to be 9.6 nm from DLS. It can be speculated that the higher hydrophilicity of $SMI_{1000}$ compared to $SMI_{2000}$ makes the polymer more elongated in solution and then more available to wrap around a larger amount of lipids.

### Salt concentration effect

In order to check the electrostatic stabilisation of the system, nanodiscs were studied at different salt concentration in the presence of different co and counter ions. In the case of purified samples using gel filtration, the concentration of the salt is exchanged through a dialysis process. The concentration of the salt was varied between 0M to 1M of NaCl for either nanodiscs made with $SMI_{1000}$ or $SMI_{2000}$ .

- $SMI_{1000}$ Figure 3.10 reports scattering patterns acquired for $SMI_{1000}$ on I22 (SAXS instrument at Diamond) and D11 (SANS instrument at ILL) for nanodiscs made using $SMI_{1000}$ at pH5 and 0.2M of NaCl. The sample was purified using gel filtration. The first peak from the gel filtration (figure 3.8) was analysed using both SANS and SAXS. In order to fit the nanodiscs made with $SMI_{1000}$, SANS data from a sample made with h-DMPC in d-ABS and h-DMCP in 36% ABS were co-refined. Values obtained for this fitting were used then to fit SAXS data. Scattering patterns and values for the fitting of these samples are reported in figure 3.10 and table 3.9, respectivelly.

  Co-refined SANS parameters were used to fit the SAXS pattern (both SANS and SAXS were run on the same sample). Certain parameters were fixed,

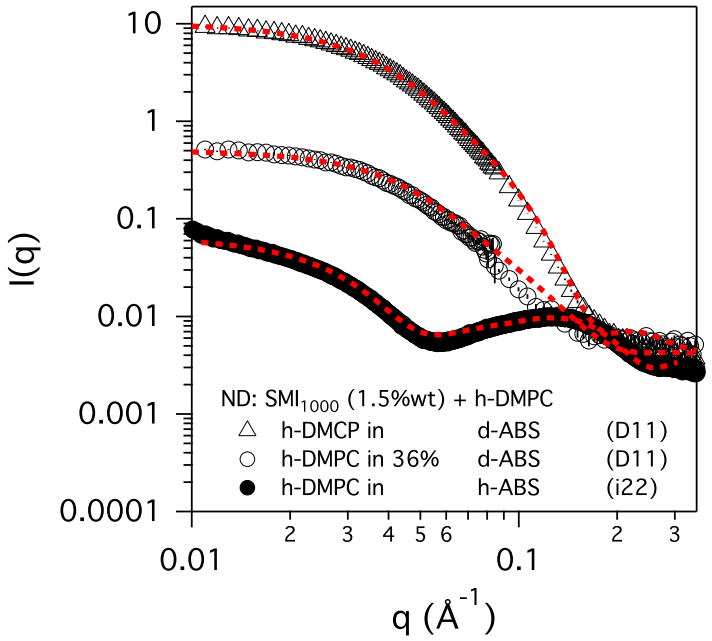


**Figure 3.10** Scattering pattern from ILL (circle and triangle) and from i22 (full circle).

**Table 3.9** Fitting parameters from corefined data get from D11 and I22 for purified nanodiscs made with $SMI_{1000}$ initial concentration of (1.5% wt) and DMPC (0.5% wt)

| | SANS/SAXS |
|---|---|
| Radius (Å) | 42 ± 2 |
| PDI | 0.26 ± 0.2 |
| Belt Thick. (Å) | 23 ± 3 |
| mol. frac. $H_2O_{rim}$ | 0.57 ± 0.1 |
| Overall Size (nm) | 13 ± 1 |

as reported in table 3.9, and yet the SAXS data could not be fitted. (This fitting is reported in figure A.2 in section A.1). In order to obtain a good fit, the SLD of the face had to be allowed to change and resulted in the SLD becoming 1.35x10$^{-5}$ Å$^{-2}$. The SLD for a "dry" phosphatidylcholine group is calculated to be 1.6x10$^{-5}$ Å$^{-2}$. This value is obtained by accounting for a molecular volume of the head of 281 Å$^3$ [138]. In the case of 57% water content [139], the SLD for the hydrated face is calculated to be 1.2x10$^{-5}$ Å$^{-2}$. The higher value found for the SLD of the face in the $SMI_{1000}$ nanodiscs is likely to be due to an increased electron density in the headgroup

region of the bilayer due to polymer penetration into the headgroups of the phospholipids. The penetration of the polymer was not found for SMA copolymers. This configuration, with the polymer inserted into the head group, could be due to the higher mobility of the tertiary amine compared to the maleic acid.

Several salt concentrations were run for nanodiscs made with $SMI_{1000}$, either with SANS or SAXS. Due to the large number of parameters of the model used, the polydisperse core shell bicelle, as many of the parameters as possible were held during the fitting. It was assumed that the core size does not change and so it was held at 42 Å(the value found from the core-fined fitting reported in table 3.9). The thickness of the belt was allowed to change assuming that for higher salt concentration of salt a charge screening effect occurred which led to changes in the size of the belt. The hydration of the rim was fitted as well. SAXS patterns and their fitting are reported in figure 3.11 and table 3.10 respectively.

**Table 3.10** Parameters for the fitting reported in figure 3.11 of purified nanodiscs made with $SMI_{1000}$ initial concentration of (1.5% wt) and DMPC (0.5% wt) in 50 mM ABS at pH=5

| [NaCl] | 0 | 0.05M | 0.1M | 0.2M | 0.5M | 1M | 2M |
|---|---|---|---|---|---|---|---|
| Mean Core (Å) | 43.2 ± 1 | 43.2 | 43.2 ± 1 | 43.2 ± 1 | 43.2 ± 1 | 42.0 ± 1 | 42.0 ± 1 |
| PDI | 0.3 ±0.1 | 0.3 ±0.1 | 0.3 ±0.1 | 0.2 ±0.1 | 0.3 ±0.1 | 0.3 ±0.1 | 0.5 ±0.2 |
| Belt Thick. (Å) | 14.0 ± 1 | 13.9 ± 1 | 13.5 ± 1 | 12.7 ± 1 | 12.0 ± 1 | 15.06 ± 1 | 32.5 ± 1 |
| $SLD_{face}$ ($x10^{-5}$) | 1.40 ±0.1 | 1.41 ±0.1 | 1.40 ±0.1 | 1.38 ±0.1 | 1.36 ±0.1 | 1.34 ±0.1 | 1.30 ±0.1 |
| mol. frac. $H_2O$ | 0.64 ±0.2 | 0.59 ±0.1 | 0.64 ±0.1 | 0.64 ±0.1 | 0.74 ±0.2 | 0.53 ±0.1 | 0.43 ±0.1 |

Looking at the thickness of the polymer belt, it decreases in size with increasing salt concentration up to 0.5 M. After this concentration, the polymer belt increases in size. A decreasing trend was matched by DLS as well. This is probably due to a screening of the charge that makes the

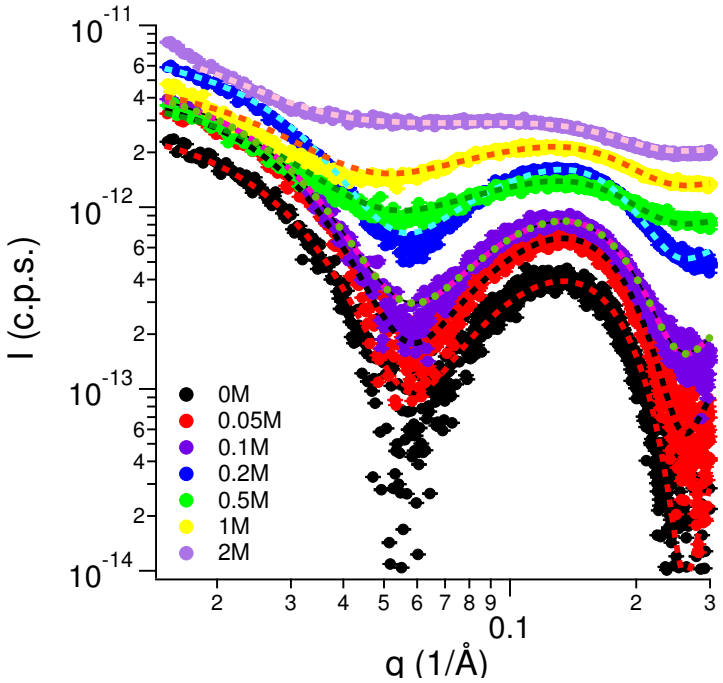


**Figure 3.11** Scattering pattern acquired on B21, beamline at Diamond Light Source. Samples are made up using $SMI_{1000}$ at 1.5% wt and using DMPC at 0.5% wt in 50 mM ABS at pH=5 fro different NaCl concentrations. Samples were purified using gel filtration and salt concentration was adjusted through dialysis. Values from fitting are reported in table 3.10

polymer more neutral, the repulsive electrostatic interactions among positive monomers are therefore less strong and the structure tends to collapse. This effect has been widely validated in the scientific community for polyelectrolytes either from a theoretical perspective [140, 141] or from experimental results [142]. Samples were also analysed using SANS (figure 3.12). For the samples made for B21 reported in figure 3.11, the salt concentration was changed through dialysis.

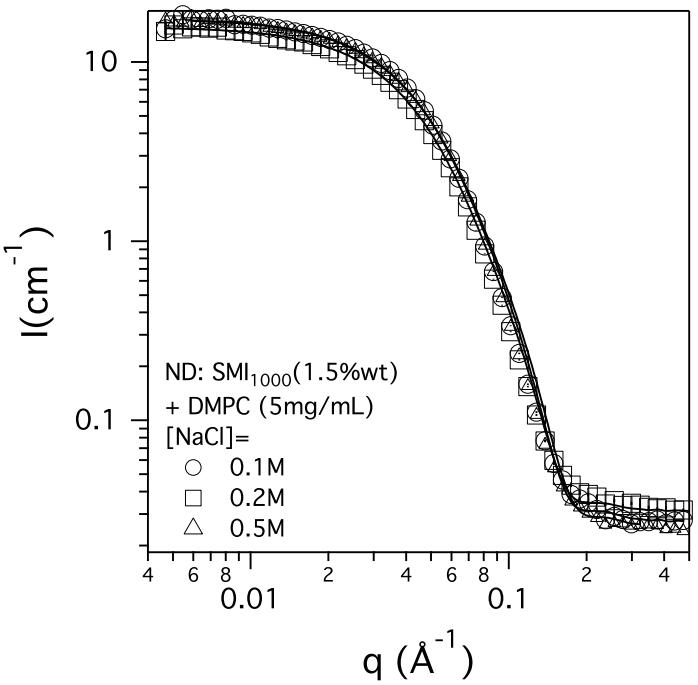


**Figure 3.12** SANS pattern acquired in SANS2d for purified nanodiscs made using $SMI_{1000}$ with standard concentration (1.5%wt of $SMI_{1000}$ and 0.5% wt of h-DMPC in 50 mM d-ABS at pH=5) and different salt concentration.

**Table 3.11** Fitting parameters for SANS pattern from figure 3.12 for purified nanodiscs made using $SMI_{1000}$ and 0.5% w of DMPC.

| | 0.1M | 0.2M | 0.5M |
|---|---|---|---|
| Mean Core (Å) | 41 ± 1 | 41.0 ± 1 | 41 ± 1 |
| PDI | 0.3 ± 0.1 | 0.3 ±0.1 | 0.3 ± 0.1 |
| Belt Thickness (Å) | 19 ± 3 | 18 ± 3 | 18 ± 3 |
| % $H_2O_{belt}$ | 0.3 ± 0.1 | 0.4 ± 0.1 | 0.4 ± 0.1 |

A slightly different radius and belt thickness are found for the samples analysed with SANS(figure 3.12) and SAXS (figure 3.11) and for belt thickness. Even though changes in absolute values for the belt thickness, the rim thickness and the hydration of the belt can be due to the preparation of a new sample, the same trend is observed. The belt thickness decreases with increasing salt concentration, along with the hydration of the belt. When a lower concentration of the salt is present in solution, fewer maleimide groups are neutralised. The charged groups on the backbone of the polymer allow intermolecular hydrogen bonding between the polymer and molecules of water, which increases the hydration of the rim. Unlike SAXS data, the penetration of the polymer into the head group was not detected in SANS because the SLDs of the polymer and the head group are not much different from each other (1.96x$10^{-6}$ $Å^{-2}$and 1.9x$10^{-6}$ $Å^{-2}$respectively). SANS is not sensitive to higher electron density as is the case for SAXS.

The effect of co- ions was also analysed using SANS for nanodiscs made using $SMI_{1000}$. Figure 3.13 shows the SANS pattern acquired at SANS2d for purified samples. Standard concentrations of polymer and phospholipid were used. Instead of using NaCl, $CaCl_2$ was used. In order to be sure that the values arising from the data collected for NaCl were suitable for fitting data from a different salt, two contrast were run for nanodiscs made using $CaCl_2$. For the fitting of this data set the parameters from the co-refined data in table 3.9 were used as initial estimate of the fitting parameters.

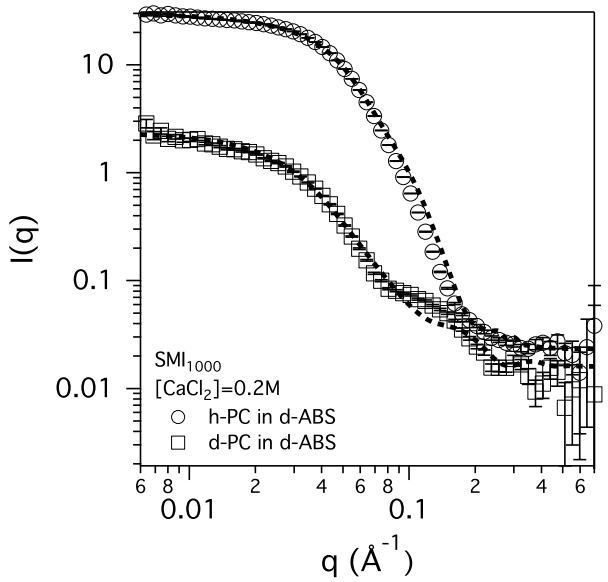


**Figure 3.13** SANS2d patterns acquired for purified nanodiscs made with standard concentration of DMPC and polymer and $CaCl_2$ 0.2M in 50 mM ABS at pH=5

**Table 3.12** Main parameters for the fitting reported in figure 3.13.

| | $[CaCl_2]$= 0.2M |
|---|---|
| Mean Core (Å) | 42 ± 1 |
| PDI | 0.3 ± 0.1 |
| Belt Thickness (Å) | 24.0 ± 1 |
| % $H_2O_{belt}$ | 0.7 ± 0.2 |

Since no dramatic changes were detected between the purified samples at different salt concentrations of NaCl or $CaCl_2$, the concentration of the several different kinds of salt were also measured at 0.2M (figure 3.14).

In the same manner as for the other fitting, the core radius was kept constant and just the hydration of the rim, the belt thickness and the PDI was allowed to change. From this fitting, it is obvious that no huge change occurs upon the addition of different salts. Values for the fitting are reported in table 3.13

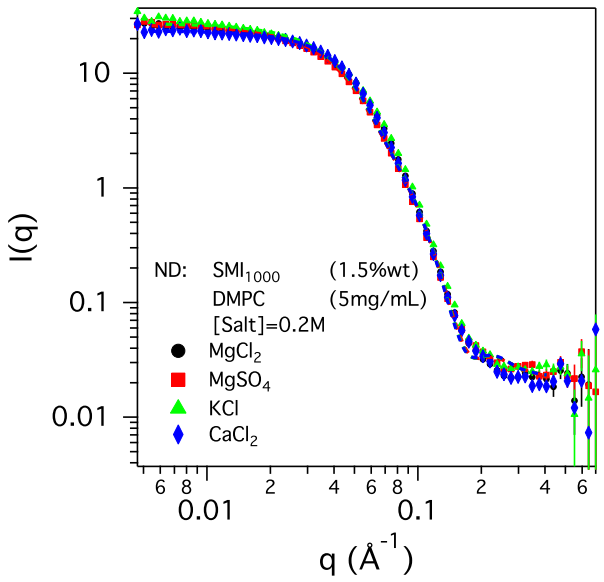


**Figure 3.14** SANS2d scattering patterns for nanodiscs made using $SMI_{1000}$ . Samples were purified using gel filtration and buffer was exchanged with 50mM ABS at pH=5 containing $MgCl_2$ (black circle), $MgSO_4$ (red square), KCl (green triangles) and $CaCl_2$ (blue diamond)

**Table 3.13** Fitting parameters for SANS pattern from figure 3.14 for purified nanodiscs made using $SMI_{1000}$ and 0.5% wt of DMPC in 50 mM ABS at pH=5 containing different salts at 0.2M.

| | $MgCl_4$ | $MgSO_4$ | KCl |
|---|---|---|---|
| Mean Core (Å) | 42 ± 2 | 42.0 ± 1 | 42 ± 1 |
| PDI | 0.3 ± 0.1 | 0.3 ±0.1 | 0.3 ± 0.1 |
| Belt Thickness (Å) | 23 ± 1 | 23 ± 4 | 23.2 ± 4 |
| mol. frac. $H_2O_{belt}$ | 0.6 ± 0.1 | 0.7 ± 0.1 | 0.6 ± 0.1 |

The stability of nanodiscs made using $SMI_{1000}$ in the presence of divalent cations make them suitable for the extraction of protein such as calmodulin or kinase C which requires the presence of calcium to keep their functional structures [143, 144].

- $SMI_{2000}$

  The same procedure as above was used to fit data collected for nanodiscs made with $SMI_{2000}$. Both from the DLS or gel filtration patterns, it is clear that the nanodiscs made with $SMI_{2000}$ are much smaller than the nanodiscs made using $SMI_{1000}$. In fact, the second peak from gel filtration for nanodiscs, which is the one analysed in SAXS and SANS, is eluted at a higher volume, which points to smaller sized structures.

  Nanodiscs purified with gel filtration were analysed using SAXS and SANS at I22 (figure 3.15) and SANS2d, respectively (3.15b) . The SLD for the polymer was calculated and held (values in table 3.4) as well as the dielectric constant, and the face and core thicknesses for the polydisperse core shell bicelle model. Fitted parameters are reported in table 3.14

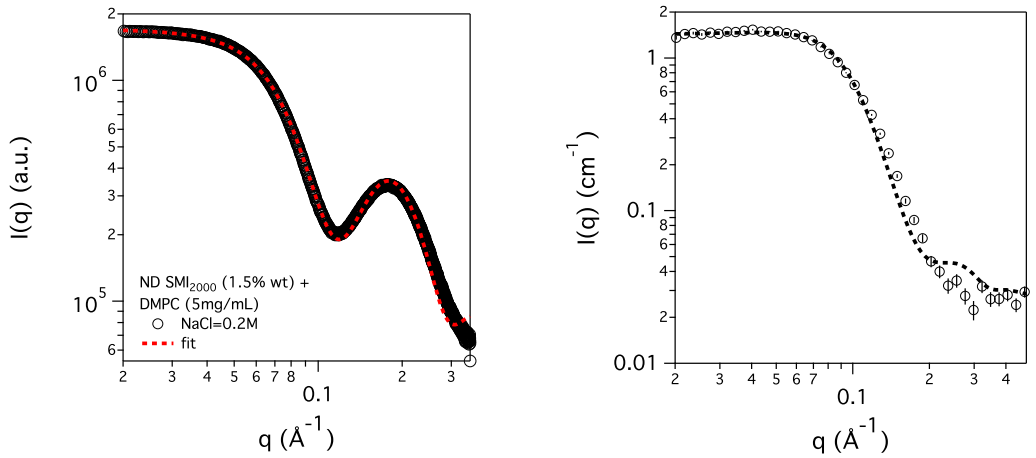


**(a)** SAXS **(b)** SANS

**Figure 3.15** (a) SAXS and (b) SANS patterns acquired on I22 and SANS2d for purified nanodiscs made using $SMI_{2000}$ and DMPC (0.5% wt intial concentration).

Gel filtration patterns (figure 3.8) also show moreover that not much poly-

**Table 3.14** Parameters for fitting reported in figure 3.15 for purified nanodiscs made using $SMI_{2000}$ at 1.5% wt of initial concentration and 0.5% wt of DMPC in 50 mM ABS at pH=5, NaCl=0.2M. Experimental and fitting patterns are reported in figure

| Parameters | Values |
|---|---|
| Core Size (Å) | 8.4 ± 1 |
| Belt Thick. (Å) | 17.4 ± 1 |
| mol.frac. $H_2O_{rim}$ | 0.53 ± 0.1 |
| Overall Size (nm) | 5.2 ± 2 |

mer is left in solution after the sample is run through a column, compared to the sample made using $SMI_{1000}$. This was verified as well from the comparison of SAXS pattern acquired for the same sample before and after the gel filtration (figure 3.16). Therefore it was possible to fit data from LOQ to a simple polydisperse core shell model, even though no purification was performed on those samples (figure 3.17).

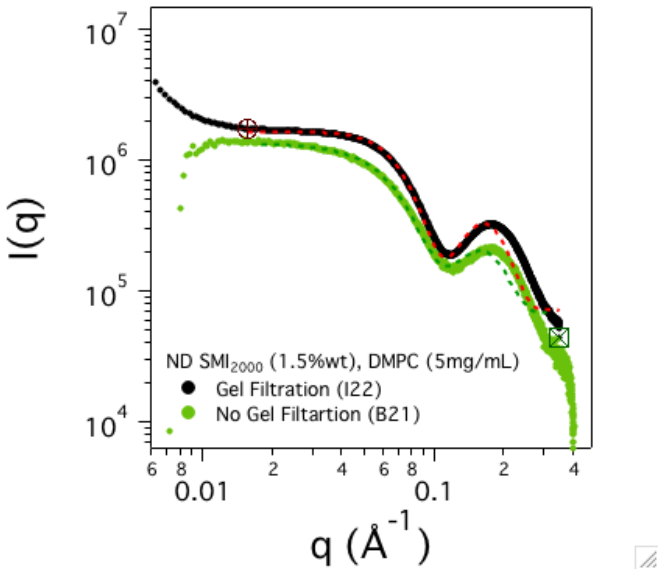


**Figure 3.16** SAXS pattern acquired on I22 for nanodiscs made using $SMI_{2000}$ before (green) and after (black) gel filtration.

The nanodiscs were made in the same way as used for the B21 sample preparation. A SANS analysis was done on the as-made samples using LOQ, in ISIS. Scattering patterns were taken with a q range of between

0.008 and 0.3 $Å^{-1}$. The standard concentration of 1.5% wt of polymer and 0.5% wt of DMPC was used for this experiment in 50 mM ABS at pH=5.

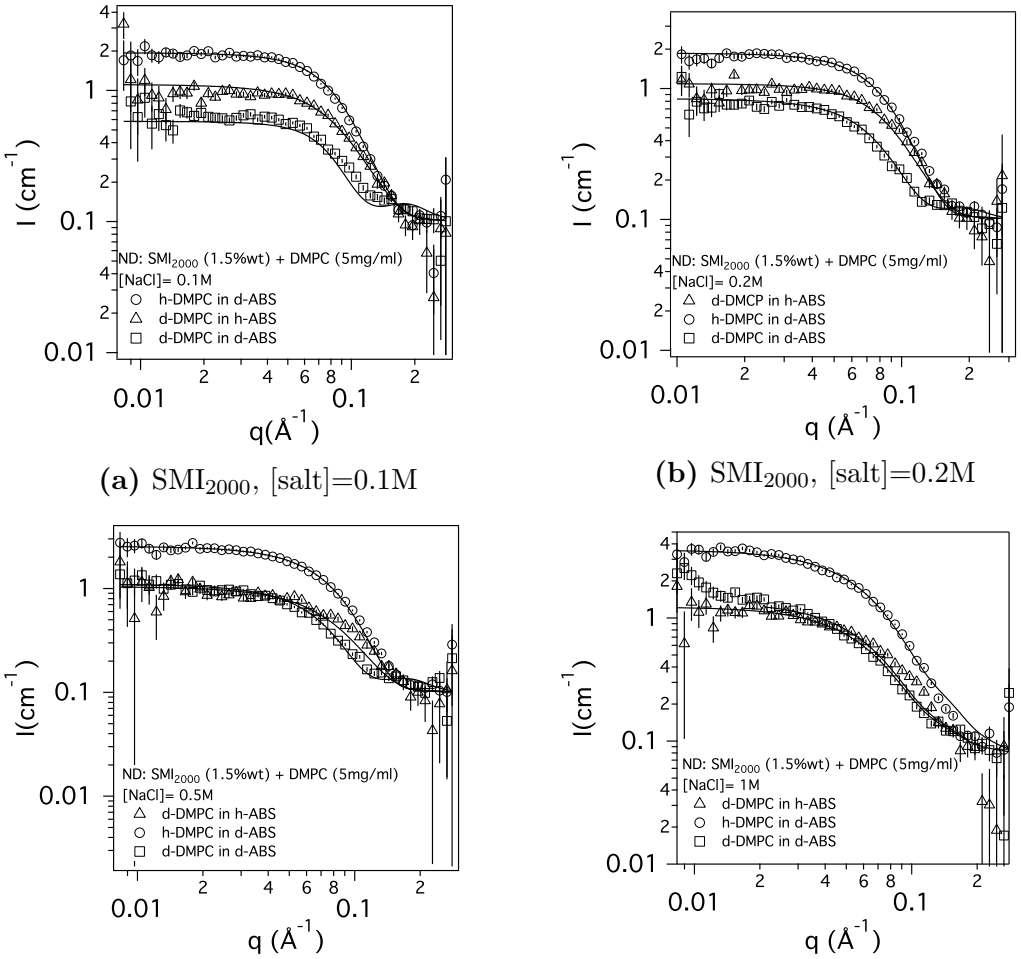


**(a)** $SMI_{2000}$, [salt]=0.1M **(b)** $SMI_{2000}$, [salt]=0.2M

**(c)** $SMI_{2000}$, [salt]=0.5M **(d)** $SMI_{2000}$, [salt]=1M

**Figure 3.17** Scattering patterns taken on LOQ for nanodiscs made using $SMI_{2000}$(1.5%wt) and DMPC (0.5% wt) at different salt concentrations dissolved in an 50 mM ABS, pH=5.

Figure 3.17 shows the scattering patterns for nanodiscs made using the same procedure as the nanodiscs that were made for SAXS samples and DLS. It is possible to get a reasonable fit for the nanodiscs made at low salt concentrations, up to 0.1M salt. However, for nanodiscs that were not purified, it is possible to see a variation in the contrast intensity for d-DMPC in d-ABS, especially when the salt concentration of the salt is increased up to 0.5M in NaCl.

Increasing the salt concentration, figure 3.17, shows that the intensity at the intercept increases for the contrast d-DMPC in d-ABS. This intensity increases from 0.06 $cm^{-1}$ for a salt concentration of 0.1 M to 1 $cm^{-1}$ for a salt concentration of 0.5 M. For a concentration of 1M NaCl, the patterns of d-DMPC in d-ABS and d-DMPC in h-ABS almost overlapped. This is a sign of a variation of the SLD of the core, due probably to a higher insertion of the polymer into the lipid tails. In fact, increasing the salt concentration causes a neutralization of the charge of the polymers, which leads to a lower solubility. This higher hydrophobicity of the polymer will result in a higher affinity for the tails, rather than for water. This hypothesis is supported by the behaviour of the solutions: when the salt concentration is too high precipitation takes place. In figure 3.17(d), it is possible to see aggregation at low Q. Data for this sample were fitted using an ellipsoid, rather than the polydisperse core shell bicelle model. For this fitting, an average SLD of the aggregate was used to fit the data and it was calculated to be $4.58x10^{-6}$ and $7.8x10^{-7}$ for structures made using d-DMPC and h-DMPC, respectively. Results from the fitting for SAXS and SANS are reported in table 3.15

Comparing the SAXS and SANS results with preliminary DLS analysis on page 82 in table3.8, a smaller size is reported for the first two experimental techniques. This is not a surprise since the DLS measurements report the hydrodynamic radius of the particle, which is affected by the solvation shell and the ionic strength of the solution.

**Table 3.15** Parameters for fitting for B21 and LoQ data, acquired for $SMI_{2000}$. Samples are made up at 1.5%wt of polymer and 0.5% wt of DMPC

| | 0.1M | | 0.2M | | 0.5M | |
|---|---|---|---|---|---|---|
| | LoQ | B21 | LoQ | B21 | LoQ | B21 |
| Mean Core (Å) | 12±1 | 13±1 | 9±1 | 9±1 | 12±1 | 11±1 |
| PDI | 0.4±0.1 | 0.2±0.1 | 0.4 ±0.1 | 0.2±0.1 | 0.4±0.1 | 0.4±0.1 |
| Belt thickness | 10±1 | 9±1 | 14±1 | 15±1 | 14±1 | 8±1 |
| mol frac $H_2O$ in rim | 0.41±0.1 | 0.82±0.1 | 0.4±0.1 | 0.4±0.1 | 0.4±0.1 | 0.8±0.1 |

Similar to the experiment undertaken with nanodiscs made using $SMI_{1000}$, the stability of nanodiscs made with $SMI_{2000}$ in the presence of divalent cation was also checked. Figure 3.18 revel that the structure of the disc does not change dramatically.

The structural stability of SMI discs in the presence of divalent cation is crucial for the biological applications for these nanodiscs.

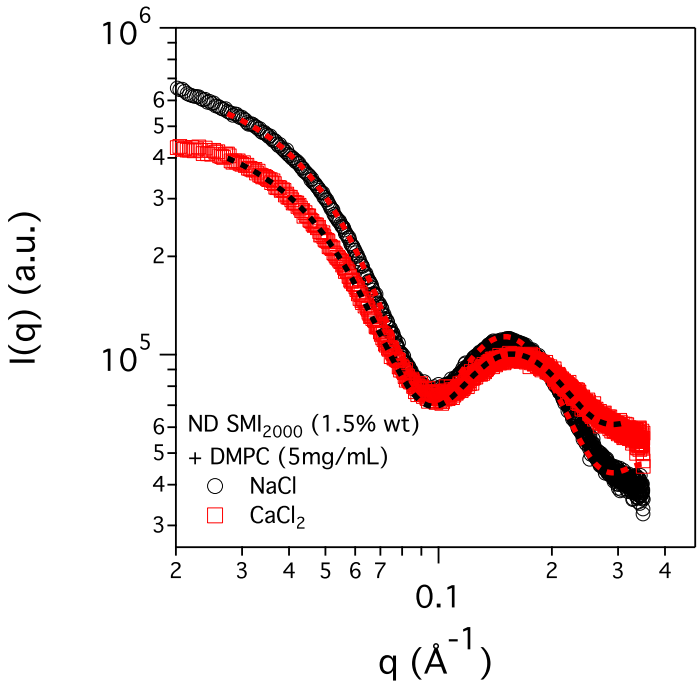


**Figure 3.18** SAXS pattern acquired on i22 for purified nanodiscs made using $SMI_{2000}$ and DMPC ( 0.5% wt intial concentration) at (red) 0.2M $CaCl_2$ and (black) 0.2M NaCl.

In order to understand the differences in the size of nanodiscs using $SMI_{1000}$ and $SMI_{2000}$, surface tension measurements were carried out for both of them. For this purpose a 0.5% wt solution of the polymer was made up. The values found were 47.3 and 40.5 mN/m for $SMI_{1000}$ and $SMI_{2000}$, respectively. The lower surface tension for $SMI_{2000}$ shows a higher affinity for the polymer to be at the air-water interface. This result is expected due the higher hydrophobic to hydrophilic ratio for $SMI_{2000}$. The surface tension for $SMI_{1000}$ and $SMI_{2000}$ were compared to the value found for SMA2000P [84] at the same polymer concentration of 38.5 mN. The size found from DLS at the same concentration of DMPC for those 3 polymers are reported in table 3.16 with the relative surface tension.

**Table 3.16** Comparison of purified nanodiscs in buffer at 50mM strength and 0.2 M NaCl

| | Size (nm) | Size Core (nm) | Size Belt (nm) | Surface tension (mN/m) |
|---|---|---|---|---|
| $SMI_{1000}$ | 10±1 | 4.2± 0.2 | 1.9±0.1 | 47.3 |
| $SMI_{2000}$ | 5.2±1 | 1.0±0.2 | 1.7±0.1 | 40.5 |
| SMA2000P | 8±1 | 3.8±0.2 | 1.1±0.1 | 38.5 |

$SMI_{1000}$ and SMA2000P make nanodiscs with comparable size. The core is found to be of approximately the same size. Nanodiscs made with $SMI_{2000}$ are much smaller than those found for $SMI_{1000}$ and SMA2000P which could be due to the fact that, as SAXS has shown for polymer alone, this polymer makes smaller micelles.

### Lipid concentration variation

From previous experimental analysis [84], the size of the commercial copolymer did not change the size of the nanodiscs in a logical manner. However, changing the amount of lipids caused the nanodiscs size to change. [42]
The ratio of phospholipids to SMI polymer was therefore varied by changing the concentration of DMPC used to make the nanodiscs and keeping the concentration of the polymer constant. The solution was made up in the same way is explained in section 2.13.2 but the final concentration of DMPC was changed to 0.3, 0.5 and 0.7% wt. The scattering patterns from these solutions collected at B21 (Diamond - Rutherford Appleton Laboratory) are reported in Appendix (figure A.3 and figure A.4 for nanodiscs made with $SMI_{1000}$ and $SMI_{2000}$ respectively). The fitting of the curves was done using a sum of the polydisperse bicelle with an ellipsoid model (a detailed description is given in section 3.4.2). Values for the ellipsoid model were obtained from previously fitting of the data for the polymer above at the same salt concentration. When the polymer was fitted to a sphere, the rotational axis and the main axis of the ellipsoid were kept at the same value as the radius of the sphere. The initial values for the fitting was obtained from the fitting of data for purified nanodiscs for $SMI_{1000}$ and $SMI_{2000}$. Keeping these values constant, the ratio between the nanodiscs and the polymer was allowed to change. At this point the size of the free polymer ,modelled with an ellipsoid, was allowed to change with the assumption that with a smaller amount of polymer in solution (since some is in the nanodiscs) the structure decreases in size. The values obtained were reasonable and the size of the polymer increased with a decreasing nanodisc to polymer ratio. This is consistent with the assumption made that a smaller ratio of nanodiscs to polymer indicates more polymer in solution. After adjusting the ratio and size of the polymer, the radius and the belt thickness of the nanodiscs were allowed to change. A summary of the fitting is reported in table 3.17 for nanodiscs made with $SMI_{1000}$ and table 3.18 for nanodiscs made with $SMI_{2000}$. Figure 3.19 shows the size of the radius, the belt thickness and the overall size of discs for $SMI_{1000}$ and $SMI_{2000}$versus the

lipid composition.

**Table 3.17** Fitting parameters for nanodiscs made with $SMI_{1000}$ at different salt and DMPC concnetration. All the samples were made in ABS, 50mM, pH=5.

| | 3 mg/mL | 5 mg/mL | 7 mg/mL |
|---|---|---|---|
| | | [NaCl] = 0.1M | |
| Radius (Å) | 35.9±2 | 38.6±2 | 40.9±2 |
| Belt (Å) | 8.7±2 | 8.8±2 | 8.8±2 |
| Overall Size (Å) | 89.4±4 | 94.7±4 | 99.2±4 |
| Ratio ND/pol | 2.2 | 0.8 | 1.2 |
| | | [NaCl] = 0.2M | |
| Radius (Å) | 31.4±2 | 31.4±2 | 40.2±2 |
| Belt (Å) | 13.8±2 | 13.8±2 | 15±2 |
| Overall Size (Å) | 90.3±4 | 90.3±4 | 11.4±4 |
| Ratio ND/pol | 0.7 | 1 | 1.1 |
| | | [NaCl] = 0.5M | |
| Radius (Å) | 28.4±2 | 29.8±2 | 35±2 |
| Belt (Å) | 14.1±2 | 14.7±2 | 14.8±2 |
| Overall Size (Å) | 85.0±4 | 89.0±4 | 99.6±4 |
| Ratio ND/pol | 1.2 | 1.7 | 1.6 |

**Table 3.18** Fitting parameters for nanodiscs made with $SMI_{2000}$ at different salt and DMPC concnetration. All the samples were made in ABS, 50mM, pH=5.

| | 3 mg/mL | 5 mg/mL | 7 mg/mL |
|---|---|---|---|
| | | [NaCl] = 0.1M | |
| Radius (Å) | 6.2±2 | 8.9±2 | 12.3±2 |
| Belt (Å) | 11.3±2 | 16.5±2 | 16.5±2 |
| Overall Size (Å) | 35.1±4 | 50.7±4 | 57.5±4 |
| Ratio ND/pol | 8.0 | 3.0 | 3.2 |
| | | [NaCl] = 0.2M | |
| Radius (Å) | 6.6±2 | 9.7±2 | 11.7±2 |
| Belt (Å) | 16.8±2 | 18.0±2 | 16.1±2 |
| Overall Size (Å) | 46.8±4 | 55.4±4 | 55.7±4 |
| Ratio ND/pol | 2.4 | 4.2 | 4.0 |
| | | [NaCl] = 0.5M | |
| Radius (Å) | 8.3±2 | 10.2±2 | 13.3±2 |
| Belt (Å) | 20.7±2 | 18.8±2 | 17.3±2 |
| Overall Size (Å) | 58.0±4 | 58.0±4 | 61.2±4 |
| Ratio ND/pol | 2.3 | 5.6 | 7.7 |

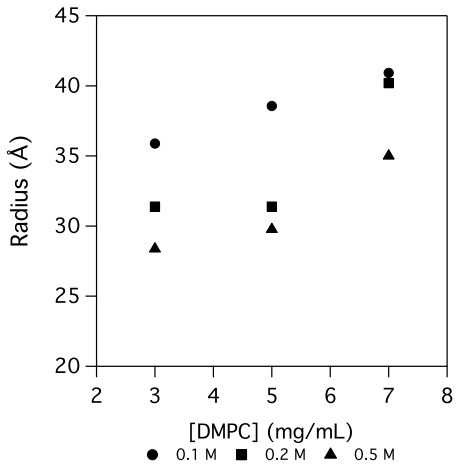


**(a)**

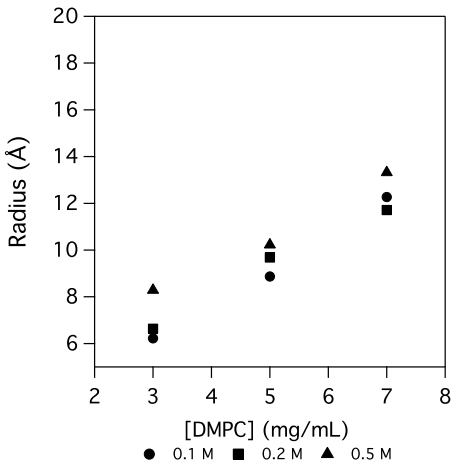


**(b)**

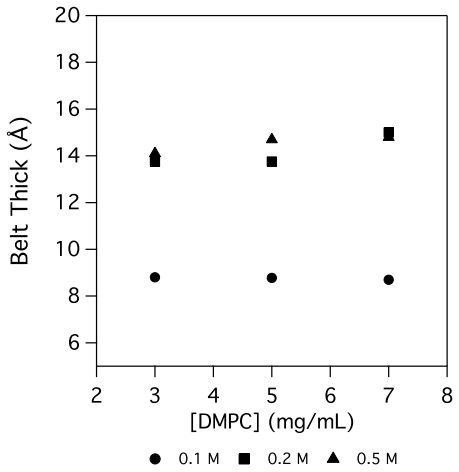


**(c)**

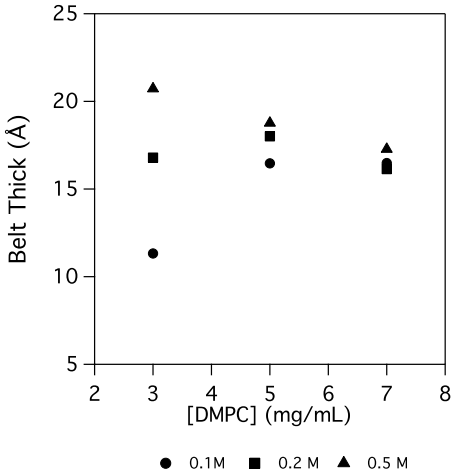


**(d)**

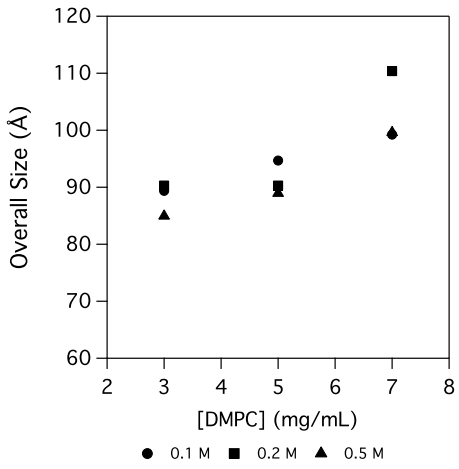


**(e)** Overall Size - $SMI_{1000}$

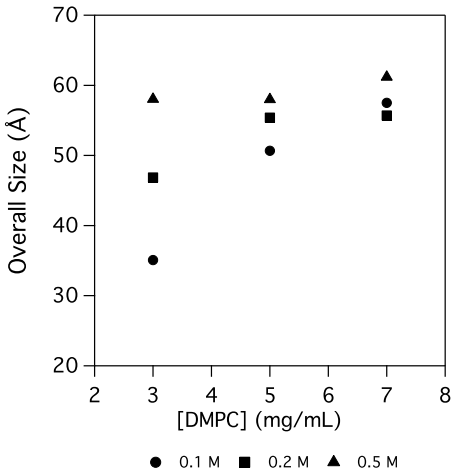


**(f)** Overall Size - $SMI_{2000}$

**Figure 3.19** Graphs reporting radius (a) and (c), belt thickness (b) and (d) and overall size of nanodiscs (e) and (f) for $SMI_{1000}$ and $SMI_{2000}$. Data from table 3.17 and 3.18

Values obtained for the nanodiscs are in good agreement with the sizes found in the DLS and scattering experiments. It is shown that the size of the discs increases with the content of DMPC. The increasing size along with the concentration of nanodiscs has been detected for other SMA co-polymers [42] and more recently for zwitterionic SMA-derived copolymer [145]. Discs made with $SMI_{2000}$ have a much smaller size than the discs made with $SMI_{1000}$. This is in agreement with the sizes found from previous experiments. Moreover, fitting data for nanodiscs at different salt and lipid concentrations using a sum model allowed the calculation of a nanodiscs to polymer ratio in solution (figure 3.20). This is in good agreement with expectations. It shown that upon increasing the amount of lipids in solution, the amount of ratio of nanodiscs to polymer increases.

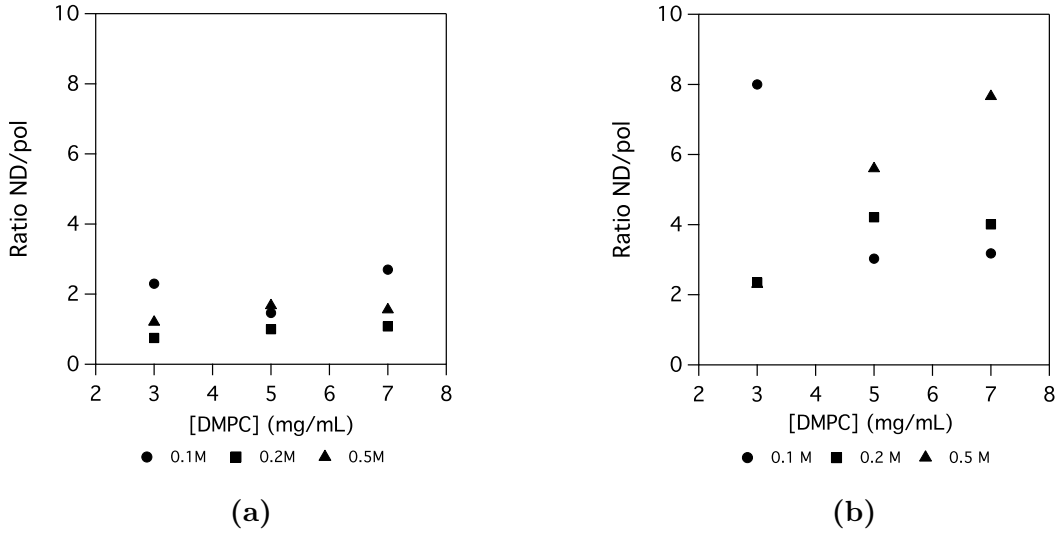


**Figure 3.20** Ratio of nanodiscs to polymer at different salt concentration for (a) $SMI_{1000}$ and (b) $SMI_{2000}$

The ratio of nanodiscs to polymer is stable for $SMI_{1000}$ at any salt concentration, but increases when $SMI_{2000}$ is used at high salt concentration (0.5M trend in figure 3.20b). The higher affinity of the polymer toward lipids is potentially due to the increased hydrophobicity of the polymer which tends to interact more with the hydrophobic core of the discs. In order to validate this hypothesis, SANS experiments at multiple contrasts can be carried out. Using deuterated DMPC, in fact, the penetration of the polymer into the core can be highlighted.

## 3.5 Lipid composition

DMPG lipids are common in lipid membranes and give rise to the potential between the inside and the outside of the cell membrane [146]. Electrostatic interactions play a key role in the partitioning of drugs into the membrane [147] as well as for the stabilisation of membrane proteins. Unfolded structures of proteins were detected when the negative charge of the membrane hit a critical point [148]. SMA stabilised discs have already been studied in the presence of DMPG [84] and to reconstruct membrane proteins [149]. SMI stabilised discs were, therefore, analysed in the presence of negatively charged lipids. For this purpose, 1,2-dimyristoyl-sn-glycero-3-phosphorylglycerol sodium salt (DMPG) was purchased from Sigma Aldrich (purity $\geq$ 98%) and used with no further purification. The solution was made with a percentage of DMPC to DMPG of 0.8 to 0.2. In the same manner as to the studies above for DMPC lipid discs, the stability of the structures in the presence of NaCl and divalent cation was analysed. Figure 3.21b and 3.21a report a summary of DLS measurements for $DMPC_{80}DMPG_{20}$ nanodiscs made using $SMI_{1000}$ and $SMI_{2000}$.

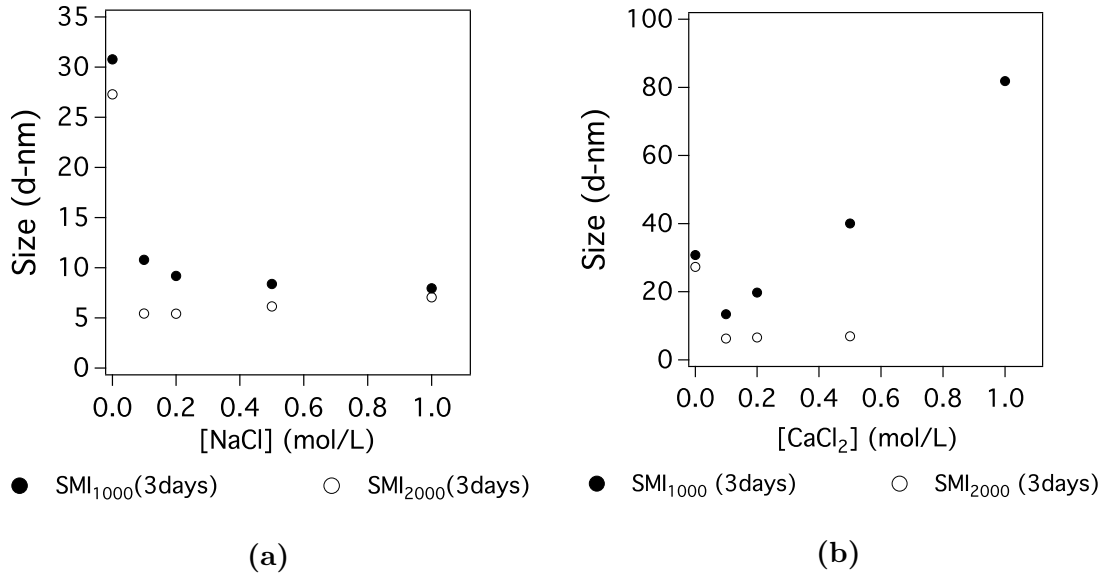


**Figure 3.21** DLS for $DMPC_{80}DMPG_{20}$ nanodiscs made using $SMI_{1000}$ and $SMI_{2000}$ in ABS, pH=5, at different concentration of (a) $CaCl_2$ and (b) NaCl

The behaviour of SMI stabilised $DMPC_{80}DMPG_{20}$ discs do not differ from the behaviour found for pure DMPC discs when NaCl is used as a salt. However, smaller structures are present for $SMI_{1000}$ when no salt is added to the buffer. This is likely to be due to the partial interaction of the negative heads of DMPG with the positive charges of the polymer. As for pure DMPC discs the size of the discs decrease and then stabilises after [NaCl] = 0.2M. A different behaviour instead is observed when $CaCl_2$ is used in solution.

Cations, in general, interact with the negative DMPG head group, binding to the phosphate group and forming a cation-lipid complex. [150] The differences between the behaviour when NaCl is present in solution rather than $CaCl_2$, is most likely to be due to the different effect that divalent cations have on negative charged lipids such as DMPG [151]. Calcium cations can bind to two adjacent head groups neutralising their charge. Previous studies on SMA, carried out at the same DMPC:DMPG composition, did not show a big difference when DMPG was used to make nanodiscs [84]. The differences between the behaviour between SMA and SMI-stabilised discs can be due to two effects: firstly, the lower pH used for SMI-stabilised discs leads to a protonation of the DMPG. At pH=8 used for SMA, the glycerol group is completely dissociated, whereas at pH=5 the glycerol group is partially protonated [151]. Secondly, the polymer used here is positively charged, therefore it is likely to interact and further neutralize the DMPG negative charge. The higher amount of amine present in $SMI_{1000}$ neutralises more charges than $SMI_{2000}$. The neutralisation of the charges on the surface leads the system to fuse.

However, more in-depth analysis using surface tension studies and small angle scattering is need to resolve the penetration and interaction of the SMI polymers in presence of negative lipids.

## 3.6 Concluding remarks on SMI-stabilised nanodiscs

In this chapter it has been investigated the structural changes of SMI co-polymers in solution, either alone or in the presence of DMPC or $DMPC_{80}DMPG_{20}$ mixtures have been studied.

The stability of the polymer at different pH has been a key point for the characterisation of the system. Moreover, SAXS and SANS have been key for the characterisation of the structures made with SMI-copolymers. It has been shown that these co-polymers can successfully make stable nanodiscs at pHs lower than the $pK_a$. It has been shown that SMI copolymers can successfully make nanodiscs. Collaborators in Birmingham have used $SMI_{2000}$ to successfully extract membrane protein. Even though the efficiency for membrane proteins extraction of SMI co-polymers is lower than the SMA2000P, their stability in the presence of divalent cations demands a more in-depth study of these copolymers.

Changing the concentration of lipids in solution has been shown to modulate of the radius of the nanodiscs. This highlights the ability of the polymer to adapt to an increasingly hydrophobic environment. The modulation of the radius, though, has not been investigated for different molecular weights polymers.

For future works, similar studies to those carried out for SMA commercial co-polymers [84], would be interesting, for example, to study the effect on the size of the structures of different molecular weights of these random copolymers.

Moreover, it would be crucial for the modulation of the structures to achieve a control over the architecture of the SMI co-polymers. As shown in this project (chapter 4) and by [152], a better control of the architecture of the copolymers and their molecular weights, leads to a control over the size of the structures made. This behaviour has not been found for commercial co-polymers of poly(styrene-comaleci acid) which have a random structure and an high polydispersity index [84].

The synthesis of SMI polymers with a control over their architecture and molec-

ular weight, thanks to their stability in the presence of divalent cations, could be a step forward for a universal platform for membrane protein extraction.

# Chapter 4

# RAFT copolymer stabilised nanodiscs

This chapter will cover the synthesis of tailored polymers with well controlled properties, as made to better control and understand nanodisc formation. First a brief introduction to polymer and RAFT polymerisation is given. Part of this work was made in collaboration with Sarah Waldie, a master project student who did the some of the syntheses of poly(styrene-co-maleic anhydride) reported in this chapter.

## 4.1 Polymers: an introduction

The polymer originates from ancient greek (*poly*=many and *mer*=parts). Indeed, a polymer is a macromolecule made of the same repeating units, so called monomers.

If the polymer is composed of just one monomer, the corresponding macromolecule is called a homopolymer. In case of two or more distinct monomers, the final macromolecule is referred to as a copolymer. Depending on the backbone architecture, as reported in figure 4.1 polymers can be subdivided into:

a - *Linear polymers*: polymers that have one single backbone.

b - *Star polymers* [153]: a type of grafted copolymer, but which are distinguished by containing just a single branching point.

c - *Graft or branched polymers*: both of which are polymers with linear deviation from a backbone, but in the first case the branching polymer is of the same nature of the backbone whereas in the second case the deviation from the backbone is made of a different monomer.

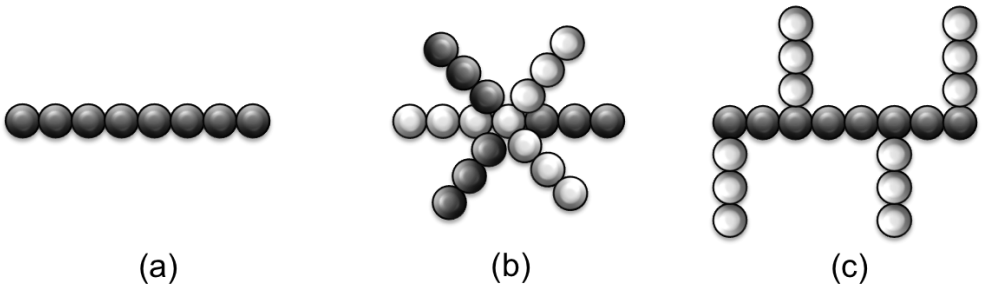


**Figure 4.1** Pictorial representation of different polymer architectures.

Moreover, in the case where the copolymer depends on the alternation of monomers in the polymer chain, another set of classification may be made:

a - *Homopolymer*: polymers made from just one kind of monomer

b - *Alternating copolymer*:polymers made of two alternating monomers

c - *Random copolymer*: polymers with no long range order among monomers

d - *Block copolymer*: linear copolymers made of long sequences of the same monomer

A pictorial representation of these architectures is reported in figure 4.2
Polymers, unlike most organic molecules that can be characterised by molecular structure and molecular weight, are described by statistical laws which return structural information about the polymers. The numbers that are needed to characterise a polymer are:

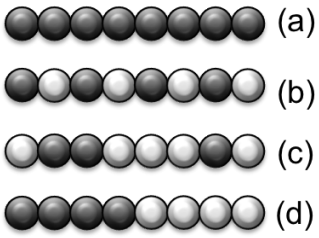


**Figure 4.2** Pictorial representation of different polymer architectures.

- Molecular Number ($M_n$): which is defined as the total weight of polymers with mass $M_i$ divided by the number of polymer molecules $N_i$ as reported in 4.1

$$M_n = \frac{\sum_i N_i M_i}{\sum_i M_i} \tag{4.1}$$

- Molecular Weight ($M_w$): which is defined as the total weight divided by the number of polymer molecules $N_i$. $M_w$ is therefore the weighted average of the weight fractions

$$M_w = \frac{\sum_i N_i M_i^2}{\sum_i N_i M_i} \tag{4.2}$$

from equation 4.1 it is evident that a long polymer chain will have a greater effect on the average than a shorter chained polymer.

The values arising from equation 4.1 and 4.2 are influenced by different parameters. $M_n$ is more influenced by the number of chains, whereas $M_w$ is more influenced by the molecular weight of a single chain (the square of the molecular weight is in the numerator in equation 4.2). As a consequence, both $M_n$ and $M_w$, can be determined by different analyses that depend on different properties of the polymer. To give an example, $M_n$ is more affected by the number of chains, hence techniques that measure colligative properties of the system are applied. In fact colligative properties do not vary for the same mole fraction concentration, either for small or big

molecules. Such techniques include end group analysis and vapour pressure osmometry. Unlike $M_n$, $M_w$ is more influenced by bigger molecules. Hence techniques used to evaluate this property rely on the mechanical and physical properties of the material, such as the diffusion coefficient or viscosity. On the other hand, techniques such as gel permeation chromatography allows evaluation of both $M_w$ and $M_n$ at the same time. The advantage of using GPC relies on its ability to return the distribution of population, hence the polydispersity of the polymer. However, solutions to equation 4.1 and 4.2 can be extrapolated in order to calculate the PDI (polydispersity index) using equation 4.3

- Poydispersity ($PDI$): defines the range of size of the molecules. The lowest value is 1 for a perfectly monodisperse polymer, but it is usually higher since $M_w$ is greater than $M_n$

$$PDI = \frac{M_w}{M_n} \tag{4.3}$$

  Due to the undefined structure, it is important to remember that both the molecular weight and the molecular number are required to determine the properties of a given polymer. However, it is not possible to gain a clear understanding using these two numbers, so it is advisable to represent the polymer using a distribution graph of the molecular weight as reported in figure 4.3.

- Degree of polymerisation ($DP$): this parameter can be defined either as the number of repeating units or as the number of monomer units.

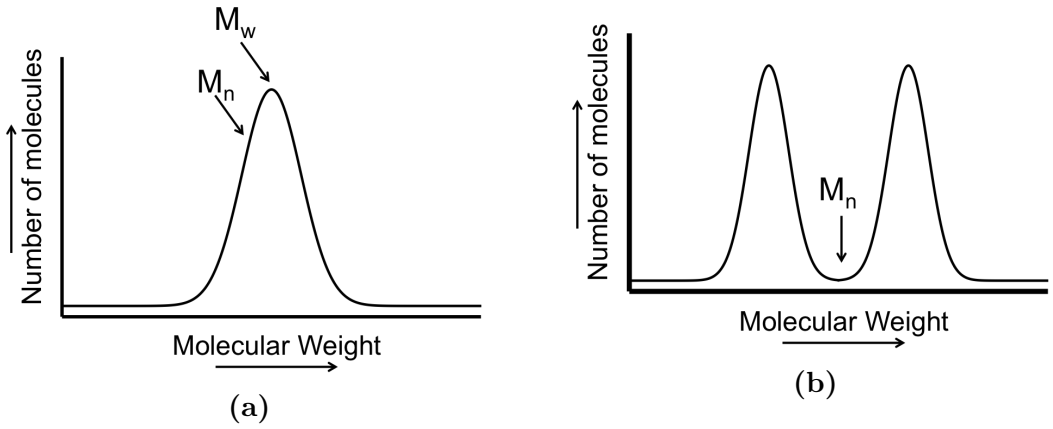


**Figure 4.3** Schematic representation of (a) normal polymer distribution and (b) irregular distribution

## 4.2 Polymerisation Techniques

Due to the wide range of polymers available, and the way they are produced, more than one classification of the reaction mechanisms has been made over the last few decades. The first classification was done by IUPAC in 1931: polymerisation techniques were divided into addition and condensation reactions[154]. In the first case the monomers have a double bond that can react with each other. The most common monomers for this type of reaction are olefins and vinyl-based monomers. In this class of polymers is included ring-opening polymerisation. For the case of condensation reactions the monomers have functional groups that react with each other; in this reaction a molecule of water is released. The most famous commercial polymer that comes from this kind of reaction is Nylon-6,6. Several different polymerisation techniques, depending on the monomer, can be used.

For brevity, since this the work in this thesis is based on RAFT polymerisation, the following text will describe radical polymerisation.

### 4.2.1 Free radical polymerisation (FRP)

Free radical polymerisation has been widely used in the past decades, and it is still one of the most used techniques among polymer producing companies.

Using free radical copolymerisation, over 110 billion pounds of polymer were synthesised in 2001 [62]. The most common polymers made from this method are PE (polyethylene)[155], Teflon (tetrafluoroethylene), PVC (poly vinyl chloride) [156] and polystyrene [157]. In general this technique allows for the polymerisation of vinyl monomers or functional groups with a double bond, which easily allows a radical initialisation and propagation. As with any polymerisation, FRP has 3 different steps:

- Initiation and propagation: This process usually involves a cleavage of a double bond and the formation of a radical. The two most common radical initiators are organic peroxides (figure 4.4a) and nitro compounds (figure 4.4b). AIBN has been used in this project as the radical initiator.

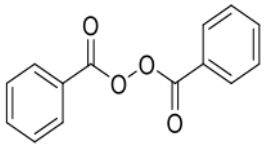


**(a)** organic peroxide

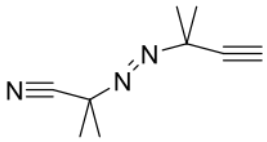


**(b)** AIBN

**Figure 4.4** Two commonly used radical initiators.

Due to the radical nature of the reaction, a wide range of polymers can be synthesised. In the propagation step, which follows the formation of radicals, monomers react with the initiator (figure 4.5a) and then with each other, forming a nascent polymer chain (figure 4.5b).

- Termination: due to the high reactivity of radicals, free radical polymerisation is often difficult to control. In fact radicals can easily react with each other to give a head-head polymer, can undergo a disproportionation reaction or can interact with oxygen. All these processes lead to the termination of the polymerisation reaction as shown in figure 4.6.

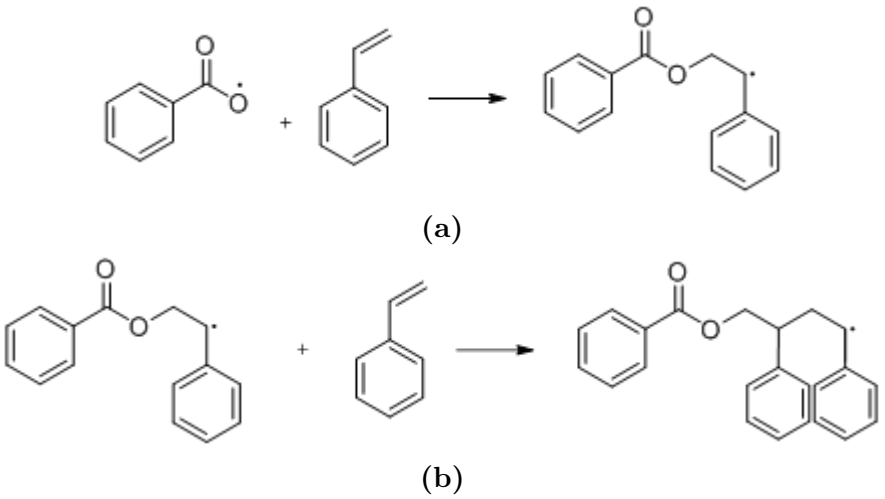

**(a)**

**(b)**

**Figure 4.5** Schematic of the propagation process.

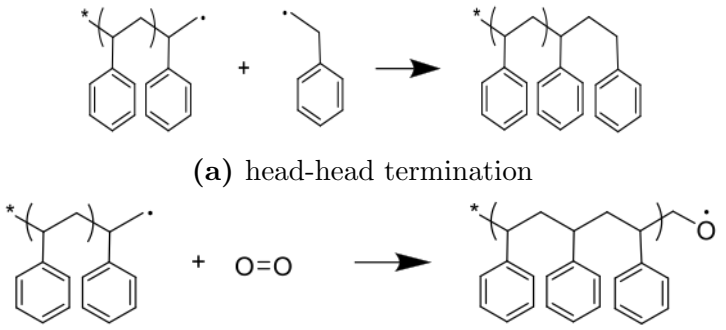

**(a)** head-head termination

**(b)** reaction with oxygen

**Figure 4.6** schematic of termination processes

## 4.3 RAFT polymerisation

First discovered in 1998 by Rizzardo *et al*[158], RAFT polymerisation has been widely investigated and used in the last decade in order to have better control of the polymer architecture. Better control over the polymerisation reaction is due to the **R**eversible **A**ddition-**F**ragmentation chain **T**ransfer agent, which will henceforth be called the RAFT agent. In general RAFT polymerisation is a specific class of a wider kind of polymerisation, so-called reversible deactivation radical polymerisation analogous to Nitroxide-mediated radical polymerization (NMP) and Atom-transfer radical-polymerization (ATRP). The mechanism of RAFT is based on the equilibrium of the dormant and propagating species. The chain transfer is mediated by a thiocarbonylthio group, which is the RAFT agent. In general a RAFT agent has the structure displayed in figure 4.7.

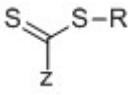


**Figure 4.7** General structure of a RAFT agent

where R is the leaving group. Depending on the nature of R and Z, the polymerisation can be controlled and a narrow molecular weight distribution of polymers can be synthesised. In fact RAFT polymerisation is based on the concept that there is an equal rate of growth for each initiated chain, which leads to a tight control of the molecular weight and a narrow distribution in the population of the polymer.

The overall RAFT reaction can be concisely described as an insertion of monomers between the S–R group as reproduced in figure 4.8.

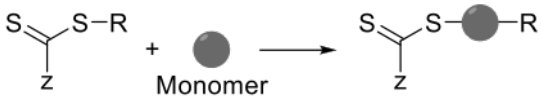


**Figure 4.8** Overall mechanism of RAFT polymerisation

The overall reaction would be enough to understand the potential of this polymerisation. However the attention of researchers is also driven by the fact that the

RAFT agent remains attached to the polymer chain, which can be used again after a polymerisation has been completed for further modification of the polymer. The detailed mechanism of RAFT polymerisation is reported in figure 4.9.

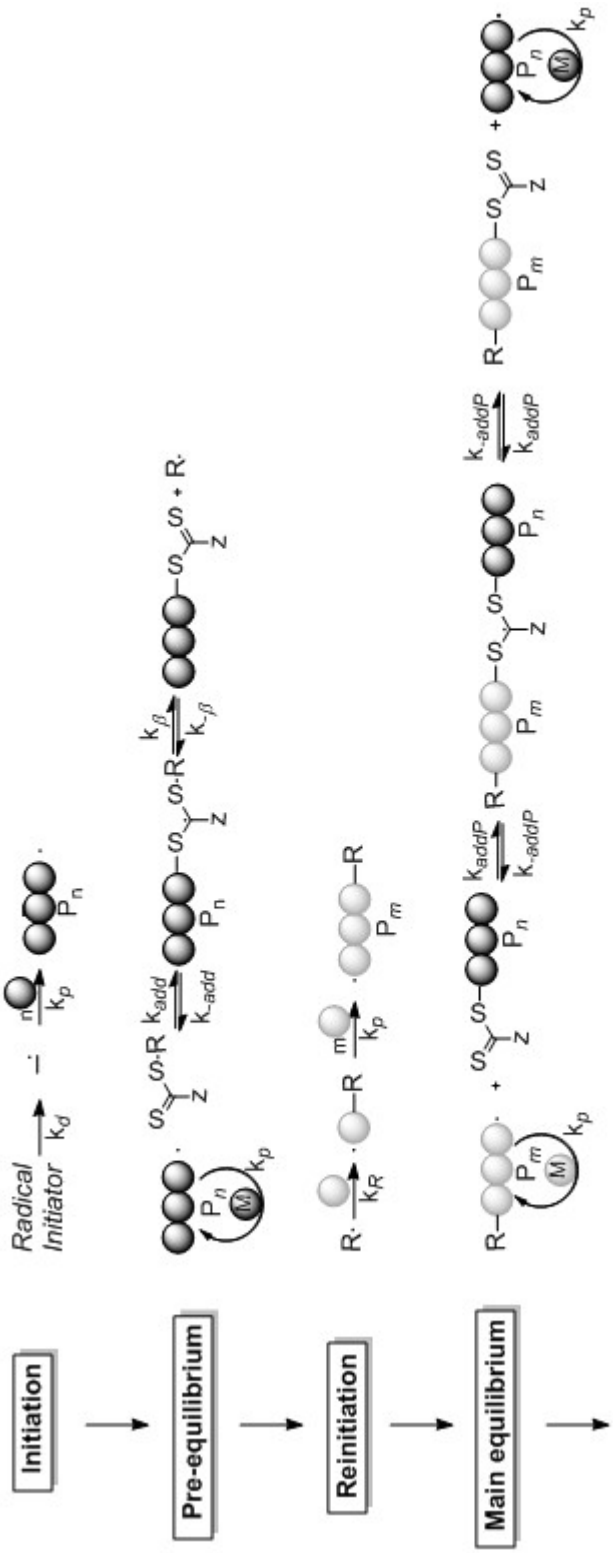


**Figure 4.9** Detailed mechanism of RAFT polymerisation

Initiation is the first process involved in the mechanism of the reaction. This reaction is characterised by the kinetic constant $k_d$. $k_d$ is the rate at which radicals of the initiator are made. It depends on the nature of the initiator and on the temperature of the reaction. At this point, the initiated radical polymer chain reacts with the RAFT agent in solution (pre-equilibrium in figure 4.9). In order to have a well controlled polymerisation, the initial radical made $P_n\cdot$ interacts rapidly with the RAFT agent to give the intermediate radical species in the pre-equilibrium step. This intermediate decomposes with a constant rate $K_\beta$ to give the macro-RAFT agent and the radical R. This last radical re-initiates the polymerisation in the reinitiation step (figure 4.9). However, the equilibrium toward the $P_n\cdot$ leads the system to undergo an uncontrolled synthesis, where the monomer instead is polymerised as a free radical. . The extent of deviation from the ideal system can be quantified as a partition coefficient (equation 4.4).

$$\phi = \frac{k_\beta}{k_{-add} + k_\beta} \tag{4.4}$$

$\phi$ describes the rates at which the intermediate is decomposed to give either the desired product through $k_\beta$ or $P_n\cdot$ with a kinetic constant $k_{-add}$.

Well controlled polymerisations have a high $\phi$. This occurs when the RAFT agent has a good homolytic leaving group. This aspect is further discussed in section 4.3.2.

The pre-equilibrium terminates when either $P_n\cdot$ or the first reacted RAFT agent have been fully consumed. This means that for a well controlled polymerisation, $k-\beta$ is higher than $k_{-add}$, and the reaction moves rapidly to the main equilibrium, allowing the growth of polymers with low polydispersity.

### 4.3.1 Living polymerisation nature

The main advantage of RAFT polymerisation arises from its "living nature". In general a living polymerisation is so called when termination processes are drastically reduced. This feature is achieved when the rate of initiation is much higher than the chain propagation. This means that all the radicals are produced at the beginning of the reaction and the propagating chain is in equilibrium with the dormant chain. This allows the propagation of all the chains at the same rate leading to a narrow distribution of molecular weight. However, due to the radical nature of RAFT polymerisation, radical-terminated chains can not be avoided but just minimised [158].

The slow propagation of the growing chain combined with the correct choice of the RAFT agent, allows the synthesis of articulated architectures such as star, graft and block copolymers. The selection of this agent is explained in section 4.3.2.

The insertion of the monomers between the thio group and the leaving (-R $\cdot$) group leads to the possibility of further modification of the polymer after it has been precipitated and purified. Complex architectures can be obtained either from branched RAFT agent such in the case of polymer brushes, or by the sequential modification of block copolymers with different affinity for the solvent they are dissolved in. Due to the radical nature of RAFT, monomers used for free radical polymerisation are also suitable for RAFT synthesis.

### 4.3.2 RAFT agent

The reactivity of the RAFT agent toward the monomers dictates the overall reaction. Therefore, the choice of an appropriate RAFT agent is essential for the synthesis of the desired polymer.

In general, the RAFT agent has to be chosen in such a way that the equilibrium in the pre-equilibrium step (figure 4.9) is favourable towards the formation of the dormant species rather than the propagating chain. In this way the RAFT agent

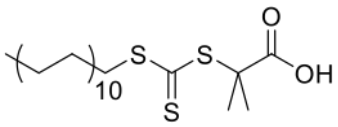


**Figure 4.10** Structure formula of DDMAT

is all reacted at once and the polymerisation quickly reaches the main equilibrium. [159]. In order to choose the right RAFT agent it is crucial to choose Z and R. Even though the double bond C=S is highly reactive, Z changes the reactivity of the RAFT agent towards the monomer. To understand this point it is useful to divide monomers and their reactivity in radical polymerisation into two categories: "less activated monomers" (LAM) and "more activated monomers" (MAM) [160]. MAM are generally vinyl monomers with the double bond conjugated to a group that can delocalise the radical such as aromatic ring or a carbonyl group. This means that the radical is produced more quickly, but it is more stable. That is why a good control of the reaction is given by a RAFT agent that is more reactive towards a radical addition. This group of RAFT agents is usually dithioesters or alkyl thiocarbonylthio species. On the other hand, for LAM, the radical formed is not stabilised by the adjacent groups which makes the radical unstable and highly reactive. That is why better RAFT agents for these monomers are less reactive in the radical reaction. Species like O-alkyl xanthates and N-alkyl-N-aryldithiocarbamates belong to this category. [161]. For the synthesis of poly(styrene-co-maleic anhydride) dithiocyanoesters have mainly been used [100, 158, 160]. For this project 2-(Dodecylthiocarbonothioylthio)-2-methylpropionic acid (DDMAT) has been used as the RAFT agent (figure 4.10).

## 4.4 Polymer self-aggregation

The conformation of big molecules in solution depends on several parameters that can be distinguished as intramolecular and intermolecular interactions [65]. These can be classified as hydrophobic and hydrophilic effects, hydrogen bonding, Columbic interactions and van der Waals forces [162]. A well known example for self-assembled structures is found throughout biology. The tertiary structure of proteins or the double helix of DNA are two outstanding examples of intra and inter molecular interactions, respectively.

In synthetic polymers, these dispersive forces are affected by the molecular weight of the polymer, the polydispersity index and, of course, the type of monomer used to make the polymer.

Flory [163] studied how the temperature and solvent influenced the aggregation of polymers in solution. As classic thermodynamics shows, an ideal solution does not have variation in the enthalpy of mixing. This physically means that the interaction between polymer and solvent molecules are of the same nature. The viscosity of a solution has been related to the quality of the solvent used through the Mark-Houwink law [164] (equation 4.5).

$$[\eta] = kM^{\alpha} \tag{4.5}$$

where $[\eta]$ is the intrinsic viscosity, $k$ and $\alpha$ are constant and M is the molecular weight of the polymer. Depending on the interaction among the polymer chain and solvent molecules, a classification of solvents for a particular polymer can be made:

- **Theta solvent** ($\alpha$=0.5) Solvents at the theta temperature for which the polymer chain follows a random coil distribution. This occurs when the monomer-monomer interactions are of the same nature as the monomer-solvent (figure 4.11b).
- **Good Solvent**($0.5< \alpha <0.8$): The polymer has favourable interactions

with the solvent. This leads the polymer to adopt an extended chain configuration. The $R_g$ that results is larger than the one found for a polymer in the theta condition (figure 4.11a).

- **Poor solvent**: ($\alpha$ >0.8): The polymer has unfavourable interactions with the solvent. This leads the polymer to have stronger interactions with itself and avoid contact with solvent molecules. This results in a collapsed configuration of the polymer (figure 4.11c).

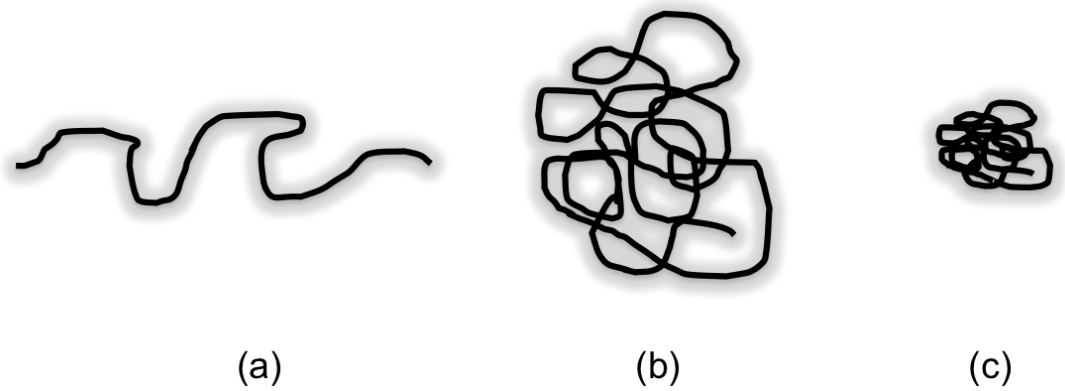


**Figure 4.11** Schematic of the arrangement of a polymer in a (a) good, (b) theta or (c) poor solvent.

However, given a good solvent, the effect of the molecular weight of the polymer is to increase or decrease the flexibility in solution. For a short chain, the arrangements of the backbone are more elongated than for a higher molecular weight polymer, which is likely to aggregate. This behaviour is more pronounced in block copolymers.

In the case of block copolymers the carbon backbone will tend to have an assembled structure in solution in order to minimise the Gibbs free energy and relax to the lowest energy configuration [162]. In the case of copolymers with amphipathic nature the hydrophobic block will tend to minimise its exposure to the water environment. In solution, for example, this is possible if the polymer forms micellar structures with the insoluble part minimising the contact with the solvent and making the core of the structure and with the soluble part of the block copolymer

forming the corona [165]. If we take into account these parameters (monomers, solvent, pH, temperature, etc) it is possible to engineer the final structure of a polymer in solution. Of course, the conformation of a polymer in solution depends on the type of monomers that make the chain and the solvent used to solubilise the polymer [33]. In previous studies it was shown that pH-responsive polymers change their architecture [166] going from a spheres to a vesicles to a flower [167, 168].

### 4.4.1 pH responsive polymers

Poly(styrene-co-maleic acid) (SMA) belongs to a wide range of polymers that change behaviour and conformation upon changes in pH [4].

A first classification of pH responsive polymers can be made using their nature, which can be either a weak poly-base or weak poly-acid. Poly-bases have functional groups that can accept protons at low pH and make a positively charged polymer. Within this group belong vinylic polymers containing amines, pyridine or imidazole. SMI discussed in chapter 3 belongs to this classification.

SMA belongs to the second classification of pH responsive polymers. These polymers have acid groups that can be protonated at low pH. Acid group types can be carboxylic, sulfonic, phosphonic or boronic. Acidic groups on the surface of a nanostructure give rise to potential biological applications. Physiological characteristics among organs can vary, while changes in the pH between the internal and external compartments of a cell can be used to disrupt and release drugs from pH responsive polymer platforms. Other than the pH, however, properties such as temperature (thermoresponsive polymers), light (photoresponsive polymers) or salt can also be used to study and optimise potential polymeric drug delivery platforms [169, 170].

Due to protonation/deprotonation of functional groups, the polymer can become completely insoluble in the media and precipitate, or can flocculate. In the case of a block copolymer with a pH responsive functional group the polymer can self assemble in several structure as discussed in section 4.4. By using a block

copolymer in which half of the block is soluble at low pH and half soluble at high pH, a phase inversion can occur (figure 4.12).

### 4.4.2 SMA self-aggregation

As for any pH responsive polymer, SMA has a different behaviour in aqueous solution when the pH is changed. This is due to the changes in the intra and intermolecular forces experienced among polymer chains arising from hydrogen bonding. Theoretical studies have shown how SMA, in a similar way to proteins, can assume primary, secondary and tertiary structures [171]. The primary structure consists of the interactions among polymer chains due to two main effects: hydrophobic interactions and hydrogen bonding. Unlike hydrogen bonding, the hydrophobic effect due to styrene-styrene interactions occurs at any pH condition. The hydrogen bonding effect, instead, relies on the pH of the solution in which the polymer is dissolved. Rigid structures can be obtained from SMA co-polymers at the first $pK_a$, in which just half of the acid group is protonated. At this condition, strong hydrogen bonding can be formed among maleic acid groups of different chains. The fewer degrees of freedom of the polymer due to the hydrogen bonding interaction, lead the polymer to arrange in solution in rigid structures such as cylinders. These theoretical studies [171, 172] were confirmed by SANS experiment carried out on SMA solutions at pH=7 [173].

## 4.5 Synthesis of poly(styrene-co-maleic anhydride)

Synthesis of poly(styrene-co-maleic anhydride) is well established in polymer chemistry. Used as a surfactant at low molecular weight or as a plastic material for high molecular weights, due to its low cost and availability, it has been produced on large scale for decades.

The copolymerisation of styrene and maleic anhydride lead to a mainly alternating co-polymer.

The kinetics of polymerisation for styrene and maleic anhydride has been studied

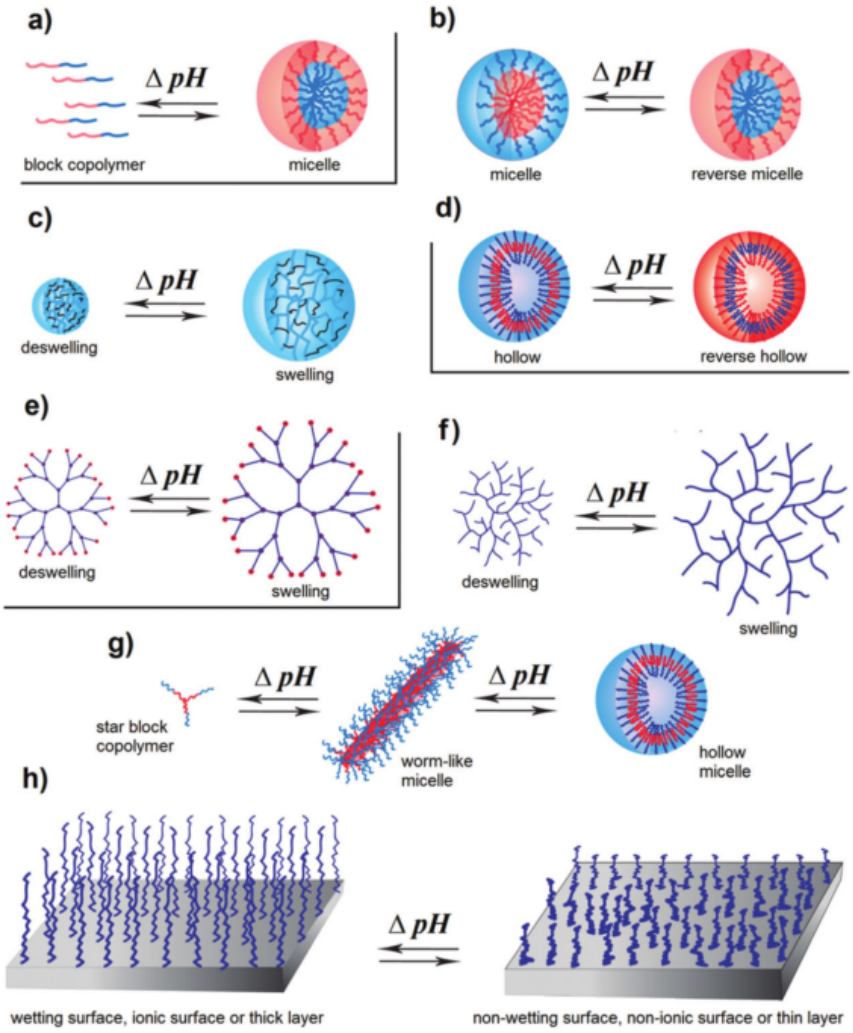


**Figure 4.12** Schematic of supramolecular structures formed by block copolymers that can be obtained upon changes of pH. Reproduced from Ref. [4] with permission from the Royal Society of Chemistry

in the literature using a continuous polymerisation process. The mechanism for this reaction was studied according to the steady state principle [174], which leads the polymer chains to have the same ratio as that of the monomers in the reactor vessel

It has been seen that when increasing the temperature of the reaction, the alternating nature of the copolymer become less and less pronounced.

Even though the synthesis of poly(styrene-co-maleic anhyride) and its reaction rate has been widely investigated, the reasons that lead to the formation of an alternating copolymer are still unclear. A few mechanisms have been proposed: a terminal model, where the rate of the propagation is affected by the propagating radical and the monomer [175] , or a penultimate unit model (PUM) [176] which proposes that the propagation rate of the polymer depends also on the penultimate unit, rather than just the terminal radical. This has been theoretically explained as a steric effect on the transition state . Another model suggests the formation of a charge transfer complex [177]. Even though this has been observed by spectrochemical analyses, the mechanism that leads to this complex to be added to the propagating chain, is still unclear.

Due to the synthesis route of the commercial copolymer, a semi-alternating block can also be observed. In general, for copolymers of styrene and maleic anhydride it must be remembered that maleic anhydride, due to its strong electrophilic nature cannot homo-polymerise. For this reason there are three possible combinations in which styrene and maleic anhydride can polymerise, as reported in figure 4.13. The semi-alternating block (SSM in figure 4.13 leads the copolymer to have a random structure.

It has been shown, however, that by carrying out a slow controlled reaction with RAFT it is possible to reduce the number of SSM triads and to synthesis a block co-copolymer of styrene-*alt*-maleic anhydride with a styrene tail if the ratio of styrene to maleic anhydride is greater than 1:1.

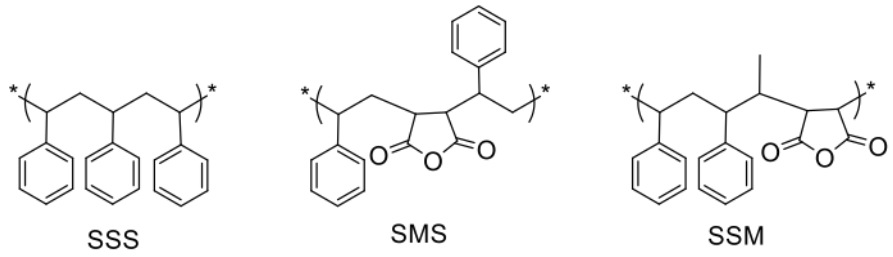


**Figure 4.13** Possible combinations of triads for SMA copolymers

## 4.6 RAFT synthesis of SMA

In this project the polymer synthesis was carried out by varying the concentration of the maleic anhydride and the styrene to make different molecular weights, using the formula reported in equation 4.6.

$$M_n = \left(\frac{mol_{M1}}{mol_{RAFT}} MW_{M1} + \frac{mol_{M2}}{mol_{RAFT}} MW_{M_2}\right) DP + MW_{RAFT} \qquad (4.6)$$

It has been shown by Bayburt and collaborators that the length of a membrane scaffold protein affects the size of the nanodiscs [24]. In previous studies in the Edler group, however, changes in the molecular weights of commercial SMA copolymers showed no correlation among these parameters [84]. TThe commercial copolymer, however, has a high polydispersity index and a random structure [178]. For this reason, it is plausible that the overall size of nanodiscs does not increase with the molecular weight of the polymer used.

For the experiments reported here several molecular weights and styrene to maleic anhydride compositions were used. Table 4.1 shows the targeted molecular weight and the amounts of styrene, maleic anhydride, RAFT agent and AIBN used.

A typical synthesis of a 6 kDa polymer with a styrene:maleic anhydride molar ratio of 2:1 was made as follows: 0.40g of maleic anhydride (puriss., 99.0% (NT), Sigma Aldrich), 1.00g of styrene (ReagentPlus, contains 4-tert-butylcatechol, Sigma Aldrich) , 0.005g of recrystallised AIBN (98%, Aldrich) and 0.040g of DDMAT (98%, HPLC, Aldrich) solubilised in 4.4 mL of 1,4-dioxane (anhydrous, 99.8%, Sigma-Aldrich). Styrene was run through a prepacked column, to remove

tert-butylcatechol. The listed reagents were purchased and used without any further purification.

Due to the radical nature of the polymerisation, three freeze-pump-thaw cycles were undertaken prior to the reaction. To make sure no oxygen would enter into the reaction vessel, the round bottom flask was left in a slightly over pressured nitrogen atmosphere and placed in a preheated oil bath or hot plate at 60°C for about 20 h. The viscous solution obtained was then suspended in the minimum amount of THF (ACS Grade, VWR) and was then precipitated in diethyl ether (99.8%, Sigma Aldrich). The resulting powder was filtered under vacuum using a Bückner funnel. This procedure was repeated 3 times in order to remove any unreacted monomer, oligomeric material and solvent. The resulting polymer was placed in the oven at 70°C overnight.

**Table 4.1** Values for amounts of reagents used in the synthesis of $SMA_{RAFT}$.

| $M_{th}$ (Sty:MA) | Sty (g) | MA (g) | DDMAT (g) | AIBN (g) |
|---|---|---|---|---|
| (A) 4 kDa (2:1) | 0.67 | 0.27 | 0.07 | 0.007 |
| (B) 6 kDa (2:1) | 1.00 | 0.40 | 0.07 | 0.007 |
| (C) 8 kDa (2:1) | 1.33 | 0.54 | 0.07 | 0.007 |
| (D) 10 kDa (2:1) | 1.66 | 0.67 | 0.07 | 0.007 |
| (E) 15 kDa (2:1) | 2.5 | 1.01 | 0.07 | 0.007 |

The maleic anhydride of the polymer needs to be hydrolysed in order to make the water soluble polymer used to make the final nanodiscs. The procedure used is reported below: For a general SMA-copolymer hydrolysis, 1g of $SMA_{RAFT}$ polymer was dissolved in 100 mL of 2M NaOH in a 250 mL round bottom flask. This solution was stored in fridge overnight. The hydrolysis was then carried out by refluxing the solution at 120°C for 3 h. The round bottom flask was cooled to room temperature and 2M HCl was added in order to precipitate the polymer, which was insoluble in the protonated state. The precipitate was centrifuged in a Eppendorf 5804R centrifuge at 6000 rpm in 50 mL eppendorf tubes for 10 minutes and washed with deionised water (Milli-Q, 18.2 MΩ) 3 times. To ensure

a full precipitation of the polymer, the pH of the supernatant was checked with pH paper and maintained at pH=5. The last precipitate was dissolved in a minimum amount of 1M NaOH solution and the pH was adjusted to 8. To obtain a powder, the polymer solution was frozen and then placed in the freeze-dryer VirtisSP Scientific Bench Top Pro at -80°Cand 20 Pa overnight.

## 4.7 Polymer characterisation

After the polymerisation was carried out, the degree of conversion of the monomer was measured using gravimetry. An aliquot of the reagents was withdrawn from the vessel reaction before the temperature was increased. This procedure was repeated before the polymerisation was stopped. A $^{1}$H NMR was carried out (figure 4.14) on the starting material and the final sample. The peaks attributed to the styrene and maleic anhydride disappears from the $^{1}$H NMT spectrum whereas the broad peak due to the polymer appears. The conversion was found to be 100% for polymerisations carried out at 60°C for 20h.

The molecular weight of the polymer was worked out in a first analysis using a gravimetric method, and then using a GPC.

For the gravimetric analysis, the polymer is weighed after being precipitated and purified. The conversion of the polymerisation is calculated as in equation 4.7:

$$conv = \frac{g_{fin}}{g_{in}} \tag{4.7}$$

where $g_{fin}$ is the amount of polymer collected at the end of the polymerisation, after being dried at 70°Cin the oven overnight and $g_{in}$ is the total amount of reagents added to the reaction vessel. This calculation is possible due to the equivalent molecular weight of both monomers before and after the polymerisation. The conversion is equivalent to the degree of polymerisation, which can be substituted in equation 4.6 to give the theoretical nominal molecular weight.

In order to make samples for GPC, 1.5mg of polymer was dissolved in 3mL of THF. The polymer was left to equilibrate overnight. In order to obtain the

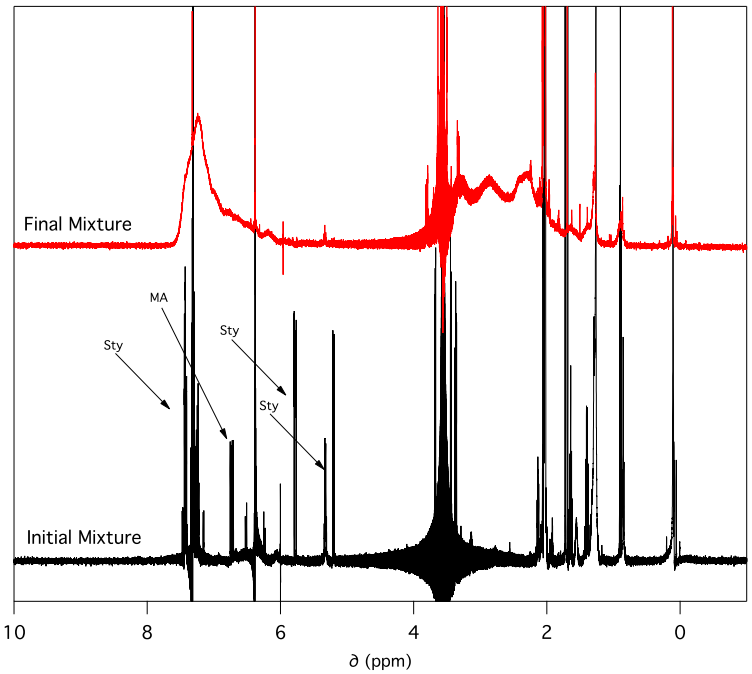


**Figure 4.14** $^{1}$H NMR spectra for an initial (black) and final (red) of reaction mixture . Peaks attributed to styrene and maleic anhydride are highlighted using arrows as Sty and MA respectively.

molecular weight of the polymer, a polystyrene of known molecular weight was run as a standard. Figure 4.15 reports a typical measurement for a GPC analysis.

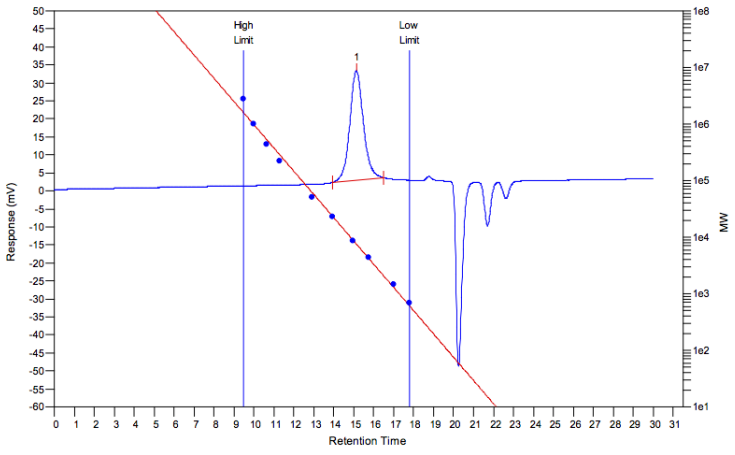


**Figure 4.15** Typical GPC analysis for $SMA_{RAFT}$ co-polymer (blue line) and polystyrene standard calibration (blue dot) at 25°C.

The characterisation of the $SMA_{RAFT}$ anhydride was followed by the hydrolysis

**Table 4.2** Molecular weight of $SMA_{RAFT}$ polymer synthesised in this work obtained from (*) gravimetric conversion analysis and from (**) GPC with PDI.

| $M_{th}$ | | Grav. Conv. (%) | $M_n$ Grav * (kDa) | $M_w$ (kDa)** | PDI ($M_w/M_n$) |
|---|---|---|---|---|---|
| (A) 4 kDa | (2:1) | 62 | 3.6 | 4.8 | 1.2 |
| (B) 6 kDa | (2:1) | 75 | 2.3 | 6.3 | 1.2 |
| (C) 8 kDa | (2:1) | 73 | 5.4 | 7.9 | 1.1 |
| (D) 10 kDa | (2:1) | 70 | 7.0 | 8.5 | 1.2 |
| (E) 15 kDa | (2:1) | 84 | 8.4 | 16.6 | 1.2 |

. Polymer solutions were then analysed using several techniques.

### 4.7.1 DLS measurements

Characterisation of polymers on their own was carried out before the polymers were combined with lipids.

Polymer solutions were run at the same concentration used to make nanodiscs (1.5%wt) using dynamic light scattering (DLS). DLS measurements are performed the day after the polymer was dissolved in phosphate buffer solutions (PBS), 50 mM, NaCl 0.2M at pH=8 checked using pH paper. This allows the polymer to relax to an optimal conformation. The results reported in figure 4.16, as expected, show an increase in size of the polymer structures in solution with increasing molecular weight.

The diameter of the structures determined from DLS measurements, with the molecular weight obtained from GPC measurements, are reported in table 4.3. The tendency of the polymer to aggregate in aqueous solution can be detected by calculating the theoretical $R_g$. If the polymer behaved ideally, the structures in solution would match a Gaussian coil distribution. In the case that the polymer had this structure, the $R_g$ can be calculated using equation 4.8

$$R_g^2 = \frac{Nb^2}{6} \tag{4.8}$$

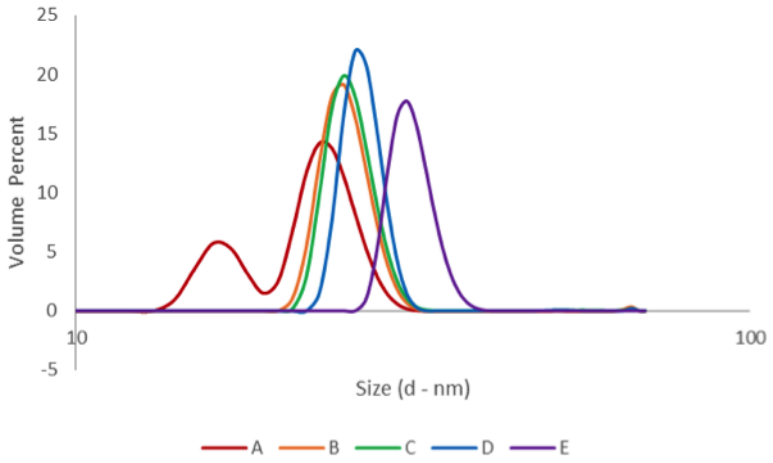


**Figure 4.16** DLS measurements of polymer solutions in PBS (50mM, 0.2M in Nacl) made at 1.5%wt of $SMA_{RAFT}$ acid at 25°C. Several molecular weight are reported : (a) 4 kDa, (b) 6 kDa, (c) 8 kDa and (d) 10 kDa.

where $b$ is assumed as the effective C-C bond length (0.1526nm) [179] and $N$ is the number of bonds in each chain. The 4 kDa polymer has two distributions, one ∼3 nm and the other one ∼ 10.5 nm. The first distribution is close to the value found for a Gaussian coil distribution. The first peak is just slightly bigger than the one found for a single polymer chain. The smaller peak is than probably due to small aggregates of polymer in solution, whereas the largest part of this polymer behaves like a surfactant making large aggregated structures, possibly similar to micelles.

**Table 4.3** Radius of gyration and structure diameter from the DLS measurement reported in figure 4.16 for polymer solutions in PBS (50mM, 0.2M in Nacl) made at 1.5%wt of $SMA_{RAFT}$ acid at 25°C

| $M_w$ | | $R_g^*$ (nm) | Diameter DLS (nm) |
|---|---|---|---|
| (A) 4.8 kDa | (2:1) | 1.11 | 3 ±1<br>10.5±3 |
| (B) 6.3 kDa | (2:1) | 1.33 | 12.8±3 |
| (C) 7.9 kDa | (2:1) | 1.44 | 13.5±3 |
| (D) 8.5 kDa | (2:1) | 1.48 | 15.5±3 |
| (E) 16.6 kDa | (2:1) | 2.14 | 32.8±5 |

As it is obvious from table 4.3, apart from the 4 kDa polymer, all the other polymers present much bigger structures than would be expected for a Gaussian coil approximation. Due to the styrene tail, which has a high tendency to avoid water, the polymer is likely to minimise the contact with the solvent by arranging in supramolecular structures. In general, core shell structures for block copolymers made of a hydrophobic and a hydrophilic region have been widely reported for amphiphilic block co-polymers [180, 181], including SMA [182].

### 4.7.2 Proton NMR

After the polymer was synthesised following the procedure reported in section 4.5 , $^{1}$H NMR was carried out to find the ratio of styrene to maleic anhydride in the polymer. Figure 4.17 shows $^{1}$H NMR spectrum spectrum for a SMA copolymer.

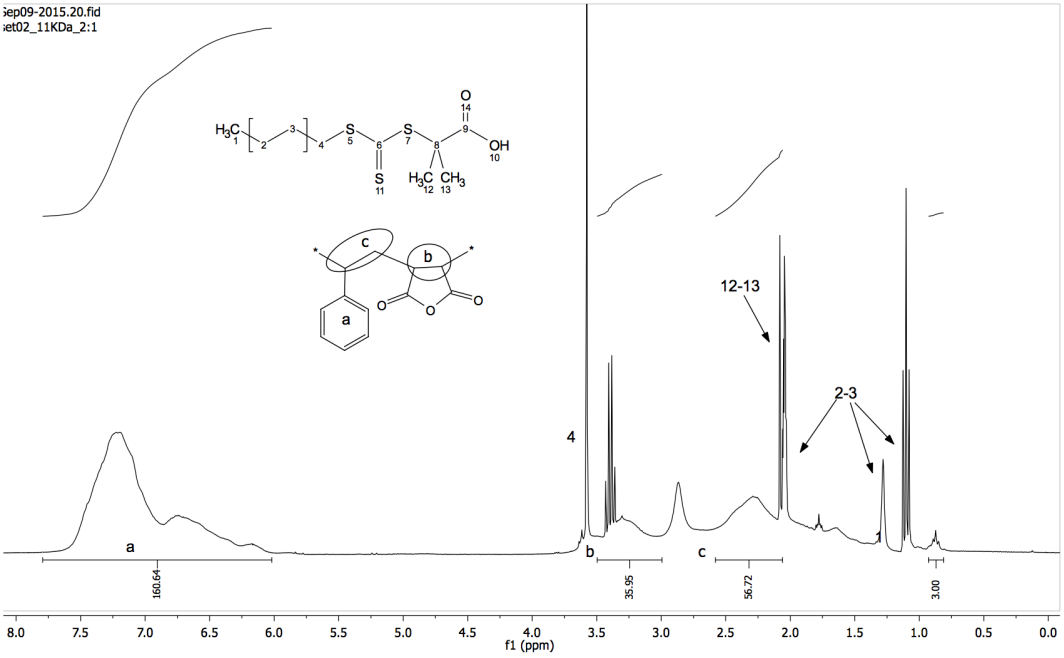


**Figure 4.17** $^{1}$H NMR spectrum for a 15 mg/mL solution of $SMA_{RAFT}$ dissolved in d-acetone.

Peaks relating to the RAFT agent in figure 4.17 are assigned using values

from the literature [183]. The end group from the RAFT agent is integrated and assigned to 3 protons. The integration of the peaks are carried out from 6.0 to 8 ppm (styrene aromatic ring), 3 to 3.5 ppm (maleic anhydride protons) and 2 to 2.5 ppm (styrene aliphatic protons). In order to obtain the ratio of styrene to maleic anhydride, the area underneath those peaks are divided by 5, 2 and 3 respectively [184]. From the area of the peak from the aliphatic and aryl regions we can calculate the ratio between styrene and maleic anhydride. Table 4.4 reports the nominal and experimental styrene to maleic anhydride ratio found using $^1$H NMR.

**Table 4.4** Ratio of styrene to maleic anhydride gained from $^1$H NMR analysis.

| Copolymer | Ratio$_{th}$ Sty:MA | Ratio$_{ex}$ Sty:MA |
|---|---|---|
| 4 kDa | 1:1 | 1.8:1 |
| 4 kDa | 2:1 | 1.9:1 |
| 6 kDa | 2:1 | 2.0:1 |
| 8 kDa | 2:1 | 2.3:1 |
| 10 kDa | 2:1 | 2.0:1 |

### 4.7.3 FTIR

FTIR was used to check the conversion from anhydride to acid, after the hydrolysis process explained in section 4.6. Figure 4.18 reports an example of the analysis for a 6 kDa copolymer.

FTIR spectra show the conversion from the anhydride to the acid form of the polymer. Peaks between 1700 and 1800 cm$^{-1}$ are typical of the carboxylic group of the anhydride. This peak is highlighted in the spectrum at 1775 cm$^{-1}$. After the hydrolysis this peak is below the limit of detection, highlighting a high degree of conversion. In the SMA acid form, instead, there is a peak present at 1555 cm$^{-1}$ which is typical of a carbonyl group and at 3200 cm$^{-1}$ which is characteristic of the -OH stretching [185, 186].

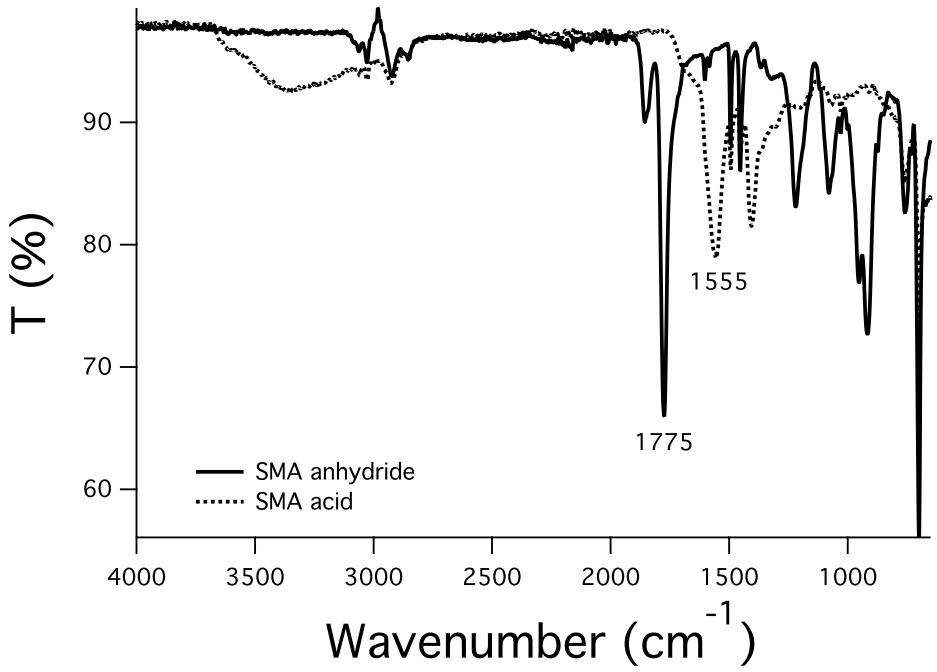


**Figure 4.18** FTIR spectra for SMA powder. The graphs reports the patterns for the anhydride (continuous line) and acid (dotted line). The wavenumbers for anhydride and the acid functional groups are shown at 1775 cm$^{-1}$ and 1555 cm$^{-1}$ are shown respectively.

## 4.8 Characterisation of nanodiscs made from SMA$_{RAFT}$ polymers

### 4.8.1 DLS and neutron scattering analysis

Nanodiscs were made using the procedure reported in section 2.13.2. Previous studies of SMA$_{RAFT}$ polymers with lipids showed that no free polymer was left in solution [84]. For this reason nanodiscs were made with no further purification. An initial analysis was carried out using the DLS in the University of Bath to check the nanodiscs stability over time and to correlate the size of the system to the molecular weight of the investigated copolymer. As shown in figure 4.19, an increase in the molecular weight of the polymer leads to an increase in the diameter of the structures in solution.

A similar experiment was carried out by Craig and co workers [152]. In their

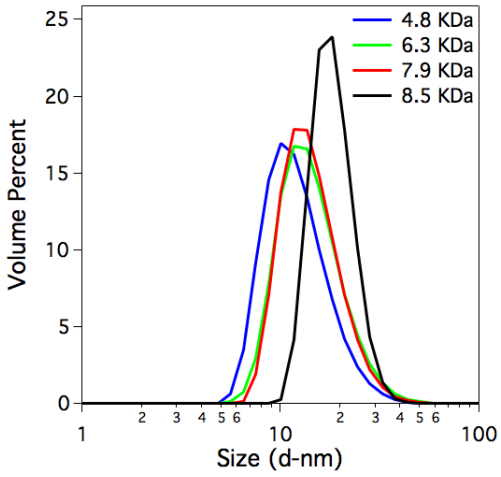


**(a)** DLS measurements - Volume percent vs Size (d - nm)

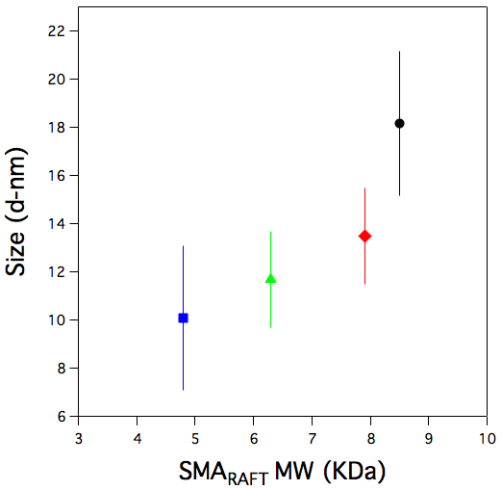


**(b)** Trend of nanodiscs size with MW of the polymer used

**Figure 4.19** DLS measurements for nanodiscs made at 0.5% wt of DMPC and 1.5% wt of $SMA_{RAFT}$ with different MWs, in 50 mM PBS, 0.2M NaCl, pH=8. Measurements were acquired at 25°C

study they had synthesised 3 different molecular weight and changed the ratio of styrene to maleic acid. No difference in the size of the particles was detected with DLS with increasing molecular weights in Craig's work. However they detected an increased size of the particles with an higher ratio of styrene to maleic acid. The main difference between this and our experimental work carried out at the University of Bath, is the choice of the phospholipid used. In their research Craig and co-worker have used POPC and POPG. . The unsaturated chains could lead to the discrepancy in the results.

In order to characterise the structure of the aggregates analysed with DLS, the same samples as those reported in figure 4.19 were examined using Small Angle Neutron Scattering (SANS) at ISIS (on the SANS2d beamline). Scattering patterns from these samples are reported in figure 4.20. For scattering patterns of freshly made samples, the background was not subtracted, but was included in the fitting as a linear flat background term. This is revealed in the high background signal for pattern reported in figure 4.20 on the left column. Data from aged samples had a background subtracted during data reduction. Due to limited

time on the beam line, only 3 MWs have been analysed using SANS.

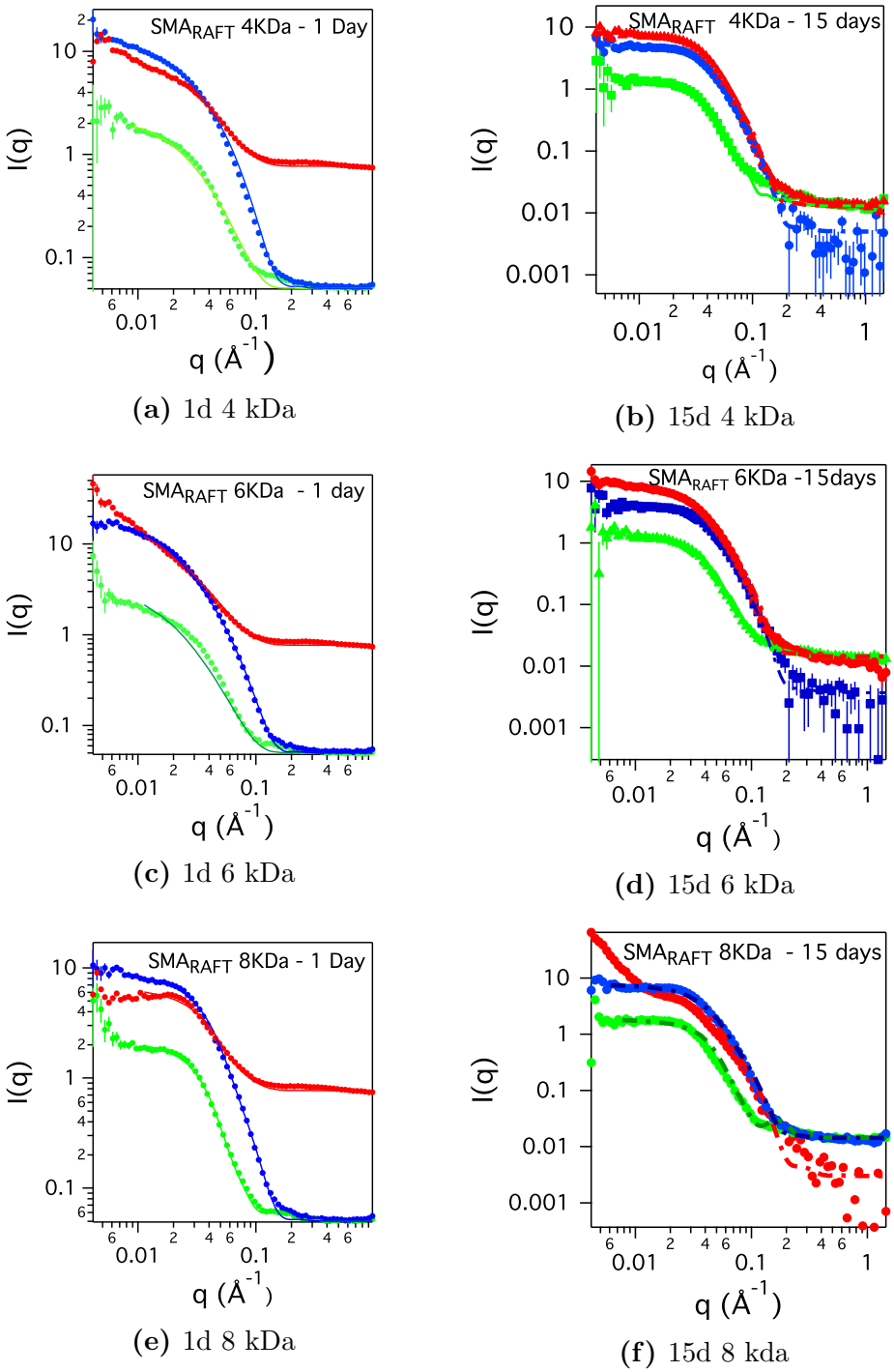


**(a)** 1d 4 kDa

**(b)** 15d 4 kDa

**(c)** 1d 6 kDa

**(d)** 15d 6 kDa

**(e)** 1d 8 kDa

**(f)** 15d 8 kda

**Figure 4.20** Scattering patterns acquired in SANS2d arising from a nanodiscs solution made at the same concentration of polymer (1.5% wt) and DMPC (0.5% wt). On the left hand side are reported scattering pattern after 1 day (a,c,e) and after 15 days (b,d,f) from the sample preparation. Contrasts run were d-DMPC in h-PBS (red), d-DMPC in d-PBS (green) and h-DMPC in d-PBS (blue). Measurements were acquired at 25°C

Due to the high number of parameters, a step-wise analysis was carried out. Parameters for the thickness of the bilayer core and head were held during the fitting at 28 Å and 8 Å, respectively [138]. The hydration of the head was fixed to 0.57 mol% [139]. Values of the temperature, dielectric constant and salt concentration were held and are reported in table 3.4. Before starting the simultaneous global fitting analysis, a preliminary fitting of the curve was done and general parameters were obtained for the core radius, PDI and rim thickness, using the data for the sample that has the highest contrast, which is h-DMPC in d-PBS. The returned values were used to fit the scattering pattern arising from solutions containing a disc with a deuterated core and deuterated buffer. Using this contrast, the scattering arises mainly from the polymer in solution, so it was used to fit the thickness of the rim and the percentage of water in the polymer rim. Moreover the penetration of the polymer into the core was fitted from the scattering pattern of deuterated lipid in hydrogenated solvent. The SLD of the deuterated core was allowed to vary, so the polymer percentage was calculated as a linear combination of both the SLD of the phospholipid and the polymer respectively. This value was then used to back-calculate the SLD of the core for the disc made with h-DMPC. These values (belt thickness, water percentage in the rim, and the percentage of polymer in the core) were fixed during the simultaneous global fitting. Parameters obtained from the aforementioned fitting are reported in table 4.5

**Table 4.5** Fitted parameters for SANS patterns reported in figure 4.20

| | 4 kDa | | 6 kDa | | 8kDa | |
|---|---|---|---|---|---|---|
| | Fresh | Old | Fresh | Old | Fresh | Old |
| Core Radius (Å) | 30±3 | 50.4± 5 | 36.9± 4 | 42±3 | 50± 3 | 49±4 |
| PDI | 0.54 ± 0.2 | 0.1 ±0.1 | 0.57±0.1 | 0.31±0.1 | 0.2 ±0.1 | 0.2 ±0.1 |
| Rim Thickness | 12 ±3 | 10.8 ±3 | 15±3 | 10.5±2 | 13.6±3 ±3 | 6.8 ±3 |
| Polymer Penetration (%) | 13 ±2 | 37 ±3 | 14±2 | 37± 3 | 13 ± | 31 ±3 |
| Rim mol frac $H_2O$ | 0.8±0.3 | 0.5±0.2 | 0.8±0.3 | 0.3±0.2 | 0.5±0.3 | 0.67±0.3 |

Even though 15 parameters were used to fit the data, in this model the strategic fitting above led to a good fit, in agreement with the preliminary DLS results. In fact, the validity of these results showing the tendency of nanodiscs to increase in

size upon increasing molecular weight of the polymer is reinforced by the tendency to get smaller with time, observed in both SANS and DLS.

The hydration of the polymer rim is calculated in the model as a linear combination of the SLD of solvent and polymer with their respective molar ratio. Fitting shows that the hydration of the rim is decreasing with time, which means that the SLD of the polymer rim region is changing. This change in the hydration is more likely to be due to a different configuration of the polymer in the discs. In fact after 15 days the polymer penetration into the core increases, which leads the rim region to have lower polymer density, which leads the SLD to change and the rim thickness to decrease, while the core radius tends to increase, also suggesting that the polymer penetrates more into the core with time.

The stability of these structures was also studied using DLS in Bath. Figure 4.21 reports the behaviour of nanodiscs when stored at different temperatures and confirms this trend first noted in the SANS patterns. Nanodiscs were analysed after 7 days using DLS, the trend of which is reported in figure 4.16. This sample was then split in two, half was stored for a further 5 days at room temperature, whereas the other half was stored in the fridge (4°C). Both samples of nanodiscs decreased in size over this time period, which is probably due to a relaxation of the polymer around the phospholipid core. This behaviour follows that detected with SANS, as reported in table 4.5. Moreover, this trend is more prominent for nanodiscs made using polymers with higher molecular weights. This is most probably due to the larger number of intramolecular interactions in higher molecular weight polymers, which take more time at the beginning to disrupt the initial core-shell structure and wrap around the lipid core.

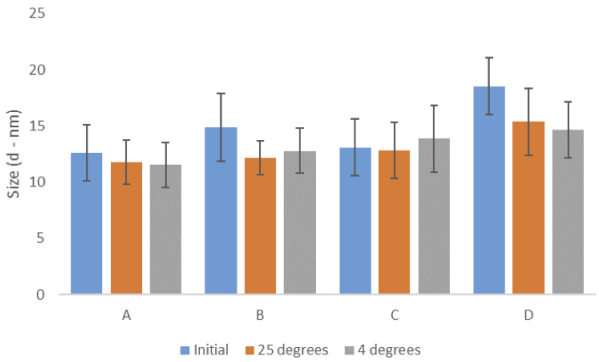


**Figure 4.21** DLS measurements of nanodiscs made with DMPC (0.5% wt) and with SMA (a)4.8, (b)6.3, (c) 7.9 and (d)8.5 kDa (1.5% wt). Blue columns report a DLS measurement after 7 days, orange columns are measurements after a further 5 days at room temperature and grey columns are DLS measurements after a further 5 days in the fridge.

## 4.9 SMA modification

Although poly(styrene-co-maleic acid) has been the most widely used copolymer to make nanodiscs, a few recent publications have shown the possibility to make nanodiscs using polymers of different physical/chemical characteristics [109, 187]. Oluwole [187] showed a successful solubilisation of membrane proteins using a copolymer where the styrene moiety is substituted with a hydrophobic chain made of isobutylene. Use of this copolymer bring advantages in terms of spectroscopic studies of membrane proteins [187].

Lindhoud and collaborators [109] showed the possibility to solubilise lipid bilayer membranes in disc-like shape structures using thyol styrene co-polymer. In order to test the important interactions allowing nanodiscs formation, in this project a modification of the copolymer in terms of hydrophobic to hydrophilic ratio was carried out.

Other than making several different $SMA_{RAFT}$ molecular weights as shown in paragraph 4.5, the chemical structures were modified as well. Two main changes were made in order to get a polymer with novel characteristics. In one case the polymer was synthesised using *para*-methylstyrene as one reagent, which led to increased hydrophobicity, whereas in the other case, the polymer was reacted with a di-amine making a zwitterionic copolymer. This gave the opportunity to work in a wide range of pHs, from acidic to basic. More details about the synthesis and the characterisation of structures made using these copolymers is given in section 4.9.1 and 4.10 for the poly(methylstyren-co-styrene-co-maleic acid) copolymer and the zwitterionic copolymer respectively.

### 4.9.1 Poly(*p*-methylstyrene-co-maleic anhydride)

*p*-methylstyrene differs from styrene by one methyl group in the *para* position with respect to the styrene group. This polymer was synthesised using RAFT polymerisation in Bath using the procedure described below.

A typical synthesis of poly(*para*-methylstyrene-co-styrene-co-maleic anhydride)

**Table 4.6** Values for the ratio of $SMA_{met}$ and molecular weight values from GPC with polydispersity index.* GPC for this polymer returned high polydispersity

| Acronym | *para*-methyl styrene | Sty | MA | MW (kDa) | PDI |
|---|---|---|---|---|---|
| $SMA_{met-1.0}$ | 1 | 1 | 1 | 8163 | 1.12 |
| $SMA_{met-0.8}$ | 0.8 | 1.2 | 1 | n/a* | |
| $SMA_{met-0.6}$ | 0.6 | 1.4 | 1 | 7354 | 1.11 |
| $SMA_{met-0.4}$ | 0.4 | 1.6 | 1 | 7190 | 1.11 |
| $SMA_{met-0.2}$ | 0.2 | 1.8 | 1 | 7256 | 1.14 |

was made such that the ratio between the arylic and aliphatic groups is kept at a 2:1 molar ratio, but the percentage of *para*-methylstyrene and styrene was varied. These ratios are reported in table 4.6.

In order to make the polymer match as close as possible to the SMA 6 kDa polymer, which was the one most frequently used in this and previous projects, the degree of polymerisation for the novel copolymer was calculated to be the same as the 6 kDa (40 aromatic repeating units and 20 repeating units of maleic anhydride). The procedure followed for this reaction was almost identical to that explained in section 4.5 for a one pot reaction. *para*-methyl styrene was purchased from Sigma Aldrich (96%, contains 3,5-di-tert-butylcatechol as inhibitor). 1.62g of maleic anhydride, 2.26g of *p*-methylstyrene, 2.00g of styrene, 0.025g of AIBN and 0.28g of DDMAT were solubilized in 4.4 mL of 1,4-dioxane. Due to the radical nature of the polymerisation, the reaction was carried out in an oxygen free environment using the same procedure explained in section 4.5.

### DLS analysis

From the structural point of view, a very small change was made in the polymer structure. The structure of the copolymer is reported in figure 4.22.

As for the analysis of $SMA_{RAFT}$ and SMI copolymers, this novel copolymer was analysed using DLS, at 1.5% wt in PBS at pH=8, NaCl 0.2M. The DLS patterns are reported in figure 4.23

Even though just a small change was made in terms of molecular structure, the

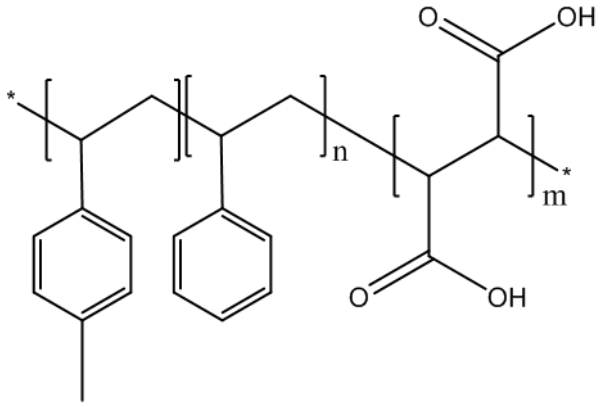


**Figure 4.22** Molecular structure of poly(*para*-methylstyrene-co-styrene-co-maleic anhydride) block copolymer.

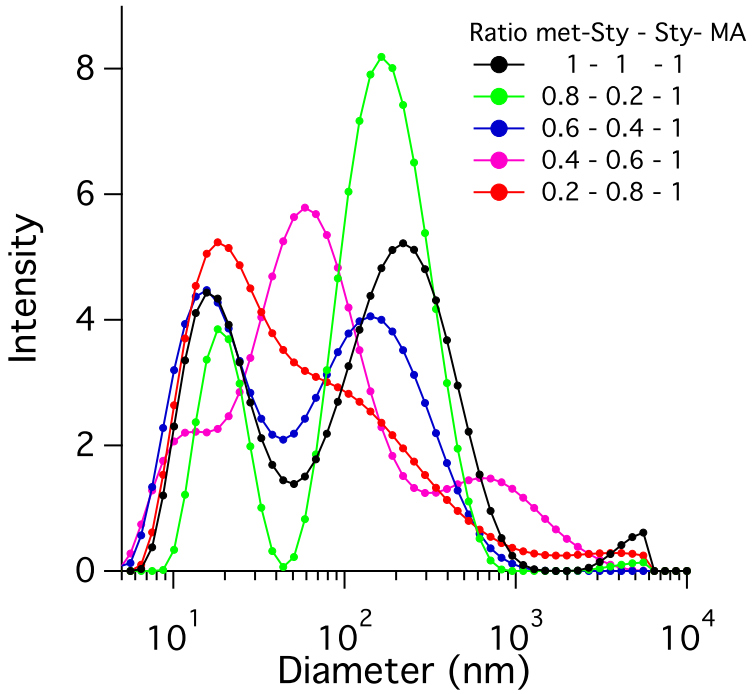


**Figure 4.23** DLS for *para*-methyl styrene copolymer at 1.5% wt, PBS 50mM, 0.2M NaCl, acquired at 25°C.

behaviour of these polymers in aqueous solution differ enormously from that of the $SMA_{RAFT}$ copolymer. A lower solubility of the polymer was expected, due to the methyl styrene in the *para* position, which increases the hydrophobicity of the polymer. However, DLS showed that the $SMA_{met}$ polymers (figure 4.23) are more aggregated than the $SMA_{RAFT}$ (4.19a), although it is still possible to

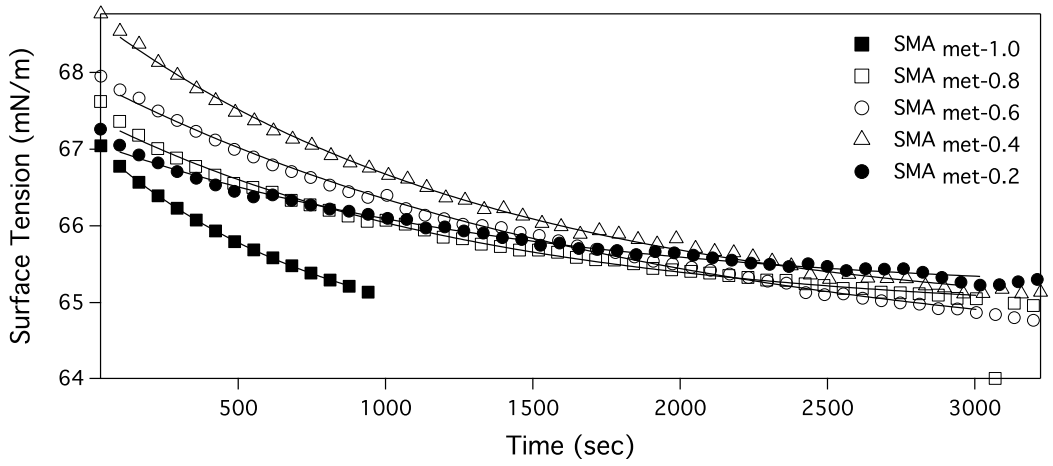


**Figure 4.24** Surface tension measurement carried out for *para*-methyl styrene copolymer solution at 0.5% wt, in PBS, pH=8. Prior to the measurement the probe was calibrated against pure water. Measurements were acquired at 25°C

see a tendency for the big aggregates in solution to decrease in intensity when the percentage of *para*-methyl styrene is decreased. Increasing the hydrophobic to hydrophilic ratio usually causes the structures of the polymer in solution to become bigger because of the hydrophobic effect among the polymer chains. [188, 189].

In order to have a qualitative assessment of the hydrophobicity of the polymer, the surface tension of the polymer in solution was measured. Due to the high relaxation time of the polymer, a 0.5% wt of the solution was made up the day before the measurement. Moreover, after the solution was placed in the vessel, the solution was left static for 1.5 h. Surface tension analysis is reported in figure 4.24

Since the measurements showed a decreasing surface tension over time, the data were fit with an exponential curve and the surface tension was extrapolated to a value at infinite time. These values are reported in table 4.7

As expected, the limiting surface tension increases with decreasing percentage of *m*-styrene content in the polymer. The surface tension of poly(*para*-methylstyrene-co-styrene-co-maleic anhydride) copolymers were compared with that of the $SMA_{RAFT}$ 6 kDa co-polymer described in section 4.6 and with SMA2000P, the commercial

**Table 4.7** Surface tension values at 25°Cfor 0.5% wt solution of *para*-methyl styrene copolymers in PBS with 0.2 M NaCl extrapolated with an exponential from figure 4.24

| | Surface Tension (mN/m) |
|---|---|
| $SMA_{met-1.0}$ | 64.3 |
| $SMA_{met-0.8}$ | 64.8 |
| $SMA_{met-0.6}$ | 64.2 |
| $SMA_{met-0.4}$ | 64.7 |
| $SMA_{met-0.2}$ | 65.1 |
| $SMA_{RAFT}$ 6 kDa | 60.2 |
| SMA2000P | 38.5 |

copolymer used commonly used to make discs [36]. For the first copolymer the limiting surface tension is around 60.2 mN/m whereas for SMA2000P surface tension was found to be 38.5 mN/m [84]. The commercial copolymer SMA2000P has a random structure and, as shown in [84], makes a Gaussian coil structure in solution. In this scenario the hydrophobic styrene moieties are more exposed to the water environment and so the polymer adsorbs much more strongly at the interface, decreasing the amount of styrene exposed to the water. Differences between the $SMA_{RAFT}$ 6 kDa co-polymer and the *para*-methyl styrene copolymer may be due to the fact that, as shown from DLS data in figure 4.23 the copolymers are much more aggregated than the $SMA_{RAFT}$ 6 kDa. The higher packing of *para*-methyl styrene can be due to either the higher molecular weight of *para*-methyl styrene than that of $SMA_{RAFT}$ 6 kDa, about 7000 and 5000 kDa respectively. The more folded structure is revealed from surface tension as well. For *para*-methyl styrene copolymer no equilibrium is reached after 26 h. In this scenario less of the hydrophobic region of the copolymer is exposed to water and so less polymer adsorbs at the interface.

### Small Angle Scattering Analysis

In order to understand the structures in solution, the copolymers were analysed using SANS. In figure 4.25 are reported scattering patterns acquired on SANS2d

at ISIS.

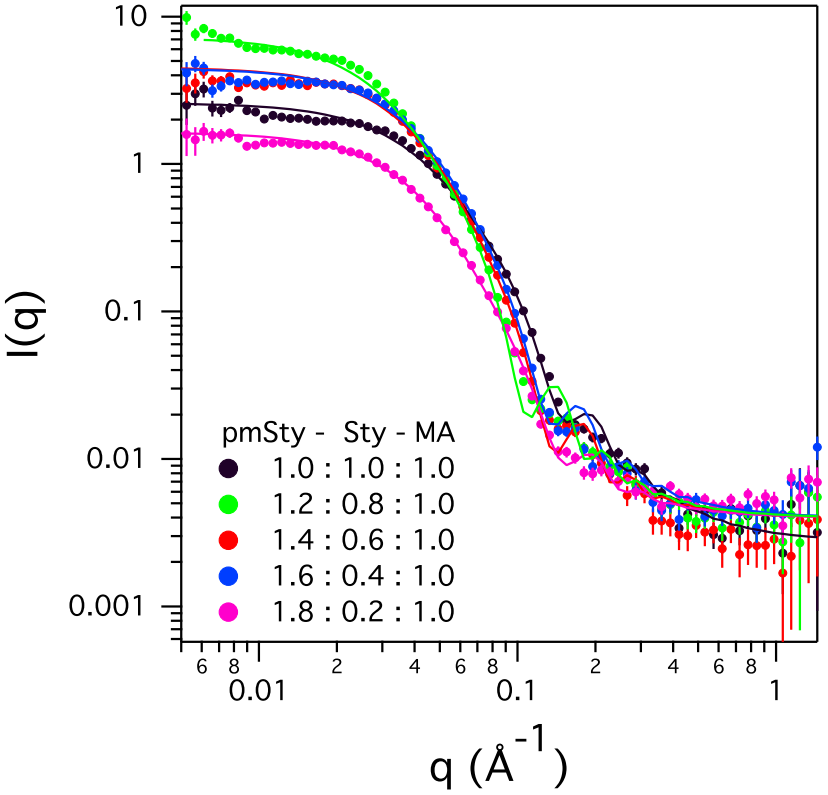


**Figure 4.25** SANS scattering patterns acquired on SANS2d for *para*-methyl styrene co-polymer in d-PBS, 50mM, 0,2M NaCl at 1.5% wt of copolymer.

Polymer solutions were made up in the same way as for DLS, but in deuterated buffer. PBS (50 mM) and 0.2M NaCl was used to make up samples. In order to fit the scattering pattern a polymer micelle model was used. This model is described in section 2.6.1. From a spatial arrangement perspective, the polymer is modelled as a core with a defined SLD and a shell made of Gaussian spheres of radius $R_g$ corresponding to the hydrophilic alternating part of the copolymer. SLDs for the core and the Gaussian coils were calculated to be 1.4X10 $^{-6}$ Å$^{-2}$ and 2.0X10 $^{-6}$ Å$^{-2}$respectively. Bumps observed in the model are due to the absence of polydispersity in the model, which would smear out these. No structure factor is included in the model.

Table 4.8 show that structures have an overall size around 100 Å, which is in

**Table 4.8** Main parameter for the fitting shown in figure 4.25

| | $SMA_{met-1.0}$ | $SMA_{met-0.8}$ | $SMA_{met-0.6}$ | $SMA_{met-0.4}$ | $SMA_{met-0.2}$ |
|---|---|---|---|---|---|
| Core Radius (Å) | 30 ± 2 | 42 ± 2 | 33 ±2 | 34 ±2 | 31 ± 2 |
| $R_g$ (Å) | 21 ± 2 | 27 ± 2 | 20 ±2 | 20 ± 2 | 20 ± 2 |

agreement with the distribution of small structures found with DLS. Bigger aggregates detected in DLS are not detected in SANS in the q range studied. The larger size of the core for $SMA_{met-0.8}$ is likely to be due to the high polydispersity found with GPC.

### 4.9.2 poly(*para*-methylstyrene-co-styrene-co-maleic anhydride) stabilised lipid structures

*para*-methyl styrene copolymers were used to make aggregates with lipids using the same procedure described in section 2.13.2. Structures were analysed according to the procedure adopted for nanodiscs made with SMA and SMI polymers. DLS data was used for preliminary analysis followed by SANS data collected on SANS2d.

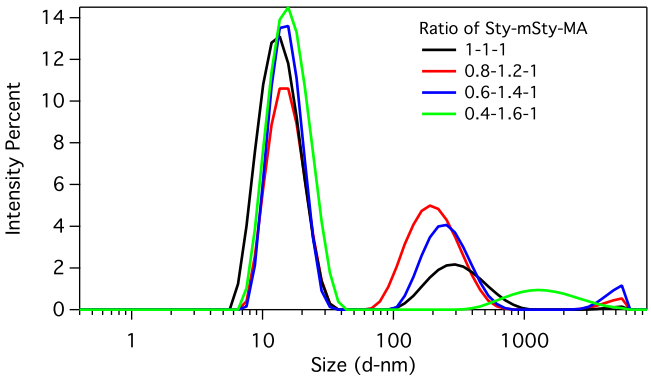


**Figure 4.26** DLS measurements of structures made using *para*-methyl styrene copolymers with DMPC (0.5% wt) in 50 mM, 0.2 M NaCl at 25°C

Figure 4.26 shows how increasing the hydrophobicity of the polymer, destabilises the formation of smaller structures when mixed with DMPC. In fact, the structures at ∼ 10nm decreased in intensity when higher percentages of *para*-methyl

styrene were present in the polymer.

A structural analysis of the sample was carried out using SANS on SANS2d. Since the DLS on these $SMA_{RAFT}$ copolymers showed that a monodispersed sample was generated before and after gel samples were freshly made and measured. An unexpected behavior, however, was shown for these samples. Figure 4.27 shows the scattering patterns acquired for the structures made using $SMA_{met-1.0}$ and several contrasts of PBS and lipids. The black square highlights the contrast of d-DMPC in h-PBS. This contrast should show the core of the structure. The bump at 0.15 $Å^{-1}$ in figure 4.27, however, shows a different structure which was not possible to analyse with conventional models available in the NIST SANS Analysis software Igor 6.3 used to fit the other sets of data.

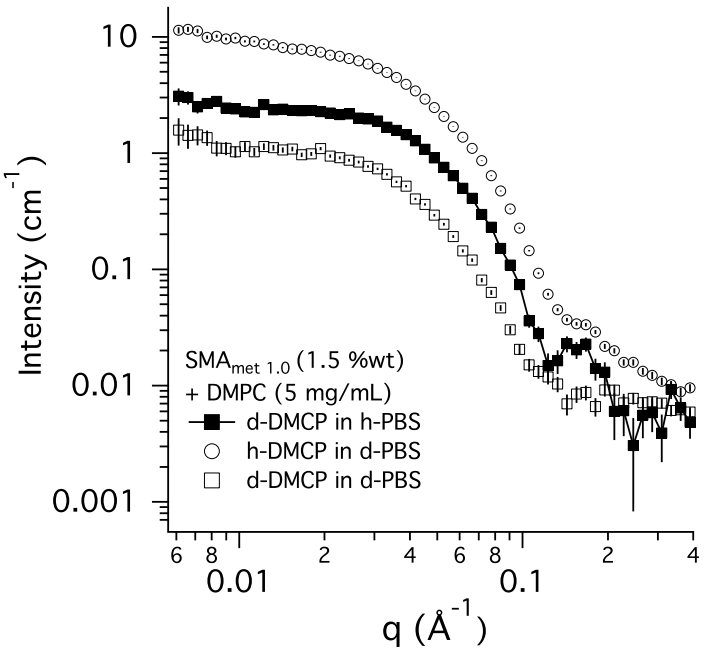


**Figure 4.27** SANS patterns acquired on SANS2d for *para*-methyl styrene copolymers at 1.5%wt in PBS 50 mM, 0.2M NaCl at different *para*-methyl styrene:styrene: maleic acid composition. Measurements were acquired at 25°C

Previous work has shown how important the effect of the hydrophobic to hydrophilic ratio of the polymer is on self-assembly [84, 110]. When copolymers with a styrene to maleic acid ratio of 1:1 are involved, the self-assembly process

that forms nanodiscs does not occur. Moreover Idini [84] showed that polymers with high molecular weight that made big aggregates in solution were less likely to form nanodiscs. Both surface tension and DLS (figure 4.24 and 4.23) show that these copolymers are aggregated and less soluble than $SMA_{RAFT}$ 6 kDa. It can be speculated that the higher packing leads the polymer to prefer the folded structure over interactions with the lipids. In this scenario, the lipids minimise their interaction with water by interacting with the hydrophilic corona of the polymer. The penetration of polymer into monolayers at the liquid air interface was assumed to involve strong SMA interactions with the the head group of the lipids, suggested by previous studies for commercial SMA diffusing into DMPC and DMCP/DMPG mixed monolayers at the liquid air interface [110]. This penetration was studied in this project as well using neutron reflectivity to identify the position of the polymer in the monolayer (see chapter 5). A schematic of the potential structure is reported in figure 4.28

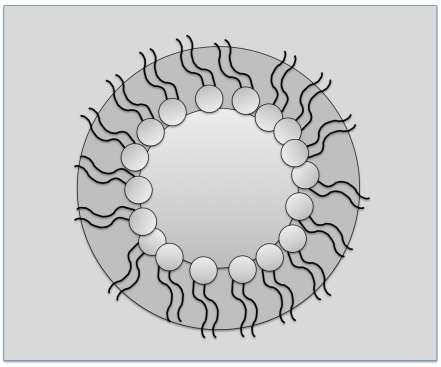

**Figure 4.28** Schematic representation of the presumed structure assumed from *para*-methyl styrenecopolymers in presence of DMPC. Dark grey represents the hydrophilic polymer shell around the light grey hydrophobic polymer core

*para*-methyl styrene SMA copolymer was transferred to Birmingham University, to collaborators in the Biology Department where it was also used to extract membrane protein from cells. These polymers were reported to perform poorly at protein extraction so this work was not pursued further

**Table 4.9** Values for amounts of reagents used in the synthesis of zwitterionic copolymers.

| init. SMA | | Code sample | SMA (g) | DMAPA (g) | conv. (%) |
|---|---|---|---|---|---|
| 6 kDa | 2:1 | $ZWI_{6kDa-2:1}$ | 0.5 | 0.156 | 30 |
| 11 kDa | 2:1 | $ZWI_{6kDa-2:1}$ | 0.5 | 0.156 | 25 |
| 20 kDa | 1:1 | $ZWI_{20kDa-1:1}$ | 0.5 | 0.260 | 32 |

## 4.10 Synthesis of Zwitterionic copolymers

Zwitterionic polymers based on SMA made from RAFT copolymers with different MW and ratios of styrene to maleic anhydride were also synthesised. Use of a zwitterionic copolymer allows a wider working pH range, going from pH= 4 to pH = 10 overcoming current restriction on commercial SMA which is only soluble above pH=7.5.

Synthesis of zwitterionic copolymers was carried out in DMF (dimethylformide) (ACS reagent, 99.8%, Sigma Aldrich). In general 0.5% wt of polymer was solubilised in DMF (0.5 g of polymer in 100mL of DMF). The solution was cooled down in an ice bath. The low concentration and the low temperatures reduced side products such as cross linked polymers. After the polymer had completely solubilised, a syringe pump (Cole-Parmer Single-syringe infusion pump, 230 VAC) was used to add 25 mL of a solution of 0.1M of 3-(dimethylamino)-1-propylamine (DMAPA)(99%, Aldrich) over 1h. Table 4.9 reports the quantities of the reagents for each zwitterionic copolymer synthesised.

The solution was stirred for 3 hours and then split in two: half was precipitated in diethylether, filtered and dried in the oven at 70°C for 2 days to obtain the zwitterionic copolymer. The other half of the solution was heated at 100°C in a vacuum oven for 3 hours or in a microwave at 70 for 15 min. It was precipitated in water and dried in the oven at 70°C for 2 days. The reaction by which the polymer was made is reported in figure 4.29. The zwitterion species is the intermediate for making SMI polymers. After the ring is opened the reaction can proceed through a ring-closing reaction and make SMI. Commercial SMI co-polymer have been

extensively discussed in chapter 3.

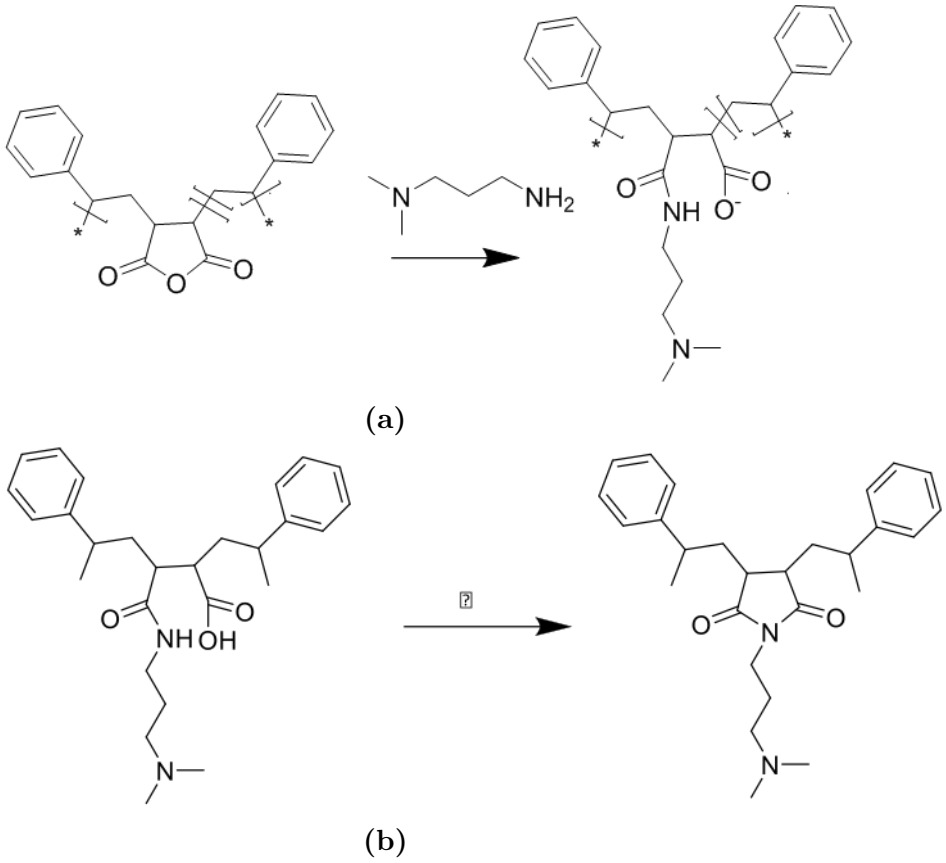


**Figure 4.29** Schematic of the reaction from (a) $SMA_{RAFT}$ 6 kDa to zwitterionic polymer and from (b) zwitterionic polymer to SMI.

Three $SMA_{RAFT}$ co-polymers were reacted with DMAPA to make the zwitterionc species. Table 3 report the starting $SMA_{RAFT}$, the amount of DMAPA and the conversion of the reaction.

Unfortunately the ring-closing reaction to make SMI, even though it was tried extensively during the project, was not successfully carried out. Difficulties with the crosslinking reaction were found, which led to insoluble polymers. The FTIR spectra of both zwitterion and crosslinked SMI are reported in figure 4.30 and compared with the starting SMA used for the reaction.

Figure 4.30 shows that, for the zwitterion step, the peak at 1700 $cm^{-1}$, which is related to the carbonyl group of the maleic anhydride, disappears completely, which suggest a total conversion for the reaction from the anhydride to the zwit-

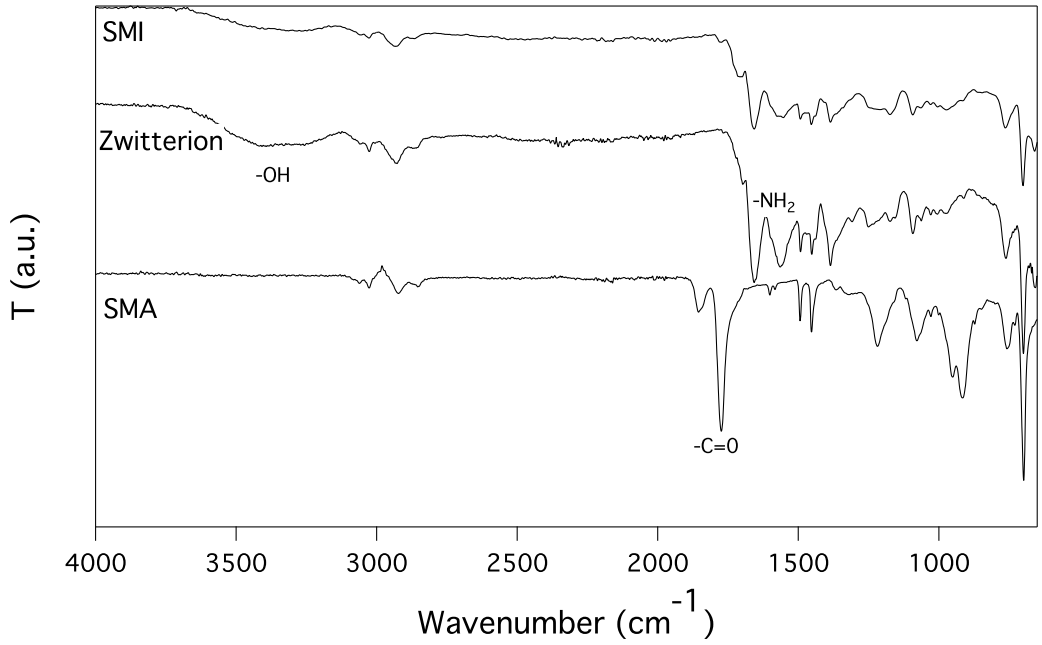


**Figure 4.30** FTIR spectra of SMA (bottom line), zwitterionic polymer (central line) and SMI (top line).

terion polymer. Moreover, a broad signal appears around the region of 3000 $cm^{-1}$ which is due to the stretching of the –OH gorup.

After the ring-closing reaction, the powder was analysed in the same way as the zwitterionic polymers using FTIR after precipitation in water and filtering. This last reaction, due to crosslinking, returned an insoluble resin. Several solvents were used: acetone, DMF, THF. None of these solubilised the SMI powder. The FTIR spectrum in figure 4.30 has a higher background in the finger print region of the spectrum. The reduction in the relative intensity of FTIR peaks was shown for crosslinked polymer of PVA in [190].

### 4.10.1 DLS and SANS analysis

As for the other polymers analysed in this thesis, 1.5% wt solutions of the zwitterionic polymer were made up at different pH using acetate buffer (pH=5) or phosphate buffer (pH=7 and 8) 50 mM and NaCl 0.2M. DLS and SANS results are reported in figure 4.31. SANS analysis was carried out for these polymers us-

ing an ellipsoid and a fuzzy sphere which are both described in section 2.6.1. No structure factor was used for the fitting. The SLD for the polymer was assumed to be 1.96x10$^{-6}$ Å$^{-2}$ as for commercial SMI.

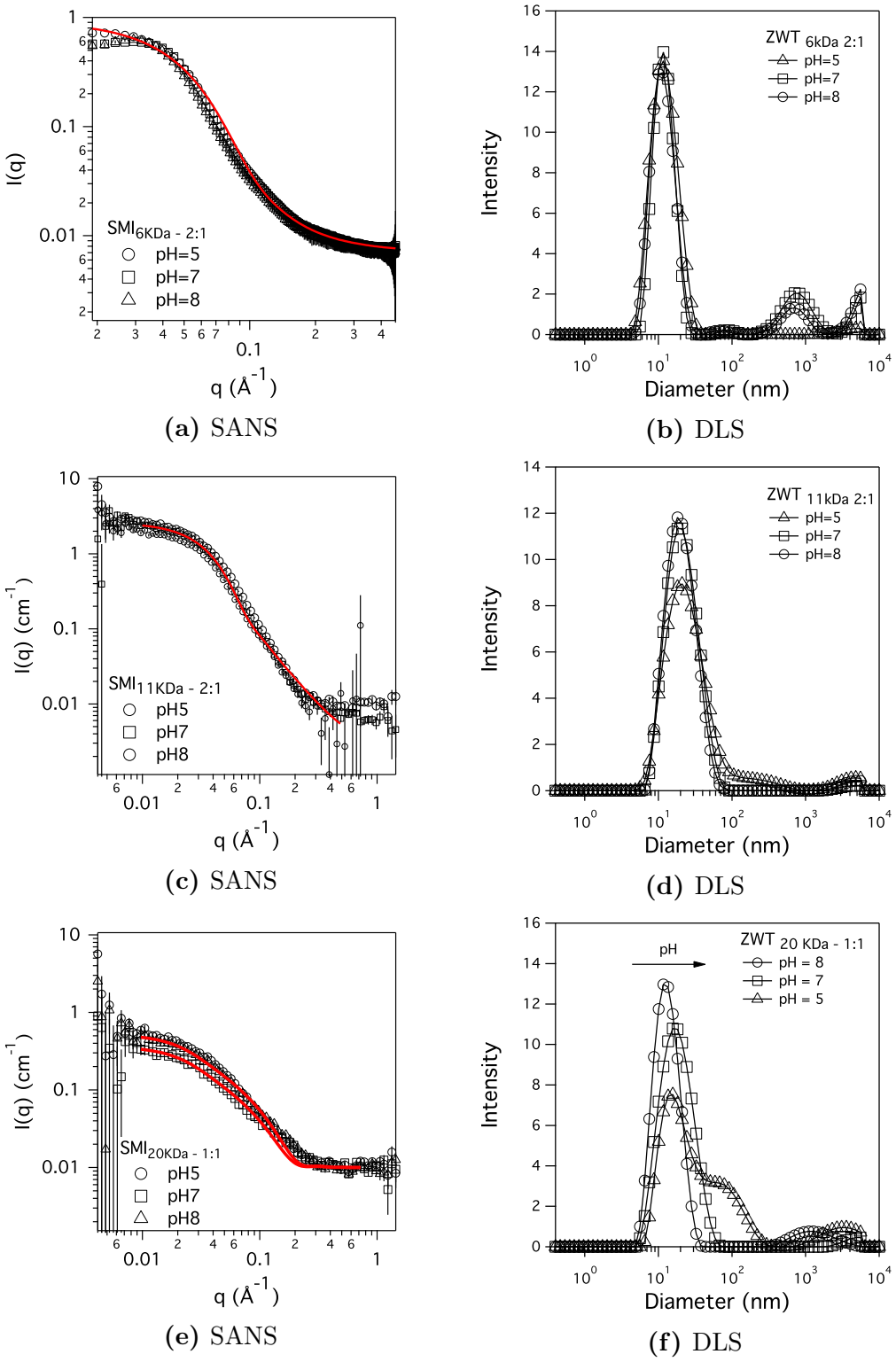


**(a)** SANS **(b)** DLS

**(c)** SANS **(d)** DLS

**(e)** SANS **(f)** DLS

**Figure 4.31** SANS measurement acquired at 3 different pH 5, 7 and 8 and NaCl=0.2M for 1.5% wt of zwitterionic polymer at 25°C. Data were acquired on D33 for (a) $ZWT_{6kDa-2:1}$ and on SANS2d for $ZWT_{11kDa-2:1}$ and $ZWT_{20kDa-2:1}$. DLS measurements for (b) $ZWT_{6kDa-2:1}$, (d) $ZWT_{11kDa-2:1}$ and (d)$ZWT_{20kDa-2:1}$ at the same concentration as for SANS measurement. Measurements were acquired at 25°C

**Table 4.10** Parameters for the fitting of $ZWT_{6kDa-2:1}$ and $ZWT_{11kDa-2:1}$ from figure 4.31a and 4.31c to a fuzzy sphere model

| | $SMI_{6kDa-2:1}$ | $SMI_{11kDa-2:1}$ |
|---|---|---|
| Mean Radius (Å) | 25±5 | 44±2 |
| Interfac. Thick. (Å) | 5±3 | 10±3 |
| Lorentz Length (Å) | 25±3 | 35±4 |
| PDI | 0.45±0.1 | 0.2±0.1 |

**Table 4.11** Parameters for the fitting of $ZWT_{6kDa-2:1}$ and from figure 4.31e

| | $SMI_{20kDa-1:1}$ |
|---|---|
| R. (a) (Å) | 122±5 |
| R. (b) (Å) | 17±3 |

Fitting parameters for SANS are reported in table 4.10 and 4.11.

Figure 4.31 shows how decreasing the pH causes the polymers to tend to aggregate. This might be due to an overall neutralisation of the polymer around the isoelectric point. Unfortunately, due to the low yield of the reaction, not enough material was left to carry out a zeta potential measurement to check at which pH the overall charge on the surface is zero. The SANS characterisation revealed a different arrangement of this polymer in solution as well. The $ZWT_{20kDa-2:1}$ behaved mostly in a similar manner as the commercial SMI, and the solution structures could be fitted to a ellipsoid for all the pH values. On the other hand, $ZWT_{6kDa-2:1}$ and $ZWT_{11kDa-2:1}$ fitted best to a hairy sphere structure. This is reasonable due to the architecture of the starting copolymer: in fact both $SMA_{RAFT}$ 6 kDa and 11 kDa have a styrene tail that will not be reacted and will tend to form the core of the structure. The fitting results reported, as expected from an increased molecular weight, an increased size in the radius. The overall size from SANS is comparable with the structure found from DLS of 12 ± 2, 20 ± 2 and 15 ± 2 nm for $ZWT_{20kDa-2:1}$ $ZWT_{11kDa-2:1}$ or $ZWT_{6kDa-2:1}$ respectively.

## 4.11 Concluding remarks and future work

In this chapter three main points have been discussed. The synthesis and the characterization $SMA_{RAFT}$ of copolymers has been successfully carried out. As expected from the literature , by using RAFT polymerization, well defined and narrow molecular weight distribution polymers have been synthesised. These synthesised polymers have been hydrolysed and used to make nanodiscs. Unlike commercial copolymers, stabilised discs, in accordance with the literature [152], increased in size with increasing molecular weight of the polymer used. This behaviour highlights how crucial it is to have an improved control over the copolymer architecture in order to tune the structures made. $SMA_{RAFT}$ 6 kDa copolymer was successfully used by our collaborators from the Biology Department at the University of Birmingham to extract membrane protein with similar efficiency to the commercial SMA.

Encouraged by the promising results obtained from $SMA_{RAFT}$ copolymers, the architecture of the copolymers was modified by adding an extra hydrophobic moiety: *para*-methyl styrene. Even though the change was not dramatic in terms of the structures formed, huge changes have been detected in the polymer behaviour. DLS and surface tension were measured and showed the presence of aggregates which led, in the presence of DMPC, to a supramolecular structure that still needs to be clarified from a structural point of view. DLS measurements detected the presence of small structures, unlike those found for the polymer alone, which was confirmed by the transition from a cloudy solution of DMPC to a clear solution when the polymer was mixed with DMPC. However, tests on protein extraction with this polymer were unsuccessful suggesting that the increased hydrophobicity is not a useful modification for this purpose.

Last, but not least, zwitterionic copolymers have been successfully made showing stable properties in a wide range of pH. Preliminary DLS analysis of the polymer on its own shows promising features for this copolymer. Unfortunately, due to the low yield of the polymerization and lack of time to prepare more material, no further analysis requiring a high amount of polymer could be carried out. An improved synthesis of this copolymer and further characterisation could potentially lead to great advantage in the scientific community for membrane proteins extraction and studies by allowing nanodisc formation at neutral pH.

# Chapter 5

# Polymer-phospholipid interactions during polymer stabilised nanodisc formation

For many purposes, investigations of polymer interactions with phospholipids have been carried out in the last decades. Techniques such as Atomic Force Microscopy and fluorescence have been used [191]. Some experiments carried out with charged polymers showed an interaction with a DMPC monolayer and its disruption when the polymer was added to the solution [192]. In 1992 [193] a study showed how pH responsive polyelectrolytes interact and disrupt lipid vesicles when pH is changed.

Over the period of this project, interactions between phospholipids and different copolymers have been investigated using several scattering techniques and also fluorescence. Neutron or X-Ray sources were used to characterise the diffusion and the interaction of polymer with vesicles or Langmuir monolayers with a high spatial resolution and penetration depth. Thanks to its fast response to changes in the surrounding environment, fluorophore probes were used to detect fast processes during lipid-polymer interactions and give information about the mechanism. In the next paragraph an outline of general polymer-lipid interactions will be given.

### 5.0.1 Polymer-lipid structures

When a polymer species interacts with lipid membranes, the structure that is formed in its final stage depends on the features of the structures at the beginning such as charge, composition and size of both initial systems. For any arrangement going on in solution, from the thermodynamic point of view, the reduction in entropy of the polymer chain as it approaches the interface has to be compensated by the energy of adsorption between the segments and the surface. A key property for the final structure is the hydrophilic/hydrophobic ratio of the polymer. As discussed in chapter 3, this ratio affects the shape of the polymer in solution due to the strength of inter and intramolecular interactions. These interactions lead the polymer to interact more or less effectively with the membrane [5]. Several different structures have been reported in literature showing different behaviours when this ratio was changed. "Mushroom" shapes were found when a hydrophilic copolymer was added to a membrane [194] where the hydrophobic part of the copolymer anchors into the membrane while the hydrophilic part of the copolymers behave like a Gaussian coil. Pores can be made in the lipid membrane upon polymer addition if the architecture of it allows this process. Pores can be made in the lipid membrane upon polymer addition if the architecture of it allows this process. Pore-making block copolymers are usually made of two or more sequences of thermodynamically incompatible homopolymers. This leads to a swelling of the copolymer into part of the membrane and a to a selective exposure of the monomers to the surrounding environment. [195]. In the literature examples are reported of pore formation for star copolymers or di- and tri-block copolymers of PEO-PPO-PEO. Figure 5.1 reports an example of the most common interactions studied when different polymers are used, being either neutral or charged [5]. The process that leads to the self assembly of polymer and lipids is driven by both structures. A polyelectrolyte, which is charged interacts first through electrostatic interactions on the surface of the lipid membrane which lead to the formation of a polymeric corona on the surface of the liposome or the membrane [196]. This first organisation causes a rearrangement of the lipids

along the layer. It has already been shown in literature how a positively charged polymer approaching a membrane can induce a flip flop of the lipids in the bilayer, which results in a negatively charged layer of lipids in contact with the positively charged polyelectrolyte (figure 5.1-b) [197]. The complexation of polymer with the membrane can be so strong that it can lead to the disruption of the membrane itself. Several structures, depending on the polymer and the membrane used have been investigated. Block copolymers of PEO-PPO-PEO with a high hydrophobic ratio showed disrupting behaviour, forming crew-cut structures [198]. In other cases micelles were formed. In the last few decades the SMA copolymer has been shown to cause membrane disruption, making nanodiscs.

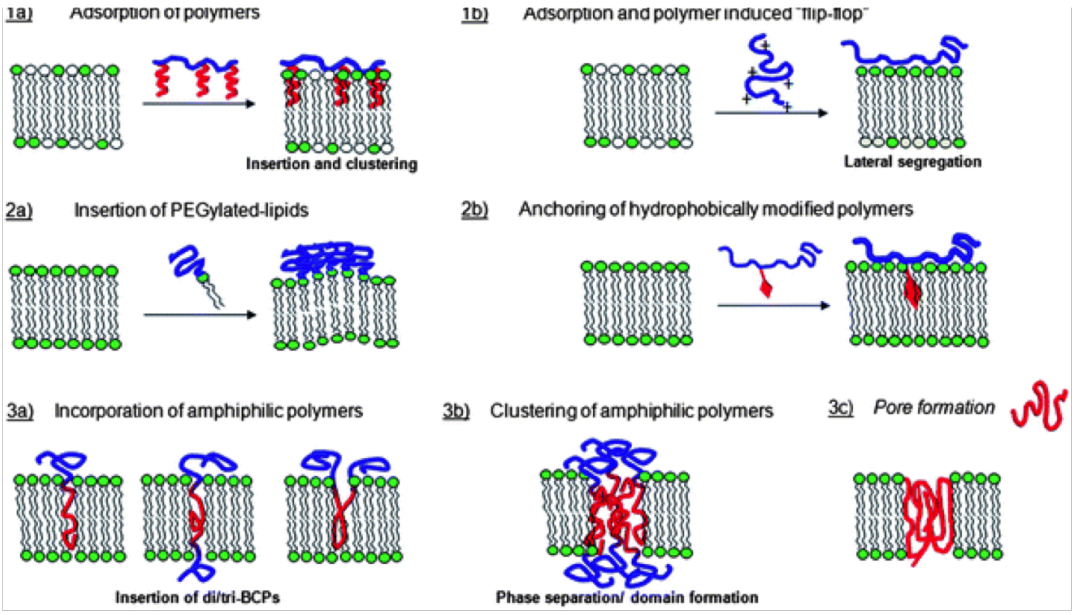


**Figure 5.1** Graphic showing the various kinds of interactions of polymers with a phospholipid bilayer. Picture reprinted with permission from [5]

Even though many experiments on polymer-lipid interactions have been carried out, the basic mechanism of the self-assembling process is not yet clarified. Self assembled vesicle structures made with polymers are now known as polymersomes. A polymersome is an artificial vesicle made using synthetic block copolymers [199]. However, even though this system is widely used for encapsulation of biological material, protein and drugs, SMALP and other polymer stabilised discs

do not belong to this category since they do not make vesicles.
In the literature several experiments have previously been carried out to understand how a polymer approaches the interface of lipid vesicles and how it disrupts the membrane. In this chapter it will be shown how SMA polymer interacts with DMPC artificial membrane using fluorescence (section 5.1.2, neutron reflectivity (section 5.3.1) and SANS(section 5.2).

## 5.1 Characterisation of phospholipid-polymer interaction using fluorescence

Fluorescence is a wide branch of chemistry where, in general, a species called a fluorophore changes its emission spectrum when it is surrounded by a different environment. This technique is commonly used because the signal to noise ratio is high enough to carry out experiments at very low concentrations and because it has a high resolution either for the spatial or temporal point of view. Last but not least, fluorescence is a non-invasive technique. For all these reasons fluorescence has been widely used in recent years because it allows in vivo detection and is used for diagnosis and treatment of diseases [200]. A few examples are reported in literature where fluorescence was used to study enzymes approaching a cell membrane [201–203]. Even though synthetic polymers are not identical to an enzyme, a few general rules must be satisfied in order to follow an interaction using fluorescence: when the diffusing species interacts with the membrane, the fluorescence properties of the probe, such as intensity, life time or emission wavelength, must change. Two types of probes can be used to study the interaction:

- *Intrinsic fluorescence*: Membrane proteins contain fluorescent amino acids such as tryptophan (Trp) and tyrosine (Tyr). Thanks to their sensitivity to the surrounding environment, a change in the fluorescence properties can be detected when a species interacts with the membrane where these groups are intercalated. Using this approach, side effects derived from the

interaction of the membrane with external agents are minimised.

- *Membrane potential-sensitive probes*: due to lack of fluorescent amino acids, intrinsic fluorescence is not always suitable to study the interaction of species with the membrane. That is why probes have been used in the last few decades to study for the interaction of species with the membrane.

For our purposes, in order to detect the interaction of the polymer with a suspension of phospholipids the second approach was used. The approach of the polymer to the vesicle surface near the headgroups and the insertion of the styrene moieties were investigate using fluorescein phosphatidylethanolamine (FPE) and 1 - (3-sulphonatopropyl) - 4 - [$\beta$ [2 - (di-n-octylamino)-6-naphthyl] vinyl]pyridinium betaine (known as Di-8-ANEPPS) respectively (figure 5.2 on page 166). Those two probes are extensively described in section 5.1.1 below. Since the fluorophore attached is to a phospholipid molecule, this probe system is biocompatible and non-invasive. The tagged lipid inserts into the membrane with no perturbation of the membrane structure.

### 5.1.1 FPE and Di-8-ANEPPS: a tool to probe polymer-vescicles interactions

Structures for FPE and Di-8-ANEPPS are reported in figure 5.2
In order to understand how FPE and Di-8-ANEPPS work, it is important to revise how the potential is distributed along a phospholipid bilayer. Changes in this potential play a key role in events such as cellular recognition and metabolism[204]. Figure 5.3 shows how the potential changes along the membrane.
The surface potential ($\Psi_s$) arises from the different kinds of lipid head groups along the surface of the membrane. The polar head of a phospholipid can be neutral (*i.e.* DMPC, DPPC), negatively charged (*i.e.*DMPG) or (*i.e.* DMPE). Natural membranes, however, are most commonly made by zwitterionic or negatively charged lipids, which leads to a negative surface potential that is established to be around -30 mV. The membrane dipole potential, instead, arises from

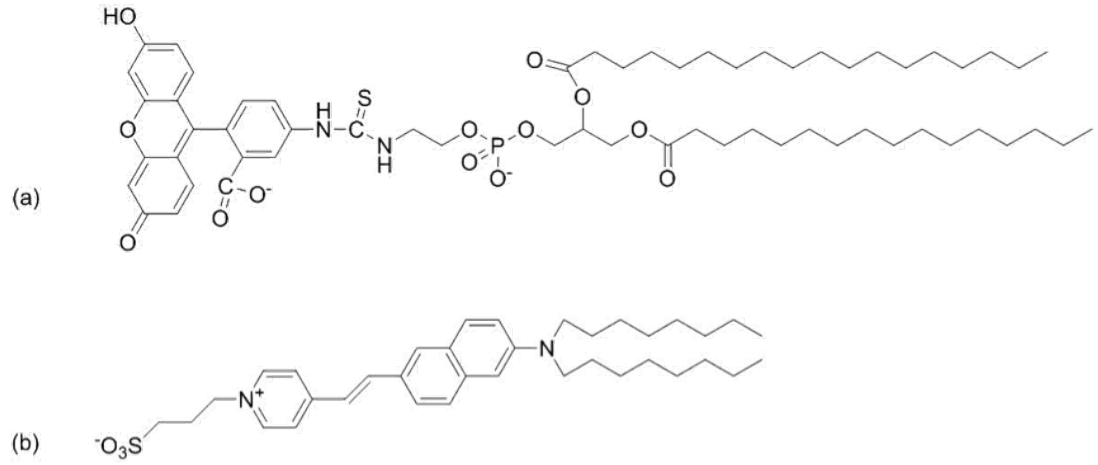


**Figure 5.2** Structural formulas of (a) FPE and (b) di-8-ANEPPS

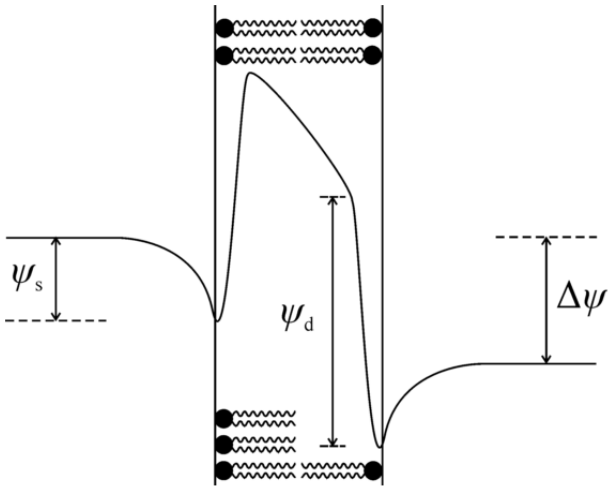


**Figure 5.3** Electrical potentials across a phospholipid membrane where $\psi_s$ is the surface potential, $\psi_d$ is the dipole potential and $\Delta\psi$ is the transmembrane potential. Picture reprinted with permission from [6]

dipole-dipole interactions among carbonyl group in the lipids. Dipolar groups are considered to be spatially organised in a way that the internal hydrophobic region has a positive potential of several hundred mV [205]. These two potentials are not influenced by the same factors. This, in physical terms, means that changing factors such as the ionic strength of the surrounding media, leads to a change in the surface potential, but it does not affect the dipole potential.

FPE was first used to probe the pH changes in the inner and outer environment of lipid vesicles [206]. It has been widely used in the biological community to probe the binding of charged molecules onto the surface of lipid membranes. This molecule consists of two regions. Like a phospholipid, FPE has a strongly hydrophobic region which inserts into the phospholipid tail region of the bilayer and a more hydrophilic one, made of fluorescein, which works as a tag. Given this structure, when FPE is suspended within a vesicle solution, it inserts into the outside layer of the vesicle with the hydrocarbon chains integrated into the lipid tails, the phosphatidylethanolamine moiety mixed with the lipid headgroups and the chromophore composed of a xanthene ring system placed on the outside of the liposome. Fluorescein is well known to undergo a shift in the emission and excitation spectra depending on its protonation state [207] which is affected by the electrostatic potential surrounding the xanthene ring system [203]. The behaviour according to which the protonation/deprotonation of xanthene occurs has been quantified using the Henderson-Hasselbalch equation, making a correction of the $pK_a$ by accounting for the surface potential $\Psi_s$ (equation 5.1 [202])

$$\log\left(\frac{c_F}{c_{HF}}\right) = pH - \left(pK - \frac{F\Psi_s}{RT\ln 10}\right) \tag{5.1}$$

where $C_F/C_{HF}$ is the ratio of deprotonated and protonated molecules of fluorescein, $pH$ is the pH of the bulk solution and $pK-(F\Psi_s)/(RT\ln 10)$ is the apparent pK. From this equation it is clear how, at a constant $pH$ of the bulk, the surface potential affects the protonated state of the fluorescein. The electrostatic potential varies depending either on the electrolyte concentration or on the charge of the binding molecule. Because of this dependence of the fluorescence spectra on the electrolyte environment, during the experiments here a control was run by adding $CaCl_2$ to FPE solution instead of polymer. Because this increased the positive charges in solution, a decrease in the magnitude of the negatively charged potential is observed. Due to this change the apparent pK of the FPE changes, leading to deprotonation of xanthene ring system and an increase in fluorescence intensity. Those characteristics made FPE an incredibly sensitive probe for the

studies of how molecules approach and bind to the cell membrane.
In order to monitor the dipole potential using Di-8-ANEPPS a ratiometric fluorescence experiment using a fixed excitation wavelength was used carried out.
It has been reported in literature that Di-8-ANEPPS has the highest and lowest variation in emission intensity at 460 and 520 nm respectively [201]. The same study reported that the surface potential of the membrane does not interfere with the dipole potential [201]. In this way an independent study of the polymer binding and the intercalation of the polymer into the bilayer can be carried out. This ratiometric potential method has been validated by many researchers [201, 208]. Here vesicles were tagged using both FPE and Di-8-ANEPPS (figure 5.2).

### 5.1.2 Titration and binding curve

For a typical experiment, a first scan of DMPC-FPE tagged vesicles is carried out. Then, 0.1 mM polymer solution was added to 1.9 mL of FPE tagged vesicles. The system was allowed to stabilise and the measurement was averaged over 100 sec. In order to check the correct insertion of the fluorescein of tagged lipid into the lipid head leaflet had occurred, excitation and emission spectra of DMPC and $DMPC_{80}DMPG_{20}$ FPE-labelled vesicles were acquired prior to the experiment. $CaCl_2$, TRIS buffer and SMA2000P were added to the labelled vesicle solutions. Figure 5.6 shows how fluorescence changes during the addition of polymer.

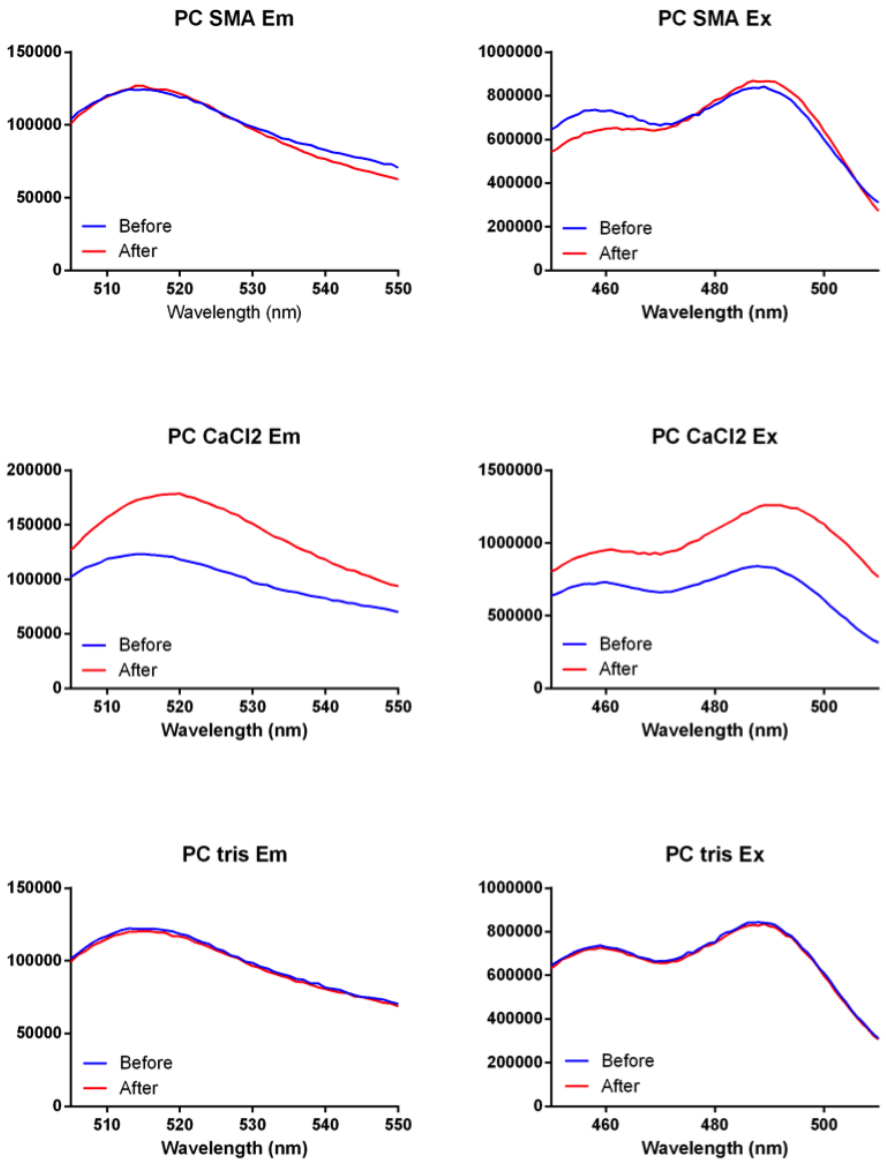


**Figure 5.4** Emission (a, c, e) and Excitation (b, d, f) of FPE-tagged vesicles made with DMPC before and after the addition of polymer (first row), $CaCal_2$ (second row) and TRIS buffer as a control (third row). The excitation and emission spectra were acquired with $\lambda_{exc} = 420nm$ and $\lambda_{em} = 520nm$ respectively. Measurements were acquired at 25°C.

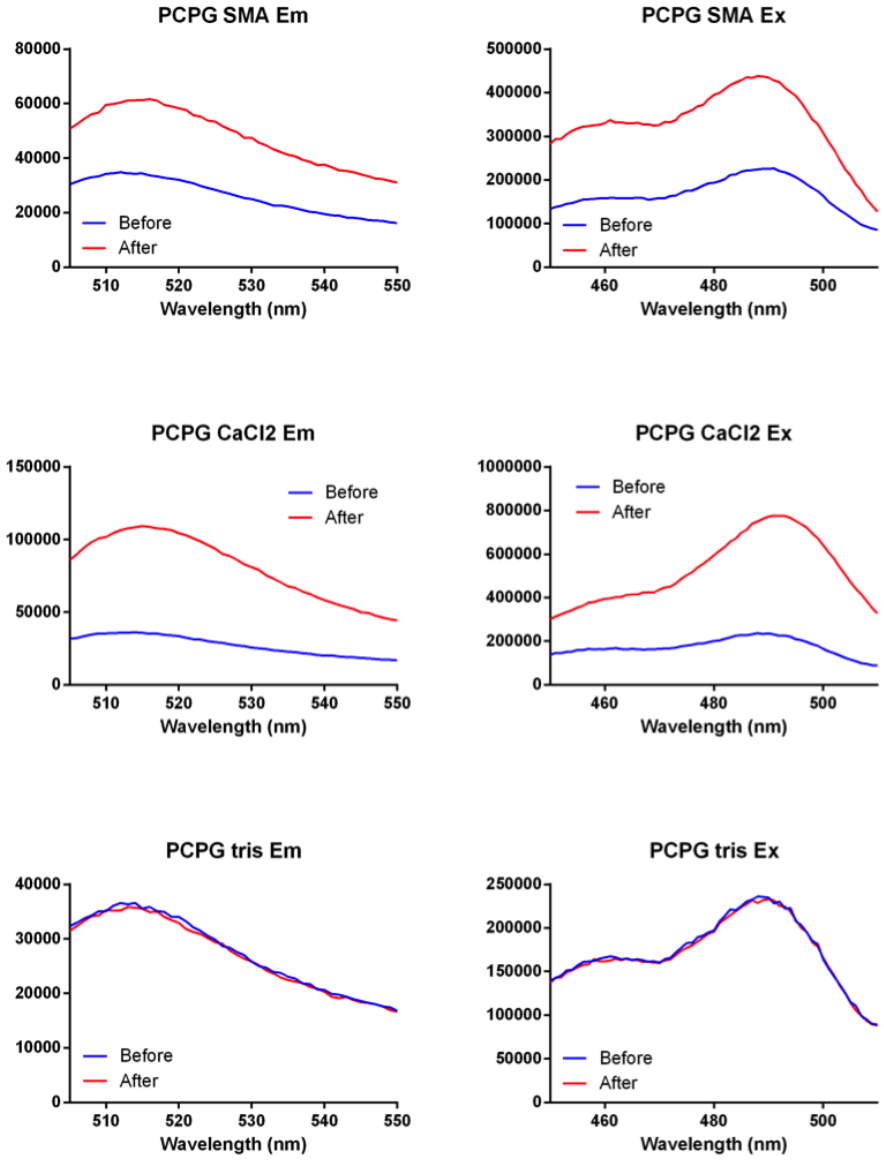


**Figure 5.5** Emission (a, c, e) and Excitation (b, d, f) of FPE-tagged vesicles made with $DMPC_{80}DMPG_{20}$ before and after the addition of polymer (first row), $CaCal_2$ (second row) and TRIS buffer as a control (third row). The emission and excitation spectra were acquired with $\lambda_{exc} = 420nm$ and $\lambda_{em} = 520nm$ respectively. Measurements were acquired at 25°C.

The graphs in figures 5.4 and 5.5 report the excitation (a, c, e) and emission (b, d, f) spectra in the left and right column respectively. Figure 5.4 reports the spectra for DMPC tagged vesicles whereas figure 5.5 is related to $DMPC_{80}DMPG_{20}$ tagged vesicles. In both figures the blue curve shows the spectra of vesicles tagged with FPE on their own. The spectra after the injection of polymer are reported in the graphs by the red line.

A control measurements was carried out by adding to the tagged lipid vesicles solution, the same volume of TRIS, containing no polymer or $CaCl_2$to the tagged lipid vesicle solution. The intensity of the emission, before and after the TRIS addition, did not change (5.4-(e),(f) and 5.5-(e),(f)). This highlights that any change seen in the other spectra is not due to dilution effects, but is due to the interaction of the polymer with the system. It is obvious comparing figure 5.4 and 5.5 that the lipid composition also affects in the changes seen in the spectra. In fact when a mixture of DMPC and DMPG is used, the decrease in intensity is more pronounced. But, since FPE is greatly sensitive to the potential of the surface, this effect could be due to the negatively charged head group of DMPG. When a negative charge is approaching the liposome surface where the FPE is inserted, a negative change in fluorescence should be observed as explained in paragraph 5.1.1.

Several optimisation experiments were carried out to obtain the best binding curve. In fact, when using a highly concentrated solution of polymer (10 mM), the first addition of the polymer was sufficient to cause a decrease of the curve, as expected, since the polymer carries a negative charge. But from the second addition of polymer, giving a polymer concentration in solution of about 100 $\mu$M the % fluorescence increases (rather than decreases) as shown in figure 5.6. This unusual behaviour could be caused by the disruption of the vesicles when the second aliquot of polymer is added to the solution. The different environment around the fluoresceine could cause an unexpected response to the addition of polymer in solution. Therefore a lower concentration of polymer was used. Binding curves for the experiment carried out by adding the lower concentration of 0.1

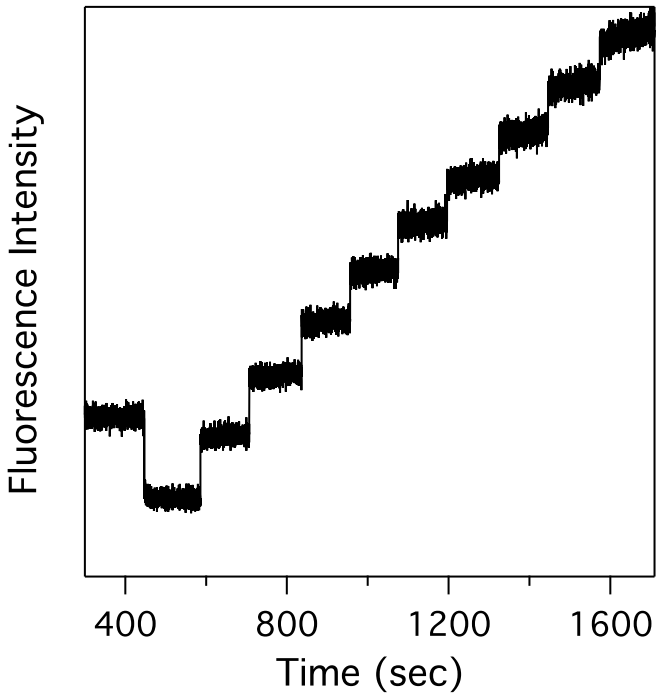


**Figure 5.6** Effect of addition of SMA2000P solution 10mM to a solution of DMPC-FPE lebelled vesicles.

mM SMA2000P and $SMA_{RAFT}$ at the lower concentration of 0.1 mM are shown in figure 5.8

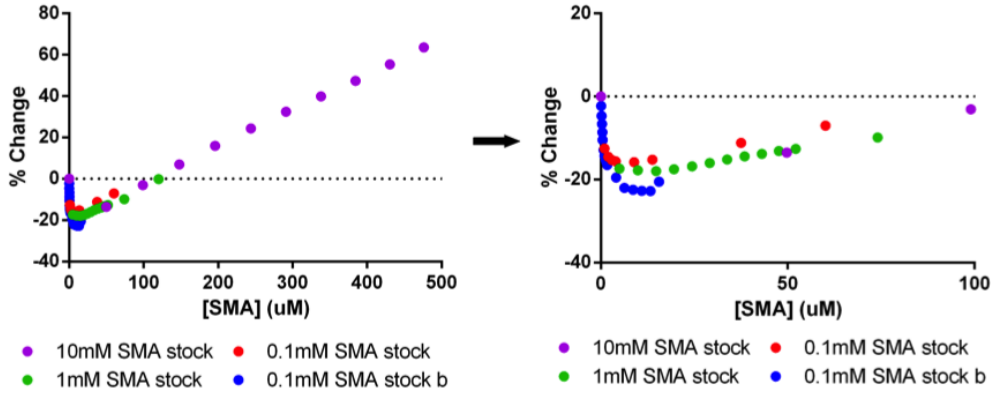


**Figure 5.7** Titration binding curve for DMPC vesicles for different concentrations of added SMA: (left) from 0 to 500 mM and (right) from 0 to 100 mM.

An unexpected behaviour was found for $DMPC_{80}DMPG_{20}$ vesicles when either SMA2000P or $SMA_{RAFT}$ was added to the solution. Even at the low polymer

concentration, the fluorescence signal undergoes an enhancement. This unexpected behaviour has been reported in literature when erythtocyte membranes were used. This membrane was labelled with FPE and then melittin and poly-L-lysine were added to the solution. Due to the positive charge of those molecules, an enhancement in the fluorescence signal is expected. However the opposite behaviour has been observed. In those membranes, where a high negative charge is present, such as for $DMPC_{80}DMPG_{20}$ ,the high charge can lead to an unexpected response of the FPE molecule. The enhancement of FPE when SMA 2000P or $SMA_{RAFT}$ is approaching could be due to a rearrangement of the lipids in the liposome.

It is possible that the polymer makes hydrogen bonds with lipid head groups. In fact at pH values lower than 8 the polymer is partially protonated, so able to hydrogen bond with the lipids potentially reducing the apparent charge on the membrane. Another explanation is that the negative polymer, approaching the surface squeezes the DMPG head away from the FPE tag leading the FPE to "experience" a more positive local environment.

The starting value for fluorescence was used to calculate the absolute % change.

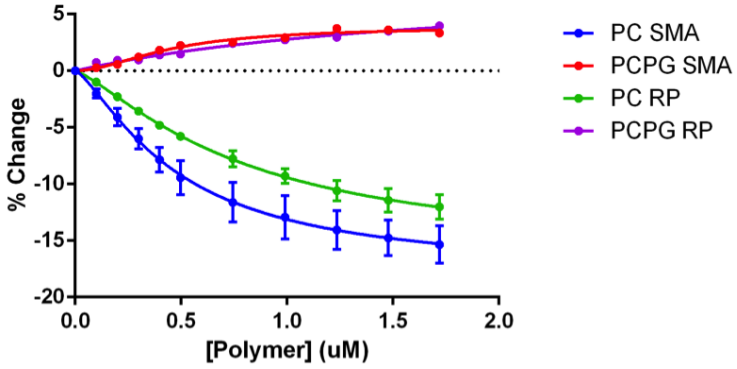


**Figure 5.8** Binding curves for SMA2000P and $SMA_{RAFT}$ with $PC_{80}PG_{20}$ (red and magenta respectively) and DMPC (green and blue respectively) vesicles.

The fitted binding curves with relative fitted parameters for either commercial SMA2000P or $SMA_{RAFT}$ polymer with 100% DMPC and $DMPC_{80}DMPG_{20}$ phospholipids are reported in table 5.1

**Table 5.1** Fitting parameters for binding curves relative to the two membranes under investigation ($DMPC_{100}$ and $DMPC_{80}DMPG_{20}$) with $SMA_{RAFT}$ and SMA2000P

| Membrane | Polymer | Best fit | $R^2$ | $B_{max}$ | $K_d$ | h |
|---|---|---|---|---|---|---|
| $DMPC_{100}$ | SMA | Sig. | 0.97 | -17.95 ± 2 | 0.48 ± 0.097 | 1.36 ± 0.2 |
| $DMPC_{80}DMPG_{20}$ | SMA | Sig. | 0.98 | 3.88 ± 0.3 | 0.45 ± 0.063 | 1.85 ± 0.4 |
| $DMPC_{100}$ | RP | Sig. | 0.99 | -16.56 ± 2 | 0.809 ± 0.2 | 1.30 ± 0.1 |
| $DMPC_{80}DMPG_{20}$ | RP | Hyper. | 0.98 | 8.19 ± 1 | 1.95 ± 0.5 | - |

Other than the binding of the polymer on the surface, the intercalation of the polymer into the tail of the liposome was investigated using Di-8-ANEPPS. To have reproducible and comparable results, the same concentration of polymer and phospholipids were used for the titration carried out with Di-8-ANEPPS.

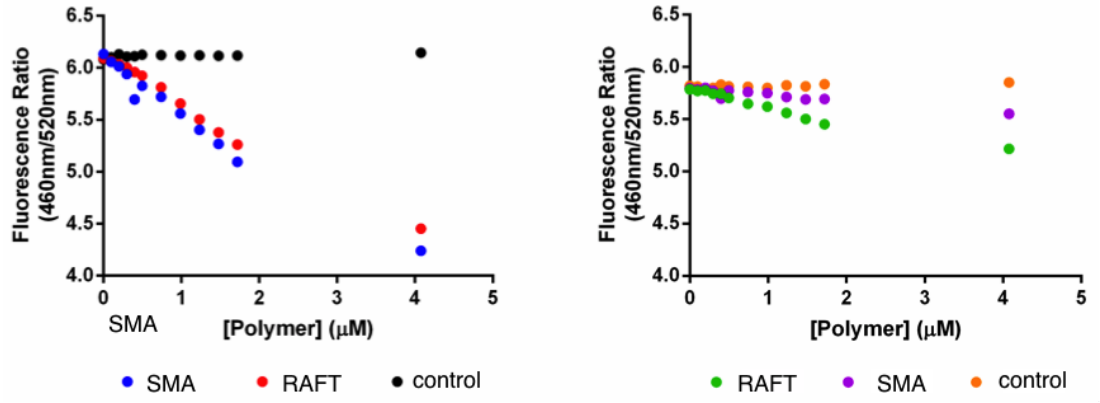


**Figure 5.9** Di-8-ANEPPS titration curve of: (left) DMCP vescicles adding SMA2000P 0.1 mM (blue dot), $SMA_{RAFT}$ (red dot) or Tris buffer pH=7.4 (black dot); (right) $DMPC_{80}DMPG_{20}$. adding SMA2000P 0.1 mM (pink dot), $SMA_{RAFT}$ (green dot) or Tris buffer pH=7.4 (orange dot).

In the literature it has been reported that the insertion of a peptide such as p25, a mitochondrial amphipathic sequence, decreases the dipole-dipole interaction among the phospholipid tails causing a decrease in the fluorescence ratio . [201]. In that study, using this peptide, it was shown that a higher concentrations of the peptide led to a higher decrease in the fluorescence ratio. The magnitude of the interaction is proportional to either the concentration of the peptide or to the membrane used, which affects the initial value of the dipole potential. However, when a DMPC liposome interacts with SMA, either the commercial or

the $SMA_{RAFT}$, the magnitude of the changes in the fluorescence ratio is comparable. The slightly smaller intercalation of the $SMA_{RAFT}$ could be due to the slower interaction also found during other experiments (see SANS data in section 5.1.3; in this case the values used for the average were potentially not at the equilibrium state, and the polymer was not fully inserted in the membrane. A substantial difference can be highlighted between the left and right hand side of figure 5.9 which reports interactions with DMPC and $DMPC_{80}DMPG_{20}$ liposomes respectively. Even though it has been reported that differences in the membrane used can lead to a difference in the magnitude of the dipole potential [202, 205], the headgroups of DMPC and DMPG are not dramatically different to explain such a different effect in the magnitude of the signal as shown in figure 5.9. Nonetheless the difference in magnitude, when the polymer inserts into the membrane is much lower for the commercial SMA when the membrane is made of $DMPC_{80}DMPG_{20}$. This can be explained by the different architecture of the copolymer in solution. Even though the molecular weight and ratio of styrene to maleic acid of both polymers are similar, a substantial difference arises in the conformation of the polymer in solution. As discussed in chapter 4, $SMA_{RAFT}$ copolymers have well defined alternating blocks of styrene and maleic acid followed by a styrene tail. This localises the negative charge of the maleic acid just on the alternating block of the polymer. The electrostatic repulsion of the styrene tail is much lower than the alternating block, and allows styrene tail block to penetrate better into the $DMPC_{80}DMPG_{20}$ membrane. On the other hand, SMA2000P has a random distribution of styrene and maleic acid, with the only restriction that two maleic acid monomers can not be next to each other. This polymer was shown to have a random coil distribution [84] which allows a faster interaction with zwitterionic membranes such as DMPC, but leads to a higher and more spread out electrostatic repulsion of DMPG negatively charged head groups along the whole structure of the copolymer. $SMA_{RAFT}$ polymer then is much more effective when the membrane to be disrupted has a negative charge on it. This is also shown by subsequent studies reported here where DLS was

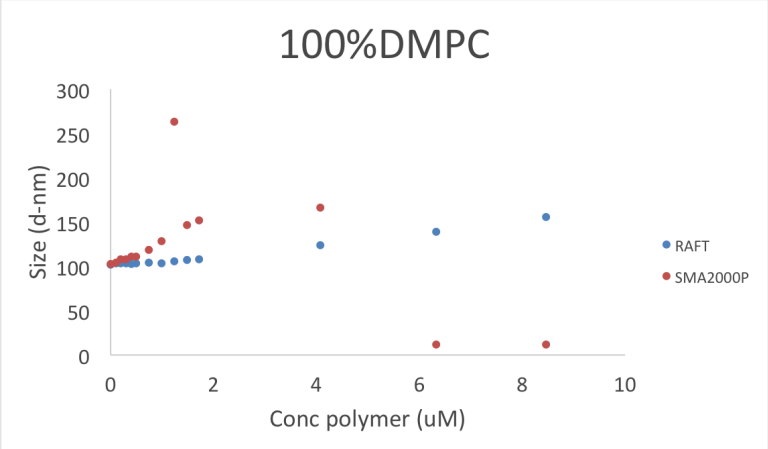


**Figure 5.10** DLS titration carried out with DMPC liposomes using either SMA2000P or $SMA_{RAFT}$.

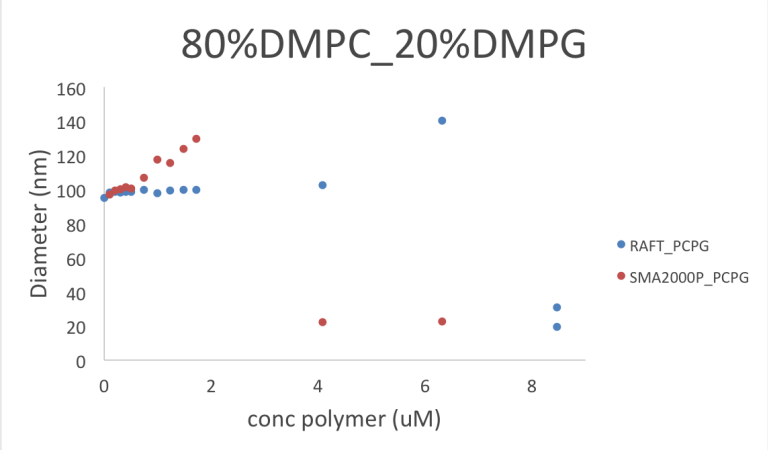


**Figure 5.11** DLS titration carried out with $DMPC_{80}DMPG_{20}$ liposomes using either SMA2000P or $SMA_{RAFT}$.

used to follow the size of structures during titration of either DMPC or vesicles using the same concentration of polymer used for the fluorescence experiment. (figure 5.10 and 5.11)

The DLS measurements show how SMA2000P and copolymer interact in two different ways with the vesicles. In fact when SMA2000P is used the vesicles swell, suggesting that the polymer is approaching the membrane, as shown from by the FPE titration, and then, at a concentration equal to 3 $\mu$M breaks the vesicles apart, for both DMPC and $DMPC_{80}DMPG_{20}$,and makes small structures with size around 10 nm. In the case of the $SMA_{RAFT}$ copolymer, vesicles do not

increase in size, until just before the polymer disrupts the liposome. For both DMPC and $DMPC_{80}DMPG_{20}$ vesicles, a higher concentration of $SMA_{RAFT}$ is needed in order to break the vesicles. In the case of DMPC vesicles, the RAFT co-polymer did not reach the concentration for which the transition from vesicles to nanodiscs occurs. It is possible to note how a lower concentration of polymer is needed when $DMPC_{80}DMPG_{20}$ is used. This is probably due the destabilisation of the membrane due to repulsive electrostatic forces between the lipids and the polymer, both negatively charged. The SMA2000P destabilises the membrane more due to its randomly distributed negative charge. Therefore it breaks the $DMPC_{80}DMPG_{20}$ membrane at a lower concentration compared to $SMA_{RAFT}$ .

### 5.1.3 Stopped - flow experiments

In order to detect the early stages of the self assembly process and the polymer-lipid interaction, stopped flow experiments were carried out using either fluorescence or small angle neutron scattering.

### 5.1.4 Stopped-flow experiments - fluorescence detection

Different concentrations of polymer were made up for a stopped flow fluorescence experiment. The final concentrations of polymer in solution were 0.3 $\mu$M, 0.75 $\mu$M, 1.25 $\mu$M and 100 $\mu$M. The first 3 concentrations are in the range that was used to measure the binding curves reported above for both DMPC and $DMPC_{80}DMPG_{20}$vesicles. For this experiment the same volume of polymer, at double the final concentration (0.6, 1.5, 2.5 and 200$\mu$M) and FPE labelled liposomes (0.4$\mu$M) were injected (0.4mL). The experiment was followed between 0 and 0.2 seconds (1000 points) and between 0.2 and 20 sec (1000 points). 8 repeats for each experiment were run. Data from this experiment are reported below in figure 5.12.

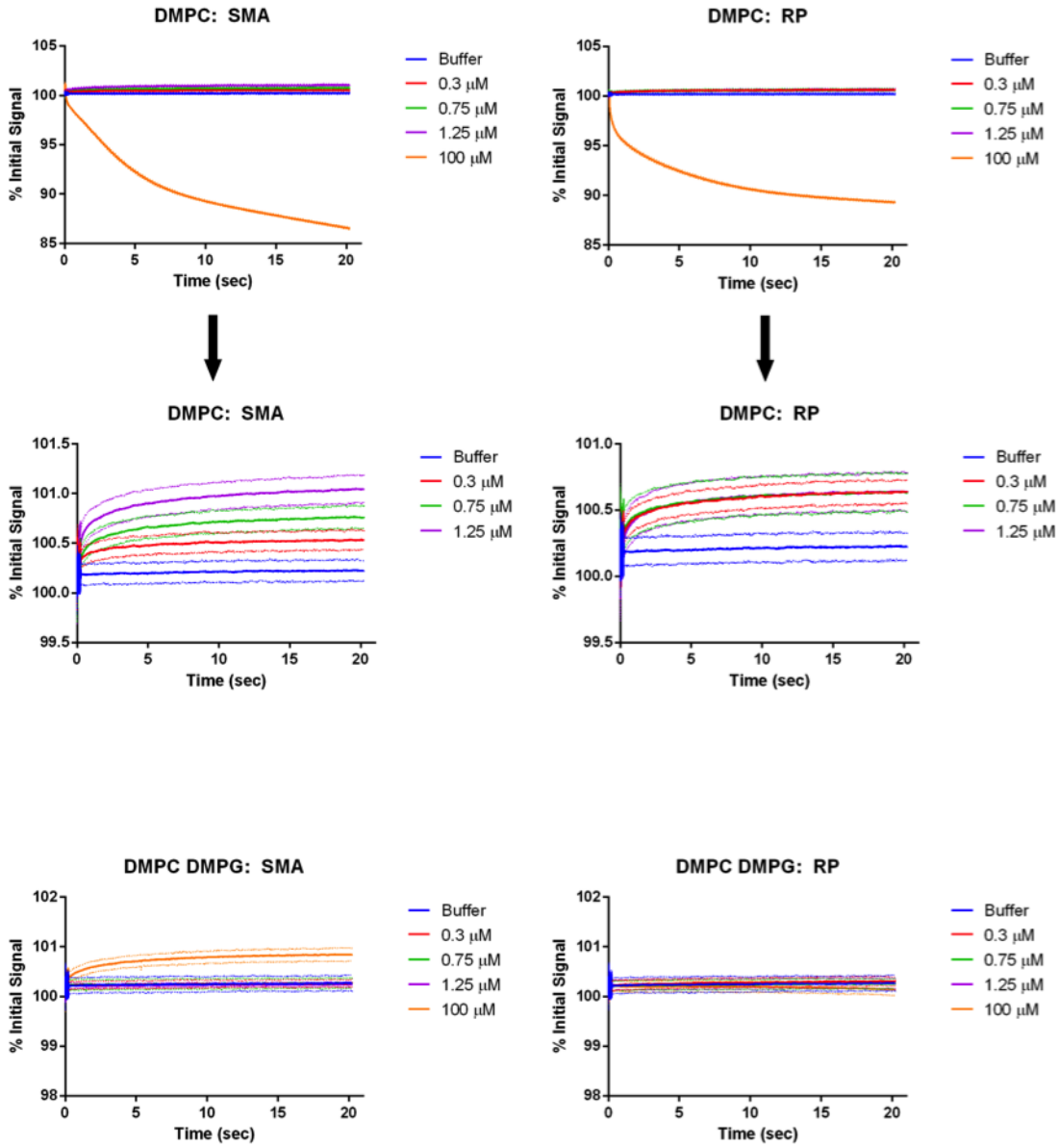


**Figure 5.12** Stopped flow experiments carried out for DMPC and for $DMPC_{80}DMPG_{20}$ when $SMA_{RAFT}$ or SMA2000P is added to the solution at different concentrations. 0.3 $\mu$M (red), 0.75 $\mu$M (green), 1.25 $\mu$M (violet) and 100 $\mu$M (orange). A control was run using TRIS buffer (blue). Data was collected at 25°C.

The top graph shows the full scale so that the 100 $\mu$M can be compared with the other data sets for DMPC vesicles. The middle graphs show the data for lower concentrations on an expanded scale to highlight the changes in fluorescence signal at lower polymer concentrations. Figure 5.12 shows on the top row the different results for $SMA_{RAFT}$ and SMA2000P as the polymer interacts with the vesicles. For SMA2000P two decays are highlighted, whereas for $SMA_{RAFT}$ the difference in percentage of fluorescence from the initial signal is smoother and looks to decay with one exponential law. This difference agrees with the different $K_d$ found for the two different polymers values of which are reported in table 5.1 Due to the massive difference in the behaviour when the high concentration polymer solution was added to the DMPC FPE-labelled vesicles, figure 5.13 and 5.14 reports the stopped flow patterns acquired for DMPC and $DMPC_{80}DMPG_{20}$were repeated in the same way as the experiment shown in figure 5.12.

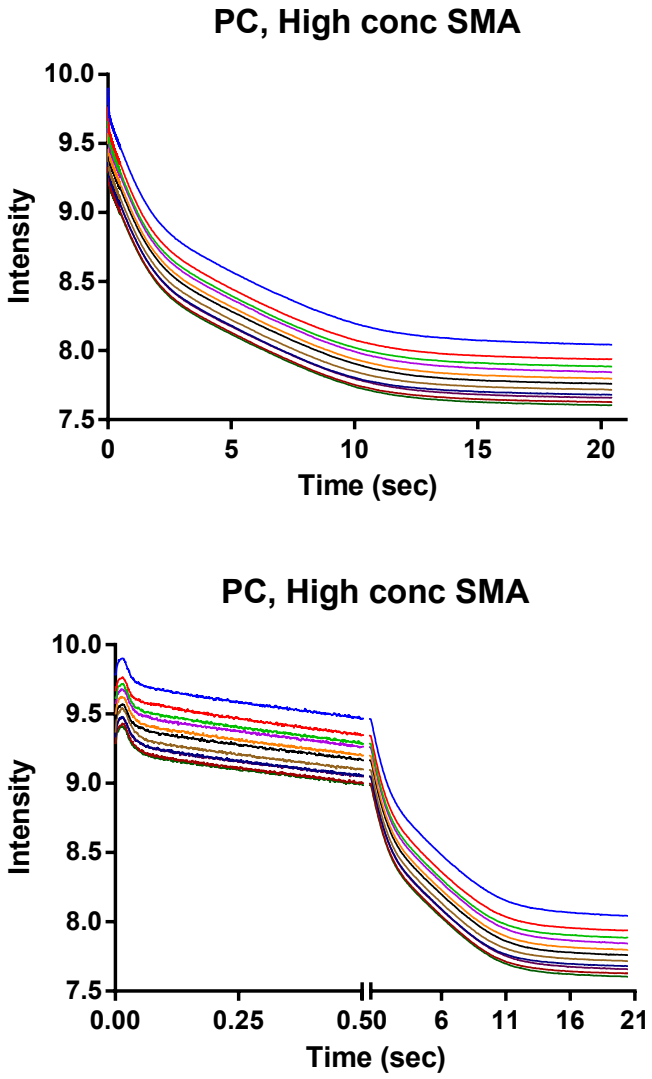


**Figure 5.13** Stopped flow expriment using DMPC FPE-laelled vesicles added with SMA2000P 1 mM. Data was collected at 25 °C. The top graph shows the data for several repeats over a 20 s time period, while the scale on the bottom graph highlights the shorter time measurements which cannot be seen on the top graph due to the x-axis scale used.

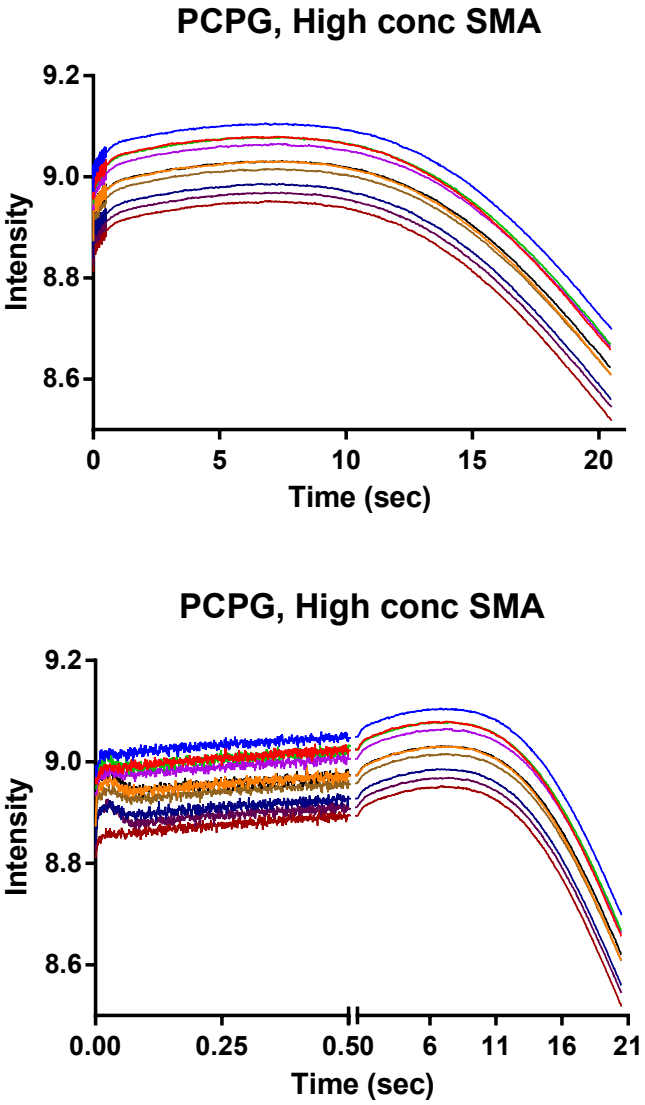


**Figure 5.14** Stopped flow expriment using $DMPC_{80}DMPG_{20}$ FPE-laelled vesicles added with SMA2000P 1 mM. Data was collected at 25 °C. The top graph shows the data for several repeats over a 20 s time period, while the scale on the bottom graph highlights the shorter time measurements which cannot be seen on the top graph due to the x-axis scale used.

## 5.2 Characterisation of phospholipid-polymer interactions using SANS

In this section the interaction of either the commercial copolymer or $SMA_{RAFT}$ with lipid vesicles will be shown. The transition from DMPC vesicles to discs was followed for $SMI_{1000}$, $SMI_{2000}$, SMA2000P and $SMA_{RAFT}$.

In order to understand the interaction of the polymer with lipid vesicles from a structural point of view, several stopped flow experiments were carried out using SANS. Experiments were performed either on D33 beamline, at the ILL and on SANS2d beamline, at ISIS. Both exeperimental set up have been discussed in section 2.6.3. In order to understand the reactivity of the polymer with vesicles when nanodiscs are formed, the same concentration of lipids and polymer normally used to prepare discs was used. Vesicles, in this case, were made according to the procedure reported in [209]. As a standard procedure 50 mg of DMPC was suspended in chloroform in a round bottom flask. Chloroform was removed using a rotary evaporator. This process makes a film on the wall of the round bottom flask. This DMPC film was then suspended in 10 mL of buffer. The solution was mixed using a vortex and sonicated for 5 min until the solution turned translucent. This solution was then filtered using a 100 nm cut off filter. The initial SANS pattern of the vesicles was fitted using a three shell hollow sphere model corresponding to lipid headgroups and tails, described in section 2.6.3 (figure 5.15)

Fitted parameters from figure 5.15 are reported in table 5.2. The SLD of the lipid heads was calculated with 0.57 % of hydration and held at 4x10 $^{-6}$ Å$^{-2}$ during the fitting. The SLD of the lipid tails was held at 7.2 x10 $^{-6}$ Å$^{-2}$. The thickness of both tails and head were fixed at 28 and 8 Å respectively and held during the fitting. The core radius of the vesicle and the polydispersity in the radius were allowed to change. The fitting is reported up to q=0.01. The lower q range was not fitted and the scattering in this range arises probably from bigger vesicles in the solution. The little bump around q=0.7 Å$^{-1}$ is likely to be due to the

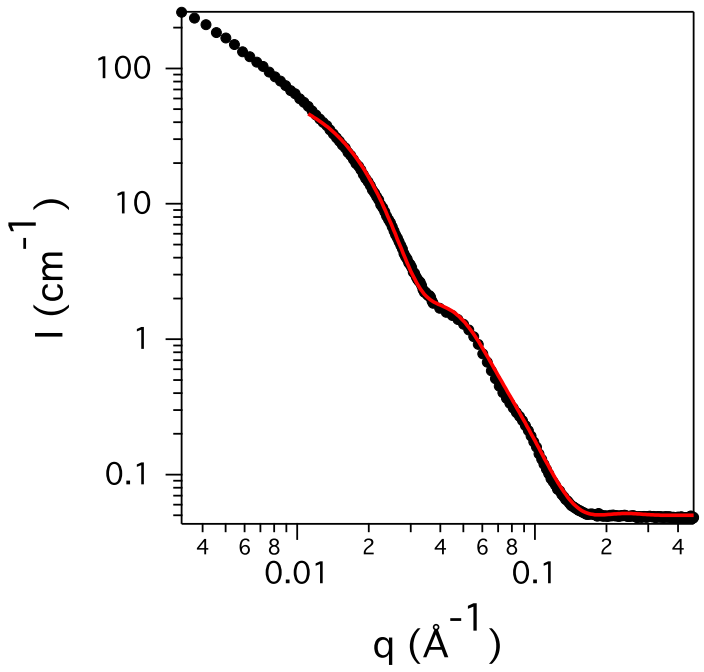


**Figure 5.15** SANS scattering pattern taken on D33 at ILL. The graph shows experimental data (black dots) and the best fit (red line). Data was collected at 25°C

presence of few multilamellar vesicles in the solution. In general the radius found from this fitting between 60 and 70 Å is in agreement with the sizes expected from the filter size used to extrude vesicles.

Polymer solution was added with a volume of 1:1 to the vesicle solution. The final concentration of vesicles and the polymer was kept at the same concentration normally used to make nanodiscs (5mg/mL of DMPC and 1.5 %wt of polymer). For commercial copolymers ($SMI_{1000}$, $SMI_{2000}$ and SMA2000P) the process was completed in few seconds. In order to measure a slower process the reaction was carried out at room temperature ( 25°C, fast process) and at low temperature (5°C, slower process) below the $T_g$ of DMPC.

When fitting these data a model of the sum of the scattering from the vesicles and the discs was used. Due to the high amount of parameters, the SLD for the lipid heads and tails and the tail thickness were kept at 4x$10^{-6}$ $Å^{-2}$, -0.4x$10^{-6}$ $Å^{-2}$and 28 Å respectively. Since the system described was not pure, an approximation was used for the model used to describe nanodiscs. Instead of using a model for

**Table 5.2** Parameters for a three shell hollow sphere model used to fit SANS data for h-DMPC vesicles in d-PBS solution at 25°Cbefore addition of polymer

| Parameters | Values |
|---|---|
| Scale | 0.01 |
| Core Radius(Å) | 60 ± 5 |
| Core PDI (sig/ave) | 0.3 ± 0.1 |
| Core SLD ($Å^{-2}$) | 6.3x$10^{-6}$ |
| Head Thick(Å) | 8 |
| Head SLD ($Å^{-2}$) | 4x$10^{-6}$ |
| Tail Thick(Å) | 28 |
| Tail SLD ($Å^{-2}$) | -0.41x$10^{-6}$ |
| Solv. SLD ($Å^{-2}$) | 6.3x$10^{-6}$ |
| Bckg ($cm^{-1}$) | 0.001 |

a polydisperse core shell bicelle, a simple core shell cylinder was used to describe nanodiscs. This is a good approximation since the polymer has a SLD comparable with the phospholipid head (1.96x$10^{-6}$ $Å^{-2}$ and 1.89x$10^{-6}$ $Å^{-2}$ respectively). The SLD of the shell was calculated for hydrated polymer and lipid head group and fixed at 3.3x$10^{-6}$ $Å^{-2}$which is the average of the SLD for the hydrated head and polymer rim. Where possible only the ratio of vesicles to nanodiscs were changed, such as for vesicles mixed with $SMI_{2000}$ at 25°C. However the mechanism seems to change when the temperature is dropped to 5°C.

In the first 400 ms for high temperature and the first 2 sec for the lower temperature, the scattering patterns were not fitted very well by using a combined vesicle and disc model. This time period is similar to the short time period seen in the fluorescence experiments described above, after a high concentration of polymer is added to the vesicles. Figures 5.13 and 5.14 highlight that the trend in the fluorescence signals at short times are distinctly different to the decreasing trend measured at longer times

Within this short time, the system is likely to be a mixture of free polymer in solution, vesicles and intermediate structures between vesicles and nanodiscs. The fitting shown was therefore done by increasing the polydispersity of the vesicles. As is shown however in figure 5.17c and figure 5.16c, the ratio of vesicles

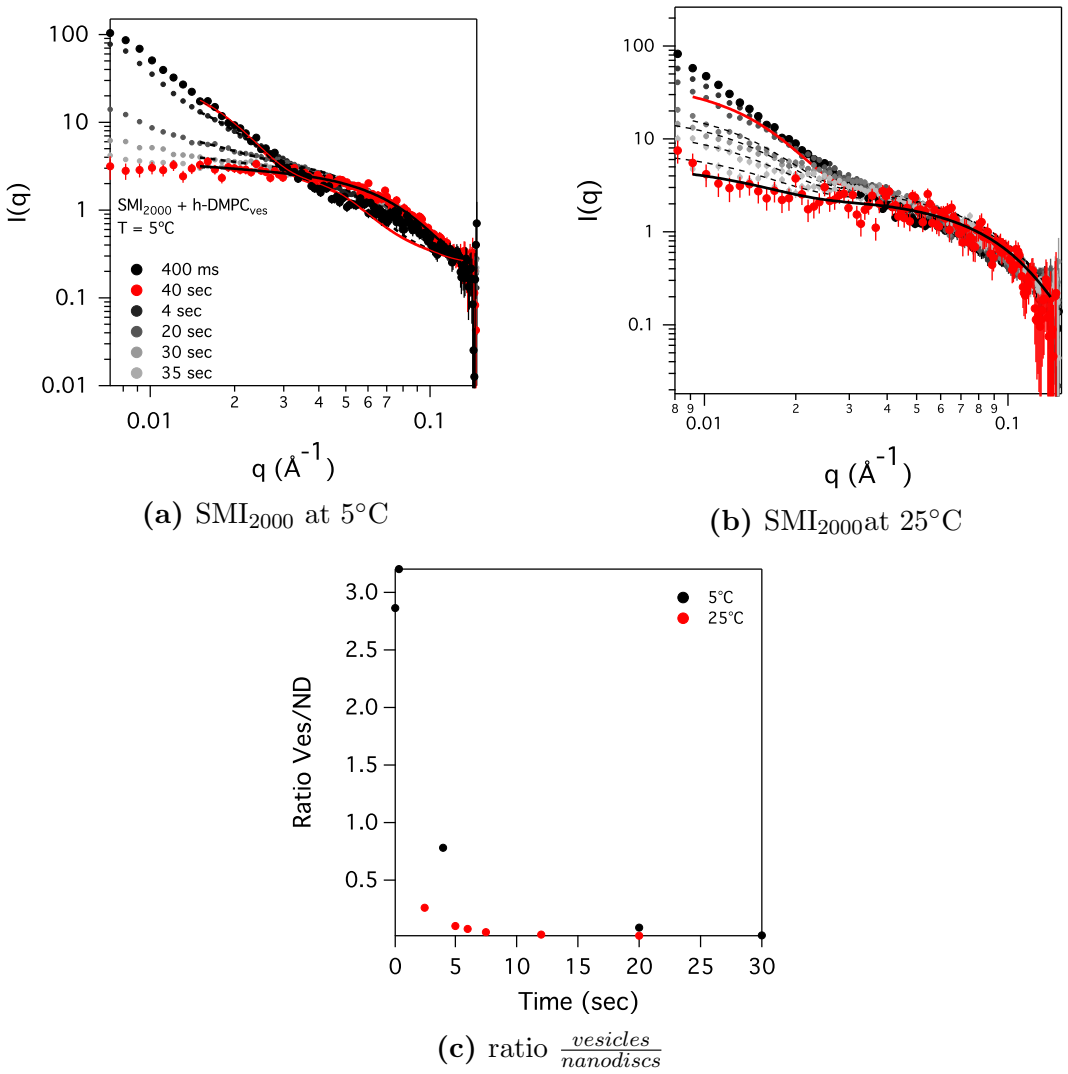


**(a)** $SMI_{2000}$ at 5°C

**(b)** $SMI_{2000}$at 25°C

**(c)** ratio $\frac{vesicles}{nanodiscs}$

**Figure 5.16** SANS patterns acquired on D33 using a stopped flow set up for $SMI_{2000}$ (1.5% wt) and DMPC vesicles (0.5% wt) at (a) 5°Cand (b) 25°C. (c) the vesicles to nanodiscs ratio found from the fitting. The black dots show the first pattern acquired and its best fit (red line), whereas the red dots show the last pattern acquired and its best fit (black line).

to nanodiscs is initially much higher when the reaction is carried out in a cold environment. When the environment is at 5°C , a slower reaction occurs. The polymer will take more time to disrupt the vesicle double layer which will result in an higher ratio of vesicles to nanodiscs. Moreover, this behaviour is highlighted in the intensity at $I_0$: the intensities for the first couple of patterns are higher on the intercept showing an higher amount of vesicles in solution. In figure 5.16b

the ratio of vesicles to nanodiscs is unexpected because it shows a higher amount of nanodiscs in the respect to the vesicles, which could be due to the fact that the fitting does not describe the system properly as discussed just above for the early stages of the process. The fitting at high q does not follow the experimental curve. This behaviour is likely to be due to free polymer in solution (small molecules will be highlighted at high q). Nonetheless using this approximation, a coherent behaviour was highlighted for kinetics observed using $SMI_{1000}$, $SMI_{2000}$ and SMA2000P for both temperatures (5 and 25°C). Patterns for these experiments are reported in figures 5.16, 5.17 and 5.18

At 5°C the diameter of the vesicles decreases with time. When the experiment is run at 25°C, even though the size of the vesicles was fitted, they did not change during the period measured unlike the experiment run at 5 for $SMI_{1000}$, which showed shrinkage in size for the vesicles.

However, a different behaviour was observed for SMA2000P. Below is reported the stopped flow experiment carried out for SMA2000P and h-$DMPC_{ves}$. In the case of SMA2000P, vesicles size does not change. Instead, the radius of the nanodiscs changes from about the size of the vesicles (radius found from the fitting is 45Åat 5°C) to a smaller radius, which is closer to values found in literature for SMA2000P stabilised discs (25Å) [84]. The size of the nanodiscs changes for both 5 and 25°C. However, when temperature is reduced, the slower interactions highlights formation of bigger structures at shorter time (i.e. structure at 45Åare not highlighted when the experiment is run at 25°C). As it is shown in the inset in figure 5.18c, for both temperature the core shell cylinder component of the fitting decreases with time to a constant radius.

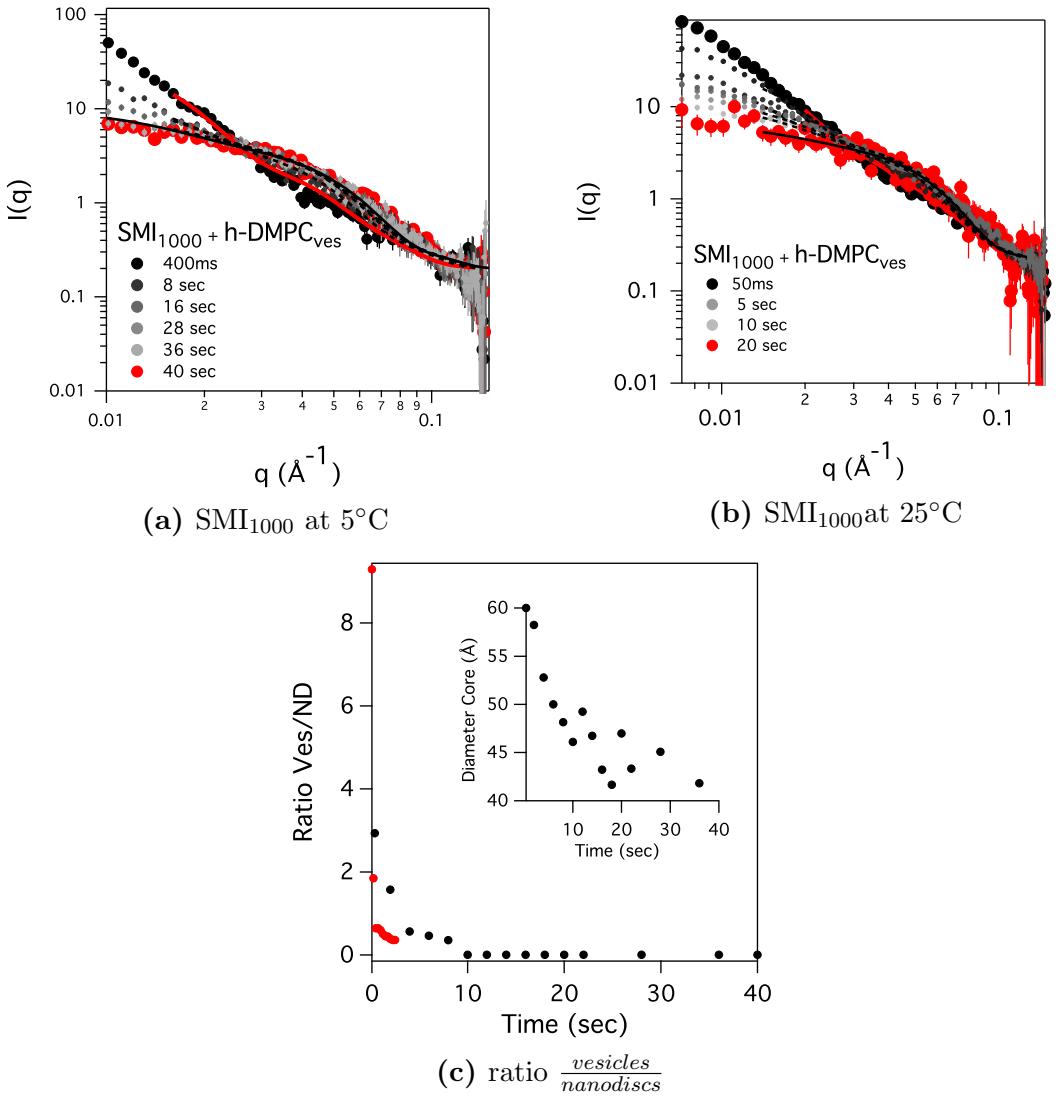


**(a)** SMI$_{1000}$ at 5°C

**(b)** SMI$_{1000}$at 25°C

**(c)** ratio $\frac{vesicles}{nanodiscs}$

**Figure 5.17** SANS patterns acquired on D33 using a stopped flow set up. 3%wt SMI$_{1000}$ was mixed with 10 mg/mL h-DMPC vesicles. In graphs (a) and (b) the black dots show the first pattern acquired and its best fit (red line), whereas the red dot shows the last pattern acquired and its best fit (black line). (c) shows the ratio of vesicles to nanodiscs at 5°C(red dots) and 25°C(black dots). The inset in graph (c) shows how the size of the vesicles change over time at 5°C.

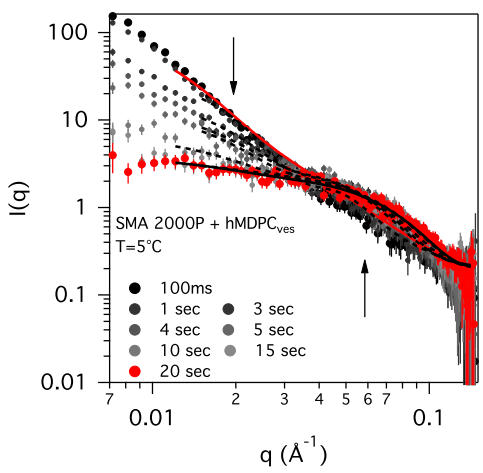


**(a)** SMA2000P at 5°C

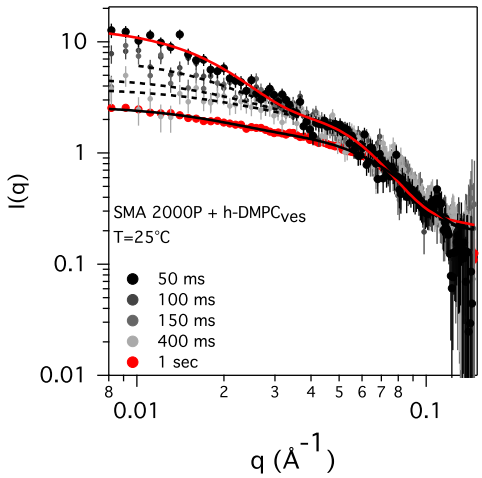


**(b)** SMA2000P at 25°C

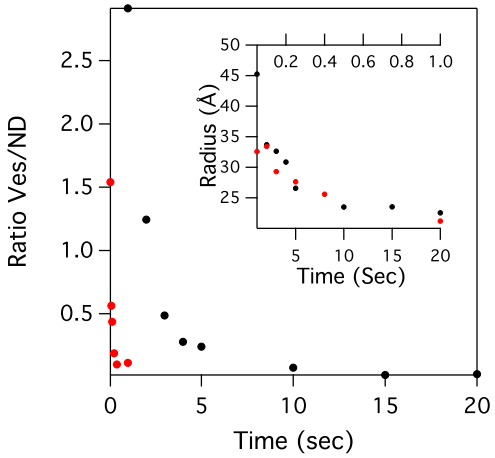


**(c)** ratio $\frac{vesicles}{nanodiscs}$

**Figure 5.18** SANS patterns acquired on D33 using a stopped flow set up. 3%wt SMA2000P was mixed with 10 mg/mL DMPC vesicles at (a) 5°C and (b) 25°C. In graphs (a) and (b) the black dots show the first pattern acquired and its best fit (red line), whereas the red dot shows the last pattern acquired and its best fit (black line). ). Graph (c) shows the ratio of vesicles to nanodiscs at 25 (red dot) and 5 (black dot). The inset in graph (c) shows how the core radius of the nanodiscs change over time. The top axis is the time scale for data taken at 25°Cwhile the bottom axis is the time scale for data taken at 5°C.

During this study it was found that the $SMA_{RAFT}$ polymer takes a long time to equilibrate, so a slow mixing experiment could be carried out. No stopped flow set up was used, but curves obtained returned similar results to the commercial SMA copolymer, just on a longer time scale. Figure 5.19a and 5.19b show scattering from the $SMA_{RAFT}$ polymers at two molecular weights (6 and 11KDa) when they are added to h-DMPC.

Even with a crude fitting it is obvious that $SMA_{RAFT}$ and commercial copolymer interact with the vesicles in a different way. Looking at the high q region, for instance, the pattern when the RAFT polymer is used does not change. So the bilayer thickness does not change during the vesicle to disc transformation. What changed in the case of the $SMA_{RAFT}$ is the amount of vesicles, seen in the scattering at low Q. This behaviour agrees with the DLS results shown in section 5.1.2. When the DLS was performed using $SMA_{RAFT}$ , vesicles did not increase in size.

The commercial copolymer, which has accessible hydrophobic styrene units, is likely to first interact with the surface of the vesicles and then disrupt the vesicles before making large flat cylinders by cutting the vesicle initially into large slabs of membrane with sizes close to that of the vesicles themselves. In the case of the $SMA_{RAFT}$ the co-polymer has a much higher hydrophobicity, which will lead the polymer to remain in polymer micelle aggregates and not interact with the surface up to a certain concentration. As is shown particularly in figure 5.11 (DLS measurements carried out with $DMPC_{80}DMPG_{20}$ vesicles), the size of vesicles increased just before the membrane is disrupted, whereas before this the size of the vesicles is kept constant around 100 nm. This allowed the SANS data fitting for the $SMA_{RAFT}$ case to be carried out just by adjusting the ratio of vesicles to nanodiscs with no change in the size of the nanodisc component. For the first pattern, however, the core radius and shell thickness of the core shell cylinder was allowed to fit. Initial guesses for nanodisc size were obtained from the fitting reported in chapter 4, from discs made with different polymer molecular weights.

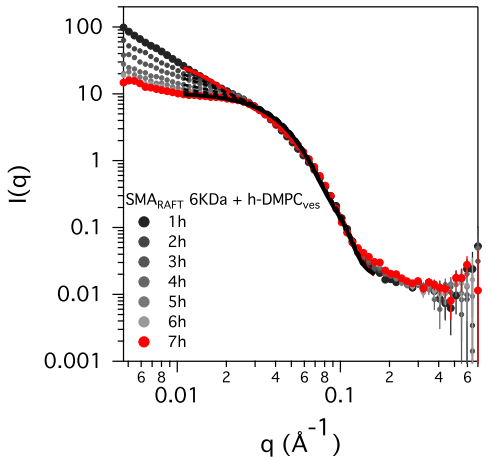


**(a)** SMA$_{RAFT}$ 6 KDa at 25°C

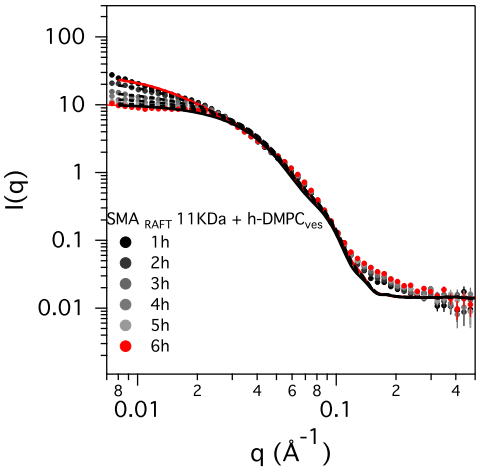


**(b)** SMA$_{RAFT}$ 11 KDa at 25°C

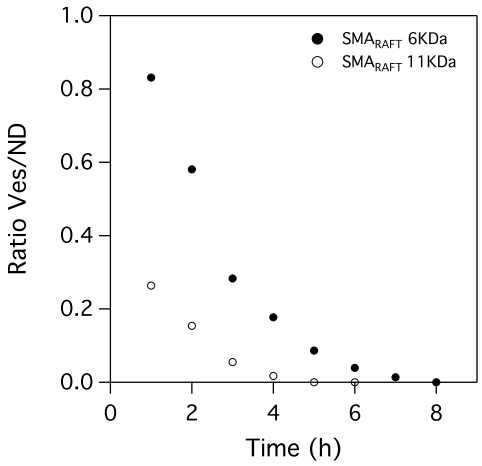


**(c)** ratio $\frac{vesicles}{nanodiscs}$ for SMA$_{RAFT}$ (6 & 11KDa)

**Figure 5.19** SANS patterns acquired on SANS2d for (a) SMA$_{RAFT}$ 6KDa and (b) 11 KDa (1.5 % wt final concentration) and DMPC vesicles (5 mg/mL final concentration) at 25°C. (c) reports the vesicles to nanodiscs ratio found from the fitting. The black dots show the ratio for SMA$_{RAFT}$ 6KDa, whereas the circles show the ratio of nanodiscs to vesicles for SMA$_{RAFT}$ 11KDa. No change was found in the nanodisc size during these experiments.

The core of the cylinder fitted here returned a bigger core radius for the inner cylinder of the core shell model for structures made using the 11 kDa SMA$_{RAFT}$ copolymer Larger discs sizes have already been shown in chapter 4 for higher molecular weight polymers. The size of the radius of the core shell cylinder was found to be 43 and 54 Å for 6 and 11 kDa SMA$_{RAFT}$ respectively. The

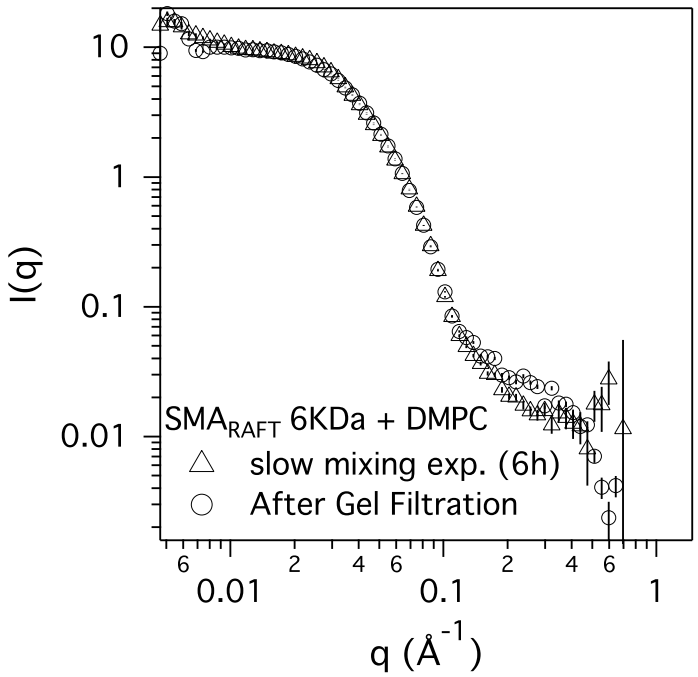


**Figure 5.20** Comparison between scattering patterns arising from SMA$_{RAFT}$ 6KDa mixed with d-DMPC vesicles after 6 hours (circles) and with nanodiscs made using the same SMA$_{RAFT}$ 6KDa copolymers after purification (triangles).

last pattern from the polymer-vesicles experiment was compared to the purified sample made with the same polymer measured on the same beamline during the same experiment. The two patterns from the 6kDa SMA$_{RAFT}$ copolymer are reported in figure 5.20 and demonstrate the complete conversion of vesicles into nanodiscs in this system. Unfortunately the same comparison could not be carried out for 11kDa SMA$_{RAFT}$. However the fitting shows that the ratio of vesicles to nanodiscs it is really low (figure 5.19c).

## 5.3 Diffusion, interaction and penetration of the polymer at the liquid-air interface, a reflectivity study.

Polymer phospholipid interactions were also followed using either neutron or X-Ray reflectivity. In fact, even though the fluorescence experiments explained in section 5.1.2 were useful to understand how the polymer approaches the membrane, they could not return any structural information on how the polymer is inserting. On the other hand, SANS data from either stopped flow or the slow mixing experiments returned a better understanding from the mechanistic point of view, but the complexity of the system made the fitting difficult and led to various approximations. The great advantage of using neutron reflectivity is that it is possible to simplify the vesicle down to a lipid monolayer with the purpose to understand the really early stages of the process. Understanding this first approach will lead to a better understanding of the whole nanodiscs self assembly process. Only SMA was used for the kinetic experiments since deuterated polymer was required for this experiment. Both SMA and SMI were studied for the stati experiment.

For this purpose the structure of a lipid monolayer at the air-water interface was probed as either SMA or SMI, were injected into the subphase.

A 6kDa $SMA_{RAFT}$ polymer was made in Bath as discussed in chapter 4. Since deuterated styrene is relatively cheap and commercially available, a deuterated co-polymer was synthesised for a neutron reflectivity experiment on Figaro, a reflectometer at the ILL. Using deuterated polymer on air-contrast-matched water with either deuterated or hydrogenated lipids enabled the rapid accumulation of polymer at the air-solution interface to be followed with time, for different lipid monolayer compositions. As discussed in the following sections 5.3.1 and 5.3.2, both kinetic and structural information were obtained from this experiment.

A surface pressure sensor was used to initially set the area per molecule in the

lipid monolayer and then monitored during the reaction. The trough used for the experiment had a volume of 40 mL; a constant volume of PBS (pH=8, 50mM, 0.2M in NaCl) was added to it, in order to know the final concentration of the polymer injected in solution. The surface was properly cleaned and monitored with a pressure sensor to ensure an uncontaminated surface. The cleaning process removes an undefined volume from the trough. For this reason a laser was used to check its height and to adjust the volume of the trough as follows. 40 mL of PBS solution were added to the trough, the height of the solution was checked using the laser. After cleaning the surface, PBS was added outside the barrier until the laser display showed the same height as for the initial volume. PBS was added to the trough on the outside of the barrier where lipids were spread to avoid any contamination of the cleaned surface. A schematic representation of the set up is reported in figure 5.21.

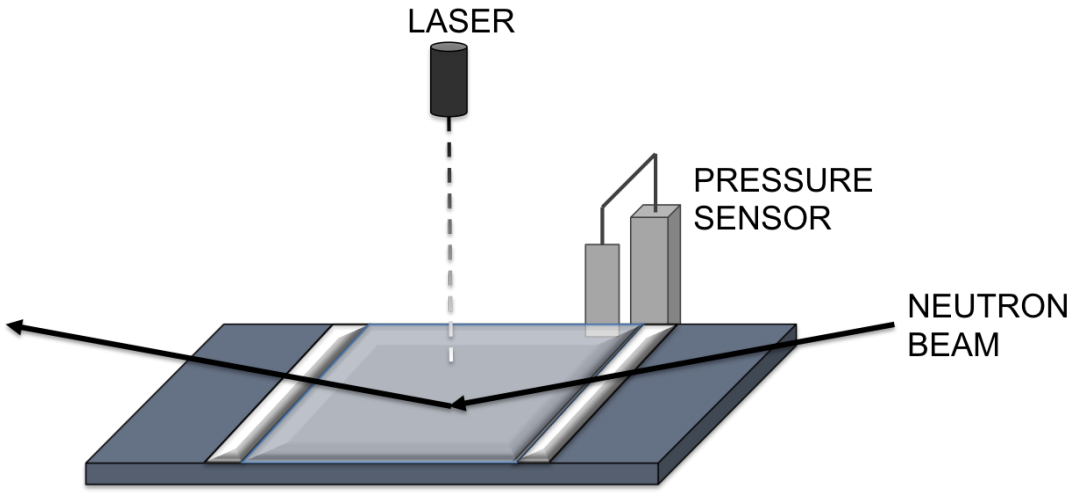


**Figure 5.21** Schematic of the experimental set up used for the neutron reflectivity experiment on Figaro.

Once the trough was cleaned and filled with a well known amount of buffer, a monolayer of either DMPC or a mixture of $DMPC_{80}DMPG_{20}$ was spread on the surface in a compressed state (about 25 mN/m), from a 0.5mg/mL solution of phospholipid solubilised in chloroform. The subphase used was PBS Air Contrast Matched Water (ACMW), 50 mM, NaCl 0.2 M which is the standard buffer in chapter 4 and was used for the previous SMA experiments in this chapter. The

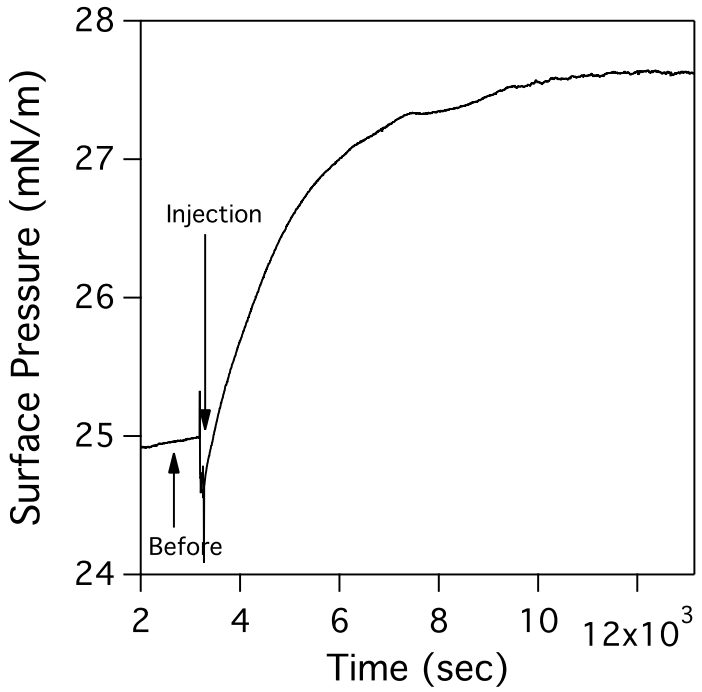


**Figure 5.22** Isotherm of $DMPC_{80}DMPG_{20}$ monolayer before, during and after d-$SMA_{RAFT}$ 6KDa injection at final subphase concentration of 0.01% wt.

spread monolayer was monitored at a pressure of 25 mN/m by controlling barriers to ensure the pressure was constant.

The polymer was injected into the subphase using a syringe with a bent needle, which was inserted between the barrier and the bottom of the trough. The spreading process took about 1.5 min and closing the hutch took about 1.5 min. The kinetics of the process was therefore acquired always with a delay time of about 180 sec. After the polymer was injected in the subphase, its concentration in solution at the final stage was either 0.1%wt or 0.01% wt. The diffusion of the polymer to the air-solution interface was followed with a pressure sensor while the neutron reflectivity experiment was run. The fact that the polymer goes to the interface results in a increased surface pressure at the interface in the experimental data. Figure 5.22 reports a typical surface tension variation for a d/d-$DMPC_{80}DMPG_{20}$ monolayer as SMA polymer diffuses into the monolayer.

In order to have structural information from the same system, static experi-

ments were run before and after the polymer injection. Several contrasts of lipid monolayers and subphase were run. Compositions used for those experiments are reported in table 5.3.

**Table 5.3** Summary of composition used for the experiment run on Figaro using deuterated $SMA_{RAFT}$ 6KDa co-polymer at final subphase concentration of 0.01% wt. The experiment was carried out at 25°Cfor one repeat.

| Lipids composition | Subphase | Initial Pressure (mN/m) | Final Pressure |
|---|---|---|---|
| h-DMPC | ACMW | 28.2 | 35.9 |
| d-DMPC | ACMW | 24.8 | 30.4 |
| d-DMPC | d-PBS | 22.7 | 25.2 |
| h/h-$DMPC_{80}DMPG_{20}$ | ACMW | 25.8 | 28.5 |
| d/d-$DMPC_{80}DMPG_{20}$ | ACMW | 27.3 | 30.6 |
| d/d-$DMPC_{80}DMPG_{20}$ | d-PBS | 24.9 | 27.6 |

### 5.3.1 Neutron reflectivity study - kinetic information

The most common problem for a neutron reflectivity experiment is its slow acquisition of data which requires at least 40 min. This disadvantage means that NR is not normally used for kinetic experiments. Instead an analysis at low-Q angle was carried out to determine how the composition of the monolayer changed over time after the polymer was injected.

As explained in section 2.5, the momentum transfer is related to the incident wavelength and angle as shown in equation 5.2

$$Q_z = \frac{4\pi}{\lambda} \sin\theta \tag{5.2}$$

The resolution of a set of data is given by the instrument and it is a convolution of both wavelength and incident angle as given in equation 5.3.

$$\left(\frac{dQ_z}{Q_z}\right)^2 = \left(\frac{d\lambda}{\lambda}\right)^2 + \left(\frac{d\theta}{\theta}\right)^2 \tag{5.3}$$

From a physical point of view, equation 5.3 shows that in the case of low resolution in either the incident angle or for a polychromatic beam, the uncertainty in the

momentum transfer does not allow a well defined reconstruction of the layer at the interface. On the other hand, reducing the tight control over the wavelength (reducing the number of choppers used) leads to a higher flux of neutrons in the incoming beam. The improved statistics due to the higher flux makes it possible to probe the concentration of deuterated compounds at the ACMW-air interface. In the case of a one component layer the surface excess can be written as in equation 5.4

$$\Gamma_a = \frac{\rho_a d}{b_a N_A} \tag{5.4}$$

where $\Gamma_a$is the surface excess, $d$ is the thickness of the layer, $N_A$ is the Avogadro's number, $b_a$ is the scattering length.

It has been shown [210] that for a high flux of neutrons and low $Q_z$ values the surface excess becomes independent from structural information such as $d$.

Therefore, at low angles the structural information is minimised and the count of neutrons arriving at the detector is directly related to the SLD of the interface. To fit the data, the following simultaneous equations were solved:

$$SLD_{int} = SLD_{d-lip}x_{d-lip} + SLD_{d-pol}x_{d-pol} + SLD_{sub}x_{sub} \tag{5.5}$$

$$SLD_{int} = SLD_{h-lip}x_{h-lip} + SLD_{d-pol}x_{d-pol} + SLD_{sub}x_{sub} \tag{5.6}$$

Using equation 5.5 and 5.6 reported above with the 2 contrasts used for the experiment (deuterated and hydrogenated lipids on ACMW), the absorbed amount of the polymer at the interface can be calculated. Using ACMW, the contribution to the $SLD_{int}$ from the subphase can be neglected. Two different polymer concentrations were used (0.1 and 0.01%wt) when a DMPC monolayer was spread on the surface. When the higher concentration is used, however, the interaction of the polymer with lipids is too fast and it was not possible to follow it from the early stages. For this reason the following experiments with DMPC and with

$DMPC_{80}DMPG_{20}$ monolayer were carried out using a lower SMA concentration. Figure 5.23 shows the surface concentration of the deuterated polymer upon injection under DMPC monolayer plotted against time.

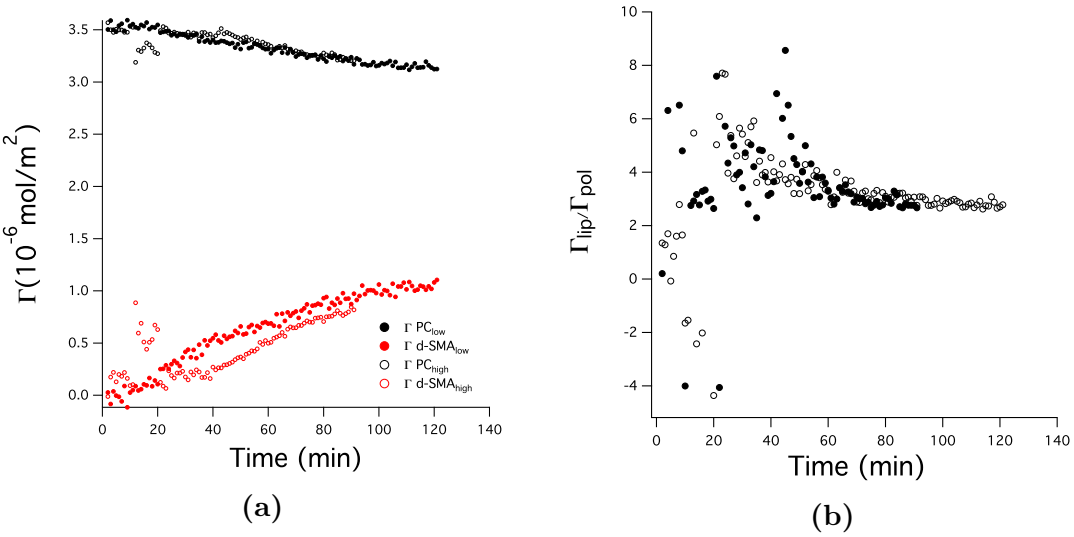


**Figure 5.23** (a) Values of surface concentration against time for deuterated $SMA_{RAFT}$ polymer diffusing into a DMPC monolayer. (b) Ratio of DMPC concentration at the interface over polymer concentration for a final solution concentration of the polymer of 0.01%wt (dots) and 0.1%wt (circles).

The same experiment was carried out at 0.01%wt of final concentration of polymer with $DMPC_{80}DMPG_{20}$ monolayers. Figure 5.24 shows the lipid loss and polymer accumulation at the interface calculated from neutron reflectivity data.

The extent of the interaction of the polymer with zwitterionic and charged lipids is different. In fact when the steady state is reached, the amount of polymer at the interface is higher when the interface is not charged.

As was shown by the fluorescence experiment, the different ratio in the surface excess at the interface, is probably due to a different interaction when charged lipid is present. In fact, as shown in table 5.4 the ratio of lipid to polymer at the interface is higher for DMPG than for DMPC (5 and 3 respectively).

Table 5.1 shows that in order to fit the $SMA_{RAFT}$ binding curve for DMPC or $DMPC_{80}DMPG_{20}$ vesicles in the fluorescence measurements, two different models had to be used. Even though is not clear from literature what precise mechanism

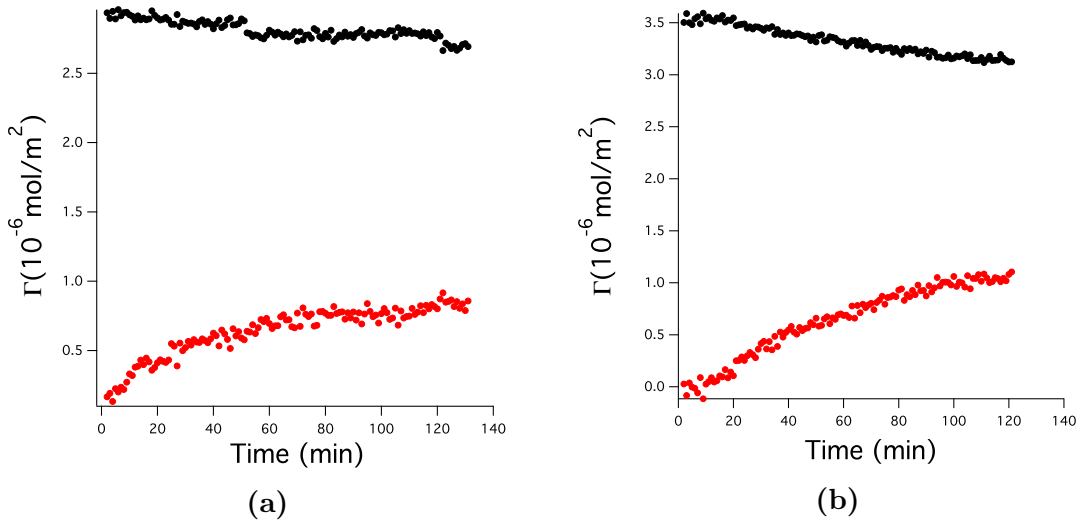


**Figure 5.24** Surface concentration values against time reporting the diffusion of d-SMA$_{RAFT}$ to the interface causing lipid loss from (a) DMPC$_{80}$DMPG$_{20}$ and (b) DMPC monolayer at a final concentration of the polymer in the subphase of 0.01% wt.

**Table 5.4** Ratio of lipid to polymer composition found for kinetics experiment data collected on Figaro for different lipid compositions and different final concentration of the polymer in the subphase

| Monolayer | [d-SMA$_{RAFT}$] | lipid/polymer |
|---|---|---|
| DMPC | 0.1% wt | 3 |
| DMPC | 0.01% wt | 3 |
| DMPC$_{80}$DMPG$_{20}$ | 0.01% wt | 5 |

implies sigmoidal or hyperbolic fitting for the binding curve, it is certain that two different mechanism of interaction are occurring. To try to determine where the polymer is located in the membrane and to explain the different mechanisms, static structures of the lipid monolayers were also measured.

### 5.3.2 SMA - lipid monolayers: static structures

Before and after the kinetic experiments reported in section 5.3.1 the equilibrium structures formed by the polymer and lipid systems at the liquid-air interface were probed using neutron reflectivity. The structures of nanodiscs formed from SMA$_{RAFT}$ co-polymer have been discussed in chapter 4, but these measurements

probe the structures which may transiently exist during disc formation.

### DMPC monolayers

First, the phospholipid monolayer alone was characterised with neutron reflectivity and was analysed using two different model discussed in section 2.6.4. NR patterns and results from the fitting are reported in figure 5.25 and table 5.5 respectively.

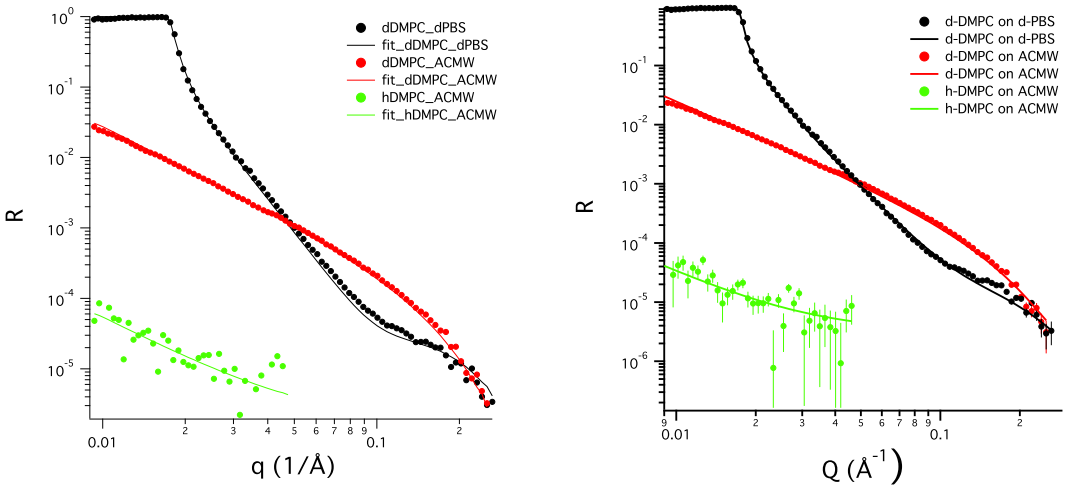


**(a)** DMPC monolayer RasCAL **(b)** MOTOFIT

**Figure 5.25** NR profiles for DMPC monolayer at 25mN before the polymer injection and fitting (line through dots) done using (a) RasCAL and (b)MOTOFIT

**Table 5.5** Fitting parameters for the DMPC monolayer, done using RasCAL and MOTOFIT

| RasCAL | | Motofit | | |
|---|---|---|---|---|
| Subphase rough. (Å) | 2±0.26 | Layer 1 | Tail Thick. | 13.77±1 |
| APM | 50± 1 | | SLD tail(x$10^{-6}$Å$^{-2}$) | -0.4/7.2 |
| Tail rough. (Å) | 2±0.1 | | Roughness (Å) | 4.4±1 |
| Waters per head | 1.9±0.3 | | Water (%) | 0 |
| Tail tilt (degree) | 22.4±0.3 | Layer 2 | Head Thick. (Å) | 8 |
| Tail hydration (%) | 2.1±0.1 | | SLD head(x$10^{-6}$Å$^{-2}$) | 1.98 |
| | | | Roughness (Å) | 4.6±1 |
| | | | Water (%) | 44.7 |

Values for this fitting agreed with those reported in literature for both models

used [211]. The advantage to use both RasCAL and MOTOFIT arises from the different parameters used to fit the reflectivity pattern. Due to the complexity of the system, having 2 comparable results from two different fitting for one identical system reinforces the knowledge of the initial status of the monolayer used. Data from this fitting will be used later to fit the polymer adsorption.

During the injection of polymer underneath the monolayer, polymer diffusion to the interface was checked with a surface pressure sensor. For all the measurements carried out, the surface pressure reaches a plateau after about 20min (5.22). This is likely to be the time needed for the polymer to diffuse to the interface in these dilute solutions. Diffusion of the polymer to the interface was studied using three contrasts, all of them were used to obtain final structure of the lipid-polymer monolayers to determine the equilibrium structures. Compositions used are reported in table 5.3. The reflectivity pattern for the DMPC monolayer after the injection of the polymer was fitted using both RasCAL or MOTOFIT (figure 5.26). Fittings reported using RasCAL software were performed by Dr. Stephen Roser. In both case similar behaviour is found. The approaches used by these two different methods are a bit different and are described in section 2.6.4. RasCal is software that allows fitting of the data after the polymer injection as a sum over the SLD of the pre-existing fit. MOTOFIT, instead, is a software that uses an optical matrix formalism to analyse data such that it was not possible to add an independent SLD profile distribution for the polymer on the top of the 2 initial layers to describe the polymer insertion and the intercalation of the polymer into the phospholipid monolayer. Therefore, to model the penetration of the polymer in MOTOFIT the SLD for the lipid head region and for the tail region was allowed to change.

At a first glance, NR patterns after the polymer injection (figure 5.26) does not have a pronounced difference in shape from the monolayer on its own (figure 5.25 ).

However a large increase in the intensity at low Q is detectable looking at the pattern from h-DMPC on ACMW before and after the polymer injection, going

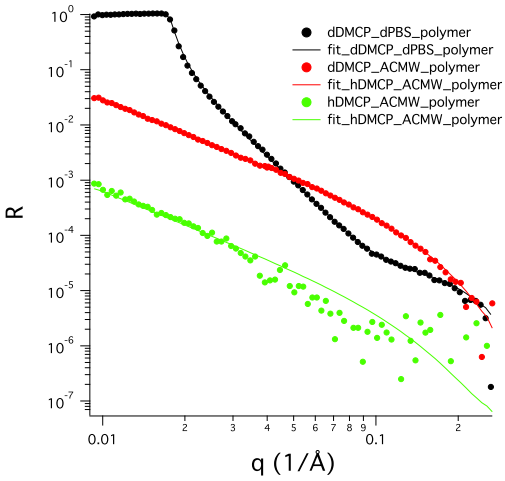


**(a)** DMPC after polymer injection (RasCAL)

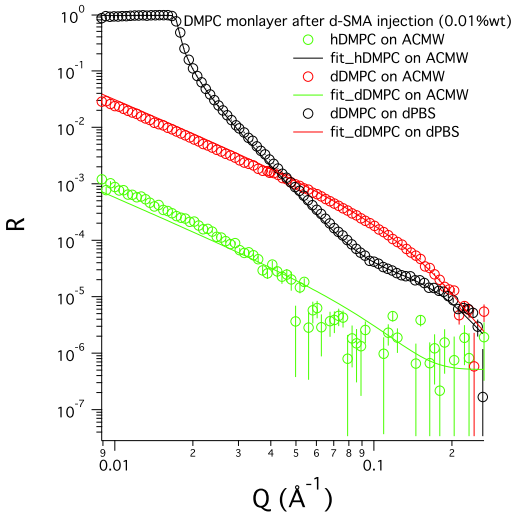


**(b)** DMPC after polymer injection (MOTOFIT)

**Figure 5.26** Neutron reflectivity patterns acquired on Figaro (ILL) for DMPC monolayers after polymer injection for 3 different contrasts: h DMPC on ACMW in green, d-DMPC on ACMW in red and h-DMPC on d-PBS in black. Fitting was performed using (a) RasCAL and (b) MOTOFIT

from 1x10$^{-3}$ to 1x10$^{-4}$ Å$^{-2}$ respectively. This change is not surprising since the contrast arising from an h-DMPC monolayer on ACMW is very low because every component in the system contains hydrogen. The injected polymer, which diffuses to the interface, is made of maleic acid and deuterated styrene, which is likely to go into the tails region of the monolayer given its high hydrophobicity, increasing the contrast of the layer at the interface. For the fitting as many parameters as possible were held. The first thing changed was the SLD for tails after the polymer injection keeping the scale constant. Assuming that the polymer absorbing will into the tail region, the tail thickness was allowed to vary. The thickness of the headgroup region was also held but the SLD of this region allowed to vary. A slight increase in this value was detected

Fitting parameters after the polymer was injected are reported in table 5.6

As expected from the differences noted in the NR pattern of h-DMPC on ACMW, values for the SLD of the tails increased from -0.4x10$^{-6}$ Å$^{-2}$ for pure monolayer to 0.45x10$^{-6}$ Å$^{-2}$ after the polymer injection.

**Table 5.6** Fitting parameters for NR patterns reported in figure 5.26 after the polymer injection.

| RasCAL | | MOTOFIT | | |
|---|---|---|---|---|
| sub. rough. | 7.9± | | SLD tail h/d (x$10^{-6}$ Å$^{-2}$) | 0.45/6.7 |
| APM | 51 ±1 | Layer 1 | Thick. Tails (Å) | 16.0±1 |
| tail rough (Å) | 5±2 | | Water % | 0 |
| Water per heads | 0.6±0.1 | | Tail Rough. (Å) | 3.7±2 |
| Tail tilt (degree) | 33±1 | | SLD heads (x$10^{-6}$ Å$^{-2}$) | 2.23±1 |
| Head Rough. (Å) | 3.0 | Layer 2 | Head Thick (Å) | 8±2 |
| d-SMA$_{RAFT}$\tails | 9.6x$10^{-6}$ | | Water % | 8±4 |
| d-SMA$_{RAFT}$\heads | 9.8x$10^{-12}$ | | Head Rough (Å) | 5.7±2 |
| subphase_d | 20.0 | | Back Rough (Å) | 6.4 ±1 |
| subphase_nb | 2.8x$10^{-3}$ | | | |
| subphase rough. | 3±1 | | | |

Assuming the change of the SLD is a linear combination of the SLD of the polymer and the tails, the penetration of the polymer into the monolayer can be calculated as reported in equation 5.7:

$$SLD_{layer} = SLDlipx_{lip} + SLDpolx_{pol} \tag{5.7}$$

where $SLD_{layer}$ is the value for the fitted SLD, $SLD_{lip}$ is the SLD of pure tails or head and $SLD_{pol}$ is the SLD of the d-SMA$_{RAFT}$. $x_{lip}$ and $x_{pol}$ is the molar fraction of tails/ head of lipids and polymer respectively. For an initial DMPC monolayer the penetration of the polymer into the lipid tail is 12% which is close to the value for the penetration of the polymer into the core reported in chapter 4 and in other work [84].

### $DMPC_{80}DMPG_{20}$ monolayer

As for the DMPC monolayer, $DMPC_{80}DMPG_{20}$ solution was spread at the liquid air interface and analysed before and after the polymer injection. In order to fit the NR pattern after the polymer injection, as for the DMPC monolayer, two layers were used. Unfortunately this did not return a good fitting with reasonable values. The fitting for the $DMPC_{80}DMPG_{20}$ monolayer before and after the polymer with two layers model is reported in figure 5.27

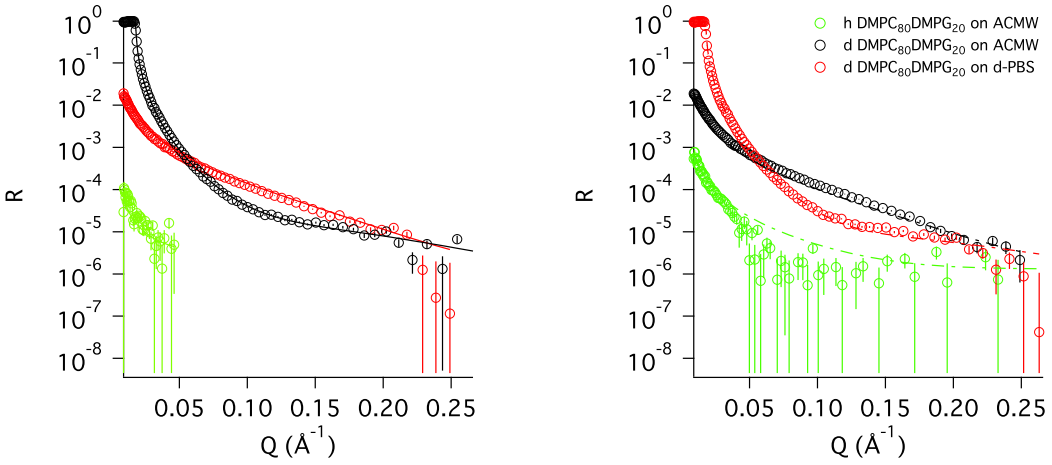


**(a)** Before d-$SMA_{RAFT}$ injection **(b)** After d-$SMA_{RAFT}$ injection

**Figure 5.27** NR patterns acquired for $DMPC_{80}DMPG_{20}$ monoalyer (a) before and (b) after the polymer injection. Several contrasts were run: h-$DMPC_{80}DMPG_{20}$ on ACMW (green), d-$DMPC_{80}DMPG_{20}$ on d-PBS (red) and d-$DMPC_{80}DMPG_{20}$ on ACMW (black)

The green curve does not fit well and, moreover, the contrast d-$DMPC_{80}DMPG_{20}$ on d-PBS shows a smooth fringe at high Q (between 0.15 and 0.25 Å$^{-2}$. In order to obtain this fitting reported in figure 5.27 the SLD of the lipid tails was increased from -0.4 to 0.9 x$10^{-6}$ Å$^{-2}$. This value is higher than that found for the DMPC monolayer. This is unrealistic for two main reasons: $SMA_{RAFT}$ is negatively charged, like the DMPG head group. Previous studies investigated the insertion of SMA copolymer into a lipid monolayer. The commercial copolymer, like $SMA_{RAFT}$, shows a lower increase in the surface pressure, compared to zwitterionic lipid monolayers, when negativelly charged lipids are used [212]. Moreover,

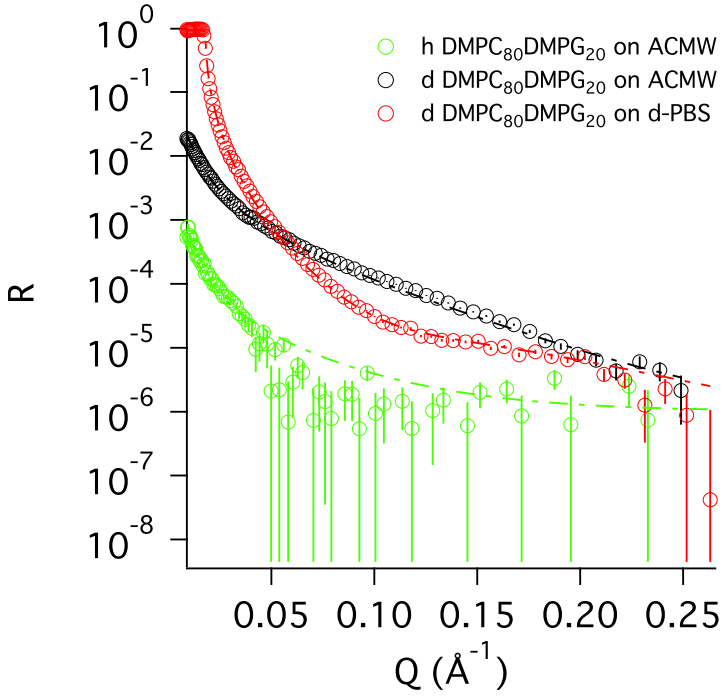


**Figure 5.28** NR patterns for $DMPC_{80}DMPG_{20}$ monolayers after d-$SMA_{RAFT}$ injection. The fitting shown arises from a 3 layer model whose paramters are reported in table 5.7

the intercalation of polymer measured using Di-8-ANEPPS in the earlier section showed that less polymer was inserted into the liposome leaflet compared to measurements undertaken with DMPC liposomes. Furthermore, the surface pressure increased was lower for $DMPC_{80}DMPG_{20}$ monolayer, which is a signal of less polymer going to the interface. Thus, in order to fit the NR pattern, a third layer was added to the subphase, and fitted as a mixture of polymer and water. The SLD of this polymer was calculated to be $3.8x10^{-6}$ $Å^{-2}$ and it was held during the fitting. Figure 5.28 shows the fitting for the NR patterns. Values for the fitting are reported in table 5.7

When the polymer is injected underneath a deuterated monolayer, the SLD does not change significantly since the SLD of the deuterated styrene and the deuterated tails is comparable. The SLD of the headgroup region changes only slightly as well. Similar to the combination of deuterated styrene with deuterated tails, the SLD of maleic acid is not too far from the SLD of the headgroups of the

**Table 5.7** Fittning parameters for $DMPC_{80}DMPG_{20}$ monolayer before and after the polymer injection. (*) values hold during fitting

| | | Before | After |
|---|---|---|---|
| Layer 1 | SLD tails (h/d) (x$10^{-6}$) | -0.4/7.2 (*) | 0.14/7.1 ±0.1 |
| | Tails Thick. (Å) | 14.0±1 | 14±1 |
| | Tails Rough. (Å) | 3±1 | 5±1 |
| | $H_2O$ % | 0 (*) | 0 |
| Layer 2 | SLD Head (x$10^{-6}$) | 2.3±0.2 | 2.4±0.2 |
| | Head Thick. (Å) | 8 (*) | 8 |
| | Head Rough. (Å) | 3±1 | 2±1 |
| | $H_2O$ % | 38±3 | 32±3 |
| Layer 3 | SLD pol (x$10^{-6}$) | | 3.5 |
| | Pol. Thick. (Å) | | 1.7 ±1 |
| | Pol. Rough (Å) | | 5.0±1 |
| | $H_2O$ % | | 58±3 |

phospholipid, being 1.98x$10^{-6}$ Å$^{-2}$ and 1.89x$10^{-6}$ Å$^{-2}$ for the maleic acid and head group respectively. The SLD profile agrees with a model that has maleic acid in addition to the phospholipid head and water in the headgroup region and the styrene in the hydrophobic layer with the phospholipid tails, in addition to a polymer-water layer below the lipid monolayer in the case of the $DMPC_{80}DMPG_{20}$ monolayer. SLD profiles before and after the polymer injection for both monolayer are reported in figure 5.29a and 5.29b

Fitting carried out with RasCAL allows an independent SLD profile for the polymer to be added to the SLD profile of the initial layer to be made. This allows a plot of the SLD profile for the polymer along the interface to be made. Figure 5.30a shows that, depending on the composition of the monolayer at the interface, the polymer behaviour changes. In fact when the polymer diffuses into a DMPC monolayer, which is neutral, it can penetrate into the tail region and almost none is found at the subphase interface. When instead it has to overcome a negative electrostatic potential to diffuse into the tail region in the case of the mixed $DMPC_{80}DMPG_{20}$ monolayer, the polymer is more diffusely arranged all along the interface. Figure 5.30a reports this behaviour.

Fitting for DMPC and $DMPC_{80}DMPG_{20}$ monolayers were carried out using two

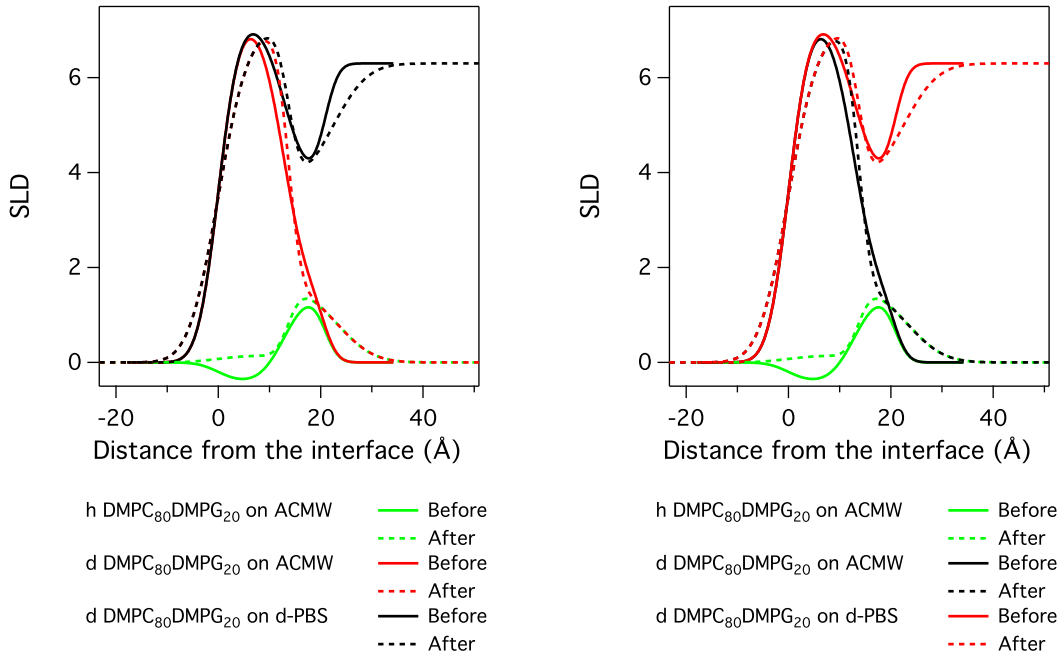


**Figure 5.29** SLD profiles for (a) DMPC and (b) $DMPC_{80}DMPG_{20}$ before (solid line) and after (dotted line) d-$SMA_{RAFT}$ injection at 0.01 % wt in the subphase.

different models, which both returned the same conclusion. The absence of polymer in the subphase detected using RasCAL, was observed in MOTOFIT as a 2 layer model. Fixing then the thickness of heads and phospholipids tails, the SLD of those was varied to model the penetration of the polymer. In the case of $DMPC_{80}DMPG_{20}$ mixtures 3 layers were used to describe the intercalated polymer in the monolayer and the polymer left in the subphase

### 5.3.3 SMI - lipid interactions: an XRR study

X-Ray reflectivity studies have also been carried out for $SMI_{2000}$ in a similar manner to the static NR experiments above. The fringe in the monolayer data moves to lower Q after polymer injection. This shows an increased thickness of the layer at the interface. After polymer injection, a preliminary fitting has been done using the values for SLD and thickness for DMPC used in previous sections.

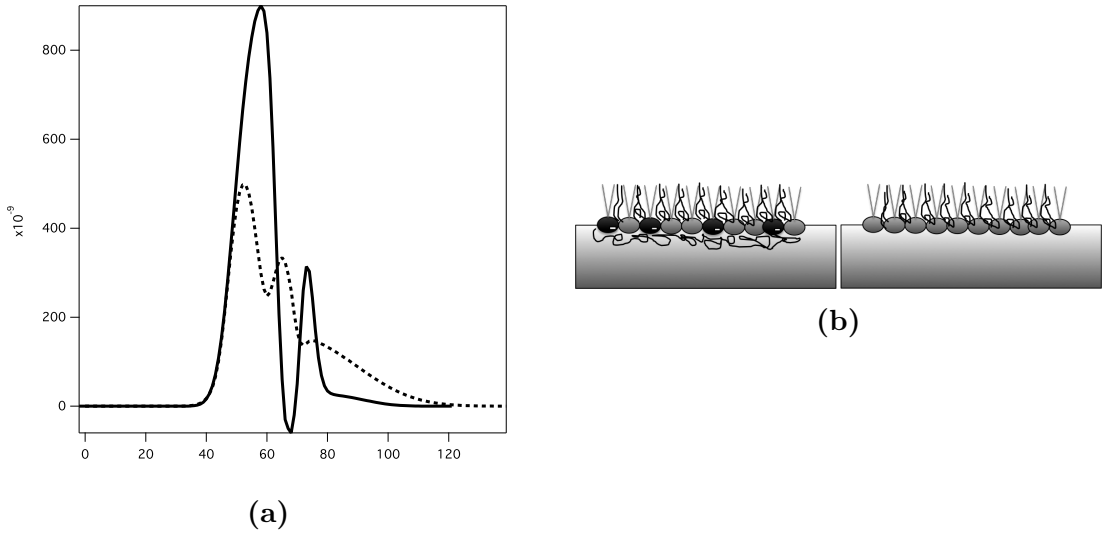


**Figure 5.30** (a)SLD profile of the polymer against the distance from the interface for DMPC (solid line) and $DMPC_{80}DMPG_{20}$ (dotted line) calculated by fitting using RasCAL and (b) schematic representations of the modelmodels for (left) $DMPC_{80}DMPG_{20}$ and (right) DMPC with adsorbed SMA.

The fitting after the polymer injection was done allowing the water content in the head and the thickness of the subphase to vary. Data could be fitted as shown in figure 5.31 by decreasing the hydration of the headgroup layer and increasing the roughness of the subphase interface. Even though it can be speculated that poly(styrene-co-maleimide) interacts with the lipid monolayer in a similar manner to the way that commercial SMA does, a more in depth analysis must be carried out before drawing conclusions.

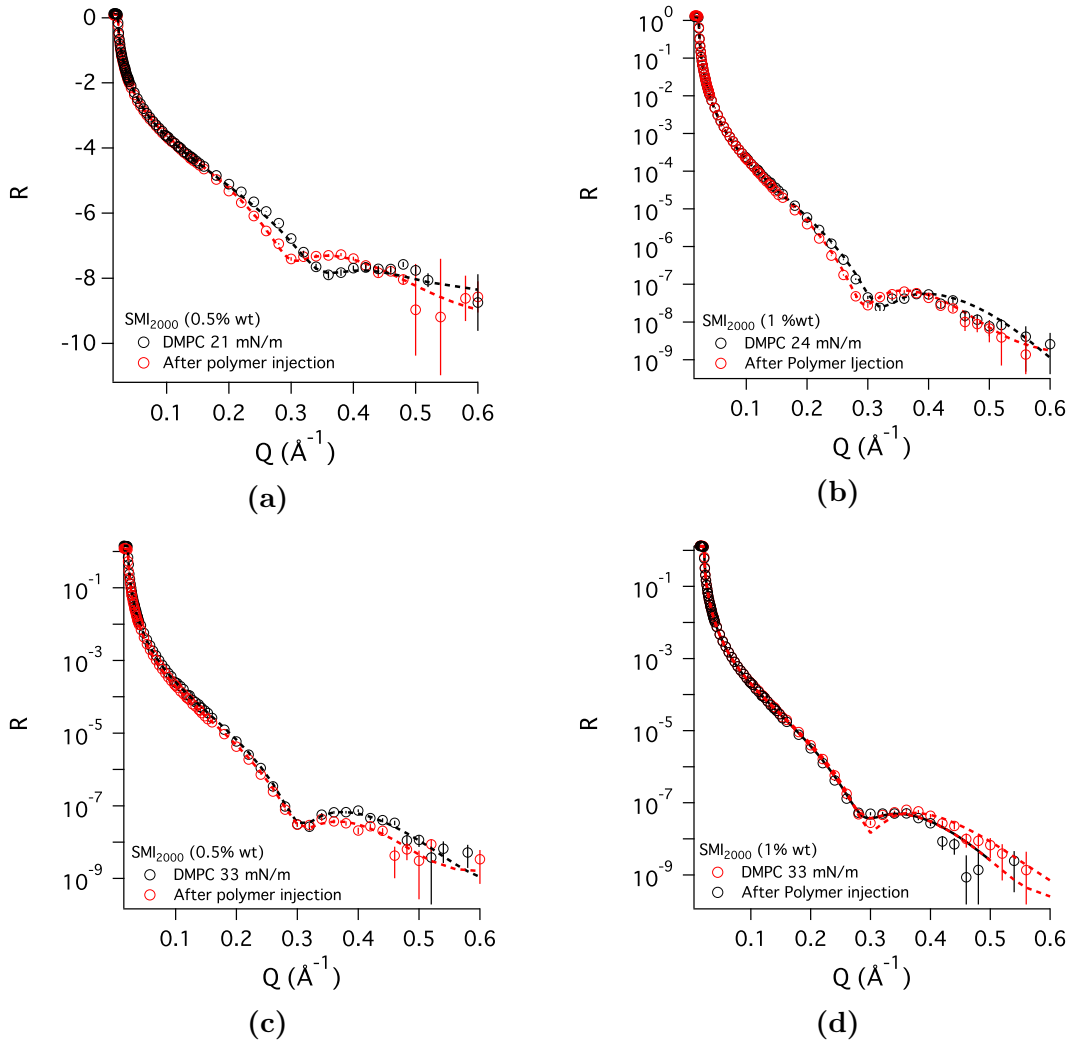


**Figure 5.31** XRR patterns for DMPC monolayer spread on ABS pH=5, [NaCl]=0.2M before (black circle) and after (red circle) the polymer injection. Best fit is shown as dashed line through experimental points before (black) and after (red) the polymer injection. Polymer was injected at 1.5% wt. Measurements were carried out at 25°C

## 5.4 Concluding remarks

In this chapter it has been shown how the disc forming polymers interact with different lipid structures. It has been found that the conformation of the polymer affects the interaction as much as the composition of the starting membrane does. In fact the commercial copolymer, with a random structure interacts in different way compared to $SMA_{RAFT}$. The mechanism of the interaction changes as well when the same polymer is used with a different lipid composition.

Fluorescence experiments have shown that the penetration of the commercial copolymer into the membrane is more effective when it interacts with a zwitterionic membrane whereas it decreases in the presence of DMPG lipids. This is probably due to the electrostatic repulsion that the polymer experiences when it approaches. The localised negative charge of the $SMA_{RAFT}$ instead allows the polymer to have an higher penetration into the lipid layer. The lower penetration of the polymer into a negatively charged monolayer has also been assessed in this chapter as in the literature [212] where experiments with a Langmuir trough have shown that less SMA polymer goes to the interface when it interacts with a negative monolayer. Due to the different mechanism observed for SMA2000P and $SMA_{RAFT}$ during the fluorescence work, for future work it would be interesting to make a random deuterated copolymer similar to the commercial SMA and study the interaction of this with DMPC or $DMPC_{80}DMPG_{20}$ using reflectivity. This might help to probe the reason for the difference observed in the interactions

Even though only preliminary studies have been carried out for commercial SMI, XRR shows the interaction of the polymer with the monolayer, while the stopped flow SANS experiment suggested that this polymer behaves similarly to commercial SMA when interacting with vesicles. An improved synthesis of this copolymer in the university laboratory would be ideal to make a deuterated SMI, similar to what have been done with $SMA_{RAFT}$.

Even though the self-assembly process is not completely clear yet, a step further has been made in characterising some of the interactions.

# Chapter 6

# Conclusion and future works

In this project three main areas were investigated in the nanodisc field.
In first instance, a few commercial copolymers ($SMI_{1000}$, $SMI_{2000}$ and $SMI_{3000}$) were used to successfully form nanodiscs. Thanks to the basic amine group at the end of the propyl chain, these copolymers are soluble at low pH. This was an achievement since SMA fails in its functionalities at pH lower than 7. It was evaluated that these copolymers make stable nanodiscs-like structures at different range of pH and salt concentrations. The promising achievement obtained in this project from the use of these copolymers is their stability in the presence of divalent cations. SMA polymers, instead, make complexes and precipitate out of the solution in the presence, for instance, of $CaCl_2$. Moreover, SMI copolymers have been successfully used by our collaborator in Birmingham to extract membrane proteins. Compared to the commercial SMA copolymers, the efficiency of the extraction is lower when it is performed with SMI copolymers. However the extraction was performed at pH=7, a pH at which, as shown in chapter 3, SMA structures are not stable.
The second part of this project was the development of new copolymers capable of tuning the size and the properties of the discs. Several molecular weights of polymers were synthesised and tested with lipids to make aggregates. DLS measurements showed the formation of small structures around the expected disc size, with SANS indicating successful formation of nanodisc-shaped structures.

The size of these structures has a linear dependence on the molecular weight of the polymer. Even though this feature has been already reported in literature by Craig an co workers [152], small angle scattering experiments performed on these samples, made the structural resolution possible. Arising from results from scattering data, it was possible to check the rearrangement of the polymer around the lipid core over time. With the purpose to stabilise further the lipid core, a poly(styrene-co-para-methylstyrene-co-maleic anhydride) was synthesised. Results for this novel copolymer were unfortunately not helpful in preparing nanodiscs. However, these experiments highlighted the delicate balance in soft matter self-assembly. Further investigations on the failure of these copolymers in making discs, could help to make progress in explaining the driving force for the self assembly process of nanodiscs. Zwitterionic copolymers have also been synthesised with the purpose to make stable structures at different pH. This copolymer have an invaluable potential. The development of these copolymers can potentially lead to an universal platform for membrane protein extraction, stable over a wide range of pH. However, an improvement must be carried out to the synthesis of these copolymers, increasing the yield of functionalized material.
In the last part of this project, an investigation on the kinetics of the polymer-lipids self assembly was been carried out. Fluorescence and reflectivity data were collected to investigate the diffusion and the penetration of the polymer at the interface with a liposome (fluorescence) or with a lipid monolayer (reflectivity). Both techniques showed that the diffusion of the polymer and the interaction with lipids changes depending on the lipids used. Changes in the structure were followed by stopped flow experiments using the same concentration of lipids, but using commercial and $SMA_{RAFT}$ copolymers. The mechanism, even though it is not completely clear, showed that the random commercial copolymer interacted with a different mechanism compared to $SMA_{RAFT}$ . Many Much progresses have been done made since SMALP entered the scientific community in 2009. Due to the versatility and biocompatible nature of this platform, there are many potential fields in the future to be investigated.

As mantioned above, the use of SMA or SMI is limited to their pH stability range. A controlled synthesis of zwitterionic copolymers could lead the development of a universal platform stable in the presence of divalent cations and in a wide range of pH.

The straightforward functionlisation of poly(styrene-co-maleic anhydride) gives rise to the possibility to prepare potential bioimaging nanodiscs labelled with a dyie or a fluorescent probe. Fluorescently labelled nanodiscs have already been shown in literature for intracellular imaging of Hela cells [213]. Furthermore, the chemical affinity of $Gd^{+3}$ with lipids allows the development of multifunctional platforms, combining the MRI properties of $Gd^{+3}$ with the fluorescentce effect.

# Appendix A

# Appendix

## A.1 SAS analysis of SMI

## A.2 SMI stabilsied nanodiscs

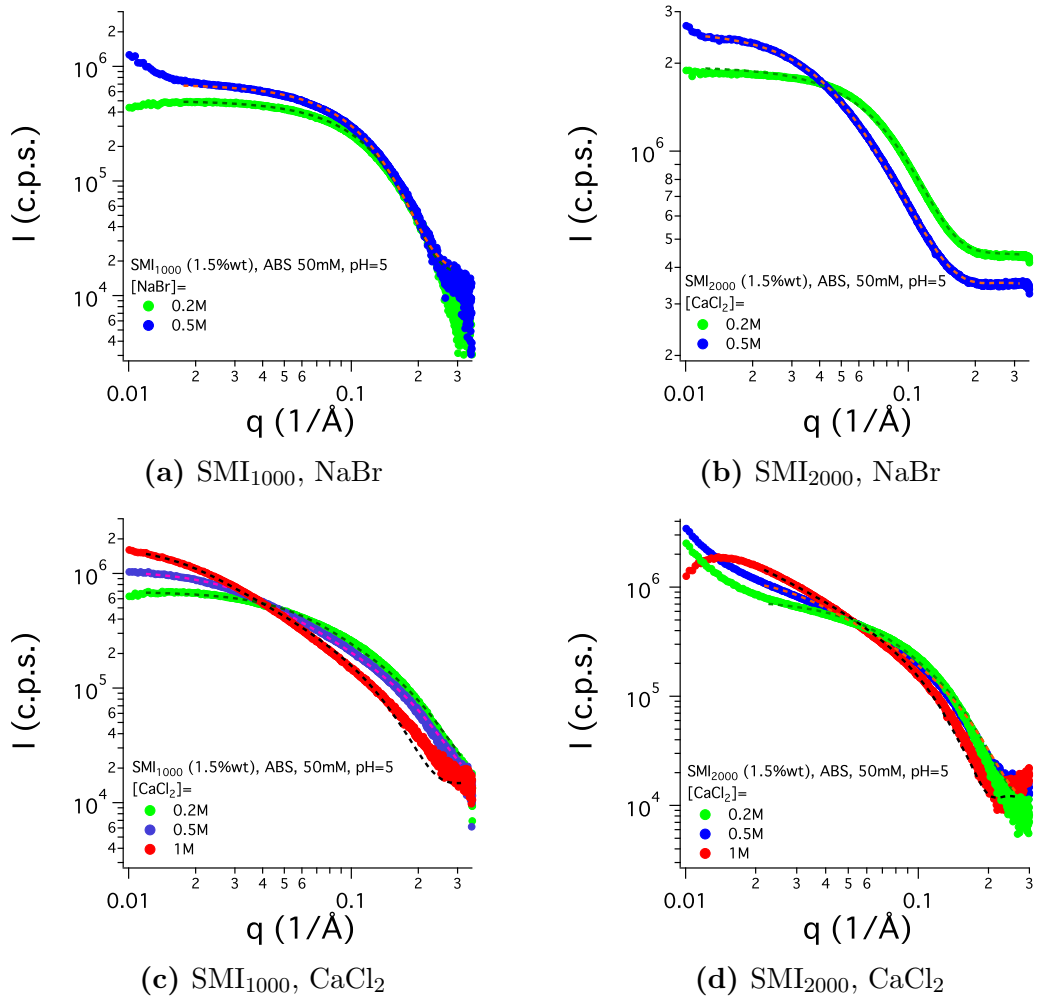


**(a)** $SMI_{1000}$, NaBr

**(b)** $SMI_{2000}$, NaBr

**(c)** $SMI_{1000}$, $CaCl_2$

**(d)** $SMI_{2000}$, $CaCl_2$

**Figure A.1** SAXS patterns acquired on (a)$SMI_{1000}$and (b)$SMI_{2000}$at 1.5%wt in ABS (pH=5, 50mM) with different salt concentration. Several salts were used: NaCl (red dot), NaBr (green square) and $CaCl_2$ (blue triangle).

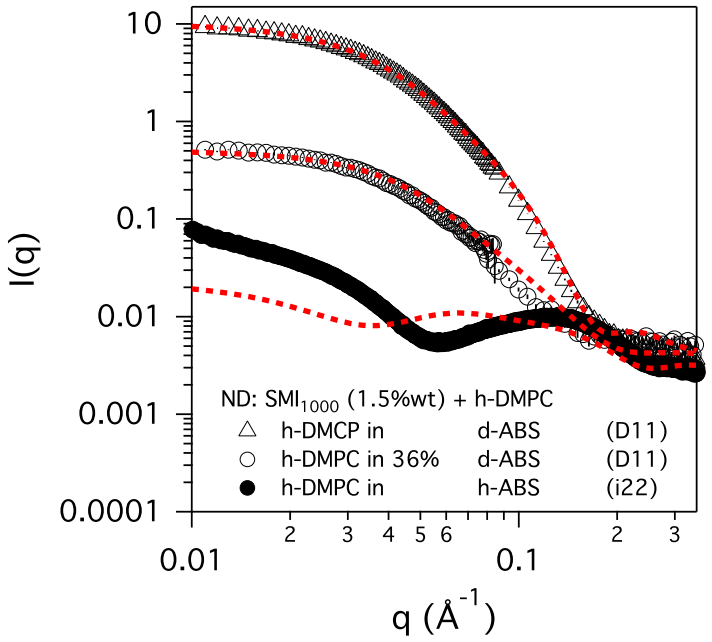


**Figure A.2** Scattering pattern from ILL (circle and triangle) and from i22 (full circle). The dotted red line shows the fitting with an SLD for the head of 1.1x10$^{-5}$ Å$^{-2}$.

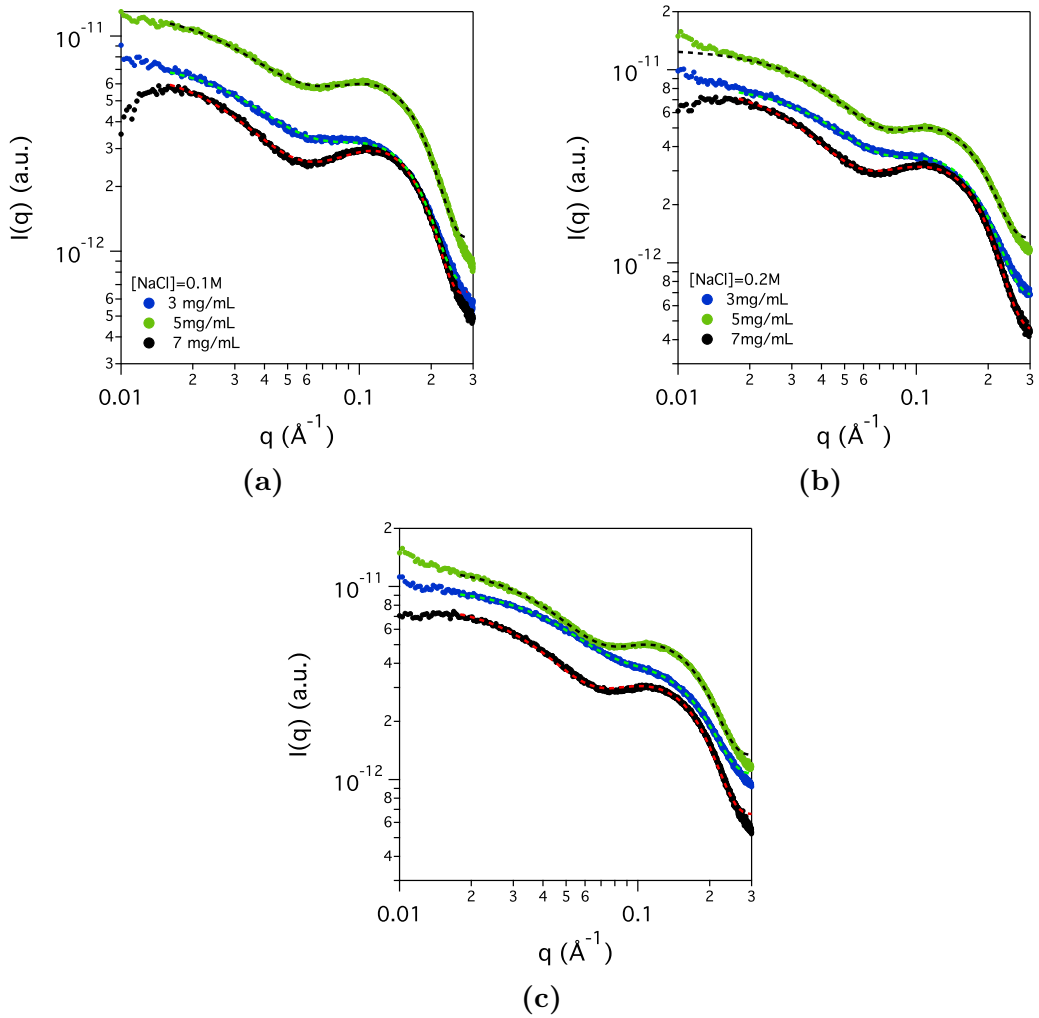


**Figure A.3** SAXS patterns acquired for nanodiscs not purified made with $SMI_{1000}$at 1.5%wt in ABS (pH=5, 50mM) with different salt concentration and lipid concentration.

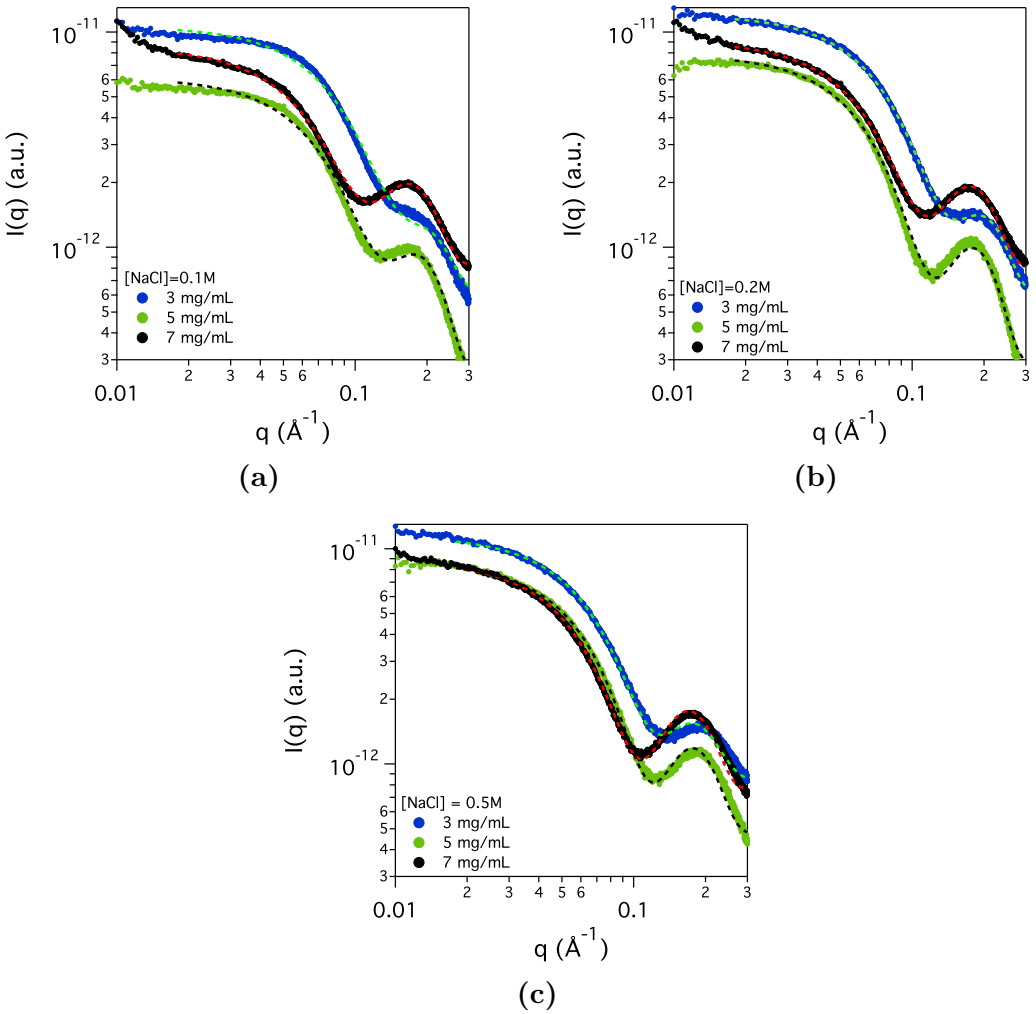


**Figure A.4** SAXS patterns acquired for nanodiscs not purified made with $SMI_{2000}$at 1.5%wt in ABS (pH=5, 50mM) with different salt concentration and DMPC concentration.

# Bibliography


[1] M. Monduzzi, S. Lampis, S. Murgia, and A. Salis, "From self-assembly fundamental knowledge to nanomedicine developments.," *Advances in colloid and interface science*, vol. 205, pp. 48–67, 2014.

[2] "Schematic of i22." http://www.diamond.ac.uk/Beamlines/Soft-Condensed-Matter/small-angle/I22/specs.html. Accessed: 18/09/2017 at 23.30.

[3] D. Singh, "Small angle scattering studies of self assembly in lipid mixtures," 2008.

[4] G. Kocak, C. Tuncer, and V. Bütün, "pH-Responsive polymers," *Polym. Chem.*, vol. 8, no. 1, pp. 144–176, 2017.

[5] M. Schulz, A. Olubummo, and W. H. Binder, "Beyond the lipid-bilayer: interaction of polymers and nanoparticles with membranes," *Soft Matter*, vol. 8, no. 18, p. 4849, 2012.

[6] M. Domingues Marco, S. Santiago Patricia, M. Castanho, and N. C. Santos, "Interaction of peptides with biomembranes assessed by potential-sensitive fluorescent probes," *Journal of peptide science : an official publication of the European Peptide Society*, vol. 14, no. 10, pp. 1084–1095, 2008.

[7] "Cray valley website." http://www.crayvalley.com/products/sma-styrene. Accessed: 09/09/2017.

[8] "Sld calculator." https://www.ncnr.nist.gov/resources/sldcalc.html. Accessed: 09/09/2017.

[9] R. Feynman, "Nobel lectures: Physics 1963–1970," 1972.

[10] d. G. Pierre-Gilles, "Soft matter (Nobel lecture)," *Angewandte Chemie International Edition*, vol. 31, no. 7, pp. 842–845, 1992.

[11] J. Yakhmi, "Soft matter: a perspective," *Journal of Materials Education*, vol. 33, no. 3, p. 149, 2011.

[12] G. Singer, S. J., Nicolson, "The fluid mosaic model of the structure of cell membranes," *Science*, vol. 175, no. 4023, pp. 720–731, 1972.

[13] P. Raven and G. Johnson, "Biology. dubuque, iowa: William c," 1996.

[14] H. Lodish, A. Berk, S. L. Zipursky, P. Matsudaira, D. Baltimore, and J. Darnell, "Molecular cell biology 4th edition," *National Center for Biotechnology InformationÕs Bookshelf*, 2000.

[15] G. von Heijne, "Membrane-protein topology," *Nat Rev Mol Cell Biol*, vol. 7, no. 12, pp. 909–918, 2006.

[16] C. Soto, "Unfolding the role of protein misfolding in neurodegenerative diseases," *Nature reviews. Neuroscience*, vol. 4, no. 1, p. 49, 2003.

[17] J. Ma, A. Yee, H. B. Brewer, S. Das, and H. Potter, "Amyloid-associated proteins [$\alpha$]1-antichymotrypsin and apolipoprotein E promote assembly of Alzheimer [$\beta$]-protein into filaments," *Nature*, vol. 372, pp. 92–94, nov 1994.

[18] H.-J. Park, K.-W. Lee, E. S. Park, S. Oh, R. Yan, J. Zhang, T. G. Beach, C. H. Adler, M. Voronkov, S. P. Braithwaite, *et al.*, "Dysregulation of protein phosphatase 2a in parkinson disease and dementia with lewy bodies," *Annals of clinical and translational neurology*, vol. 3, no. 10, pp. 769–780, 2016.

[19] V. P. Torchilin and A. N. Lukyanov, "Peptide and protein drug delivery to and into tumors: challenges and solutions," *Drug discovery today*, vol. 8, no. 6, pp. 259–266, 2003.

[20] P. C. Jost, O. Griffith, R. Capaldi, and G. Vanderkooi, "Evidence for boundary lipid in membranes," *Proceedings of the National Academy of Sciences*, vol. 70, no. 2, pp. 480–484, 1973.

[21] E. Stier, A., Sackmann, "Spin labels as enzyme substrates heterogeneous lipid distribution in liver microsomal membranes," *Biochimica et Biophysica Acta (BBA)-Biomembranes*, vol. 311, no. 3, pp. 400–408, 1973.

[22] A. Lee, "Lipid–protein interactions in biological membranes: a structural perspective," *Biochimica et Biophysica Acta (BBA)-Biomembranes*, vol. 1612, no. 1, pp. 1–40, 2003.

[23] S. Inagaki, R. Ghirlando, and R. Grisshammer, "Biophysical characterization of membrane proteins in nanodiscs," *Methods*, vol. 59, no. 3, pp. 287–300, 2013.

[24] T. H. Bayburt and S. G. Sligar, "Membrane protein assembly into nanodiscs," *FEBS Letters*, vol. 584, no. 9, pp. 1721–1727, 2010.

[25] J. Nichols, "Phospholipid transfer between phosphatidylcholine-taurocholate mixed micelles," *Biochemistry*, vol. 27, no. 11, pp. 3925–3931, 1988.

[26] R. Kalmbach, I. Chizhov, M. Schumacher, T. Friedrich, E. Bamberg, and M. Engelhard, "Functional cell-free synthesis of a seven helix membrane protein: in situ insertion of bacteriorhodopsin into liposomes," *Journal of molecular biology*, vol. 371, no. 3, pp. 639–648, 2007.

[27] F. Ursini, M. Maiorino, M. Valente, L. Ferri, and C. Gregolin, "Purification from pig liver of a protein which protects liposomes and biomembranes from peroxidative degradation and exhibits glutathione peroxidase activity on phosphatidylcholine hydroperoxides," *Biochimica et Biophysica Acta (BBA)-Lipids and Lipid Metabolism*, vol. 710, no. 2, pp. 197–211, 1982.

[28] B. E. Gregoriadis, G., Ryman, "Fate of protein-containing liposomes injected into rats," *The FEBS Journal*, vol. 24, no. 3, pp. 485–491, 1972.

[29] F. J. Morera, G. Vargas, C. González, E. Rosenmann, and R. Latorre, "Ion-channel reconstitution," *Methods in Membrane Lipids*, pp. 571–585, 2007.

[30] J. Lehn, "Toward self-organization and complex matter," *Science*, vol. 295, no. 5564, pp. 2400–2403, 2002.

[31] G. M. Whitesides and B. Grzybowski, "Self-assembly at all scales," *Science*, vol. 295, no. 5564, pp. 2418–2421, 2002.

[32] G. Whitesides, J. Mathias, and C. Seto, "Molecular self-assembly and nanochemistry- a chemical strategy for the synthesis of nanostructures," *Science*, vol. 254, no. 5036, pp. 1312–1319, 1991.

[33] V. Percec, C. Ahn, G. Ungar, D. Yeardley, M. Möller, and S. S. Sheiko, "Controlling polymer shape through the self-assembly of dendritic side-groups," *Nature*, vol. 391, no. 6663, pp. 161–164, 1998.

[34] I. Denisov, Y. Grinkova, A. Lazarides, and S. Sligar, "Directed self-assembly of monodisperse phospholipid bilayer nanodiscs with controlled size," *Journal of the American Chemical Society*, vol. 126, no. 11, pp. 3477–3487, 2004.

[35] T. Bayburt, Y. Grinkova, and S. Sligar, "Self-assembly of discoidal phospholipid bilayer nanoparticles with membrane scaffold proteins," *Nano Letters*, vol. 2, pp. 853–856, 2002.

[36] T. J. Knowles, R. Finka, C. Smith, Y.-P. Lin, T. Dafforn, and M. Overduin, "Membrane proteins solubilized intact in lipid containing nanoparticles bounded by styrene maleic acid copolymer," *Journal of the American Chemical Society*, vol. 131, no. 22, pp. 7484–7485, 2009.

[37] J. Borch and T. Hamann, "The nanodisc: a novel tool for membrane protein studies," *Biological chemistry*, vol. 390, no. 8, pp. 805–814, 2009.

[38] A. Nath, W. M. Atkins, and S. G. Sligar, "Applications of phospholipid bilayer nanodiscs in the study of membranes and membrane proteins," *Biochemistry*, vol. 46, no. 8, pp. 2059–2069, 2007.

[39] V. Koppaka, L. Silvestro, J. Engler, C. Brouillette, and P. Axelsen, "The structure of human lipoprotein ai evidence for the belt model," *Journal of Biological Chemistry*, vol. 274, no. 21, pp. 14541–14544, 1999.

[40] A. Wlodawer, J. Segrest, B. Chung, R. Chiovetti, and J. Weinstein, "High-density lipoprotein recombinants: evidence for a bicycle tire micelle structure obtained by neutron scattering and electron microscopy," *FEBS letters*, vol. 104, no. 2, pp. 231–235, 1979.

[41] C. Vargas, R. C. Arenas, E. Frotscher, and S. Keller, "Nanoparticle self-assembly in mixtures of phospholipids with styrene/maleic acid copolymers or fluorinated surfactants," *Nanoscale*, vol. 7, no. 48, pp. 20685–20696, 2015.

[42] R. C. Arenas, J. Klingler, C. Vargas, and S. Keller, "Influence of lipid bilayer properties on nanodisc formation mediated by styrene/maleic acid copolymers," *Nanoscale*, vol. 8, no. 32, pp. 15016–15026, 2016.

[43] S. Lee, T. J. Knowles, V. Postis, M. Jamshad, R. A. Parslow, Y. Lin, A. Goldman, P. Sridhar, M. Overduin, S. Muench, and T. Dafforn, "A method for detergent-free isolation of membrane proteins in their local lipid environment," *Nature Protocols*, vol. 11, no. 7, pp. 1149–1162, 2016.

[44] V. Postis, S. Rawson, J. K. Mitchell, S. C. Lee, R. a. Parslow, T. R. Dafforn, S. a. Baldwin, and S. P. Muench, "The use of SMALPs as a novel membrane protein scaffold for structure study by negative stain electron microscopy," *Biochimica et Biophysica Acta (BBA) - Biomembranes*, vol. 1848, no. 2, pp. 496–501, 2015.

[45] S. Gulati, M. Jamshad, T. J. Knowles, K. A. Morrison, R. Downing, N. Cant, R. Collins, J. B. Koenderink, R. C. Ford, M. Overduin, I. D. Kerr, T. R. Dafforn, and A. J. Rothnie, "Detergent-free purification of abc (atp-binding-cassette) transporters," *Biochemical Journal*, vol. 461, no. 2, pp. 269–278, 2014.

[46] J. M. Dörr, M. C. Koorengevel, M. Schäfer, A. V. Prokofyev, S. Scheidelaar, E. A. W. van der Cruijsen, T. R. Dafforn, M. Baldus, and J. A. Killian, "Detergent-free isolation, characterization, and functional reconstitution of a tetrameric k+ channel: The power of native nanodiscs," *Proceedings of the National Academy of Sciences*, vol. 111, no. 52, pp. 18607–18612, 2014.

[47] W. M. Penny, H. B. Steele, J. Ross, and C. P. Palmer, "Phospholipid bilayer affinities and solvation characteristics by electrokinetic chromatography with a nanodisc pseudostationary phase," *Electrophoresis*, vol. 38, no. 5, pp. 738–746, 2017.

[48] D. Li, J. Li, Y. Zhuang, L. Zhang, Y. Xiong, P. Shi, and C. Tian, "Nano-size uni-lamellar lipodisq improved in situ auto-phosphorylation analysis of e. coli tyrosine kinase using 19f nuclear magnetic resonance," *Protein & cell*, vol. 6, no. 3, pp. 229–233, 2015.

[49] J. S. McDowall, I. Ntai, J. Hake, P. R. Whitley, J. M. Mason, C. R. Pudney, and D. R. Brown, "Steady-state kinetics of $\alpha$-synuclein ferrireductase activity identifies the catalytically competent species," *Biochemistry*, vol. 56, no. 19, pp. 2497–2505, 2017.

[50] T. Radeva, *Physical chemistry of polyelectrolytes*, vol. 99. CRC Press, 2001.

[51] T. Cao, W. Yin, and S. Webber, "Poly (2-vinylnaphthalene-alt-maleic acid)-graft-polystyrene as a photoactive polymer micelle and stabilizer for polystyrene latexes," *Macromolecules*, vol. 27, no. 25, pp. 7459–7464, 1994.

[52] P. S. Nair, T. Radhakrishnan, N. Revaprasadu, G. Kolawole, A. Luyt, and V. Djoković, "Polystyrene-co-maleic acid/cds nanocomposites: Preparation and properties," *Journal of Physics and Chemistry of Solids*, vol. 66, no. 7, pp. 1302–1306, 2005.

[53] F. Suzuki, R. B. Pollard, and H. Maeda, "Stimulation of non-specific resistance to tumors in the mouse using a poly (maleic-acid-styrene)-conjugated neocarzinostatin," *Cancer Immunology, Immunotherapy*, vol. 30, no. 2, pp. 97–104, 1989.

[54] E. F. Palermo, I. Sovadinova, and K. Kuroda, "Structural determinants of antimicrobial activity and biocompatibility in membrane-disrupting methacrylamide random copolymers," *Biomacromolecules*, vol. 10, no. 11, pp. 3098–3107, 2009.

[55] L. E. Prevette, D. G. Mullen, and M. M. Banaszak Holl, "Polycation-induced cell membrane permeability does not enhance cellular uptake or expression efficiency of delivered dna," *Molecular pharmaceutics*, vol. 7, no. 3, pp. 870–883, 2010.

[56] M. Teerenstra, D. Suwier, B. Van Mele, L. Teuwen, M. Maassen, H. Van Den Berg, and C. Koning, "Flexibilized styrene-n-substituted maleimide copolymers. i. multiblock copolymers prepared from styrene-maleimide telechelics and polytetrahydrofuran," *Journal of Polymer Science Part A: Polymer Chemistry*, vol. 38, no. 19, pp. 3550–3557, 2000.

[57] E. R. Moore, "Properties of styrene-maleic anhydride copolymers," *Industrial & engineering chemistry product research and development*, vol. 25, no. 2, pp. 315–321, 1986.

[58] E. Moore and D. Pickelman, "Synthesis of styrene/maleimide copolymers and physical properties thereof," *Industrial & engineering chemistry product research and development*, vol. 25, no. 4, pp. 603–609, 1986.

[59] I. Vermeesch, G. Groeninckx, and M. Coleman, "Poly (styrene-co-n-maleimide) copolymers: preparation by reactive extrusion, molecular characterization by ftir, and use in blends," *Macromolecules*, vol. 26, no. 24, pp. 6643–6649, 1993.

[60] B. Derkus, "Applying the miniaturization technologies for biosensor design," *Biosensors and Bioelectronics*, vol. 79, pp. 901–913, 2016.

[61] K. Velonia, A. E. Rowan, and R. J. Nolte, "Lipase polystyrene giant amphiphiles," *Journal of the American Chemical Society*, vol. 124, no. 16, pp. 4224–4225, 2002.

[62] G. Odian, "Radical chain polymerization," *Principles of Polymerization, Fourth Edition*, pp. 198–349, 2004.

[63] H. Higgins, J.S., Benöit, *Polymers and neutron scattering*. Clarendon press Oxford, 1994.

[64] J. V. D. R.A. Pethrick, ed., *Modern tecniques for polymer characterisation*. John Wiley, 1999.

[65] P. L. Th. Zemb, ed., *Neutron, X-rays and Light. Scattering Methods Applied to Soft Condensed Matter*. Elsevier, 2002.

[66] A. Lopez-Rubio and E. P. Gilbert, "Neutron scattering: a natural tool for food science and technology research," *Trends in Food Science & Technology*, vol. 20, pp. 576–586, dec 2009.

[67] N. Stribeck, *X-ray scattering of soft matter*. Springer Science & Business Media, 2007.

[68] R. Heenan, J. Penfold, and S. King, "Sans at pulsed neutron sources: present and future prospects," *Journal of Applied Crystallography*, vol. 30, no. 6, pp. 1140–1147, 1997.

[69] M. Mantid, "Analysis toolkit for instrument data," *Mantid Project*, 2013.

[70] P. Lindner, "Water calibration at dll verified with polymer samples," *Journal of applied crystallography*, vol. 33, no. 3, pp. 807–811, 2000.

[71] G. J. K. D. Richard, M. Ferrand, *LAMP*. A. D. Bradley.

[72] R. Heenan, S. King, D. Turner, and J. Treadgold, "Sans2d at the isis second target station," *Proc ICANS-XVII*, pp. 780–785, 2006.

[73] C. Dewhurst, "D33a third small-angle neutron scattering instrument at the institut laue langevin," *Measurement Science and Technology*, vol. 19, no. 3, p. 034007, 2008.

[74] M. Basham, J. Filik, M. Wharmby, P. Chang, B. El Kassaby, M. Gerring, J. Aishima, K. Levik, B. C. Pulford, and I. Sikharulidze, "Data analysis workbench (dawn)," *Journal of synchrotron radiation*, vol. 22, no. 3, pp. 853–858, 2015.

[75] A. Gibaud and G. Vignaud, *Specular Reflectivity from Smooth and Rough Surfaces*, pp. 85–131. Berlin, Heidelberg: Springer Berlin Heidelberg, 2009.

[76] J. Als-Nielsen, K. Jacquemain, D adn Kjaer, and et al, "Principles and applications of grazing incident x-rayand neutron scattering from ordered molecular monolayers at the air-water interface," *Physics Reports*, vol. 246, pp. 251–313, 1994.

[77] R. Campbell, H. Wacklin, I. Sutton, R. Cubitt, and G. Fragneto, "Figaro: The new horizontal neutron reflectometer at the ill," *The European Physical Journal Plus*, vol. 126, no. 11, pp. 1–22, 2011.

[78] C. Nicklin, T. Arnold, J. Rawle, and A. Warne, "Diamond beamline i07: a beamline for surface and interface diffraction," *Journal of synchrotron radiation*, vol. 23, no. 5, pp. 1245–1253, 2016.

[79] G. Zaccai and B. Jacrot, "Small angle neutron scattering," *Annual review of biophysics and bioengineering*, vol. 12, no. 1, pp. 139–157, 1983.

[80] C. G. Brouillette and G. Anantharamaiah, "Structural models of human apolipoprotein ai," *Biochimica et Biophysica Acta (BBA)-Lipids and Lipid Metabolism*, vol. 1256, no. 2, pp. 103–129, 1995.

[81] J. P. Segrest, "Amphipathic helixes and plasma lipoproteins: thermodynamic and geometric considerations," *Chemistry and physics of lipids*, vol. 18, no. 1, pp. 7–22, 1977.

[82] A. E. Klon, M. K. Jones, J. P. Segrest, and S. C. Harvey, "Molecular belt models for the apolipoprotein ai paris and milano mutations," *Biophysical journal*, vol. 79, no. 3, pp. 1679–1685, 2000.

[83] C. G. Brouillette, G. Anantharamaiah, J. A. Engler, and D. W. Borhani, "Structural models of human apolipoprotein a-i: a critical analysis and review," *Biochimica et Biophysica Acta (BBA) - Molecular and Cell Biology of Lipids*, vol. 1531, no. 1 - 2, pp. 4 – 46, 2001.

[84] I. Idini, "Polymer Stabilised Phospholipid Nanodiscs," 2014.

[85] J. G. Speight *et al.*, *Lange's handbook of chemistry*, vol. 1. McGraw-Hill New York, 2005.

[86] J.-P. Hansen and J. B. Hayter, "A rescaled msa structure factor for dilute charged colloidal dispersions," *Molecular Physics*, vol. 46, no. 3, pp. 651–656, 1982.

[87] A. Nelson, "Co-refinement of multiple-contrast neutron/x-ray reflectivity data using motofit.," *Journal of Applied Chrystallography*, vol. 39, pp. 273–276, 2006.

[88] "Schematic of i22." https://sourceforge.net/projects/rscl/. Accessed: 20/09/2017 at 10.30.

[89] J. Penfold, "Instrumentation for neutron reflectivity," *Physica B: Condensed matter*, vol. 173, pp. 1–10, 1991.

[90] R. Pecora, *Dynamic light scattering: applications of photon correlation spectroscopy*. Springer Science & Business Media, 2013.

[91] V. Filipe, A. Hawe, and W. Jiskoot, "Critical evaluation of nanoparticle tracking analysis (nta) by nanosight for the measurement of nanoparticles and protein aggregates," *Pharmaceutical research*, vol. 27, no. 5, pp. 796–810, 2010.

[92] H. I. Zgurskaya and H. Nikaido, "Acra is a highly asymmetric protein capable of spanning the periplasm," *Journal of molecular biology*, vol. 285, no. 1, pp. 409–420, 1999.

[93] J. Liu and Q. Peng, "Protein-gold nanoparticle interactions and their possible impact on biomedical applications," *Acta Biomaterialia*, 2017.

[94] U. Nobbmann, M. Connah, B. Fish, P. Varley, C. Gee, S. Mulot, J. Chen, L. Zhou, Y. Lu, F. Sheng, J. Yi, and S. E. Harding, "Dynamic light scattering as a relative tool for assessing the molecular integrity and stability of monoclonal antibodies," *Biotechnology and Genetic Engineering Reviews*, vol. 24, no. 1, pp. 117–128, 2007.

[95] E. Eiser, *Multi Length-Scale Characterisation*. John Wiley & Sons, Ltd, 2014.

[96] T. Hida, *Brownian motion*. Springer, 1980.

[97] R. Finsy, "Particle sizing by quasi-elastic light scattering," *Advances in Colloid and Interface Science*, vol. 52, pp. 79 – 143, 1994.

[98] J. T. Edward, "Molecular volumes and the stokes-einstein equation," *Journal of Chemical Education*, vol. 47, no. 4, p. 261, 1970.

[99] S. Mori and H. G. Barth, *Size exclusion chromatography*. Springer Science & Business Media, 2013.

[100] H. De Brouwer, M. A. Schellekens, B. Klumperman, M. J. Monteiro, and A. L. German, "Controlled radical copolymerization of styrene and maleic anhydride and the synthesis of novel polyolefin-based block copolymers by reversible addition–fragmentation chain-transfer (raft) polymerization,"

*Journal of Polymer Science Part A: Polymer Chemistry*, vol. 38, no. 19, pp. 3596–3603, 2000.

[101] E. Chernikova, P. Terpugova, C. Bui, and B. Charleux, "Effect of comonomer composition on the controlled free-radical copolymerization of styrene and maleic anhydride by reversible addition-fragmentation chain transfer (RAFT)," *Polymer*, vol. 44, no. 15, pp. 4101–4107, 2003.

[102] R. Aveyard and D. A. Haydon, *An introduction to the principles of surface chemistry*. CUP Archive, 1973.

[103] P. L. Du Noüy, "A new apparatus for measuring surface tension," *The Journal of general physiology*, vol. 1, no. 5, p. 521, 1919.

[104] P. L. du Noüy, "An interfacial tensiometer for universal use," *The Journal of general physiology*, vol. 7, no. 5, p. 625, 1925.

[105] E. Rame, "The interpretation of dynamic contact angles measured by the wilhelmy plate method," *Journal of colloid and interface science*, vol. 185, no. 1, pp. 245–251, 1997.

[106] B. C. Smith, *Fundamentals of Fourier transform infrared spectroscopy*. CRC press, 2011.

[107] M. Kasha, "Characterization of electronic transitions in complex molecules," *Discussions of the Faraday society*, vol. 9, pp. 14–19, 1950.

[108] J. Lakowicz, *Principles of fluorescence spectroscopy*. Springer Science & Business Media, 2013.

[109] S. Lindhoud, V. Carvalho, J. Pronk, and M. Aubin-Tam, "SMA-SH: Modified Styrene-Maleic Acid Copolymer for Functionalization of Lipid Nanodiscs," *Biomacromolecules*, vol. 17, pp. 1516–1522, 2016.

[110] S. Scheidelaar, M. C. Koorengevel, C. A. van Walree, J. J. Dominguez, J. M. D'orr, and J. A. Killian, "Effect of Polymer Composition and pH on Membrane Solubilization by Styrene-Maleic Acid Copolymers," *Biophysical Journal*, vol. 111, no. 9, pp. 1974–1986, 2016.

[111] A. Fane, C. Fell, and A. Suki, "The effect of pH and ionic environment on the ultrafiltration of protein solutions with retentive membranes," *Journal of Membrane Science*, vol. 16, pp. 195–210, 1983.

[112] P. Z. O'Farrell, H. M. Goodman, and P. H. O'Farrell, "High resolution two-dimensional electrophoresis of basic as well as acidic proteins," *Cell*, vol. 12, no. 4, pp. 1133–1142, 1977.

[113] S. R. Tonge and B. J. Tighe, "Responsive hydrophobically associating polymers: A review of structure and properties," *Advanced Drug Delivery Reviews*, vol. 53, no. 1, pp. 109–122, 2001.

[114] D. Schmaljohann, "Thermo- and pH-responsive polymers in drug delivery," *Advanced Drug Delivery Reviews*, vol. 58, no. 15, pp. 1655–1670, 2006.

[115] A. Hodgkin and P. Horowicz, "The influence of potassium and chloride ions on the membrane potential of single muscle fibres," *The Journal of physiology*, vol. 148, no. 1, pp. 127–160, 1959.

[116] F. Castelli, G. Pitarresi, and G. Giammona, "Influence of different parameters on drug release from hydrogel systems to a biomembrane model. evaluation by differential scanning calorimetry technique," *Biomaterials*, vol. 21, no. 8, pp. 821–833, 2000.

[117] P. Gupta, K. Vermani, and S. Garg, "Hydrogels: from controlled release to pH-responsive drug delivery," *Drug discovery today*, vol. 7, no. 10, pp. 569–579, 2002.

[118] S. Ikeda, "Sphere-rod transition of surfactant micelles and size distribution of rodlike micelles," *The Journal of Physical Chemistry*, vol. 88, no. 10, pp. 2144–2149, 1984.

[119] M. E. Cates and S. J. Candau, "Statics and dynamics of worm-like surfactant micelles," *Journal of Physics: Condensed Matter*, vol. 2, no. 33, p. 6869, 1990.

[120] J. Zhang, Z. Ge, X. Jiang, P. Hassan, and S. Liu, "Stopped-flow kinetic studies of sphere-to-rod transitions of sodium alkyl sulfate micelles induced by hydrotropic salt," *Journal of Colloid and Interface Science*, vol. 316, no. 2, pp. 796 – 802, 2007.

[121] O. V. Borisov and E. B. Zhulina, "Morphology of micelles formed by diblock copolymer with a polyelectrolyte block," *Macromolecules*, vol. 36, no. 26, pp. 10029–10036, 2003.

[122] K. Khougaz, I. Astafieva, and A. Eisenberg, "Micellization in block polyelectrolyte solutions. 3. static light scattering characterization," *Macromolecules*, vol. 28, no. 21, pp. 7135–7147, 1995.

[123] R. Georgieva, R. Dimova, G. Sukhorukov, G. Ibarz, and H. Möhwald, "Influence of different salts on micro-sized polyelectrolyte hollow capsules," *Journal of materials chemistry*, vol. 15, no. 40, pp. 4301–4310, 2005.

[124] O. V. Borisov and E. B. Zhulina, "Effect of salt on self-assembly in charged block copolymer micelles," *Macromolecules*, vol. 35, pp. 4472–4480, 2002.

[125] F. Hofmeister, "Zur lehre von der wirkung der salze," *Naunyn-Schmiedeberg's Archives of Pharmacology*, vol. 25, no. 1, pp. 1–30, 1888.

[126] E. Leontidis, "Hofmeister anion effects on surfactant self-assembly and the formation of mesoporous solids," *Current Opinion in Colloid and Interface Science*, vol. 7, no. 1-2, pp. 81–91, 2002.

[127] M. Boström, D. R. Williams, and B. W. Ninham, "Surface tension of electrolytes: specific ion effects explained by dispersion forces," *Langmuir*, vol. 17, no. 15, pp. 4475–4478, 2001.

[128] M. Chaplin, "A proposal for the structuring of water," *Biophysical chemistry*, vol. 83, no. 3, pp. 211–221, 2000.

[129] A. Daulat, P. Maurice, and R. Jockers, "Techniques for the discovery of gpcr-associated protein complexes," *Methods Enzymol*, vol. 521, pp. 329–345, 2013.

[130] K. Liu, N. Southall, S. A. Titus, J. Inglese, R. L. Eskay, P. Shinn, C. P. Austin, M. A. Heilig, and W. Zheng, "A multiplex calcium assay for identification of gpcr agonists and antagonists," *Assay and drug development technologies*, vol. 8, no. 3, pp. 362–374, 2010.

[131] P. Hassan, S. R. Raghavan, and E. W. Kaler, "Microstructural changes in sds micelles induced by hydrotropic salt," *Langmuir*, vol. 18, no. 7, pp. 2543–2548, 2002.

[132] N. Christov, N. Denkov, P. Kralchevsky, K. Ananthapadmanabhan, and A. Lips, "Synergistic sphere-to-rod micelle transition in mixed solutions of sodium dodecyl sulfate and cocoamidopropyl betaine," *Langmuir*, vol. 20, no. 3, pp. 565–571, 2004.

[133] L. Jiang, K. Wang, M. Deng, Y. Wang, and J. Huang, "Bile salt-induced vesicle-to-micelle transition in catanionic surfactant systems: steric and electrostatic interactions," *Langmuir*, vol. 24, no. 9, pp. 4600–4606, 2008.

[134] T. Imae and S. Ikeda, "Characteristics of rodlike micelles of cetyltrimethylammonium chloride in aqueous nacl solutions: Their flexibility and the scaling laws in dilute and semidilute regimes," *Colloid and Polymer Science*, vol. 265, no. 12, pp. 1090–1098, 1987.

[135] L. Magid, Z. Han, G. Warr, M. Cassidy, P. Butler, and W. Hamilton, "Effect of counterion competition on micellar growth horizons for cetyltrimethylammonium micellar surfaces: electrostatics and specific binding," *The Journal of Physical Chemistry B*, vol. 101, no. 40, pp. 7919–7927, 1997.

[136] H.-P. Lin, C.-P. Kao, and C.-Y. Mou, "Counterion and alcohol effect in the formation of mesoporous silica," *Microporous and mesoporous materials*, vol. 48, no. 1, pp. 135–141, 2001.

[137] M. Jamshad, V. Grimard, I. Idini, T. J. Knowles, M. R. Dowle, N. Schofield, P. Sridhar, Y. Lin, R. Finka, M. Wheatley, O. R. T. Thomas, R. E. Palmer, M. Overduin, C. Govaerts, J.-M. Ruysschaert, K. J. Edler, and T. R. Dafforn, "Structural analysis of a nanoparticle containing a lipid bilayer used for detergent-free extraction of membrane proteins," *Nano Research*, 2014.

[138] N. Kučerka, M. A. Kiselev, and P. Balgavỳ, "Determination of bilayer thickness and lipid surface area in unilamellar dimyristoylphosphatidylcholine vesicles from small-angle neutron scattering curves: a comparison of evaluation methods," *European Biophysics Journal*, vol. 33, no. 4, pp. 328–334, 2004.

[139] J. M. Boggs, "Lipid intermolecular hydrogen bonding: influence on structural organization and membrane function," *Biochimica et Biophysica Acta (BBA)-Reviews on Biomembranes*, vol. 906, no. 3, pp. 353–404, 1987.

[140] R. Winkler, M. Gold, and P. Reineker, "Collapse of Polyelectrolyte Macromolecules by Counterion Condensation and Ion Pair Formation: A Molecular Dynamics Simulation Study," *Physical Review Letters*, vol. 80, no. 17, pp. 3731–3734, 1998.

[141] P.-Y. Hsiao and E. Luijten, "Salt-induced collapse and reexpansion of highly charged flexible polyelectrolytes," *Physical review letters*, vol. 97, no. 14, p. 148301, 2006.

[142] N. Cohen, L. Binyamin, Y. Levi-Kalisman, G. Y. Berguig, A. Convertine, P. Stayton, and R. Yerushalmi-Rozen, "PH and Salt Effects on Surface Activity and Self-Assembly of Copolymers Containing a Weak Polybase," *Langmuir*, vol. 32, no. 36, pp. 9286–9292, 2016.

[143] A. J. Trexler and J. W. Taraska, "Regulation of insulin exocytosis by calcium-dependent protein kinase c in beta cells," *Cell Calcium*, vol. 67, pp. 1–10, 2017.

[144] T. A. McKeon and M. L. Lyman, "Calcium ion improves electrophoretic transfer of calmodulin and other small proteins," *Analytical biochemistry*, vol. 193, no. 1, pp. 125–130, 1991.

[145] T. Ravula, S. Ramadugu, G. Di Mauro, and A. Ramamoorthy, "Bioinspired, size-tunable self-assembly of polymer-lipid bilayer nanodiscs," *Angewandte Chemie International Edition*, 2017.

[146] C. Peetla, A. Stine, and V. Labhasetwar, "Biophysical interactions with model lipid membranes: applications in drug discovery and drug delivery," *Molecular pharmaceutics*, vol. 6, no. 5, pp. 1264–1276, 2009.

[147] M. Deleu, J.-M. Crowet, M. N. Nasir, and L. Lins, "Complementary biophysical tools to investigate lipid specificity in the interaction between bioactive molecules and the plasma membrane: A review," *Biochimica et Biophysica Acta (BBA) - Biomembranes*, vol. 1838, no. 12, pp. 3171 – 3190, 2014.

[148] M. B. Decca, V. V. Galassi, M. Perduca, H. L. Monaco, and G. G. Montich, "Influence of the lipid phase state and electrostatic surface potential on the

conformations of a peripherally bound membrane protein," *The Journal of Physical Chemistry B*, vol. 114, no. 46, pp. 15141–15150, 2010.

[149] E. Lyukmanova, Z. Shenkarev, N. Khabibullina, G. Kopeina, M. Shulepko, A. Paramonov, K. Mineev, R. Tikhonov, L. Shingarova, L. Petrovskaya, D. Dolgikh, A. Arseniev, and M. Kirpichnikov, "Lipid-protein nanodiscs for cell-free production of integral membrane proteins in a soluble and folded state: Comparison with detergent micelles, bicelles and liposomes," *Biochimica et Biophysica Acta (BBA) - Biomembranes*, vol. 1818, no. 3, pp. 349 – 358, 2012.

[150] D. S. Marynick and H. F. Schaefer, "Theoretical studies of metal-phosphate interactions: interaction of $Li^+$, $Na^+$, $K^+$, $Be^{2+}$, $Mg^{2+}$, and $Ca^{2+}$ with $H_2PO_4$-and $(ch_3o)_2po_2^-$: implications for nucleic acid solvation," *Proceedings of the National Academy of Sciences*, vol. 72, no. 10, pp. 3794–3798, 1975.

[151] P. Garidel and A. Blume, "1,2-Dimyristoyl-sn-glycero-3-phosphoglycerol (DMPG) monolayers: Influence of temperature, pH, ionic strength and binding of alkaline earth cations," *Chemistry and Physics of Lipids*, vol. 138, no. 1-2, pp. 50–59, 2005.

[152] A. F. Craig, E. E. Clark, I. D. Sahu, R. Zhang, N. D. Frantz, M. S. Al-Abdul-Wahid, C. Dabney-Smith, D. Konkolewicz, and G. A. Lorigan, "Tuning the size of styrene-maleic acid copolymer-lipid nanoparticles (smalps) using raft polymerization for biophysical studies," *Biochimica et Biophysica Acta (BBA)-Biomembranes*, vol. 1858, no. 11, pp. 2931–2939, 2016.

[153] J. M. Ren, T. G. McKenzie, Q. Fu, E. H. H. Wong, J. Xu, Z. An, S. Shanmugam, T. P. Davis, C. Boyer, and G. G. Qiao, "Star Polymers," *Chemical Reviews*, vol. 116, no. 12, pp. 6743–6836, 2016.

[154] W. H. Carothers, "Polymerization.," *Chemical Reviews*, vol. 8, no. 3, pp. 353–426, 1931.

[155] K. Van Cauter, V. Van Speybroeck, P. Vansteenkiste, M.-F. Reyniers, and M. Waroquier, "Ab initio study of free-radical polymerization: Polyethylene propagation kinetics," *ChemPhysChem*, vol. 7, no. 1, pp. 131–140, 2006.

[156] D. Cuccato, M. Dossi, D. Moscatelli, and G. Storti, "A density functional theory study of poly (vinyl chloride)(pvc) free radical polymerization," in *Macromolecular Symposia*, vol. 302, pp. 100–109, Wiley Online Library, 2011.

[157] M. K. Georges, R. P. Veregin, P. M. Kazmaier, G. K. Hamer, and M. Saban, "Narrow polydispersity polystyrene by a free-radical polymerization process-rate enhancement," *Macromolecules*, vol. 27, no. 24, pp. 7228–7229, 1994.

[158] J. Chiefari, Y. Chong, F. Ercole, J. Krstina, J. Jeffery, T. P. Le, R. T. Mayadunne, G. F. Meijs, C. L. Moad, G. Moad, *et al.*, "Living free-radical polymerization by reversible addition- fragmentation chain transfer: the raft process," *Macromolecules*, vol. 31, no. 16, pp. 5559–5562, 1998.

[159] C. Barner-kowollik, *Handbook of RAFT Polymerization*. 2008.

[160] M. Benaglia, J. Chiefari, Y. K. Chong, G. Moad, E. Rizzardo, and S. H. Thang, "Universal (switchable) raft agents," *Journal of the American Chemical Society*, vol. 131, no. 20, pp. 6914–6915, 2009.

[161] D. J. Keddie, "A guide to the synthesis of block copolymers using reversible-addition fragmentation chain transfer (RAFT) polymerization.," *Chemical Society reviews*, vol. 43, no. 2, pp. 496–505, 2013.

[162] M. Muthukumar, "Competing Interactions and Levels of Ordering in Self-Organizing Polymeric Materials," *Science*, vol. 277, no. 5330, pp. 1225–1232, 1997.

[163] P. J. Flory, *Principles of polymer chemistry*. Cornell University Press, 1953.

[164] M. A. Masuelli, "Mark-houwink parameters for aqueous-soluble polymers and biopolymers at various temperatures," *Journal of Polymer and Biopolymer Physics Chemistry*, vol. 2, no. 2, pp. 37–43, 2014.

[165] A. Garnier, S. , Laschewsky, "Non-ionic amphiphilic block copolymers by RAFT-polymerization and their self-organization," *Colloid and Polymer Science*, vol. 284, no. 11, pp. 1243–1254, 2006.

[166] J. W. Qian, M. Wang, D. L. Han, and R. S. Cheng, "A novel method for estimating unperturbed dimension $[\eta]_\theta$ of polymer from the measurement of its $[\eta]$ in a non-theta solvent," *European polymer journal*, vol. 37, no. 1, pp. 1403–1407, 2001.

[167] J. Rodriguez-Hernández and S. Lecommandoux, "Reversible inside- out micellization of pH-responsive and water-soluble vesicles based on polypeptide diblock copolymers," *Journal of the American Chemical Society*, vol. 127, no. 7, pp. 2026–2027, 2005.

[168] P. Petrov, C. B. Tsvetanov, and R. Jérôme, "Twocomponent "Onionlike" micelles with a PPO core, a PDMAEMA shell and a PEO corona: formation and crosslinking," *Polymer International*, vol. 57, no. 11, pp. 1258–1264, 2008.

[169] S. Banerjee, K. Sen, T. K. Pal, and S. K. Guha, "Poly (styrene-co-maleic acid)-based pH-sensitive liposomes mediate cytosolic delivery of drugs for enhanced cancer chemotherapy," *International journal of pharmaceutics*, vol. 436, no. 1, pp. 786–797, 2012.

[170] S. M. H, M. E. EM, C. M. Pirie, A. S. Hoffman, and P. S. Stayton, "pH-responsive poly (styrene-alt-maleic anhydride) alkylamide copolymers for intracellular drug delivery," *Biomacromolecules*, vol. 7, no. 8, pp. 2407–2414, 2006.

[171] T. D. Lazzara, M. A. Whitehead, and T. G. van de Ven, "Linear nanotemplates of styrene and maleic anhydride alternating copolymers," *European Polymer Journal*, vol. 45, no. 7, pp. 1883–1890, 2009.

[172] C. Malardier-Jugroot, T. Van De Ven, T. Cosgrove, R. M. Richardson, and M. A. Whitehead, "Novel self-assembly of amphiphilic copolymers into nanotubes: Characterization by small-angle neutron scattering," *Langmuir*, vol. 21, no. 22, pp. 10179–10187, 2005.

[173] T. C. R. M. R. M. A. W. C. Malardier-Jugroot T. G. M. van de Ven, "Novel Self-Assembly of Amphiphilic Copolymers into Nanotubes: Characterization by Small-Angle Neutron Scattering," *Langmuir*, vol. 21, no. 22, pp. 10179–10187, 2005.

[174] T. Alfrey Jr and G. Goldfinger, "The mechanism of copolymerization," *The Journal of Chemical Physics*, vol. 12, no. 6, pp. 205–209, 1944.

[175] F. R. Mayo and F. M. Lewis, "Copolymerization. i. a basis for comparing the behavior of monomers in copolymerization; the copolymerization of styrene and methyl methacrylate," *Journal of the American Chemical Society*, vol. 66, no. 9, pp. 1594–1601, 1944.

[176] B. Klumperman, "Mechanistic considerations on styrene–maleic anhydride copolymerization reactions," *Polymer Chemistry*, vol. 1, no. 5, pp. 558–562, 2010.

[177] K. Dodgson and J. Ebdon, "On the role of monomer-monomer donor-acceptor complexes in the free-radical copolymerisation of styrene and maleic anhydride," *European Polymer Journal*, vol. 13, no. 10, pp. 791 – 797, 1977.

[178] L. Klumperman, "Free radical copolymerization of styrene and maleic anhydride: kinetic studies at low and intermediate conversion," p. 120, 1994.

[179] W. M. Haynes, *CRC Handbook of Chemistry and Physics*. Boca Raton, Fla. : CRC, 2011.

[180] N. Kang, M. Perron, R. E. Prud'Homme, Y. Zhang, G. Gaucher, and J. Leroux, "Stereocomplex block copolymer micelles: core- shell nanostructures with enhanced stability," *Nano letters*, vol. 5, no. 2, pp. 315–319, 2005.

[181] G. Gaucher, M. Dufresne, V. Sant, N. Kang, D. Maysinger, and J. Leroux, "Block copolymer micelles: preparation, characterization and application

in drug delivery," *Journal of controlled release*, vol. 109, no. 1, pp. 169–188, 2005.

[182] S. Harrisson and K. L. Wooley, "Shell-crosslinked nanostructures from amphiphilic ab and aba block copolymers of styrene-alt-(maleic anhydride) and styrene: polymerization, assembly and stabilization in one pot," *Chemical Communications*, no. 26, pp. 3259–3261, 2005.

[183] S. Wang, X. Huang, G. Wang, Y. Wang, J. He, and P. Jiang, "Increasing the energy efficiency and breakdown strength of high-energy-density polymer nanocomposites by engineering the ba0. 7sr0. 3tio3 nanowire surface via reversible addition–fragmentation chain transfer polymerization," *The Journal of Physical Chemistry C*, vol. 119, no. 45, pp. 25307–25318, 2015.

[184] S. M. Henry, M. E. El-Sayed, C. M. Pirie, A. S. Hoffman, and P. S. Stayton, "pH-responsive poly (styrene-alt-maleic anhydride) alkylamide copolymers for intracellular drug delivery," *Biomacromolecules*, vol. 7, no. 8, pp. 2407–2414, 2006.

[185] G. M. Qiu, B. K. Zhu, Y. Y. Xu, and K. E. Geckeler, "Synthesis of ultrahigh molecular weight poly(styrene-alt-maleic anhydride) in supercritical carbon dioxide," *Macromolecules*, vol. 39, no. 9, pp. 3231–3237, 2006.

[186] K. Mpitso and P. Science, "Synthesis and characterization of styrene maleic anhydride copolymer derivatives," no. September, 2009.

[187] A. Oluwole, B. Danielczak, A. Meister, J. O. Babalola, C. Vargas, and S. Keller, "Solubilization of membrane proteins into functional lipid-bilayer nanodiscs using a diisobutylene/maleic acid copolymer," *Angewandte Chemie International Edition*, vol. 56, no. 7, pp. 1919–1924, 2017.

[188] G. Hadziioannou and A. Skoulios, "Molecular weight dependence of lamellar structure in styrene isoprene two-and three-block copolymers," *Macromolecules*, vol. 15, no. 2, pp. 258–262, 1982.

[189] H. Bermudez, A. K. Brannan, D. A. Hammer, F. S. Bates, and D. Discher, "Molecular weight dependence of polymersome membrane structure, elasticity, and stability," *Macromolecules*, vol. 35, no. 21, pp. 8203–8208, 2002.

[190] H. S. Mansur, C. M. Sadahira, A. N. Souza, and A. A. Mansur, "Ftir spectroscopy characterization of poly (vinyl alcohol) hydrogel with different hydrolysis degree and chemically crosslinked with glutaraldehyde," *Materials Science and Engineering: C*, vol. 28, no. 4, pp. 539 – 548, 2008.

[191] S. Hong, P. R. Leroueil, E. Janus, J. Peters, and M. Kober, "Interaction of polycationic polymers with supported lipid bilayers and cells : Nanoscale hole formation and enhanced membrane permeability," no. 3, pp. 728–734, 2006.

[192] N. Murthy, J. Robichaud, D. Tirrell, P. Stayton, and A. Hoffman, "The design and synthesis of polymers for eukaryotic membrane disruption," *Journal of Controlled Release*, vol. 61, no. 1-2, pp. 137–143, 1999.

[193] D. A. Thomas, J. L., Tirrell, "Polyelectrolyte-sensitized phospholipid vesicles," *Accounts of Chemical Research*, vol. 25, no. 5, pp. 336–342, 1992.

[194] M. Benhamou, I. Joudar, and H. Kaidi, "Phase separation between phospholipids and grafted polymer chains onto a fluctuating membrane," *The European Physical Journal E: Soft Matter and Biological Physics*, vol. 24, no. 4, pp. 343–351, 2007.

[195] Y. Wang and F. Li, "An emerging pore-making strategy: Confined swelling-induced pore generation in block copolymer materials," *Advanced Materials*, vol. 23, no. 19, pp. 2134–2148, 2011.

[196] A. A. Yaroslavov, A. A. Rakhnyanskaya, E. G. Yaroslavova, A. A. Efimova, and F. M. Menger, "Polyelectrolyte-coated liposomes: Stabilization of the interfacial complexes," *Advances in Colloid and Interface Science*, vol. 142, no. 1, pp. 43 – 52, 2008.

[197] A. A. Yaroslavov, N. S. Melik-Nubarov, and F. M. Menger, "Polymer-induced flip-flop in biomembranes," *Accounts of chemical research*, vol. 39, no. 10, pp. 702–710, 2006.

[198] Y. Y. Chieng and S. B. Chen, "Interaction and complexation of phospholipid vesicles and triblock copolymers," *The Journal of Physical Chemistry B*, vol. 113, no. 45, pp. 14934–14942, 2009.

[199] B. Discher, Y. Won, D. Ege, J. Lee, F. Bates, D. Discher, and D. Hammer, "Polymersomes: Tough vesicles made from diblock copolymers," *Science*, vol. 284, no. 5417, pp. 1143–1146, 1999.

[200] T. Terai, T., Nagano, "Small-molecule fluorophores and fluorescent probes for bioimaging," *Pflugers Archiv European Journal of Physiology*, vol. 465, no. 3, pp. 347–359, 2013.

[201] J. Cladera and P. O'Shea, "Intramembrane molecular dipoles affect the membrane insertion and folding of a model amphiphilic peptide.," *Biophysical Journal*, vol. 74, no. 5, pp. 2434–42, 1998.

[202] P. O'Shea, "Intermolecular interactions with/within cell membranes and the trinity of membrane potentials: kinetics and imaging.," *Biochemical Society transactions*, vol. 31, no. Pt 5, pp. 990–996, 2003.

[203] N. Fitchen, P. O'Shea, P. Williams, and K. Hardie, "Electrostatic sensor for identifying interactions between peptides and bacterial membranes," *Molecular Immunology*, vol. 40, no. 7, pp. 407–411, 2003.

[204] J. Wall, F. Ayoub, and P. He, "Interactions of macromolecules with the mammalian cell surface," *Journal of Cell Science*, vol. 108, no. 7, pp. 2673–2682, 1995.

[205] R. J. Starke-Peterkovic, T., Clarke, "Effect of headgroup on the dipole potential of phospholipid vesicles," *European Biophysics Journal*, vol. 39, no. 1, p. 103, 2009.

[206] M. Thelen, G. Petrone, P. O'Shea, and A. Azzi, "The use of fluorescein-dipalmitoylphosphatidylethanolamine for measuring pH-changes in the internal compartment of phospholipid vesicles," *Biochimica et Biophysica Acta (BBA)-Bioenergetics*, vol. 766, no. 1, pp. 161–168, 1984.

[207] M. M. Martin and L. Lindqvist, "The pH dependence of fluorescein fluorescence," *Journal of Luminescence*, vol. 10, no. 6, pp. 381–390, 1975.

[208] V. Montana, D. L. Farkas, and L. M. Loew, "Dual-wavelength ratiometric fluorescence measurements of membrane potential," *Biochemistry*, vol. 28, no. 11, pp. 4536–4539, 1989.

[209] M. E. Barbinta Patrascu, L. Tugulea, I. Lacatusu, and A. Meghea, "Spectral characterization of model systems containing lipids and chlorophyll," *Molecular Crystals and Liquid Crystals*, vol. 522, no. 1, pp. 148/[448]–158/[458], 2010.

[210] L. Braun, M. Uhlig, R. von Klitzing, and R. A. Campbell, "Polymers and surfactants at fluid interfaces studied with specular neutron reflectometry," *Advances in Colloid and Interface Science*, 2017.

[211] L. Clifton, M. Skoda, E. Daulton, A. Hughes, A. Le Brun, J. Lakey, and S. A. Holt, "Asymmetric phospholipid: lipopolysaccharide bilayers; a gram-negative bacterial outer membrane mimic," *Journal of The Royal Society Interface*, vol. 10, no. 89, p. 20130810, 2013.

[212] S. Scheidelaar, M. C. Koorengevel, J. D. Pardo, J. D. Meeldijk, E. Breukink, and J. A. Killian, "Molecular Model for the solubilization of membranes into nanodisks by styrene maleic acid copolymers," *Biophysical Journal*, vol. 108, no. 2, pp. 279–290, 2015.

[213] A. I. Petrache, D. C. Machin, D. J. Williamson, M. E. Webb, and P. A. Beales, "Sortase-mediated labelling of lipid nanodiscs for cellular tracing," *Molecular BioSystems*, vol. 12, no. 6, pp. 1760–1763, 2016.